EXPERIMENTAL INVESTIGATION OF THE IMPACTS OF EXPANSIVE SOILS ON THE LONG-TERM STABILITY OF MOUNTAINOUS TUNNELS

膨潤性地山が山岳トンネルの長期安定性に及ぼす影響に関する実験的研究

SAQIB ASHRAF

2022

GRADUATE SCHOOL OF URBAN INNOVATION
YOKOHAMA NATIONAL UNIVERSITY

EXPERIMENTAL INVESTIGATION OF THE IMPACTS OF EXPANSIVE SOILS ON THE LONG-TERM STABILITY OF MOUNTAINOUS TUNNELS

BY

SAQIB ASHRAF (19WA902)

A dissertation submitted in partial fulfillment of the requirements for the degree of

DOCTOR OF ENGINEERING

Examination Committee:

Associate Professor Dr. Ying CUI (Chair)

Professor, Dr. Kimitoshi HAYANO

Professor, Dr. Mamoru KIKUMOTO

Professor, Dr. Koichi MAEKAWA

Associate Professor, Dr. Chikako FUJIYAMA

SEPTEMBER 2022

DEDICATED TO MY PARENTS

MR. MUHAMMAD ASHRAF (Late) and MS. FARZANA ASHRAF

The blessings of ALLAH ALMIGHTY

جنت میری..... والدین ہمارے

ACKNOWLEDGEMENTS

In the name of Allah Almighty, The most beneficent, The most merciful.

I would like to express the deepest appreciation and heartiest gratitude to my committee chair and academic advisor, Dr. Cui Ying, who continually and convincingly conveyed a spirit of adventure in regard to this research throughout the study period. Without her guidance and persistent help, this thesis and research would have not been possible.

I would like to express sincere gratitude to my examination committee members, Prof. Kimitoshi Hayano, Prof. Mamoru Kikumoto, Prof. Koichi Maekawa and Associate Prof. Dr. Chikako Fujiyama for their constructive criticism, suggestions and valuable guidance. Their precious comments and recommendations helped a lot for the improvement of my thesis.

I acknowledge the financial support provided by Japanese Government (MEXT) Scholarship Program in collaboration with Japan International Cooperation Agency (JICA) to pursue my Doctoral degree at Yokohama National University (YNU), Japan. I have to express my special thanks to the Punjab Irrigation department, Pakistan for their cooperation and continuous support throughout the educational period.

Appreciation is also extended to all students and my colleagues who helped me several times during my study period. I am highly obliged to Mr. Zhenqing Liu and Mr. Changjian Liu for performing experiments in the laboratory with me. I wholeheartedly appreciate Dr. Saddy Ahmed, Dr. Muhammad Ali Hafeez, Usman Ali, Fang Xu, Nguyen Trong Nghia and Min Koan Kim for their continuous guidance and support during my research. Special Thanks to all my fellow members for their support during my stay at YNU, Japan.

Above all, I wholeheartedly express my appreciations to my parents, my brother, sisters, my wife and all other family members for their firm love, sacrifices, endeavors and moral support. I owe to my friends for their help and continuous spiritual support to accomplish this study. Gratitude is also extended to many individuals and well-wishers who make my stay at YNU memorable.

SAQIB ASHRAF

ABSTRACT

One of the critical problems faced in the geotechnical engineering field is the presence of expansive soils in the geological strata. Expansive soils are susceptible to volumetric changes upon contact with water. These highly plastic soils depict the possibility of expansion in presence of water and consequent shrinkage upon drying. Such alteration in the soil strata additionally causes changes in the strength of soil media around underground structures. This unique behavior of soils poses serious threats to the stability and long-lasting security of underground structures especially tunnels.

The objective of this this study was to consider compacted samples of highly expansive bentonite mixed with Toyoura sand in fixed weight ratios as possible geological formations around the existing underground tunnel structures. The cyclic loading and unloading were carried out to better comprehend the shrink-swell behavior. The swelling pressure of the expansive soils is critical in design and long-term stability assessments of the tunnels. The mechanical behavior of expansive soil and their disparity upon saturation were studied through free swell tests performed on lab prepared samples. The strength parameters of expansive soil samples were separately studied through unconfined compression tests. Selected samples were further utilized in model tests performed on a tunnel model reduced down to a scale of 1:100. Expansive soil layers were placed at different sections of the tunnel to comprehend the time-dependent impacts of expansive soils on stability of tunnel structure. The surrounding ground stiffness was varied to evaluate the impacts of expansive soils on tunnels with varying surrounding ground with respect to time. The movement of the surrounding ground upon saturation of expansive soils was further magnified by performing image analysis on the tunnel model.

Significant swelling of the soil samples upon saturation projected substantial swelling pressures with rise in expansive content, bentonite, in the sample soil mixture. The unconfined compression strength of the expanded samples reduced as compared to the un-expanded samples. Model tests projected high pressures on different sections of the tunnel with time due to expansion of the soil around it. Surrounding ground stiffness played an important role in the application of expansive pressure on tunnel itself. As the surrounding ground stiffness increased, more swelling pressure was experienced by the tunnel structure. A part of the swelling pressure was absorbed by the surrounding ground owing to its stiffness.

The image analysis projected the surrounding ground movement upon saturation of the expansive soils with time. The surrounding ground moved in correspondence with the location of the expansive soil. The stiffness of the surrounding ground reflected upon the magnitude of the displacement and corresponding strains in the surrounding ground. The magnitude of swelling pressure and corresponding surrounding ground movements exhibited through model tests performed in laboratory on a reduced scale model aided in comprehension of impacts of expansive soils on existing underground structures with respect to time. Such volume and strength changes in the geological repositories around underground structures can amplify the possibilities of long-term stability issues or even failure of the tunnel structures. Therefore, quantification and time-dependent stress-change behavior of underground structures and corresponding alterations in the surrounding ground is inevitable to carve-out mitigation strategies.

TABLE OF CONTENTS

LIST OF FIGURES

LIST OF TABLES

CHAPTER 1 INTRODUCTION

Expansive soils often present a distinctive challenge in the field of geotechnical engineering. As in tunnelling, they may cause serious excavation obstacles during construction and remain a threat to the long-term security of the tunnel structures thereafter during the service life of the tunnel. Presence of expansive strata in the geological repositories has been widely reported in literature and a number of cases have been explored where geological strata with swelling zones have caused tunnel failures altogether. A considerable damage involving additional expenses of construction and delayed projects have also been testified. Swelling risks have driven in-service underground facilities to shut down thereby failing to accomplish their intended functions like road connectivity, water distribution and hydroelectric power generation tunnels etc.

Another stimulating feature of expansive soil formations is the difficulty to distinguish their occurrence in the strata which makes this field highly interrogative and interest worthy. Similarly, the discontinuities in the rock mass in the surrounding ground of construction, position of faults or joints and weak zones etc. add up to the swelling pressure on tunnels thereby exaggerating the problems assisting the tunnel failures. The swelling contents are primarily a part of rock mass in certain geological repositories throughout the world. The underground construction carried out in past is now facing additional pressures from swelling of such clay minerals which were not taken into consideration during design and construction phases of such projects. In addition, the high-pressure applying ability of such minerals upon water interaction was undervalued.

1.1 RESEARCH BACKGROUND

Expansive soils, also referred to as active soils, are the soils possessing the capability to swell upon water interaction and shrink upon drying. This feature makes them fractured unsaturated clays with high possibility of over consolidation history (Bei-xiao Shi, Sheng-shui Chen, 2014). The development projects in certain areas prone to presence of expansive minerals are delicately executed. As the possibility of such repositories arise, the cost of stabilization of expansive soils come into play consequently, affecting the project's feasibility. In a number of studies, the projects are all together rejected due to expansive soils in areas (Selmer-Olsen et al., 1989). Expansive soils are not only a hazard for design and construction periods, in fact they remain a source of continuous problems even during the service periods of the tunnels. As soon as such soils come in contact with water, the volume change puts additional pressure on the structure built around them (Tiwari and Satyam, 2021a). The mechanical behaviour of expansive soils is mainly adjudicated by the moisture content variation yet, it is also influenced by the parent rock minerals, overburden pressures, density and hydraulic field situations etc. (Estabragh et al., 2013). As these soils pose a potential hazard to the structures, several studies have been conducted to improve their properties before construction is carried out (Al-Rawas et al., 2005; Soltani et al., 2019, 2017; Zaini et al., 2021).

As the world progresses towards rapid development projects, the utilization of underground space for connectivity has speedily been expanding in the top urban centres of the world. Tunnels are imperative structures built in modern world for carrying out essential services like water conveyance, mass transit transportation, laying pathways in hilly terrains and hydropower projects etc. Being such an important facet of the society, these structures are given particular importance during design, construction, and service periods (Panji et al., 2016). The performance of the tunnels is majorly

dependent upon the characteristics of the rock mass present around them. These characteristics involve the chemical composition, in-situ stresses and quality of the surrounding media (Wang et al., 2019). The tunnel structure is as stable as the surrounding ground media. Subsequently, the failure in the structural integrity of the tunnels is induced by the disjointedness, fault lines, strength reduction and chemical composition of the rock strata (Abdellah et al., 2018; Stille and Palmström, 2008).

Figure 1-1 Invert heave damage caused by swelling of expansive strata under the tunnel (Butscher et al., 2011)

The deteriorations of the tunnel structures are a time-dependent process. Long after the construction period, changes in the stress state conditions, overburden fluctuations, surrounding ground deteriorations, and most importantly the variation in the moisture content either by seepage or by groundwater fluctuations can initiate these damages (Selen et al., 2021). The stability of tunnels is further threatened by the presence of expansive soils around them. A number of tunnel structures have shown structural deteriorations like uplifting of the floor heave or lining weakening including spalling and cracks (Selmer-Olsen et al., 1989). These irregularities are caused by different processes like time dependent alterations in the rock strata, swelling of expansive minerals in the rock media, slaking, and dilation etc. Recently, presence of expansive minerals around tunnels have raised serious concerns for the tunnel stabilities (Seki et al., 2008; Wang et al., 2019; Y. Wang et al., 2021) as such shown in Figure 1-1. Such cases justify special attention towards structural integrity of tunnels due to expansive soils presence and consequent changes in the surrounding rocks to estimate the additional pressure on tunnel linings.

1.2 RATIONALE AND PROBLEM STATEMENT

The role of rock engineering particularly tunnelling has gained wide attention to utilize underground spaces in urban areas. The initial feasibility studies are carried out to adjudicate the project and consequent response of the underground strata to the construction of a tunnel for a specified purpose. The initial emphasis at this stage of designing is typically concentrated on material properties of the surrounding ground which is assessed based on brief laboratory testing to illustrate the influences of excavation and supporting capability of the strata etc. More emphasizes is laid on the static response of tunnel by applying traditional methodologies and design procedures during the design and construction stage of the projects. The initial design and construction may lead to satisfactory outcomes however, the real problems may arise in the aspect of time as most conventionally tunnels are designed for 100 years of life span. The time-dependant complications are often related to unique mechanisms reliant upon the type of surrounding rock media and are generally not considered vital

in the initial phases of design and construction. Complex phenomenon like stress variations, water table fluctuations and creep etc. occur in the longer run during the service life of the tunnels. Several studies have been carried out to numerically simulate such processes however in many field projects, probable incorporation or, in worst case scenario, ignoring these factors may lead towards misjudgement of the supporting systems applied at the construction phase of the tunnels. These problems can magnify even during construction thereby impacting the overall cost of the projects and even cancellation foreseeing the safety issues later.

One of these time-dependent processes can be the swelling of expansive rock mineral upon water interaction. Many tunnel failure cases reported in literature are attributed to expansion of surrounding ground of the tunnels. The unique ability of the expansive minerals in the strata to expand upon moisture interaction and shrink upon drying makes the recognition more complicated to comprehend. The process initiates and causes cracks in the tunnel linings leading to slow rupturing and consequent strength reduction of the structure followed by ultimate yielding or even complete service failure. This mechanism may not be associated with foreseen stress variations and creep behaviours.

Time-dependent variations in stresses due to expansive soils and consequent stresses in the surrounding ground are of utmost importance for existing in-service tunnels. Consequently, it is imperative to estimate the long-term impacts of the expansive soils on stability of tunnels and consequent changes in the surrounding rock media through laboratory investigations. This can lead to additional safety measures taken during construction and applied to real field situations to ensure long-term stability of mountainous tunnels constructed in expansive geological repositories.

Significant progress has been made in the field of rock mechanics and tunnelling taking time-dependent deteriorations and related consequences into account over the past several years yet, it is imperative to cover the gap between numerical models and analytical approaches through model experimentations. This will help strengthen the engineering tools that are utilized to understand the time-dependent comportment. It is important to clarify this mechanism to excel and have a sound practical engineering tool backed by theoretical knowledge in the said field.

1.3 AIMS AND OBJECTIVES OF THE RESEARCH

This research is an attempt to investigate the time-dependent behaviour of expansive soils by addressing their expansion and strength mechanisms and emphasising their influences on tunnel structures for technical and practical applications in the field. Laboratory model tests were conducted to examine the time-dependent variations in swelling pressures and their repercussions on the surrounding ground in this regard. The distinctive target of this study is to encourage a diverse perspective of analysing and forecasting the time-dependent performance of the swelling rocks with its application on mountainous tunnels and the accompanying underground environment. The study is founded on current state of the art knowledge regarding impacts of expansive soils on tunnel structures and strengthens it by familiarity achieved through the model tests conducted in the laboratory on a reduced-scale tunnel model. The mechanical behavior of the expansive soils and consequent pressure increments on the underground tunnel structures and the surrounding ground movements particularly in perspective of time provides an insight to the field engineers and

researchers in examination and estimation of the long-term behavior of underground mountainous tunnels to the presence of expansive rocks in the geological repositories.

This research is an independent effort for assessment of the time-dependent impacts of the expansive soils on long-term stability of mountainous tunnels through model tests. Initially, the mechanical behaviour of lab-prepared expansive soil samples is evaluated, and selected samples are utilized in a small-scaled tunnel model. The impacts are studied by varying the location of expansive soil around the tunnel. The role of surrounding ground is studied by variation of surrounding ground stiffness and conducting model tests. The strain in the surrounding ground is estimated by image analysis. The core objectives are enlisted below:

1- Assessment of the time-dependant variation in the mechanical properties of the lab-prepared expansive soils samples upon saturation

2- Analysing the time-dependent stress redistribution on the tunnel lining for a shallow overburden tunnel with expansive soil placed at different locations of the tunnel and with variation in the surrounding ground stiffness through laboratory experimentation under static and saturated conditions.

3- Evaluating the displacements and strains in the vicinity of the tunnel and surrounding ground owing to the expansion of the expansive soils in the geological strata through image analysis.

1.4 LAYOUT OF THE THESIS

This dissertation has been written in partial fulfilment of the requirements for the degree of Doctor of Engineering in geotechnical engineering at Yokohama National University. The thesis is divided into nine chapters. All the cited references in the thesis are presented at the end of the document.

CHAPTER 1: INTRODUCTION

Summarizes the topic in general, followed by the research background. The problem statement is formed following the rationale of the study. The purpose and objectives of the study are enlisted.

CHAPTER 2: LITERATURE REVIEW

A comprehensive assessment of the theoretical, numerical and practical background in the field of expansive soils and their relationship with underground structures has been carried out. A few case studies in relation to model tests performed in the subject field have been covered. A view of overall literature and knowledge pertaining to the problem available has been presented followed by the summary.

CHAPTER 3: EXPANSION AND STRENGTH CHARACTERISTICS OF EXPANSIVE SOILS

The outline of laboratory tests performed on expansive soils samples including cyclic loading and unloading tests, free swell tests and unconfined compression tests are explained. The explanation is followed by the results and discussion on different strength and expansion characteristics of expansive soils.

CHAPTER 4: OUTLINE OF THE MODEL TESTS

The outline of the model tests, their procedure, conditions and different scenarios are explained.

CHAPTER 5: RESPONSE OF TUNNEL LINING TO EXPANSIVE SOILS

This chapter included the results obtained from model tests showing the time-dependent impacts of expansive soils on tunnels. The comparison is made between tests performed for cases with no expansive soils and the cases including expansive soils. The time-dependent impacts are further elaborated by time-dependent changes in pressure due to expansive soils on tunnel structure.

CHAPTER 6: IMPACTS OF LOCATION OF EXPANSIVE SOILS ON TUNNELS

This chapter explains the impacts of location of expansive soils in geological repositories on underground structures. The model tests were performed by varying the location of expansive soils and consequent impacts on different sections of tunnel are explained.

CHAPTER 7: IMPACTS OF SURROUNDING GROUND STIFFNESS AND EXPANSIVE SOILS ON TUNNELS

In this chapter, the stiffness of surrounding ground has been varied while keep the expansive soil under the tunnel. The impact of surrounding ground stiffness along with expansive soils on tunnels is explained in context of time.

CHAPTER 8 TIME-DEPENDENT IMPACTS OF EXPANSIVE SOIL AT A DISTANCE FROM TUNNEL INVERT

In this chapter, the expansive soil was placed at a distance from the invert of the tunnel section under the tunnel. The impact of expansive soils on tunnels is explained in context of time. The surrounding ground movements are explained in context of formation of a trapdoor.

CHAPTER 9: CONCLUSIONS AND RECOMMENDATIONS

This chapter summarizes the outcomes of the research and concludes the results based on model tests and ground movements in expansive soils. overall accomplishments, findings, and analysis of the research are reviewed. Lastly, the achieved advantages and the development of the current study for future research have been recommended.

CHAPTER 2 LITERATURE REVIEW

2.1 INTRODUCTION

Tunnels have become imperative structures in modern day engineering fields and are constructed to accomplish several requirements like transportation, irrigation and hydroelectric power stations. They are now considered an essential infrastructure component in urban centres (Panji et al., 2016). The performance of the tunnels during their entire service life is of chief importance. The serviceability of the underground mountainous tunnels is majorly dependent upon the characteristics of the rock mass present around them. These characteristics include strength, in-situ stresses, chemical composition and quality of the surrounding ground etc. The long-term stability of the tunnels is dependent upon stability of the rock mass present around it. Consequently, the failure of the tunnel is influenced by the behaviour of the disjointedness like shear plains, joints and inappropriate chemical composition of the rock mass present around them (Abdellah et al., 2018; Stille and Palmström, 2008). World is progressing towards rapid infrastructure development and countries are undergoing tremendous number of civil structures including dams, highways and tunnels etc. to achieve different aspects of developed life standards. However, presence of expansive clays underneath such structures has many times been overlooked. Consequently, these soils upon interaction with moisture reveal their ability of swelling and shrinkage thereby causing structures to damage or in worst case scenario, complete demolition to avoid any catastrophic events. It is reported that if the percentage expansion of a soil is equal or less than 10%, it is considered as safe expansion (Jones & Jefferson, 2012).

2.2 EXPANSIVE SOILS

Expansive soils show significant volumetric changes upon contact with water. The volume of these highly plastic soils increases in presence of water causing expansion and shrinkage upon drying. These soils can be found in arid or semi-arid climatic conditions however, if found in humid conditions they can be a serious threat to any construction. The behaviour of the swelling soils mainly depends upon moisture intrusion along with other factors like particle size distribution. Sometimes the expansion is related to the chemically induced changes to the soil which are expansive in nature. This behaviour can cause serious problems for the structures founded on them (*Nature of expansive soils*, 1938). The volume of these soils as represented in Figure 2-1 can go up to 20% upon expansion (Estabragh et al., 2013).

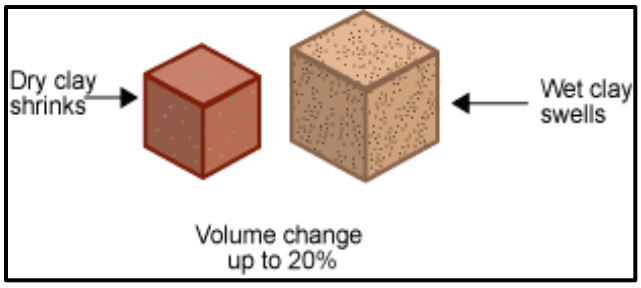

Figure 2-1 Volume change in expansive soils upon expansion and shrinkage (Estabragh et al, 2015)

Geotechnical engineering involves a serious challenge if expansive soils are faced during a development project. The stabilization of expansive soils involves huge costs that is why either the road and tunnel projects are rejected initially, or other alternatives are considered. The swelling characteristics of these soil pose another threat even long after construction. These soils are unsaturated fractured soils having strong shrink-swell potential along with over consolidation assets (Shi & Chen 2014). The behaviour of expansive soils is primarily governed by the amount of expansive clay minerals and availability of moisture around them. Their characteristics however, are also affected by dry density, overburden pressures, parent type of the expansive soil, hydraulic fields and surrounding non expansive rocks/soils etc. (Estabragh et al, 2013). Several researchers have studied the relationship of volumetric changes in expansive soils upon water interaction and consequent changes in their mechanical or structural properties based on both in-situ natural state and lab prepared samples (Gens and Alonso, 1992; Simms and Yanful, 2002; Zhang et al., 2010). The comprehension of shrink-swell mechanisms are also broadly discussed by carrying out wetting and drying cycles tests (Alonso et al., 1999; Stoltz et al., 2012).

Considering expansive soil, a potential hazard to any construction carried out around them, several studies have concentrated on their treatment prior to construction. Since water interaction is the key component in the process, researchers have introduced potential techniques to enhance the properties of these soils to overcome damages associated with huge intensifying volumes and consequent strength reduction. The treatment is broadly classified as chemical and Mechanical types (Soltani et al., 2017). Treatment of these soils with lime prior to construction on / around them is one of the best techniques as it supresses the potential expansion as well as keep the vulnerable soils intact even after exposure to water. It is also concluded that treatment of these soils can significantly reduce the swelling potential exposed to moisture variations (Al-Rawas et al., 2005; Jan and Walker, 1963).

Apart from volumetric expansion, expansive soils can depict another problem of consequent strength reduction of the soil mass. The mechanical strength of expansive soils depends upon their macrostructure which is composed of shape, geometry and interaction force in between the soil grains. The effective and shear stress is usually passed on by the contact points of the soil grains (Xu and Sun, 2001). The strength behaviour of unsaturated soils has also been widely studied. Several methods have also been suggested to predict the strength of unsaturated soils using shear strength and soil-water characteristics curve (D.G. Fredlund, 1994; Miao et al., 2002).

A number of researchers have worked on the locality of expansive soils as the expansive soils are widely distributed all over the world. Expansive minerals in underground strata are of serious concerns hence many studies have been carried out to explore their damaging potential in different countries like Japan, China, United States, Iraq and Pakistan etc. (Daraei et al., 2018; Shi et al., 2002; Takagi, 1994; Zamin et al., 2021) and causes of expansion, treatments and the damages associated with construction in presence of them (Dennis, 1994; Faezehossadat and Jeff, 2016; Osman, 2018).

Experimentation on bentonite as a mixture with sand has also been widely explored to comprehend the mechanical behaviour of expansive soils upon saturation and water interaction (Cui et al., 2015; Fattah and Al-Lami, 2016; Htut et al., 2019; Nelson, 2015; Pimentel, 2015; Pruška and Šedivý, 2015; Zeng et al., 2020; Zhang et al., 2010). Similarly, the comprehension of micro-structural formations of expansive soil to investigate the expansion mechanisms have been studied (Beloborodov et al., 2017; Tiwari et al., 2020). The mechanical behavior and shrink-swell mechanisms of unsaturated expansive soils have also been explored based on numerical modelling

and analytical methods (Bei-xiao Shi, Sheng-shui Chen, 2014; Ofoegbu et al., 2017; Wang and Wei, 2015). Several studies have concentrated on improvement of expansive soils to overcome the associated damages due to expansion by addition of various strengthening agents in the soil prior to any construction (Al-Rawas et al., 2005; Stoltz et al., 2012).

2.2.1 Composition

Expansive soils are mainly composed of swelling minerals like marls, silty mudstones, bentonite, argillaceous mudstones and conglomerates etc. Presence of smectite clay minerals adds up to the swelling potential of soils in tertiary rocks or quaternary soils. Moisture excess in atmosphere aids in volumetric expansion of expensive minerals in soil and cause heaving problems. On the other hand, if the climate is arid and rate of evaporation is higher, the ground tends to lose moisture and there is always a moisture deficiency which causes shrinkage of soil and cracks are developed. As the swelling and shrinkage processes are not entirely reversible processes (Holtz & Kovacs, 1981), shrinkage might end up with cracks in the soil surface which never come back to their original condition. These cracks may aid the moisture penetration in the deeper layers of soil during humid and/or rainy season. Also, if some more expansive minerals are carried by moisture to deeper layers, they cannot be removed, and soil might turn up more expansive than before. On the contrary if non swelling sediments get inside cracks, the complexion of the soil mass changes. The deformations characteristics of swelling soils suggests that the deformations are considerably larger as compared to the deformation obtained from classic elastic and plastic theories (Jones & Jefferson, 2012). The expansion mechanisms for expansive soils in relation to the water absorbed by the interlayers of expansive minerals for compacted samples has been explained by Komine and Ogata (1996) as represented in Figure 2-2.

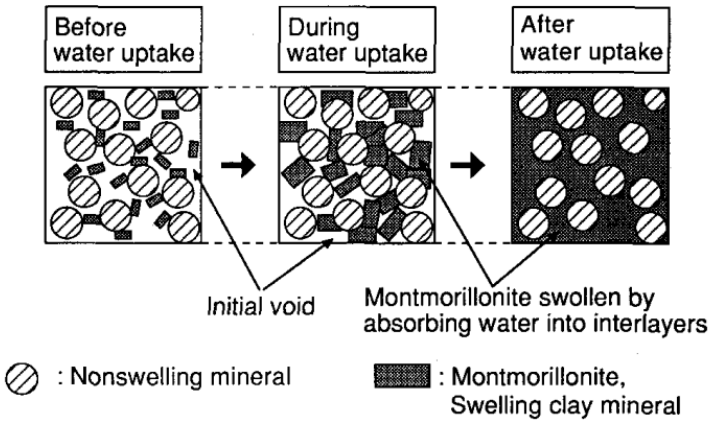

Figure 2-2 Swelling pressure mechanism of compacted bentonite (Komine and Ogata 1996)

2.2.2 Expansion characteristics of expansive soils

The expansion characteristics of expansive soils are thoroughly studied worldwide based on laboratory experimentation, analytical solutions and numerical models. As frequently reported in literature, the swelling mechanisms of expansive soils is strictly triggered by changes in soil moisture conditions. The swelling pressure resulted as the soils expand is adverse for civil structures.

It is inevitable to comprehend the expansive soil behaviour upon saturation for engineering projects, civil infrastructure and geotechnical engineering sectors. This assessment involves understanding the changes in the moisture conditions of the soil followed by the combination of wetting and loading simultaneously. As the process goes on, the unloading after water contact plays its part. Swelling pressure is the pressure that prevents any further swelling of the specimen. This method of determining the swell pressure is recognized as a standard method (ASTM, 2013) and extensively applied for expansive soils and their swelling pressure related studies (Y. J. Cui et al., 2013; El Bahlouli & Bahi, 2014; Soltani et al., 2019; Sridharan et al., 1991; Vanapalli et al., 1998).

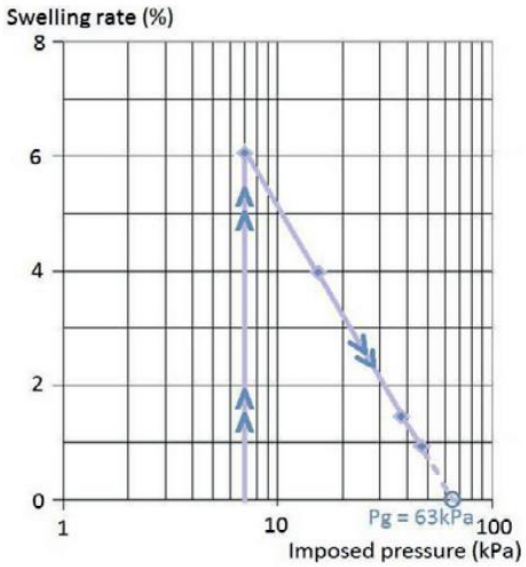

Figure 2-3 Determination of swelling pressure (El Bahlouli and Bahi, 2014)

El Bahlouli and Bahi, (2014) studied the swelling pressures of the green clay in Morocco and its soil-moisture situation. The assessment was carried out by placing the sample into the oedometer. The sample was loaded initially inducing the settlement and followed by soaking with water. The sample was allowed to expand unidirectionally until no more swelling was recorded. The loading was carried out to compress the sample back to its original state to estimate the pressure exerted by the soil sample upon saturation. Figure 2-3 represents the process graphically.

Similarly, Komine and Ogata, (2004) conducted a number of tests to select the appropriate bentonite mixture to be used as buffer and backfill material for high nuclear waste repositories. The swelling characteristics of different kinds of bentonite were evaluated in detail and a new prediction method was proposed in their selection.

The method involved a series of equations previously presented for estimation of the swelling volumetric strains of montmorillonite and its relationship with pore water pressure and specific surface of bentonite. The study was backed by experimental results for five kinds of bentonites found in United States and Japan. The swelling was determined by two tests namely the swelling pressure test and the axial swelling deformation test with detailed procedure explained by the authors in their earlier studies.

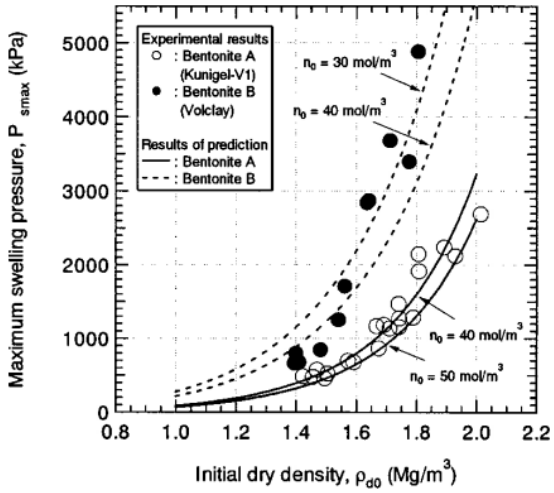

Figure 2-4 Determination of swelling pressure (Komine and Ogata, 2004)

Figure 2-4 represents the experimental and predicted results for swelling pressure with variation in initial dry density of the specimen. The results showed close relationship for bentonite having sodium as the main exchangeable ion however, the swelling behaviour of the bentonite with calcium ion was not clarified hence the sodium type bentonite was advised to be used as backfill material for active nuclear waste disposal site.

Ashayeri and Yasrebi, (2009) studied the swelling pressure of unsaturated compacted clays through neural networks modeling countered by lab experimentation. The swelling pressure and compaction state of expansive soils were studied and compared with the limiting collapse pressure. They compared the results of experiments with artificial neural networks to predict the free swell potential and consequent swelling pressure of expansive soils based on compaction state and their important properties. The lab experiments for free swell and constant volume pressures were performed as per ASTM standard D4546 on clays which depended on compaction state and degree of saturation. The neural networks responded well with mapping functions for evaluating the impaction of compaction and composition on the swelling potential of expansive soils.

Similarly, Kyokawa et al., (2020) studied the mechanical, electrical and chemical behaviour of expansive soils in detail based on their mineral composition. As this behaviour significantly impact their behavior at macro level. A constitutive model was developed to describe clay minerals and soil structure. Swelling pressure and deformational analysis were simulated by the model. The osmotic and mechanical swelling of expansive soils were verified and explained by saturated soil mechanics. The typical elasto-plastic manner and shear parameters of expansive soils were explored. Several other researchers have utilized constitutive modelling approach to explain the behaviour of expansive soils in connection to different structures and time-dependent variations in mechanical properties of expansive soils (Adem and Vanapalli, 2013; Alonso, E. E., Gens, A. & Josa, 1990; Gens et al., 2006; Nujid and Taha, 2016; Ofoegbu et al., 2017; Pedroso and Farias, 2011; Qi and Vanapalli, 2016; Yin and Tong, 2011).

Another interested phenomenon associated with clays undergoing saturation is loading and unloading loops. The soil compression curves and the effect of viscosity of soil explains this

mechanism. The soils with higher fines constituents like clays and silts show larger loops owing to their higher viscosity as compared to sandy soils being less viscous (Cui et al., 2013). The compression tests performed on sandy soils usually represents a negligible hysteresis loss with very small loops or even none. These loops become much more significant for clayey soils like bentonite or mixture of bentonite with sand etc. (Tong and Jian-Hua, 2011). In compressibility of soil these loops are ignored however, they may be of prime importance in dictating the volume change behaviour of partially saturated clays undergoing loading and unloading cycles. Comprehension of this phenomenon for expansive soils can be particularly complex. Limited studies have explored the loading/unloading cyclic loops for expansive soils. Cui et al., (2013) investigated this behaviour and performed several oedometer tests along with loading and unloading cycles on stiff clays existing naturally and proposed a verified mechanism to comprehend the swelling characteristics of expansive soils. A similar attempt has been made in this research and is explained in the results section later. Figure 2-5 (a) represents the loading and reloading performed on clay while (b) represents the method of swell-consolidation swelling pressure measurement as per the said research.

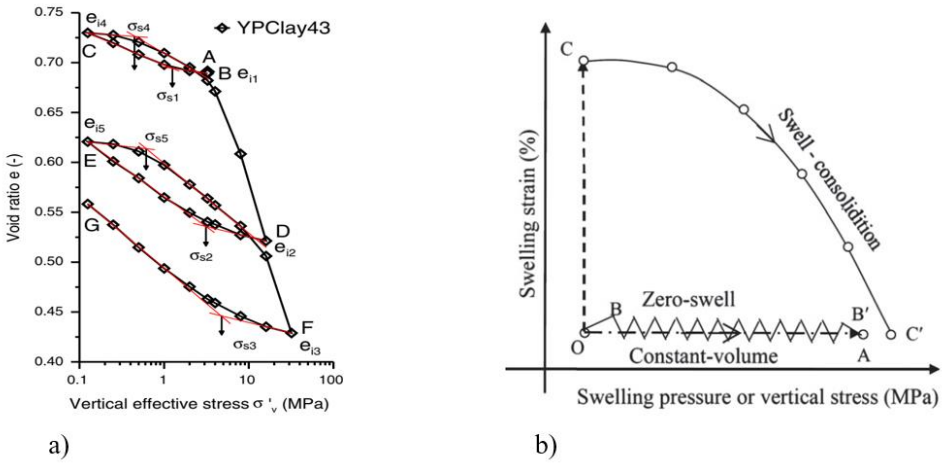

Figure 2-5 Loading and reloading (a) on clay and (b) swelling pressure (Cui et al., 2013)

2.2.3 Strength characteristics of expansive soils

Apart from volumetric expansion, another important component of expansive soil is the strength upon water interaction. The conduct of expansive soils strongly depends on their geometry and particle size distribution. Consequently, the dominant relationship to comprehend the expansive soil behaviour upon saturation are the soil-water characteristics curves. Many empirical relationships are proposed in literature (Pham and Fredlund, 2008). The shear strength of soils is given by following equation as per Fredlund et al., (1978):

$$\tau_f = c' + (\sigma - u_a)\tan\phi' + (u_a - u_w)\tan\phi^b \qquad \text{Eq. 2-1}$$

Where, T_f represents the shear strength of unsaturated soils, c' is cohesion, ϕ' is the angle of internal friction of soil, $(\sigma - u_a)$ effective normal stress, $(u_a - u_w)$ is the soil suction value and ϕ^b is the angle

of shear resistance in relation to suction. In this equation the latest parameter is difficult to determine. Several numerical models have also been presented to determine the strength of expansive soils (Miao et al., 2002). Consequently, Miao et al., (2002) performed an experimental and analytical study on expansive soils in Nanyang, China to evaluate the shear strength and soil-water curve characteristics. Conventional tri-axial compression tests were performed on remoulded samples of the soil samples taken from the field. The strength of expansive soil upon saturation was observed to be reduced as compared to the unsaturated soil samples. Figure 2-6 represents the strength comparison for saturated and unsaturated soil. It was recommended to utilize the model of suction presented in the paper to evaluate the cohesion, suction strength, and predictability of slope failures for expansive soils found in the region.

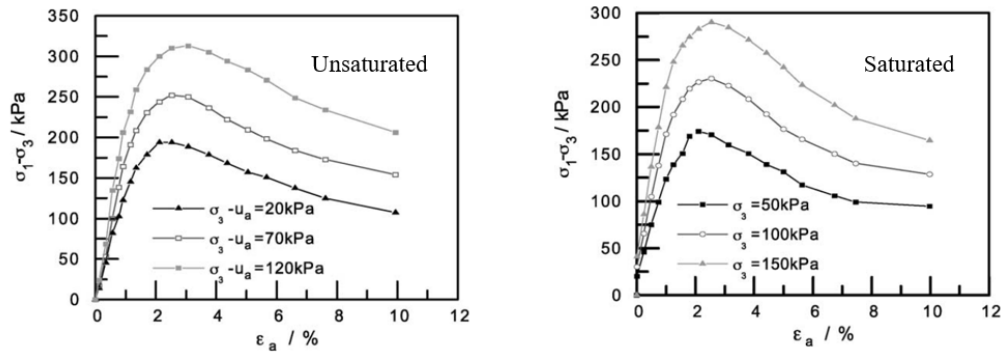

Figure 2-6 Shear strength of unsaturated and saturated soil sample of Nanyang, China (Miao et al., 2002)

Kong and Guo, (2011) studied the influence of density, swelling potential and water content on expansive soils found in Jingmen, China using California Bearing ratio (CBR) values. Empirical relationships were developed comparing these parameters. CBR values were found to have strong dependency on the dry density and water content of the expansive soils upon expansion. Expansive soil's ability to expand and the corresponding swelling potential grade was found to be similar to their compaction curves.

The parametric study was carried out for low swelling grade soil samples and medium swelling grade samples. CBR values were significantly lower for medium swelling grade soil sample as compared to low swelling grade soil. This reduction is further elaborated in Figure 2-7. As the study concentrated on water content, it was found that the water content for which CBR is maximum is slightly higher than the optimum moisture content of the soil. Consequently, it was proposed that water content for subgrade construction of road comprising of the said expansive soil should be kept higher as compared to the optimum moisture content of the soil and the dry density should be reduced in comparison to the maximum dry density. The CBR values and degree of compaction cannot reach the maximum value simultaneously.

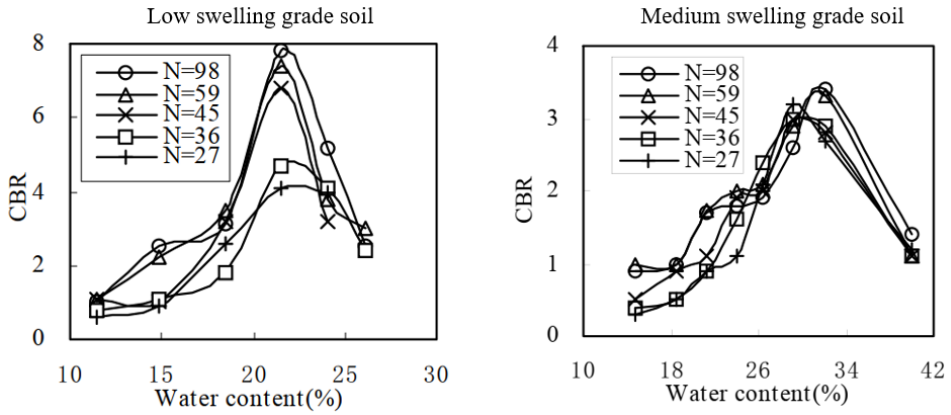

Figure 2-7 CBR and water content relationships for the low and the high swelling grade expansive soils in Jingmen, China (Kong and Guo, 2011)

Xu and Sun, (2001) proposed a fractal model to determine the strength of the expansive soils. The consideration of slope stability in expansive soil strata is important therefore, its accurate determination is vital. The shear strength determination of the expansive soil depends upon the bearing capacity and stability of strata. A micro-pore surface fractal model was proposed, and corresponding shear strength equation was presented. The short comings in the equation No. 2-1 were rectified for better determination of shear strength. The determined shear strength from the model was validated against the shear strength of the expansive soil in Ningxia, China found by conventional tri-axial compression tests. It was stated that the proposed formula has parameters that are all independent of the metric suction presented by the soil during water interaction. Also, the formula is applicable for not only expansive soils but for other unsaturated soils as well. It was concluded that micro-pore distribution of expansive soils is fractal, and they were filled with water ensuring that degree of saturation is sufficient.

Since strength of expansive soils is a concern for structures around them, much research has been carried out to comprehend the strength of expansive soils upon taking measures of improving their strength and involving numerical techniques. Tiwari and Satyam, (2021) controlled the strength and durability of expansive soils by adding pond ash and polypropylene fibres. The lab experimental data is processed by machine learning approach using artificial neural networks predicting the strength of soils accurately. The durability and mechanical strength of the soil was reported to have increased upon fibre additions. Similarly, Tang et al., (2008) reinforced the expansive soils of Xinxiang, China with fibres and experimentally studied their strength mechanisms under water content, fibre content, degree of compaction and grain size distribution. Unconfined compression tests for strength were performed and the failure mode was analysed. A rise in unconfined compression strength (UCS) of soils was observed due to addition of fibres in comparison to the soil itself. The rise in moisture content reduced the strength and the effect of size of sample was comprehended such that larger the size, lesser is the strength. The failure mode of soil also changed from brittle to plastic with no significant shear planes.

The strength of expansive soils upon expansion is critical to evaluate their stability around different structures. In this research, the UCS of soils has been evaluated based on time-dependent variation

of moisture by keeping the samples in a humid-controlled environment. Various degrees of saturations are applied to samples and unconfined compression tests are performed to adjudicate the strength before and after expansion of the soil samples prepared in the laboratory. The sections to come explain the process and results further.

2.3 EXPANSIVE SOILS AND TUNNELS

The time dependent deformations in rock mass strata underground can occur due to shear distortion, volume change or dilation. These distortions lead towards late yielding of rock mass and causing it to damage internally. This process can cause absolute failure of rock around underground structures. It is rather complex to estimate the magnitude of these deformation with respect to time. The construction of tunnels in soft rocks always presents challenges not only during construction but also in long-term stability consideration and have become centre of attention now-a-days. The swelling of expansive rock minerals causes additional pressures on invert, deteriorates the lining and in worst cases, causes the uplift of whole tunnel sections. The major tunnel projects involving expansive soils face major difficulties in construction as it involves huge costs to cater the additional pressures. In addition, the maintenance of tunnels in such repositories becomes expensive (Butscher et al., 2011). The engineering practices to cater such problems involve opposing the additional pressure by introducing reinforced tunnel lining and by provision of rock anchors or resisting the probability of expansive pressure altogether (Anagnostou, 1993). The time-dependent deformations are a combination of many factors including the composition of rock, status of groundwater table or water intrusion in the geology, the magnitude of overburden pressure, humidity or temperature and the stress state of the strata. Consequently, the failure of the tunnel is influenced by the behaviour of the disjointedness like shear plains, joints and inappropriate chemical composition of the rock mass present around them (Abdellah et al., 2018; Selmer-Olsen et al., 1989; Stille and Palmström, 2008).

Long after the tunnel construction has been completed, the overburden fluctuations, surrounding ground deteriorations, changes in the stress state conditions and more importantly the moisture content variations can induce additional pressures on tunnel securities. Tunnels and expansive soils are closely related. The tunnel performance after construction has recently shown problems due to presence of expansive soils. Some aged tunnels have shown heaving phenomenon that includes the uplift of the base floor. Sometimes owing to huge deformations in the process, very expensive counter measures like complete replacement of invert section or instalment of piles deep in the ground under tunnel floor are proposed. The heaving of the invert is strongly stimulated by several factors including but not limited to surrounding ground characteristics, type of clay mineral, process of swelling, slaking, dilation, and time dependency. The presence or fluctuation of groundwater levels and its interaction with soft rock and cyclic loading and unloading features are also common causes of heave phenomenon. Such problems have enlightened the stability issues of in-service tunnels susceptible to presence of expansive soils in the geological formations around them (Seki et al., 2008; Selmer-Olsen et al., 1989).

Swelling is reported to be a complex behaviour involving argillaceous rock characteristics having ability to adsorb water. The volume change is associated with combination of physical and chemical reactions that are aided by water presence and stress retrieval by the passage of time (Bonini et al., 2009).

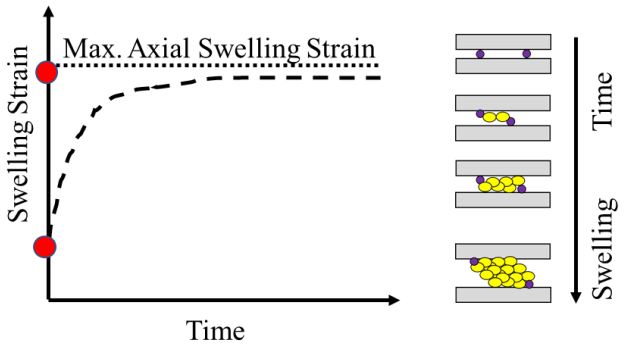

Figure 2-8 Time-dependent swelling and process in clay layers (Bonini et al., 2009)

Also, the swelling may not be associated directly with stress changes on soil and the stress increment may become a cause to cater the swelling altogether. Rock swelling is driven by water adsorption and osmosis of the expansive clay mineral as represented in Figure 2-8. The anhydride dissolves causing macroscopic changes in the soil structures, yet it is a complex process to comprehend as long durations of time are involved.

There is a significant relationship the swelling strain and the initial degree of saturation. It indicates that the higher is the degree of saturation, the smaller the swelling is. It is also true the case of the contrary, which means that the lower is the initial degree of saturation, the biggest the swelling is (Latar et al., 2015).Yin and Tong, (2011) explained the Effects of time and rate on the stress-strain-strength behavior of expansive soils. This behaviour is time or rate dependent. The two main aspects of clayey soils are swelling and creep. The term creep is referred to as the viscous compression of the soil particles under a constant loading condition in oedometer testing while swelling is volumetric expansion and is opposite to creep. These two factors have significant relationship with the deformation and failure characteristics of structures built in geological strata. Another phenomenon of relaxation zone where stress reduces while strain keeps constant was explained. The rate effects include the strain rate and stress-rate effects in which the effective stress increases with the rate. Higher the strain rate, greater is the effective vertical stress.

Since it is difficult to estimate the change in degree of saturation of the expansive soil and consequent alteration in the swelling stress and strains, it was assumed that the degree of saturation of the expansive soil changed with time. Consequently, several studies have reflected the relationship between time and swelling strains, and the strains was divided based on primary and secondary rate of swelling as represented in Figure 2-9. The swelling mechanics may be originated based on the inter-granular voids of a particular sample (Tran et al., 2014). The comparison between the treated swelling clay with lime and untreated one showed that the treated one exhibited faster swelling due to higher intra-particle voids. This was corresponded to Biot's theory of consolidation (Tran et al., 2014).

Nelson, (2015) explained that the initial phase of swelling is the result of an increase in the size of the adsorbed cation as it becomes wet. As the hydration energy of the cations is very high, water that enters the soil contributes to the mechanism of crystalline swelling. Additional water enters the micelles by osmotic forces.

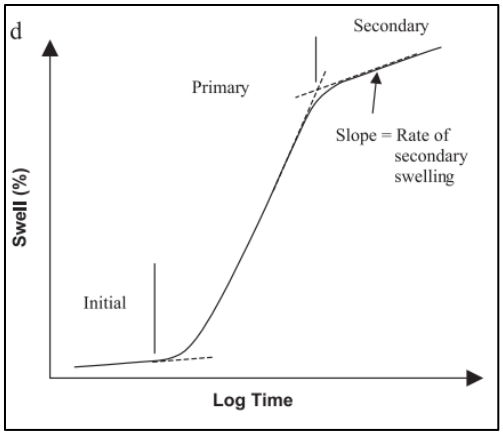

Figure 2-9 Primary and secondary swelling process with time

As swelling progresses over time, there is no distinct change from the crystalline phase to osmotic phase. The osmotic phase comprises both completion of the outer shell of the water of hydration and osmotic flow of water to cations in the micelle. The time for heave to occur will be a function of the particular phase happening and the ability of water to migrate within the soil. The migration takes place as both molecular flows in the crystalline phase and viscous flow in the osmotic phase. These differences in mechanisms will influence the time required for swelling to be completed in an oedometer test.

Okui and Nishimura, (2020) conducted a study to predict tunnel deformation and mechanical behaviour of expansive soils. Following Grob's law of swelling (Figure 2-10), which explains that the deformations due to swelling tend to cease in relation with log of the applied stresses. The swelling strains tend to decrease with increase in the stresses. Volumetric strains can cause faster approach faster final swelling strains. This mechanism accounts for the dependency of swelling strains on rate of penetration of water in soil voids. This rate changes with the permeability and thickness of the expansive soil layer.

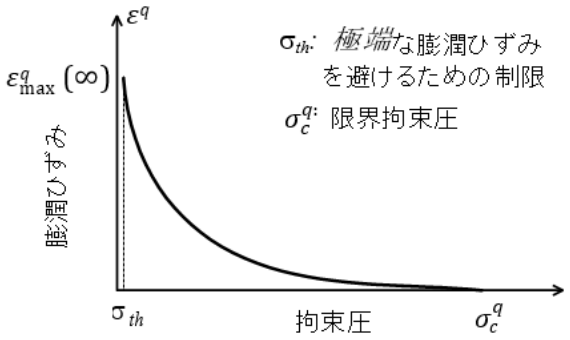

Figure 2-10 Grob's Law of swelling Okui and Nishimura, (2020)

The swell kinetics of the expansive pressure were divided into four states of stability in this study which corresponds to accelerated swelling of soil upon initial contact, a creep (or relaxation) zone where stress remained constant and strain kept on increasing, the re-rise of swelling pressure as the

water interaction with expansive soil entered the osmotic phase followed by steady state where all the swelling has occurred. A number of studies (Al-Yaqoub, Parol, and Znidarcic 2017; Albusoda 2018; Ito and Azam 2010; Latar, Hardiyatmo, and Adi 2015; Sridharan and Gurtug 2004) have represented the primary and secondary phase of swelling. The transformation of this concept from elementary expansive soil studies to model tests for tunnels with expansive soils in their vicinity was carried out in this research.

2.3.1 Tunnel failures in swelling rock zones

Many cases of tunnel failures are reported in literature owing to the insufficient support provided by the surrounding rock media including the expansive rocks. The design of tunnels often skips the high possibility of excessive pressures exerted by the expansive soils upon saturation on them. Underestimation of these swelling pressures during design is one of the key reasons of tunnel failures during their service period. As soon as geological survey of the site presents the possibility of presence of expansive soil minerals, it is essential to device a method that clearly specifies the detection of their occurrence and consequent rock support mechanisms to cater the probability of high pressures on tunnel upon expansion. In this regard, several methods based on laboratory experimentation are proposed to calculate the maximum swelling potential of different expansive soils and these are considered in the design of tunnels before carrying out the construction. Although, some of the tunnels constructed without consideration of excess swelling pressure have shown significant deteriorations and even complete collapses upon swelling pressure increment in the geological repositories around them.

Selmer-Olsen et al., (1989) reported several cases of tunnel collapses where expansive rock minerals were detected during construction but excessive increment of pressure on tunnel due to their expansion was underestimated and there was no sufficient tunnel support provided to cater these additional pressures. An example of Hemsil hydropower plant tunnel related to swelling zones comprising of granites and gneisses is reported where the collapse was seen in the head race tunnel. Steep faults in the rock were observed in the nearby vicinity of tunnel. Although, during construction, the tunnel lining was reinforced by rock support and shotcrete in several sections, however, when tunnel water was removed for inspection after 8 years of construction, a 200 m^3 collapse was seen in the tunnel section where shotcrete reinforcement was provided. Upon further evaluation of the collapse zone, it was found that 2.5m thick zone having veins of expansive material was responsible for the damage. In another example of Tirnnsjoedal hydropower plant (Figure 2-11), the collapse in geology was observed shortly after the excavation was carried out. In this case the expansive soils were not present as material, but they were associated with alteration of adjacent rock of feldspar into montmorillonite which is highly expansive in nature. The tailrace tunnel of the plant passed through granitic zone of gneiss and initially no stability issues were observed. However, the water usage during construction leaked into the strata from small joints and a 30m long collapse was seen within 2 weeks of excavation. This caused a costly rock support process to start immediately, and cast-in-situ concrete lining was provided to avoid further damages. An interesting outcome of this collapse was the conversion of strong looking granite into muddy clay upon water contact.

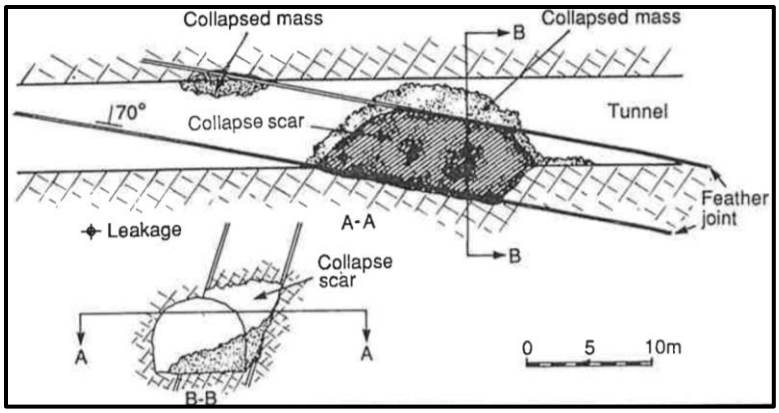

Figure 2-11 Expansive strata causing tunnel failure in Tirnnsjoedal hydropower plant (Selmer-Olsen et al., 1989)

Another tunnel collapse occurred due to swelling and softening of granite rocks with leaking calcite zone on railway in Norway. Two of these zones crossed each other and the water leakage from eroded holes caused the expansion mechanism to trigger 8 years after construction and caused cracks in the lining. A collapse of 30m length happened within two days of observance. The reason explained was the drainage failure at tunnel section which aided the surrounding ground material to swell and caused significant damage. Very expensive and time-consuming mitigation measure were forced to be carried out to repair the tunnel. Similarly, in Rafnes, a tunnel built under sea intersected the expansive zones of 5m thickness. Initially the zones were dry and no serious stability issues were expected however, upon filling the tunnel with water, a few months later when tunnel was inspected, a significant damage in 30m thick reinforced and shotcrete lining was observed at various locations. The tunnel was blocked at four locations causing its failure. The reason reported was the excessive pressure exerted by the surrounding swelling clays in combination with altered rock repositories on tunnel lining upon water interaction.

Liu et al., (2020) conducted a study on Dugong Ling tunnel in China. It was observed during the operation of the tunnel that lining has cracks, the pavement lifting up and overturning of cable trench. These factors finally resulted in closure of the operation. Upon investigation of these phenomenon, the geological composition was found responsible. The softening and expansion of the surrounding rock caused lining to crack. The research program was set by considering several sections of the tunnel and numerical analysis was performed using software FINAL by back analysis method and cracks were analysed. Field geological conditions were replicated in the program. Figure 2-12 represents one of the sectional simulations. The main cause of deterioration was due to the expansion of surrounding rock upon water contact.

Zhang et al., (2016) studied the instability of tunnel in Yun-Gui, China due to humidity variation in the surrounding ground. The humidification process and consequent expansion was simulated by utilizing finite difference software named Flac3D. It was found that a soon as model is moistened, the expansive stress adds on the tunnel haunch and vault. A large bending moment tended to fail the structure while lateral increment of stress caused bias failure. Sufficient reinforcement was recommended to tackle the additional stress due to expansion of surrounding ground.

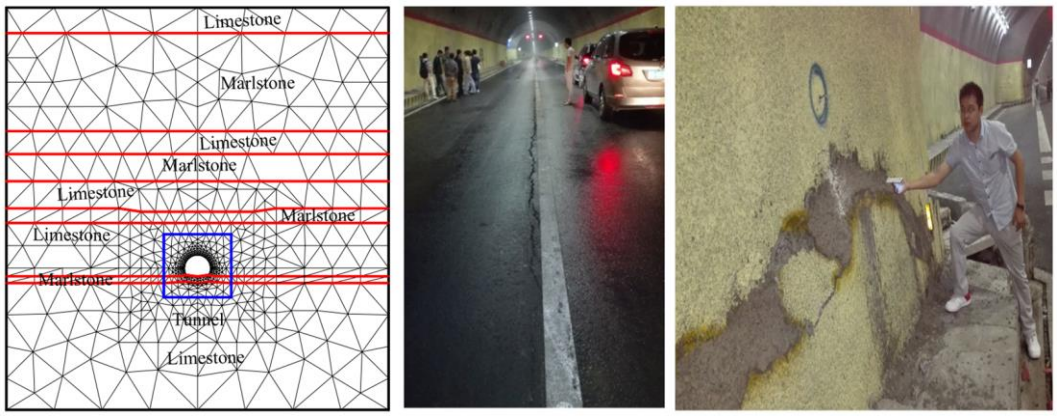

Figure 2-12 Numerical model and lining/pavement cracks in Dugong Ling tunnel due expansive rocks (Liu et al., 2020)

Similarly Barla, (2008) took a case study of Caneva–Stevena tunnel in Italy which collapsed due to expansion of stiff clay around it. The stress paths developed during the excavation were simulated to signify the evidence through numerical analysis and strengthened by laboratory examination for swelling of the surrounding rock by innovative tri-axial compression tests. The results were compared with site observations. Volumetric strains in response to pore water pressure variation were evaluated. Figure 2-13 represents the tunnel collapse at site and simulated failure state.

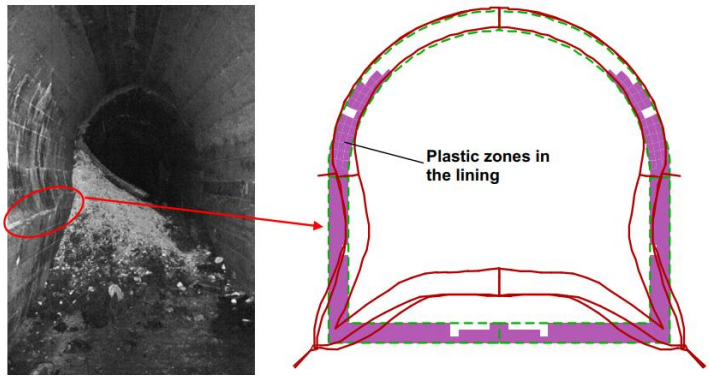

Figure 2-13 Tunnel failure at site and simulated deformed lining (Barla, 2008)

Wanjun et al., (2019) studied the relationship between water content and expansion of red clay expansive soil on tunnel constructed in Qingyang China. The expansive mechanical behaviour and shear strength characteristics of expansive soils were analysed through laboratory experimentation. Water content variation under thermal conditions built in ABAQUS software were comprehended. Figure 2-14 represents the water content around different sections of the tunnel based on field data and pressure distribution nephogram of surrounding rock. They results showed that initially upon rise in water content of surrounding ground, the displacements of invert and foot sections increases while for shoulder, spring line and crown decreases consequently, the factors of safety for different

sections and reserve deformation of tunnel were proposed. It was significantly endorsed that water content variations around the tunnel causes significant deformation followed by additional pressure on tunnel.

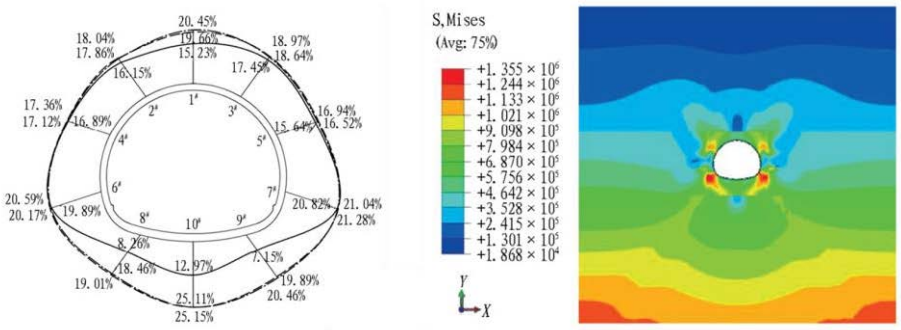

Figure 2-14 Water content around tunnel and pressure distribution of surrounding rock in China (Wanjun et al., 2019)

2.3.2 Numerical simulation for tunnels in swelling rock zones

Butscher et al., (2011) estimated the swelling ability of rocks in tunnelling. The geological conditions and groundwater aquifer systems were studied in reference to tunnelling to better comprehend the swelling mechanisms in surrounding rock. The study was focused on Chienberg tunnel in Switzerland. The tunnel was constructed in four different kinds of hydrogeological zones and two of them contained minerals with high swelling potential. The swelling occurred as the excavation for tunnel was carried out. Meanwhile, the groundwater regime was studied through numerical analysis for comprehension of expansion. The results showed that there was a hydraulic connection between the expansive and non-expansive zone and the weathered rock of expansive zone aided the non-weathered rock to transform from anhydride to gypsum making it swell upon water contact. The role of the excavation damaged zone (EDZ) has also been discussed. Figure 2-15 represents the numerically simulated surrounding ground around the tunnel. The different abbreviations in Figure are the geological zones in the research area.

(Tang and Tang, 2012) proposed a humidity-diffusion based numerical model to simulate the process of swelling of surrounding rock and its impact on tunnel invert exposed to high humidity. The stress redistribution combined with vapor diffusion on tunnel was considered and was found helpful to simulate heave without going into the details of complex chemical changes in the surrounding rock as it is the prime concern of existing tunnels in the field. Figure 2-15 represents the numerical model setup where two points on tunnel were observed for deformation measurements including invert and side wall.

The time-dependent deformations for different confining pressures, elastic modulus, swelling coefficients and humidity with corresponding failure of floor invert of the tunnel by replicating the swelling phenomenon under humid conditions were explained. More deterioration was observed at invert section as compared to wall of the tunnel. The displacement of the floor heave was observed to trigger swiftly in the beginning part of excavation and subsided as the time goes on. The humidity interaction was declared to have significant impact on surrounding rock causing it to degrade quickly with time. Figure 2-17 represents the time-dependent displacement graphs for these mechanisms.

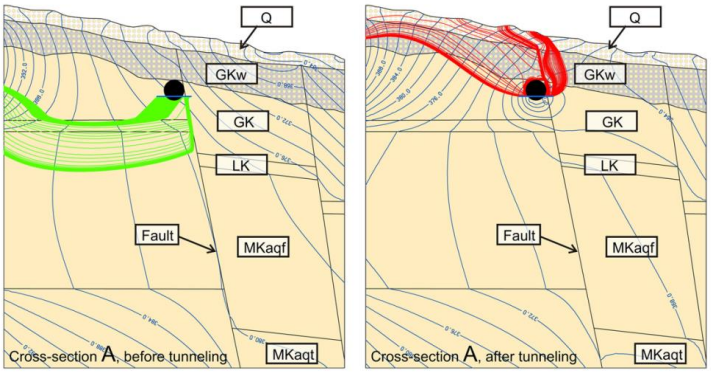

Figure 2-15 Modelled geology and hydraulic conditions for Chienberg tunnel in Switzerland before and after tunnelling (Butscher et al., 2011)

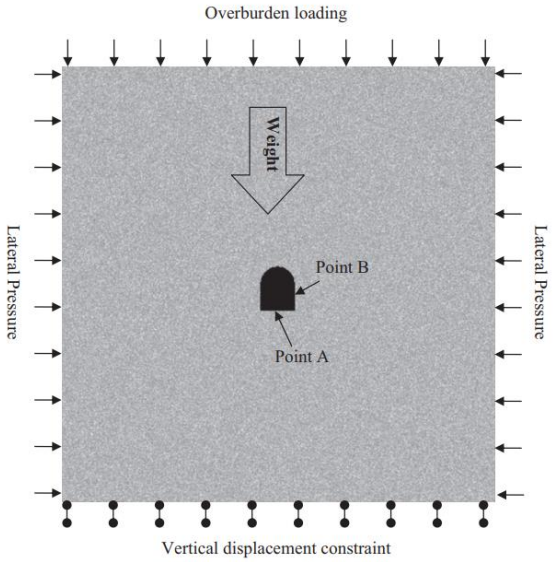

Figure 2-16 Numerical model developed by (Tang and Tang, 2012) for heave in swelling ground

Another such numerical model was presented by Anagnostou, (1993). Alonso et al., (2013) to describe the damage to Lilla tunnel in Spain during construction and during service due to expansion in surrounding rock. The geological condition of the area and field observations of swelling were analysed to clarify that growth of gypsum crystal in the fault zones. It was aided by water circulation in the tunnel vicinity resulting in deteriorations. Consequently, the tunnel cross section was changed to circular from horseshoe and was reinforced with concrete lining to cater the swelling.

Having reinforced the tunnel, the swelling pressure was recorded, and long-term evolution of swelling was studied to compute the resulting stresses. Even with provision of steel reinforcements, high swelling pressures were observed. The progression of displacements with time are shown in Figure 2-18 for Lilla tunnel.

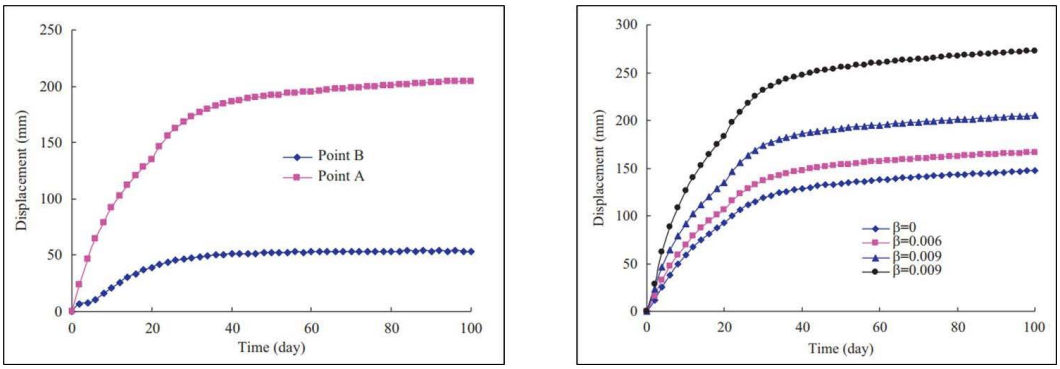

Figure 2-17 Comparison of displacement at invert and wall section of tunnel and time-dependent displacement for different swelling coefficients (Tang and Tang, 2012)

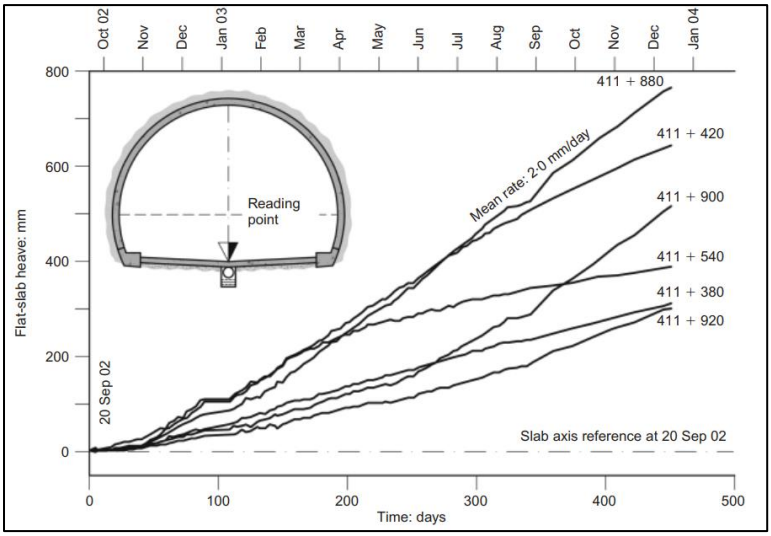

Figure 2-18 Time-dependent floor heave in Lilla Tunnel (Alonso et al., 2013)

(Yu et al., 2020) studied the time-dependent visco-plastic deformation mechanisms around tunnels in swelling surrounding ground using Nishihara model and flow rule mathematically. The time-dependent stress dilation with the process of swelling was explained through Zhang 3D Hoek-Brown criteria for yield and humidity field theory simultaneously. Parametric analysis was carried out based upon the sensitivity of parameters and their consequent impact on the outcomes of the mathematical model. The research concluded that time-dependent deformation is directly proportional to swelling and poison's ratio while inversely proportional to elastic modulus. Unstable conditions of swelling were observed mainly in secondary stage of creep.

(Wittke-Gattermann and Wittke, 2004) proposed a 3D constitutive model for calculations of strains and pressure on tunnel structures constructed in swelling rocks applicable to mudstone as well as anhydrite type rocks. The visco-plastic behavior along with time-dependent strains and corresponding stresses due to anisotropic swelling were described. The mathematical results were

compared to field observations of Freudenstein tunnel in Germany which showed floor heave due to swelling of invert rock and good agreement was found. Consequently, a design of self-sealing for tunnels in swelling strata was proposed.

2.3.3 Physical modelling for tunnel response in swelling rock zones

Mingqing et al., (2019) studied high-speed railway tunnel constructed in expansive soil strata and failure mode and mechanisms involved in floor heave due to expansion of expansive soils were analysed. Finite element analysis and indoor model tests were conducted to comprehend the floor heave on invert arch expansive surrounding rock strata. Model tests revealed that expansive pressure would act simultaneously on tunnel structure and surrounding ground causing it to displace and cause cracks in tunnel lining. The invert arch failure was comprehended by using hydro-press machine to induce hydraulic pressure replicating the swelling pressure and pressure sensors installed on tunnel were reporting the pressure increment. Figure 2-19 represents the sensor locations and model test assembly for this research. It was recommended that W-shaped uplift failure mode should be catered significantly. The slow increment of pressure at the beginning followed by rapid rise suggests the initial settlement of surrounding ground particles followed by pressure being taken by the soil directly displacing it later.

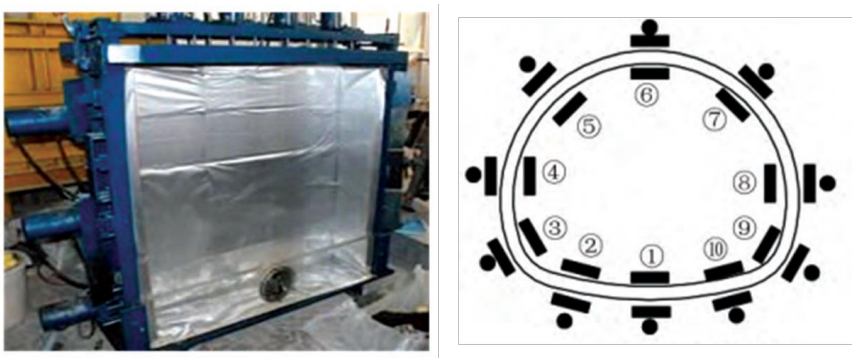

Figure 2-19 Model test assembly and location of pressure sensors installed on tunnel model (Mingqing et al., 2019)

Seki et al., (2008) conducted model tests to examine the heaving phenomenon in tunnels. The model experiment apparatus is represented in Figure 2-20. Different loading patterns were used to apply pressure to the tunnel invert and other different sections. The loading conditions were vertical, horizontal and a combination of these. The stress and displacement curves were observed for bilinear characteristics of tunnel sections. The curve gradients were sharp in the beginning and subsided at certain stress values referred to as turning points. A trial material was prepared, and unconfined compression strength of the material was found by unconfined compressive tests. The results represented that the turning point usually occurred in the elastic region on curves with displacement of the base course. Upon loading in the model test, symmetrical heave displacement was seen for symmetrical loading patterns and consequent base course displacement on top replicating the road. The heaving was replicated by numerical simulations. The ground deteriorations in field tunnels and through model tests in this research were collected and compared. It was concluded that index of stress reaches 1.7 times of the overburden pressure inducing heaving at top surface road. The trial

material was not expansive in nature and pressing mechanism was used to replicate the probable availability of swelling soils that can add pressures on tunnels therefore causing the heaving.

Figure 2-20 Model test for heaving displacement in tunnels (Seki et al., 2008)

2.4 SUMMARY OF LITERATURE REVIEW

The literature review is explained in detail in this chapter. Several studies to evaluate the expansion characteristics are explained. The volumetric expansion upon saturation and shrinkage upon drying is the major concern of expansive soils for structures constructed in their vicinity. The loading and unloading of expansive soils resulting in soil compression curves are discussed. The methods for swelling pressure exerted by expansive soils upon saturation have been explained and free-swell method is adopted. The strength of these soils is dependent upon particle size distributions and geometrical setting. Many empirical relationships are studied for soil-water characteristics curves. The strength variation of expansive soil has not been studied significantly although research has been carried out to evaluate strength of expansive soils by adding strengthening agents. The time-dependent strength variation requires exploration consequently, it is evaluated before and after expansion in this research.

Finally, the impacts of expansive soils or rocks on tunnels are discussed. Literature has been reported on failure of under-construction and in-service tunnels due to swelling strata. The process has been explained by analytical methods and numerical simulations. A few studies have also explained these mechanisms based on reduced-scale model tests but by replicating the swelling forces by artificial pressure. The time-dependent pressure variations of an actual expansive soil have not been widely deliberated. The impacts of expansive soils based on their location, surrounding ground stiffness and the consequent ground movements in the vicinity of tunnels are yet to be apprehended. Therefore, the core of this research was to monitor the time-dependent impacts of expansive soils on existing tunnels upon saturation through model tests. The impacts are extended by considering the location of expansive soil in surrounding ground and varying the surrounding ground stiffness. A detailed analysis is presented on how the non-expansive surrounding ground responds to the expansive forces as the expansive soil undergoes the swelling with each model test using the image analysis technique. The summary of this chapter is represented in Table 2-1.

Table 2- 1 Summary of literature review

Authors	Core of research	Relevance	Research gap
Expansion characteristics of expansive soils			
Y. J. Cui et al., 2013; El Bahlouli & Bahi, 2014; Soltani et al., 2019; Sridharan et al., 1991; Vanapalli et al., 1998, Komine and Ogata, (2004)	Determination of swelling pressure of expansive soil samples	Swelling pressure by free swell tests in oedometer test	--
Ashayeri and Yasrebi, (2009)	swelling pressure determination through neural networks modeling	Swelling pressure through numerical modeling	Lack of experimental evidence
Adem and Vanapalli, 2013; Alonso, Gens et al., 2006; Nujid and Taha, 2016; Ofoegbu et al., 2017; Pedroso and Farias, 2016; Yin and Tong, 2011	constitutive modelling for mechanical properties of expansive soils	Swelling pressure through numerical modeling	Lack of experimental evidence
Tong and Jian-Hua, 2011 Cui et al., (2013)	loading and unloading loops	Cyclic loading and unloading loops	--
Strength characteristics of expansive soils			
Miao et al., (2002) Kong and Guo, (2011)	Strength before and after expansion	Strength before and after expansion	--
Xu and Sun, (2001)	Strength of expansive soil by fractal model	Strength before and after expansion	--
Tunnel failures in swelling rock zones			
Selmer-Olsen et al., (1989), Liu et al., (2020), Zhang et al., (2016), Barla, (2008)	Tunnel failures in swelling rock zones	Tunnel failure mechanisms in expansive soil strata	Time-dependent mechanisms
Numerical Simulations for tunnel failures due to expansive soils			
Wanjun et al., (2019), Butscher et al., (2011) Tang and Tang, (2012), Anagnostou, (1993). Alonso et al., (2013) Yu et al., (2020)	Tunnel failures in swelling rock zones	Tunnel failure and surrounding ground movements in expansive strata	Consideration of impacts of expansive soil on tunnels after failure, Time-dependent behaviour discussion, Lack of experimental evidence

Physical modelling for tunnel response in swelling rock zones			
Mingqing et al., (2019), Seki et al., (2008)	Physical modelling for tunnel response in swelling rock zones	Conduction of model tests, Expansion and tunnels relationship	Model tests using actual expansive soil, Varying the location and differentiating for surrounding ground, Evaluating the surrounding ground movements

CHAPTER 3 PROPERTIES OF EXPANSIVE SOILS AND SURROUNDING GROUND FOR MODEL TESTS

3.1 INTRODUCTION

This chapters features the expansion and strength characteristics of expansive soil sample prepared in the lab. The expansive soil sample mix ratios along with their formulation method is described followed by the engineering properties of the samples based on several fundamental lab testing techniques. The procedure of free swell pressure determination is elaborated for different mix ratios of the soil sample. Selected samples were further tested under loading and unloading conditions for soil-water compression curve determination. The outcomes of the free-swell pressure of these samples are explained with respect to existing literature in perspective. The lab prepared samples were classified based on the swelling pressure and swell potential of each sample. The mechanical behaviour of expansive soil samples is comprehended. The sections to follow discuss the strength evaluation of expansive soil samples based on unconfined compression tests before and after expansion scenarios. The methodology and outcomes of these tests are elaborated. The surrounding ground of the model test prepared by silica sand No. 8 or No. 6 are explained in the chapters to follow. The strength and stiffness of the surrounding ground material was evaluated by direct shear tests and Yamanaka soil stiffness measuring device. The procedure and results for surrounding ground shear strength and its stiffness have been covered in this chapter.

3.2 EXPANSIVE SOIL SAMPLING AND PROPERTIES

Swelling is generally a result of expansion of certain clay minerals upon wetting e.g., montmorillonite and smectites (F. N. Wang et al., 2021). As the swelling minerals come in contact with water, the interlayer volume increases resulting in swelling. If the conditions are undrained, the additional stresses are developed in the vicinity of the expansive soils which are transferred to nearby structures. The expansive soils used in this study and their compositions is discussed below.

3.2.1 Soil sampling

The expansive soil samples used in this study were prepared in lab by mixing bentonite with Toyoura sand in different mix ratios. Four different combinations were employed to evaluate the mechanical behavior of different samples upon saturation. Initially, 10% bentonite was mixed with 90% Toyoura sand by weight ratio. This sample is referred to as B1090 hereafter. The mixing was carried out as per the volume of the oedometer testing equipment. The sample was divided into five equal part both for bentonite and Toyoura sand and was mixed separately before placing in the oedometer to ensure the homogenous mixing of the sample. On similar lines, the bentonite share of the sample was increased to 15% thereby reducing the Toyoura sand to 85% and the sample was referred to as B1585. Two more samples were prepared with bentonite being 25% and 40% mixed with 75% and 60% Toyoura sand respectively. Consequently, the nomenclature for these samples was B2575 and B4060.

3.2.2 Engineering properties of expansive soils

The engineering properties of expansive soil samples utilized in this study are enlisted in Table 3-1. The dry density of the soil mixtures was kept as 1.60 Mg/m^3 (Cui et al., 2015). As the samples were expansive in nature, the liquid limit, plastic limit and plasticity index were determined through

consistency limit tests. The liquid limit is defined as the moisture content of the soil at which a 10mm groove formed by standard tool in Casagrande's liquid limit testing apparatus closes by applying 25 falls in a standard manner. It signifies general properties of soil and their stress history. This parameter can be used to find out the compressibility index of soil which is utilized in settlements analysis in soils. Therefore, liquid limit is also narrated with natural moisture content of the soil in field. As this moisture content approaches the liquid limit, the soil becomes softer and vice versa. Similarly, plastic limit of soil is the moisture content of soil at which it exists in the boundary where soil is at the verge of acting as a plastic material before entering the zone of semi-fluid state. Plastic limit signifies the clayey nature of soil and used in classification of fine-grain soils. The index for toughness is based upon this limit too. It can also predict the consolidation characteristics of soil with time-dependent loadings on the soil as faced during additional loadings due to construction of different projects. Plasticity index is also calculated based on plastic limit values.

Table 3- 1 Engineering properties of expansive soil samples

Engineering Property	**Toyoura Sand Mixture**			
Mixed Bentonite Percentage	10	15	25	40
Dry unit weight (Mg/m^3)	1.6	1.6	1.6	1.6
Specific Gravity	2.649	2.648	2.647	2.646
Liquid Limit %	41.97	55.49	77.61	125.22
Plastic Limit %	28.13	32.47	26.17	36.54
Plasticity Index %	13.84	23.02	51.44	88.68

3.3 FREE-SWELL PRESSURE OF EXPANSIVE SOILS

3.3.1 Testing procedure

The free-swell pressure exerted by expansive soil sample is the pressure that prevents any further swelling of the specimen upon saturation. The test is usually performed in a standard oedometer apparatus in geotechnical engineering field. This method of determining the swelling pressure exerted by the expansive soils has been extensively adopted in a number of studies found in literature (Cui et al., 2013; El Bahlouli and Bahi, 2014; Miao et al., 2002; Soltani et al., 2017; Vanapalli et al., 1998). The applied method resembles to ASTM standard D4546-14 (ASTM, 2013). The said standard distinguishes into Method A where swelling test is performed under constant load of 1kPa, Test B in which the vertical load applied on sample is equal to load on the soil in actual field and Test C in which the sample is reloaded in sequential order to find the strains after wetting induced swelling. So, the method used in this research is a combination of method B and C of the ASTM standard D4546-14. The swelling pressure of an expansive soil sample can successfully be determined using this methodology. Consequently, in this research program, the swelling pressure of the soil samples prepared in lab was evaluated based on free-swell pressure method. Standard oedometer equipment was utilized for this purpose. Figure 3-1 represents the schematic diagram of oedometer, the oedometer apparatus and sample container.

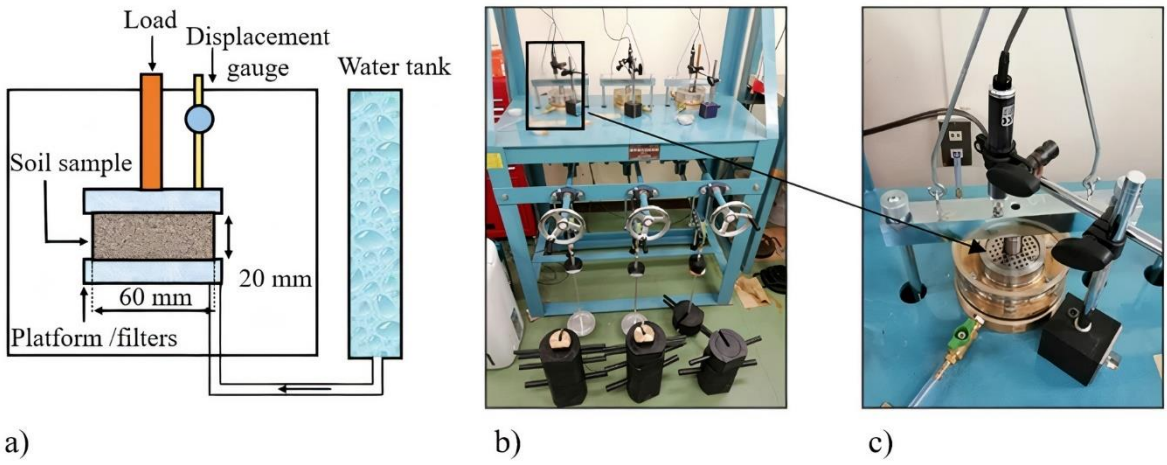

Figure 3-1 Free-swell testing a) Schematic diagram b) oedometer apparatus c) sample container

The detailed procedure of testing method is explained in Figure 3-2. The sample container in oedometer is cylindrical in shape. The diameter of the cylinder is 60mm while the height is 20mm. The soil sample prepared in 5 layers as explained earlier is placed in the container ensuring the desired volume is achieved. The loading frame is placed in its position and an initial load of 9.8 kPa is applied on the sample which was in accordance with the overburden pressure in the model tests. This load also ensured the consolidation of the sample has completed and is referred to as the token load (ISRM, 1999). The token load applied on sample rendered the initial consolidation and as soon as the 90% or more consolidation of the sample was completed, the sample was provided with water for the process of saturation to be started. The initial consolidation of the sample was calculated on the basis of root time method as per described by Robert, (2006). The water provision to the sample caused expansive minerals in the soil mixture to swell. As the sample is restrained in horizontal direction, the sample swell unidirectionally freely in vertical direction only. The height of the sample was continuously recorded through data logger attached at the top of the sample as represented in the Figure 3-1 (c). As the time went on, the sample kept on expanding and the height kept on increasing.

Figure 3-2 further clarifies the procedure. The application of token load brought consolidation and the consequent void ratio of the sample decreased and reached point A in the graph. Upon water addition to the sample, as soon as the change in height of the sample reached its peak and the rate of change of height becomes constant for a significantly long time or less than 0.1%, it was presumed that the maximum swelling has occurred, and sample has expanded to its maximum potential. This point is highlighted as point B in Figure 3-2. The height and consequent void ratio of the sample corresponding to this point was calculated. The load on the sample was kept to 9.8 kPa at this point.

As the sample swelled completely, the soil was loaded back in sequential order by addition of 9.8 kPa on it. At this point the cumulative load on sample is 19.8 kPa and the expanded height of the sample was suppressed as highlighted by point C. Significant time was given to incorporate any consolidation before adding another load of 19.8 kPa which is double of the total load on the sample making the cumulative load of 39.2 kPa represented as point D.

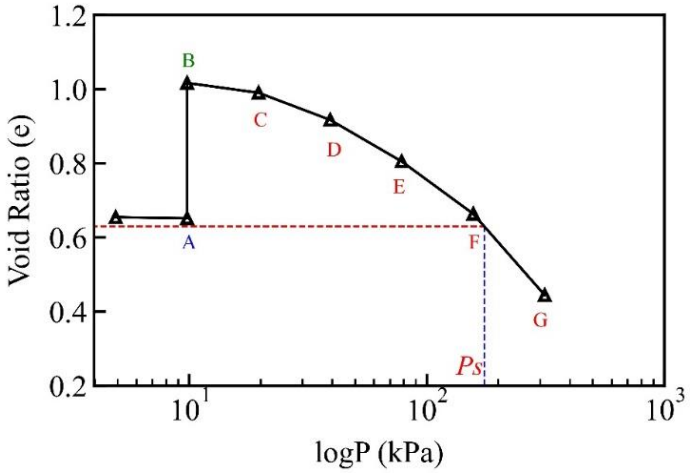

Figure 3-2 The procedure for free-swell testing

Similarly, the sample was loaded in sequential order such that each next load was twice the total load on the sample and represented by E, F and so on as the case may be, until a point was reached where the void ratio and height of the sample was equal to the initial height of 20mm. The magnitude of load applied to bring a fully expanded sample to its initial state and void ratio was referred to as the swelling pressure (P_s) while the maximum potential of a particular sample to expand freely during free swell examination was termed as swelling potential (Bahlouli and Bahi, 2013; Cui et al., 2013).

3.3.2 Mechanical behavior of expansive soil upon expansion

The results of free swell tests on different soil samples are represented in Figure 3-3. The swelling kinetics represent the path followed by different samples as the saturation was started and the height of the sample started to increase. The graphics represent the kinetics between point A and B as represented in Figure 3-2. The duration of the expansion corresponded to the amount of bentonite in each sample. The B4060 sample represented the longest duration to reach the maximum swell potential. The swell potential of different samples utilized in this study depicted that higher the potential, greater the pressure would be required to bring the sample to its original state.

Figure 3-4 represents the swelling pressure calculations for the four samples used in this study. The sample with 40% bentonite took the longest duration hence exhibiting the highest swelling pressure of 289.92 kPa. It was observed that the rate of swelling was quicker than the rate of the consolidation of the sample upon pressure application. Consequently, the decrease in swelling rate was prevented by counter greater vertical pressure during recession (Bahlouli & Bahi, 2013).

Also, during soaking the sample with water under low pressure, rapid interaction of water under gravitation leaded towards the formation of double defused layer implying swelling pressure (Robert, 2006). The soil structure internal connections and loads can demonstrate assorted swelling pressures in the process of loading. The experiments were conducted in duplication to ensure precision and reproducibility. The soil sample with lower percentages of bentonite showed small swell potentials and consequently smaller swelling pressures. As the bentonite percentage was increased, the swelling pressure got higher. The swelling pressure tendency showed typical behavior of an expansive soil (Tahasildar et al., 2018).

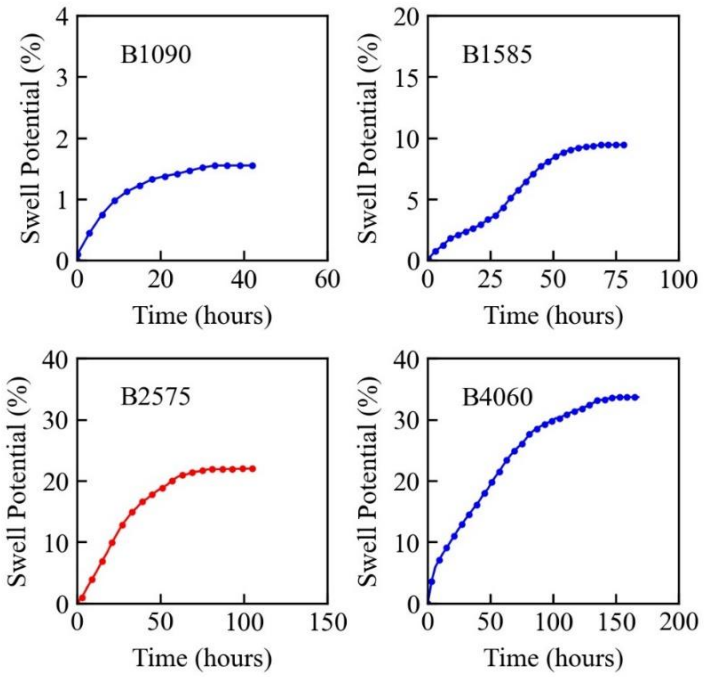

Figure 3-3 The swelling kinetics for free swell tests

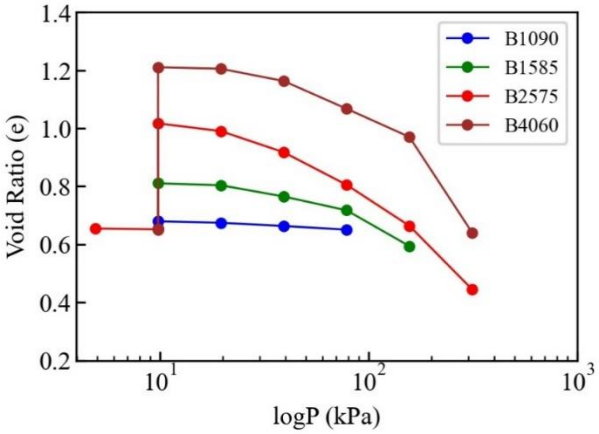

Figure 3-4 Variation of void ratio with saturation and reloading on the sample and determination of free swell pressure

The sample B2575 exhibited 161.72 kPa of swelling pressure swelling potential of nearly 22% which classifies the soil as highly expansive (Sridharan and Prakash, 2000). This sample had been selected for model tests. The selection is based on significant, nonetheless, moderate swelling pressure of the sample evaluated during free swell pressure calculations. Figure 3-5 represents the relationship of swelling potential with swelling pressures of these samples. A fairly linear relationship exists between the two with the coefficient of determination (R^2 score) of 0.97.

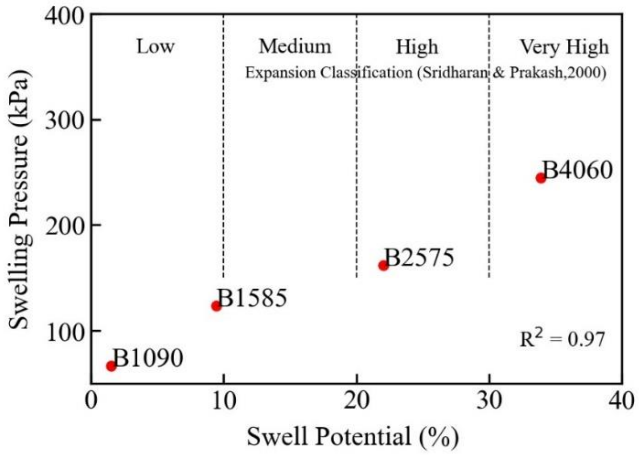

Figure 3-5 Relationship of swelling potential with swelling pressures

The slope of the samples with different fractions of bentonite content is almost constant, the intercept, however, is lower in case of samples with lower percentage of bentonite. The final value of swelling pressure and potential is curtailed by the corresponding non-swelling component of the mixture i.e., Toyoura sand thereby fading the general competence of the pure bentonite sample to swell. Komine H. and Ogata N., (1999) performed an experimental study on similar lines for swelling characteristics of sand-bentonite mixture for nuclear waste disposal. The results in this study are in-line with the swelling pressure measured by them. The swelling potential and swelling pressures of the soil samples are enlisted in Table 3-2.

Table 3- 2 Swelling potential and swelling pressure of expansive soil samples

Expansive Soil Sample	Swell Potential (%)	Swelling Pressure (kPa)
B1090	1.55	66.7
B1585	9.44	134.44
B2575	21.9	161.72
B4060	33.88	289.92

3.4 LOADING / UNLOADING RESPONSE OF EXPANSIVE SOILS

The compression and expansion curves were plotted for specified samples of expansive soils. As stated earlier, the loops formed as a result of loading and unloading the soil samples explain the viscosity characteristics of the soil. Sandy soils have narrow loops owing to smaller viscosity and are very clear for silty soils and clays like the bentonite and sand mixtures samples used in this study. As the swelling ability of expansive soils bring in the physiochemical response of soil in addition to the mechanical response to the external stresses applied. These loops are widely used in time-dependent stability studies of expansive soils. As this study is based on evaluating the time-dependent impacts of expansive soils on tunnels, the expansive soil sample B1585 and B2575 falling in category of

medium expansive and highly expansive category were considered for loading, unloading and reloading compression expansion curves and are discussed below.

3.4.1 Testing procedure

The procedure adopted for performing the long-term loading/unloading tests include preparing the sample as per the free swell tests explained earlier and were placed in the same oedometer testing apparatus. The sample was loaded with 9.81 kPa of vertical pressure. As soon as the initial consolidation of the sample was over, the load was doubled i.e., 19.8 kPa. The consolidation magnitude was adjudged through root time method. The sample upon application of further loading compressed as was loaded again with double of the previous load on it. The consequent loading was carried on until the maximum load of 1.25 MPa was applied to the sample. As the sample compressed to its maximum extent by application of load, the sample was flooded with water to saturate it. The sample showed a slight compression under load and the saturation went on until the displacement remained constant for a long enough time. The process of unloading was started and the load of 628 kPa was removed. The sample expanded under relieved pressure and as soon as the height of the sample become constant again for long enough time, another load of 314 kPa was removed. Similarly, the unloading was carried on until the pressure on sample was 19.6 kPa. The height and void ratio were evaluated on each and every point of loading, saturation and unloading etc. This rotation exercise of loading and unloading was repeated until the loops overlapped.

3.4.2 Results and discussions

Figure 3-6 represents the oedometer test results for loading, saturation and unloading cycles for the B1585 sample. The initial loading of the sample compressed lightly, and the slope of the descending line remained mild and as the load magnitude was increased, the slope of loading got steeper as represented in L1 curve. The maximum compressed sample upon saturation compressed another bit during S curve. The unloading curve is represented as UL1 where the gradual reduction of the sample was carried out. Since the sample had 15% bentonite, the retrieval curve depicted a minute expansion with coefficient of expansion (kappa) value 0.03 as compared to compression in first loading curve.

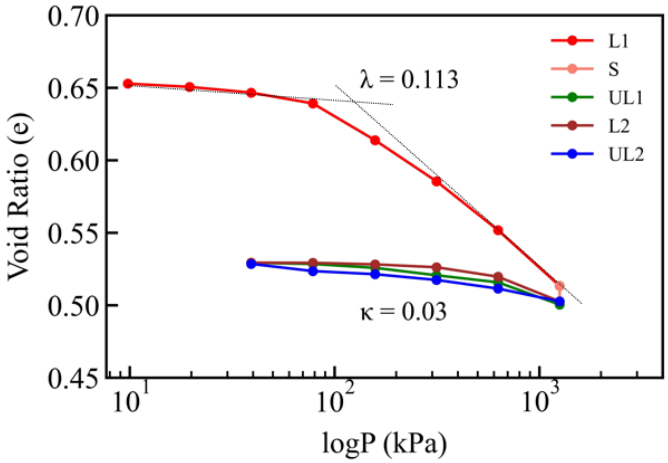

Figure 3-6 Oedometer test results for loading/unloading on B1585 sample

Assessment of the unloading curve reveals a hysteresis loop. As the further loading of the sample was carried out, the sample had already gone through enough compression under stresses higher than pre-consolidation. The particle setting had changed during the initial loading cycle and void ratio had already been taken to minimum. As the expansive content is only 15%, the loops did not represent a wider gap between the loading and unloading rings. The mechanical response of the expansive soil sample upon loading and unloading is more dependent upon the setting of the soil particles while the physio-chemical behavior is triggered by the bentonite content in the mixture. The contact angle in-between the particles had been reduced during the initial loading and the consequent re-loading did not replicate the initial compression curve. The unloading loops were accompanied by the swelling potential and a minor contribution of the mechanical re-bound of the soil sample. The re-loading curve for the sample did not reflect any further compression hence the any further cycle would have resulted in the same path for loading and unloading curves.

A similar test for B2575 represented contrasting results with a rise in bentonite content in the soil sample. Figure 3-7 represents the loading / unloading compression expansion curves for B2575. The initial loading of the sample before saturation represented a mild slope compression curve which got steeper as the magnitude of the load was raised. A slight compression during the saturation further reduced the sample height. As the sample achieved saturation, the lifting of pressure triggered the chemical response of sample and it represented expansion.

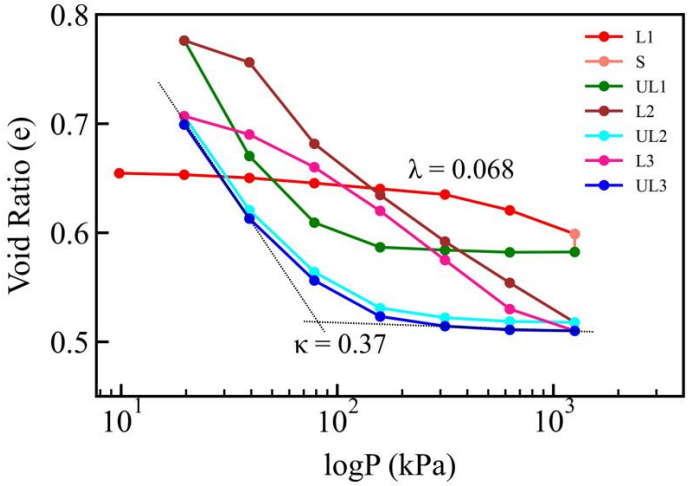

Figure 3-7 Oedometer test results for loading/unloading on B2575 sample

The consequent lifting of the segmental pressure from the sample showed expansion and as the magnitude of the overburden pressure got lower, significant expansion was observed. The expansion behavior from unloading due to reduction of pressure is administered by the balancing of mechanical and chemical response of the soil sample together. When the swelling force is higher than the pressure on the sample, the physio-chemical behavior dominates the mechanical behavior, yet the volume change is a combination of both. Similarly, in the point of time where stress dominates the expansive pressure, the volume change is driven by mechanical means. These explanations can help the distinction of the zone where mechanical participation of volume change can be separated from the chemical one. The initial unloading curve UL1 in Figure 3-7 (green) is an example where the mechanical contribution to swelling can be separated from physio-chemical one. The mild slope part

of the curve indicates the mechanical rebound whereas steep rising slope represents the volume change utterly attributed to bentonite's ability to chemically react to water presence for expansion. The lower pressure range has presented this part of the swift swelling. The coefficient of expansion (kappa) value for this case was 0.37.

As the swelling pressure of a soil sample is the pressure at which the sample would not show any expansion in wet state, the threshold pressure between chemical and mechanical swelling explained above is referred to as the swelling pressure of the sample. The determination of this pressure has been carried out through several ways as reported in the literature. The constant volume swelling test is the method in which the sample after flooding is monitored for any swelling and as soon as the height of the sample increases by a magnitude of 0.1%, the sample is reloaded to keep the height to its original position. Similarly, the load is kept increasing until no more swelling is observed and the pressure required to keep the sample in its original height is called swelling pressure (Basma et al., 1995). The other method is the free swell one explained in earlier sections. It is to be noted that the pressure applied in excess of the swelling pressure would lead to collapse in the soil particles and unloading beyond swelling pressure would create diffuse layer in between particles and they will change the orientation of their inter-particle setting to face-to-edge type. However, it is recommended to study the micro-level investigations for the particle orientation during loading and unloading.

Significant variation in the paths followed by soil sample during loading and unloading cycles were observed and as soon as the path followed became constant the loops were concluded. The unloading loops were accompanied by majority of the swelling potential and a minor contribution of the mechanical re-bound of the soil sample.

3.5 STRENGTH CHARACTERISTICS OF EXPANSIVE SOILS

As the expansion of the expansive soil occurs, a consequent alteration in their strength is essential to consider before construction of underground structure in strata accompanied by expansive soils. Expansion is a time-dependent process therefore the strength of the expansive soils is needed to be considered in the fourth dimension of time. In this study an effort has been made to evaluate the strength of expansive soil samples in combination of simultaneous expansion. The methodology followed and the outcome of the results has been discussed in detail below:

3.5.1 Testing scheme and experimental conditions

The expansive soil samples used for strength properties of expansive soils were the same as used for the expansion properties. The testing was carried out through unconfined compression tests (UCT) as represented in Figure 3-8.

The sample dimensions for UCT were 100 mm in height and 50mm in diameter. The samples were prepared in 5 layers to ensure homogeneity. Each layer 10mm high sample was placed in the mould and compressed to its designated volume. The experimental conditions involved preparing the B1090 sample at 30% of degree of saturation. The same sample was prepared for degrees of saturation of 40, 50, and 60%. Similarly, the samples B1585, B2575, and B4060 were prepared at

four degrees of saturation. The sample strength for each of the above cases was evaluated immediately after the preparation. This strength was designated as the strength before expansion.

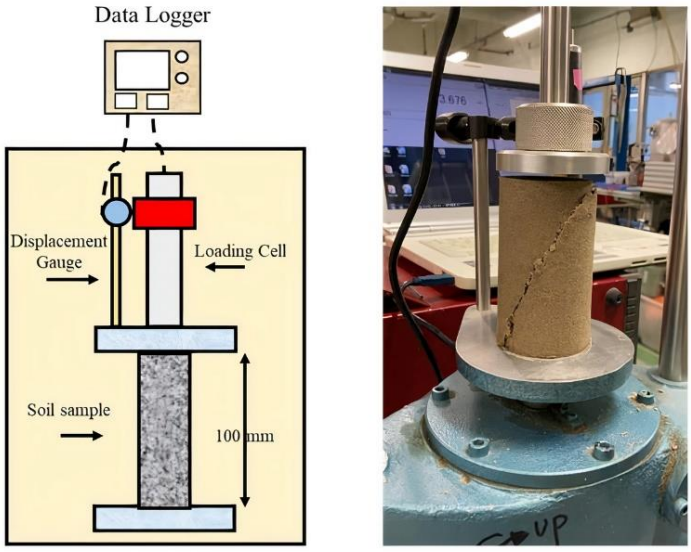

Figure 3-8 Unconfined Compression test apparatus

In another scenario, the similar samples were prepared and placed in the plastic mould to ensure that their water content is not lost to the environment and to maintain one-dimensional expansion in accordance with free-swell testing scheme. These samples were further placed at a constant temperature and humidity-controlled environment in an air-tight desiccator. Continuous readings for temperature and humidity were recorded to maintain the humid environment in the desiccators. The samples kept in desiccator were taken out after 20 days presuming that the maximum expansion under the requisite degree of saturation has occurred. The samples were tested for their unconfined compression strengths. These strengths are referred to as strength after expansion in the discussions to follow. The strength of the expansive soil samples before and after the expansion were compared and evaluated for differences.

3.5.2 Results and discussions

The unconfined compression test result for B1090 sample at different degrees of saturation before and after the expansion are discussed. The unconfined compression strength of the samples was within the range of 45 kPa. At 30% degree of saturation, the sample collapsed drastically as majority of the content was Toyoura sand. A slight reduction in the strength was observed for sample allowed to expand in the desiccator. The plasticity of the sample was not enough to incorporate the plastic behaviour of the bentonite to play a part in enhancing the cohesion of the sample against the externally applied compression stress. As the degree of saturation was increased to 40%, no significant change in the UCS was observed before and after expansion. The elastic range of the test was well defined and upon reaching the peak strength, the sample depicted a slight plastic behaviour where stress remained same while the strain carried on. The failure path to followed until the residual stress was identical. The expanded sample strength increased by a very minute magnitude.

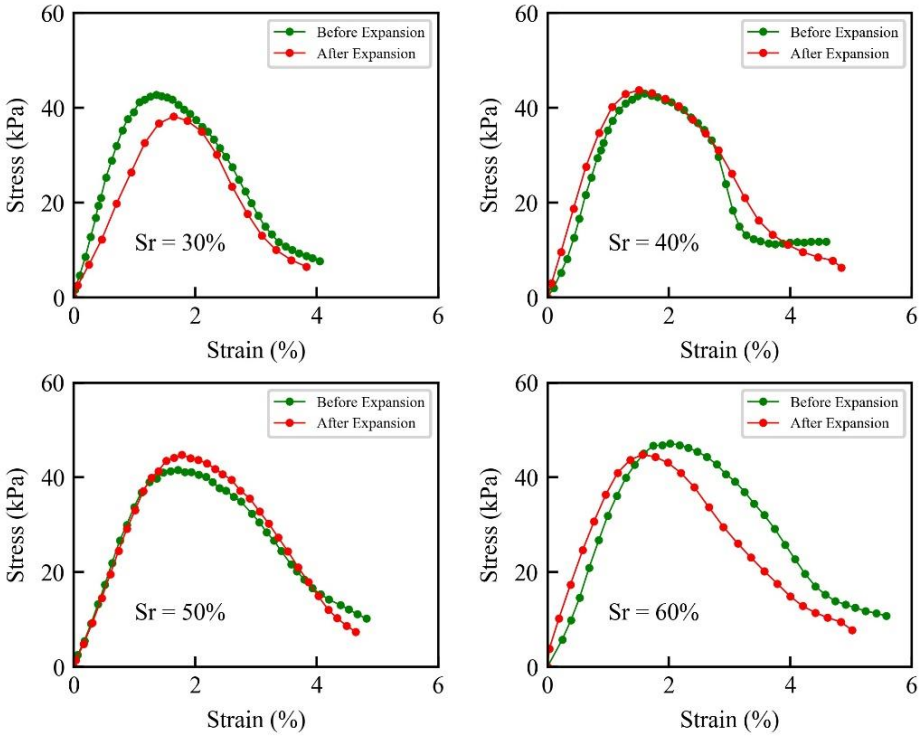

Figure 3-9 UCT for B1090 before and after expansion

Similar kinetics were observed for sample with 50% of degree of saturation and sample reflected better strength upon expansion as the increase in water content would have induced the bentonite particles to swell but not being the predominant part of the sample, the non-cohesive Toyoura sand share developed a bond in presence of clay minerals. Also, the moisture content of the sample would have approached the optimum level where better compaction was achieved during the preparation. However, with a further rise in moisture content, the strength of the sample reduced for 60% of degree of saturation. The path followed by the sample in this case were slightly separated due to the plasticity enhancement of the expanded sample achieved owing to higher water content This represents that as the expansive soil absorbs water and the moisture content increases, the strength parameters show improvements until a certain level after which the strength starts to decrease. The samples being sand-dominant, represented with clear shear failure within a strain range of 5%. Figure 3-9 represents the UCS curves for the samples.

Similarly, the UCTs for sample B1585 performed resulted in the statistics shown in Figure 3-10. An increase in the strength was seen of all the samples overall as compared to the B1090 sample due to higher fine bentonite content.

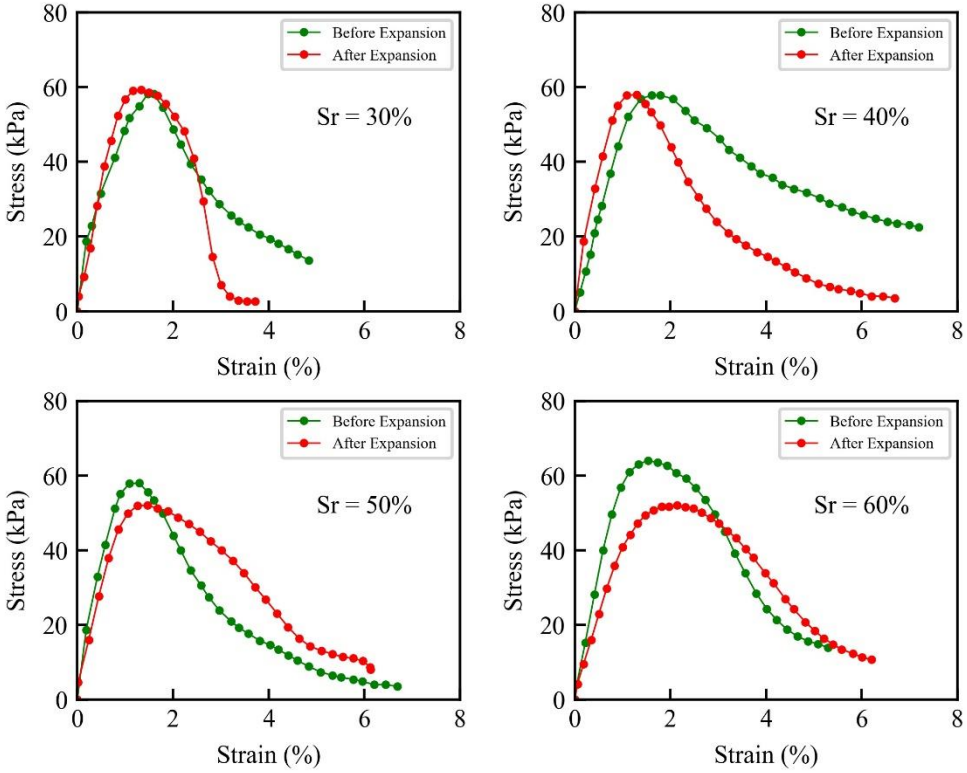

Figure 3-10 UCTs for B1585 before and after expansion

The unconfined compression strength of the samples was within the range of 45 kPa. At 30% degree of saturation, the unconfined compression strength of the expansive soil before and after expansion was 58.21 and 59.33 kPa respectively representing no significant difference. Similarly for 40% of saturation it was 57.96 and 57.88 kPa. The sample showed the consequences of increased saturation for 50% sample and the fatigue was observed in the expanded sample. A reduction in strength amounting to 6 kPa in case of expanded sample justified that the strength of expansive soils reduces upon expansion. This reduction is the result of change in the orientation of the particle-to-particle contact from face-to-face to face-to-edge. As the bentonite content increased, height of the sample increased to 100.89 mm with 60% degree of saturation. A significant reduction in strength i.e., 12 kPa was observed for this sample after expansion was allowed.

As the bentonite content further increased to 25% in the sample, the plastic nature of the sample dominated the brittle nature. The strength of the sample increased as compared to samples with lower bentonite contents. As the degree of saturation rose, the strength difference between the expanded sample and the immediate sample significantly increased. The difference of 18.77 kPa was observed for sample with 60% degree of saturation. The delayed response in elastic range of expanded sample also signifies that brittle nature of the sample has been dominated by the ductility of the sample owing to increased clayey content. The strength of expanded samples at all the saturation levels in discussion represented lowering of strength. Figure 3-11 represents the UCTs for B2575 sample before and after expansion at different levels of saturation.

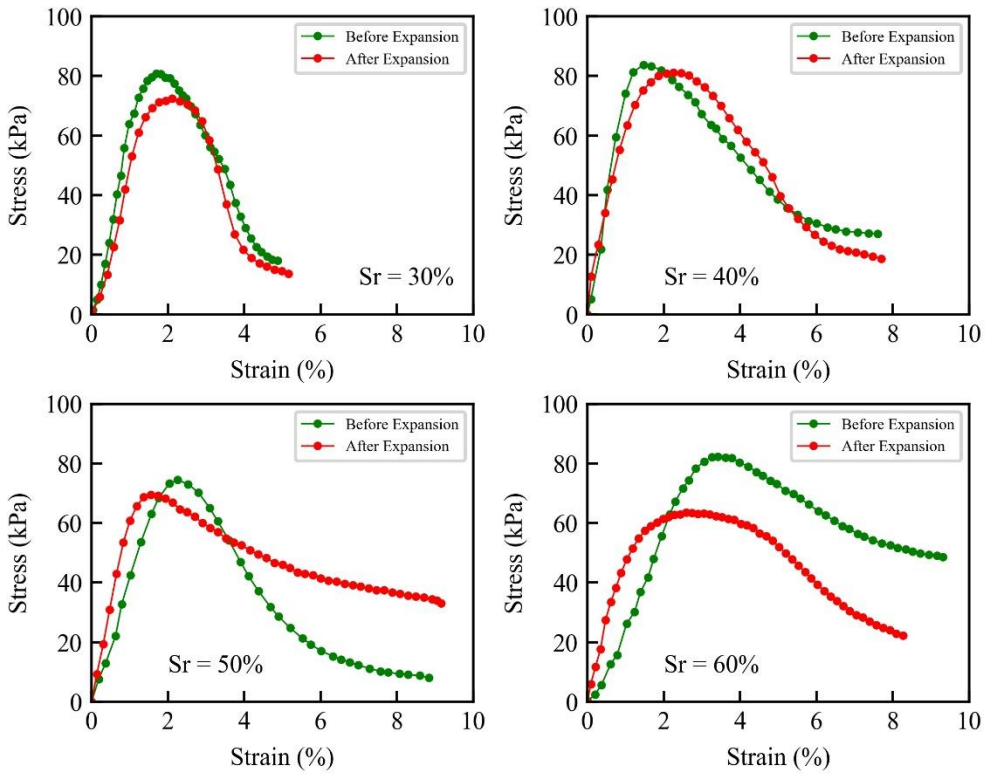

Figure 3-11 UCTs for B2575 before and after expansion

Figure 3-12 represents the UCT results for B4060 sample. The sample projected an elongated strain range as compared to other samples as the significant part of the sample was bentonite. The initial and final strengths of the sample were higher as compared to previous samples. The elastic range characteristics were quite similar for all the different degrees of saturation. The strength of the expanded samples was more than the before expansion samples for degrees of saturation of 30 and 40%. The reason could be the optimum quantity of moisture that aided the compaction of the sample during preparation. The role of the chemical adhesion of increased bentonite content with the Toyoura sand in the mixture strengthened the sample. On the contrary, as the water content further increased, the expanded samples presented with drastic reduction in strength. This signifies how quickly the expansive soils lose their strength with rise in water content.

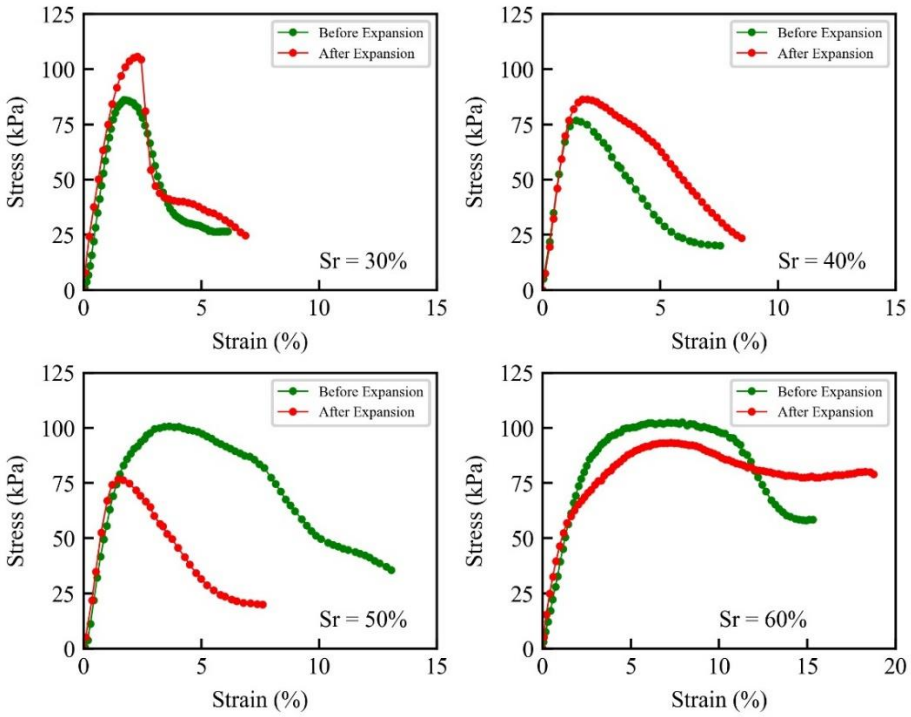

Figure 3-12 UCTs for B4060 before and after expansion

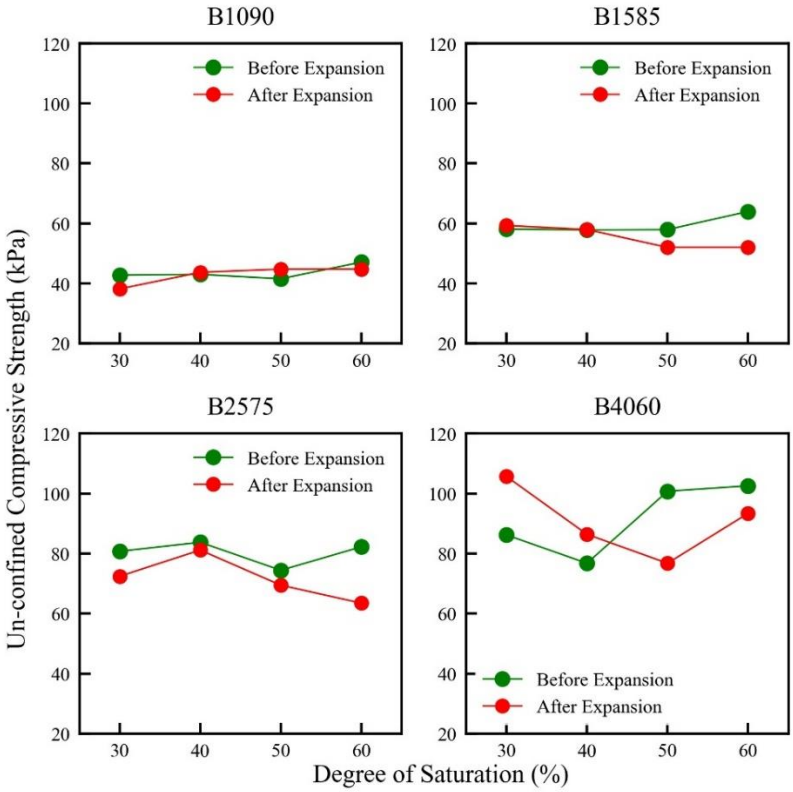

Figure 3-13 Variation of UCS at different water level for expansive soil before/after expansion

The sample with 60% saturation showed a long range of ductility where strain kept on increasing with stress remained constant. A reduction in unconfined compressive strength of 9% was observed after expansion. the results signify that with higher water contents, the expansive soils can degrade at a rapid pace and can be a source of deterioration for structures constructed in strata comprising of them. Figure 3-13 summarizes the variation of unconfined compression strength of expansive soil samples with different levels of saturation before and after the expansion occurred. As explained, most of these represented reduction of strength after expansion and rise in water content.

3.6 SURROUNDING GROUND STRENGTH

The model tests carried out in this research were performed in a small-scaled model in which expansive soil and the surrounding ground of the tunnel were placed. The engineering properties of the non-expansive surrounding ground around the tunnel are explained here. The surrounding ground for this matter was chosen as Silica sand No. 6 and No. 8. The physical properties of these sands are enlisted in Table 3-3:

Table 3- 3 Physical properties of surrounding ground material for model tests

Surrounding Ground	Specific Gravity	Maximum void ratio	Minimum void ratio	Mean particle size	Maximum particle size
Silica Sand	G_s	e_{max}	e_{min}	d_{50} (mm)	d_{max} (mm)
No. 8	2.622	1.414	0.717	0.076	0.21
No. 6	2.623	1.084	0.663	0.216	0.42

As stated earlier, the 25% bentonite and 75% Toyoura sand soil sample in free swell test projected a swelling pressure of 161.25 kPa. This pressure was expected to impact the tunnel model employed in this study during the performance of model test. As the expansive soil was modelled as a layer surrounded by surrounding ground material, naturally the material of surrounding ground would also be subjected to additional stress due to the pressure exerted by the swelling force. The stiffness of the surrounding ground material was supposed to play a key role is adjudicating the time-dependent impacts of the expansive soils on tunnel. Therefore, it was deemed necessary to evaluate the strength and stiffness of the surrounding ground material. Direct shear tests were performed to evaluate the shearing strength of the silica sand No. 8 and No.6 (referred to as S8 and S6) in this study. The procedure and the outcomes of the tests are explained in detail as follows.

3.6.1 Testing scheme and experimental conditions

The strength of the surrounding ground material around tunnel was evaluated by standard direct shear tests. The shear strength of a soil sample is the resistance of soil particles against shearing upon pressure application. The test is applicable for sandy or silty textured soils / cohesionless soils. The test is widely applied to report the strength of soil in field engineering situations like retaining walls, bearing capacity and slope stability analysis etc. The direct shear test apparatus is represented in Figure 3-14.

The diameter of the sampler was 60 mm and 20 mm in height. The shearing box was assembled and installed with porous base and filter paper. The soil sample was prepared for silica sand No. 8 and

No. 6 at 80% of its relative density as model tests were carried out at this density. Model tests were also performed by placing the surrounding ground at 90% of its relative density consequently, the tests for 90% relative density were performed too. The sample was prepared in 3 layers with addition of 5% water replicating the conditions in the model test. The layers were tamped to fit in the requisite volume. The shear box was placed in in its position and the predetermined confining pressure was applied on the sample. The three dial gauges represented in apparatus are for vertical and horizontal displacements, and the shearing force gauge. The initial consolidation under the load is recorded and the shearing of the sample was carried out.

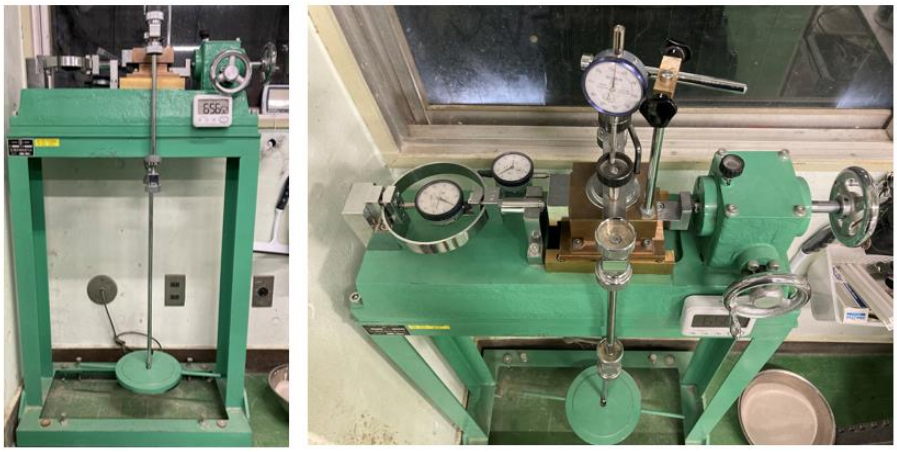

Figure 3-14 Direct shear test apparatus and measurement gauges

The shear force for shear displacement rate of 0.2 mm per minute was recorded. The horizontal displacement during the shearing was recorded for variation in the height of the sample during shearing. The samples were tested for three confining loads of 39.14, 52.4 and 78.5 kPa. The analysis was carried out by converting the dial gauge readings into appropriate loads and displacements. Using the area of the sample, the shear stress (τ) was determined as a ratio of shearing force to area. The shearing stress was plotted against the shear displacement to find the maximum shear stress for each confining load on the sample. This maximum shearing is plotted against each vertical stress for the determination of angle of internal friction and cohesion of the sample utilizing the Mohr-coulombs failure envelope criteria.

3.6.2 Results and discussions

Figure 3-15 represents the direct shear test results for S8 soil at 80% of its relative density. Shear strength of 59.78 was represented by the sample under a normal stress of 78.5 kPa. The partially saturated sample represented significant non-linear response to shearing and after attaining the peak, followed a steady residual strength state. The shear strength of the sample rose by the increment of the confining pressure. The peak strength plotted against normal stress showed a linear relationship with coefficient of determination score (R^2) of 0.987. The angle of internal friction of 34.5 degrees was observed. The vertical displacement during the shearing was 0.01 mm and remained more or less constant during the test.

The free swell pressure of 161.75 kPa was observed for B2575 sample. The pressure would have impacted the surrounding ground as well while undergoing the expansion due to water interaction. During the performance of S8-B model test (explained in Chapter 5), only a maximum of 25 kPa pressure was shown by the gauges that were in direct contact with the soil layer which is only 15.5% of the swelling pressure.

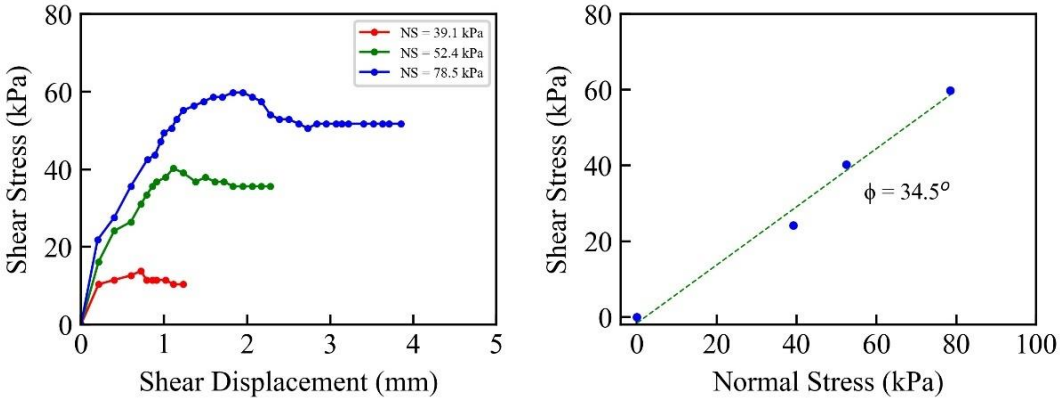

Figure 3-15 Direct shear tests for S8 at 80% of its relative density

Such reduced representation of expansive pressure encouraged to evaluate the strength of the surrounding ground and replacing it with stiffer material to assess the impacts of expansive soil on tunnels based on stiffness of surrounding ground. Therefore, it was deemed necessary to evaluate the strength of silica sand No. 8 at an enhanced density of 90% of its relative density. Figure 3-16 represents the shear test results for this case.

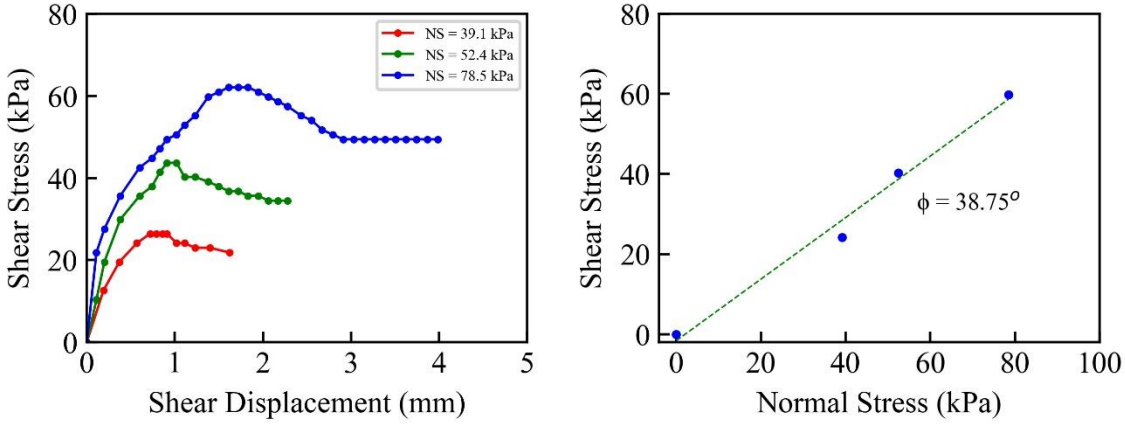

Figure 3-16 Direct shear tests for S8 at 80% of its relative density

Shear strength of 62.08 kPa was represented by the sample under a normal stress of 78.5 kPa which was higher than the previous case. The partially saturated sample represented significant non-linear response to shearing and after attaining the peak, followed a steady residual strength state. The shear

strength of the sample rose by the increment of the confining pressure. The peak strength plotted against normal stress showed a linear relationship with coefficient of determination score (R^2) of 0.988. The angle of internal friction of 38.75 degrees was observed. The vertical displacement during the shearing was 0.02 mm compression during the test.

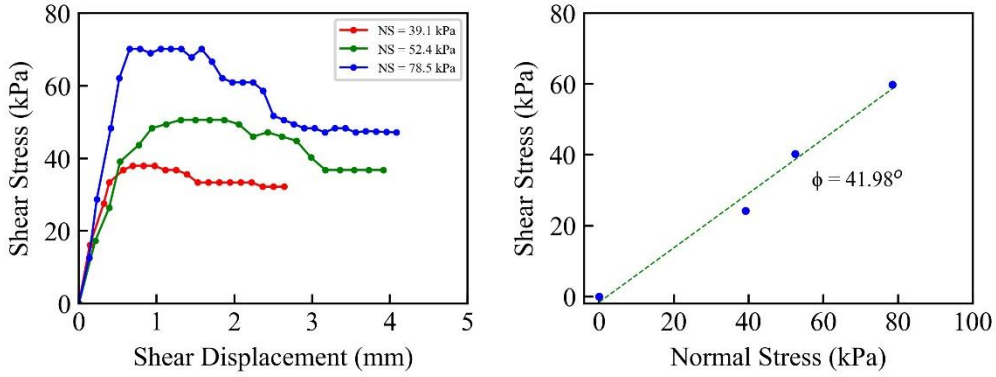

Figure 3-17 Direct shear tests for S6 at 80% of its relative density

Although the shear strength of the surrounding ground increased by increasing the density still the expansive pressure presented by the gauges amounted to 62.33 kPa in model test (explained as S8(90)-B in chapter 7) which is 38.53% of swelling pressure. Therefore, it was deemed necessary to replace the surrounding ground by silica sand No. 6. Following the shear tests for S8, Figures 3-17 and 3-18 represent the direct shear test results for silica sand No.6 performed at its relative density of 80 and 90% respectively.

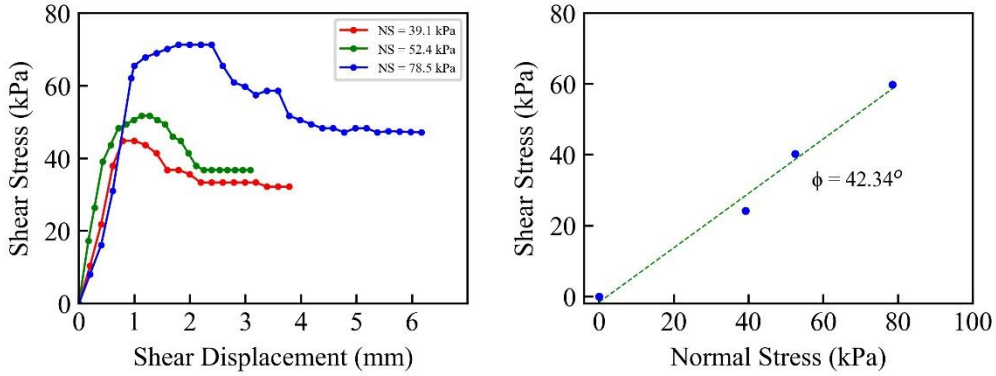

Figure 3-18 Direct shear tests for S6 at 90% of its relative density

Shear strength of 62.08 kPa and 71.28 kPa was represented by the samples under a normal stress of 78.5 kPa for 80% and 90% of the relative density of silica sand No.6 respectively. This strength was higher than the No. 8 sand owing to granularity and higher resistance of soil to shearing. The partially saturated sample represented significant non-linear response to shearing and after attaining the peak, followed a steady residual strength state. The shear strength of the sample rose by the

increment of the confining pressure as depicted in the graphs. The peak strength plotted against normal stress showed a linear relationship with coefficient of determination score (R^2) of 0.97 and 0.99 respectively. The angle of internal friction rose as the shearing strength increased. The peak vertical displacement during the shearing were 0.03mm and 0.04mm. Table 3-4 summarizes the direct shear tests for surrounding ground material for model tests performed in this study.

Table 3- 4 Direct shear tests for surrounding ground material for model tests

Surrounding Ground and density	Normal Stress (kPa)	Shear Stress (kPa)	Internal friction
No. 8 (80%)	39.14	24.14	$\phi = 34.51^o$
	52.4	40.24	
	78.5	59.78	
No. 8 (90%)	39.14	26.44	$\phi = 38.75^o$
	52.4	43.69	
	78.5	62.08	
No. 6 (80%)	39.14	37.94	$\phi = 41.98^o$
	52.4	50.59	
	78.5	70.13	
No. 6 (90%)	39.14	44.84	$\phi = 42.34^o$
	52.4	51.74	
	78.5	71.28	

3.6.3 Friction between the surrounding ground soil, expansive soil and model boundaries and model tunnel material

As the surrounding ground movement was evaluated using PIV analysis. The model equipment boundaries would have impacted the movement of the ground upon expansion of expansive soil. The friction between the front acrylic plate and tunnel material would have interfered with the net displacement. The evaluation of the friction between two different boundaries and the silica sand No. 6 was evaluated using direct shear test. The test was performed between acrylic plate with sand and for metal material of model boundary with sand. The silica sand layer was sheared against the fixed acrylic plates and metal. Figures 3-19 and 3-20 represent the results for these direct shear tests.

The coefficient of friction between the sand and acrylic plate was found to be 0.17 times of the confining lateral pressure and 0.15 for metallic plate. This pressure would be smaller than the vertical pressure. Since the ratio between the maximum friction and confining pressure is considerably small. Also, the evaluated coefficient of friction is for critical state (maximum shear stress) its value for model tests would be equal or less than this value. This smaller fraction of resistance of soil to move can have slight boundary impact but insignificant hence it can be ignored against the high expansive push of the expansive soil, and it would not hamper the ground movement significantly, yet this friction was further reduced by applying the Teflon spray on the acrylic surface before performing the model tests to make the testing conditions as close as possible to the plain-strain conditions.

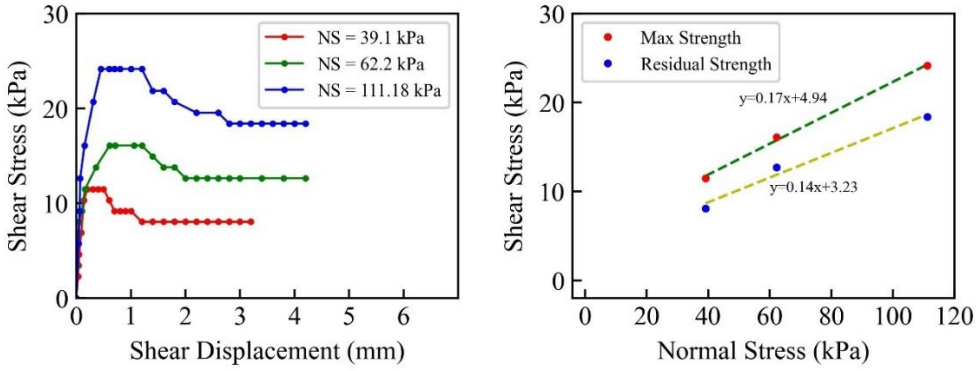

Figure 3-19 Friction between the acrylic front and silica sand No.6

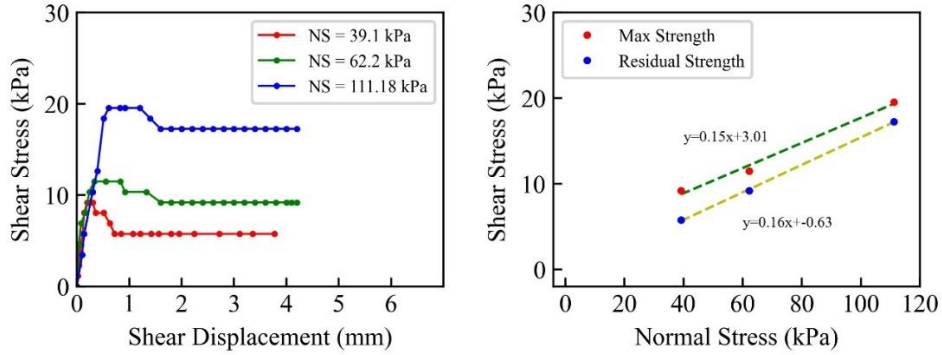

Figure 3-20 Friction between the metal material and silica sand No.6

Similarly, the friction between the expansive soil and the acrylic front was evaluated to adjudicate if expansive soil would resist the ground movement. Figure 3-21 represent the direct shear test results for these cases. The coefficient of friction between the expansive soil and acrylic plate was found to be 0.16 times of the confining lateral pressure.

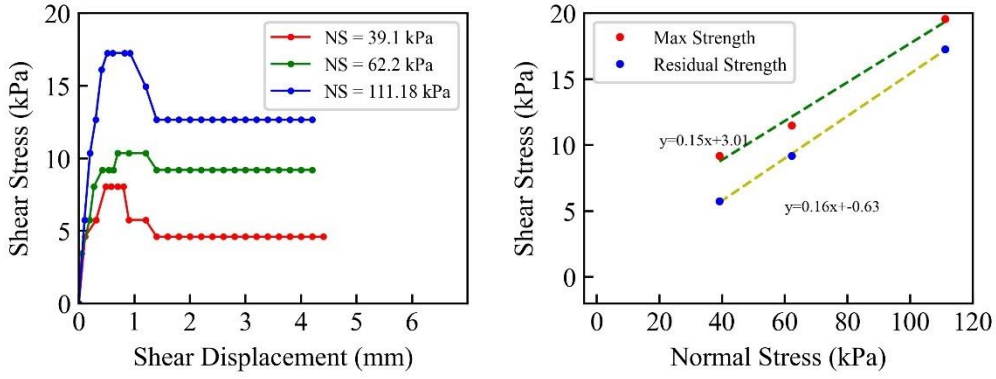

Figure 3-21 Friction between the acrylic front and expansive soil

3.7 SURROUNDING GROUND STIFFNESS

In addition to strength tests for surrounding ground, its stiffness was determined by quick tests using the Yamanaka soil stiffness measuring meter. The specifications and method of the stiffness tests along with the outcomes for surrounding ground employed for this study are explained.

3.7.1 Yamanaka Soil Stiffness Measuring Meter

The Yamanaka soil hardness meter is a special device developed by FUJIWARA SCIENTIFIC CO., LTD. to measure the stiffness of soil based on principle of a calibrated spring contraction. This meter has a press-fitted cone which is used perpendicular to the flatten cross sections of soil surface. The depth of penetration corresponds to soil reaction force change (spring contraction) and is measured as a number X. The stiffness of the soil (P) in kg/cm^2 is then measured by using the following formula:

$$P = (100X) / 0.7952 (40 – X)^2$$

Figure 3-23 represents the Yamanaka soil stiffness measuring instrument. The meter has a flat face disk of area 2 cm^2 attached to a standard cone by a special device. It can precisely measure the hardness (consolidation resistance) of soft soils and other materials. The meter is a valuable equipment for obtaining data regarding quick and general measurement of stiffness of materials.

Figure 3-22 Yamanaka Soil Stiffness Meter (https://satosokuteiki.com/item/detail/1998)

3.7.2 Stiffness of silica sand No. 8 and No. 6

The stiffness of sand no.8 was measured by the Yamanaka stiffness instrument. The sand was prepared at 80% and 90% of its relative density and adding 5% of water to replicate the test conditions in S8, S8-B and S8(90)-B as per experimental conditions explained in Chapter 4. The sample was made in layers and placed in a container of size $100cm^3$. The stiffness at 80% of the relative density was observed to be 1.86 MPa. Similarly, the stiffness of Silica sand No. 6 was measured. Silica sand No. 6 (referred to as S6 in model test) is slightly coarser as compared to No. 8. The test conditions for S6 were kept as same with S8 i.e., 80% of relative density with 5% added water to assist the compaction process and 90% for S6(90)-B test. Table 3-5 represents the corresponding stiffness for S8 and S6 for different relative densities as determined by Yamanaka soil stiffness meter. The ascending stiffness values again justified that the surrounding ground material became stronger with increasing the relative density of the soil for model tests.

Table 3-5 Surrounding ground stiffness for different Silica sands at different relative densities

Soil Sample	Relative Density (%)	Stiffness
No. 8	80	1.86 MPa
No. 8	90	2.04 MPa
No. 6	80	2.06 MPa
No. 6	90	2.27 MPa

3.8 SUMMARY

The expansion and strength characteristics of expansive soils sample are discussed in this chapter. The lab-prepared samples mixed at different weight ratios were tested for swelling pressure and expansion. A swelling pressure of 161.75 kPa was observed for B2575 sample. This sample fell in the range of highly swelling type soil. This sample was selected for model tests in further research. The cyclic loading, unloading, and reloading were carried out to evaluate the soil-water interaction curves. The strength of these samples was evaluated by unconfined compression tests before and after the expansion occurred. It was observed that the strength of the soil reduced in general after the expansion was allowed. The surrounding ground material for model tests was evaluated by performing direct shear tests and rapid stiffness tests. It was observed that silica sand No. 8 had lower shear strength at 80% of its relative density as compared to 90%. Similarly, the silica sand No. 6 was found to be stiffer than No. 8. Silica sand No. 6 at 90% of its relative density was stiffer of all and was selected to be employed in different model tests explained in the chapters to come.

CHAPTER 4 FRAMEWORK OF THE MODEL TESTS

4.1 INTRODUCTION

The comprehension of expansive phenomenon with underground structures is a complex process. The time-dependent implications of expansive soils on tunnels are imperative to quantify the additional stresses on them and their consequent long-term performance. The fluctuations in overburden pressure, changes in stresses and moisture variation in expansive surrounding ground strata are key factors influencing the tunnel stability. The expansion mechanisms and consequent deteriorations of the tunnels in expansive strata is of prime importance. As tunnels are constructed in varying dimensions, full-scaled laboratory experimentation is hard to manage because of huge costs, difficulty in execution and repetitions. Although, reduced-scale model studies can be effectively carried out to realize the core mechanisms. The model studies can replicate the actual field conditions to the closest possible however there may still be some shortcomings appraising the complex field phenomenon. However, it is vital to replicate field conditions at laboratory scale to have an insight of real processes. This study has been based upon conduction of model tests. A number of research studies have been carried out by utilizing the reduced-scaled model tests. The unique feature of this research is to employ real expansive soil and surrounding ground medium to evaluate the time-dependent behaviour of tunnel experiencing the swelling pressure upon saturation. One of the critical constraints of the model test was to ensure homogeneity of ground preparation around the tunnel for each trail test. The location and placing of the tunnel, overburden ground preparation, and water application for saturation were carefully taken care of to ensure maximum accuracy and repeatability. Model tests with presence of expansive soils, varying the location of the expansive soil, and varying the surrounding ground stiffness were performed for their consequent time-dependent impacts on underground structures. This chapter is based on the outline of the model test apparatus and procedure utilized in this study to evaluate the long-term impacts of expansive soils on mountainous tunnels.

4.2 SIMILITUDE PRINCIPLES FOR MODEL TESTS

It is imperative to guarantee the similarity between the replication of the field geotechnical processes in the laboratory prototypes. The similitude principles must satisfy the relationships for boundary conditions, material arrangement and symmetrical forms etc. for physical model-based studies. The basic similarity rules (Castro et al., 2007; Li et al., 2021) were followed in this research. As the size plays a critical role and can have a minor effect on exact similarity rules (Castro et al., 2007) , the similitude analysis has significant importance for model studies. The similarity conditions are inferred based on principles of physical and geometric equivalence, boundary conditions and differential equations satisfying the equilibrium (Huang et al., 2013). It is hard to manage exact similarities between the prototype and field geotechnical situations hence some of the parameters with diversions have to be accepted (Yan et al., 2015). The model test tank for this study was designed at a scale of 1:100 for evaluating the log-term impacts of expansive soils on tunnels. The general laws of similarity deduced for this study as per the similarity theory are enlisted in Table 4-1. The subscript ‘p’ is presented for prototype while ‘m’ is for model test conditions.

Table 4- 1 General law of similitude for model tests

Parameters	Description	Reduced scale
Length	L_p / L_m	100
Displacement	d_p / d_m	100
Elastic Modulus	E_p / E_m	100
Stress	σ_p / σ_m	100
Time	T_p / T_m	100
Permeability (saturated)	μ_p / μ_m	1
Strain	ε_p / ε_m	1
Density	γ_p / γ_m	1

4.3 MODEL TEST EQUIPMENT

Figure 4-1 represents the model test setup and its schematic diagram. The setup comprised of a steel tank of size 600 mm in length and height while 200 mm in width. The tank has opening at the base for water inlet. The tank was designed to incorporate a down-scaled horse-shoe tunnel model having a length of 200 mm, diameter of 100 mm, and height of 80 mm. The tunnel had appropriate size openings for installing the pressure measurement gauges at various locations. The pressure measuring circular gauges of 7.5 mm diameter and 0.5 mm thick were installed at the crown, shoulder, spring-line, wall and invert section of the tunnel.

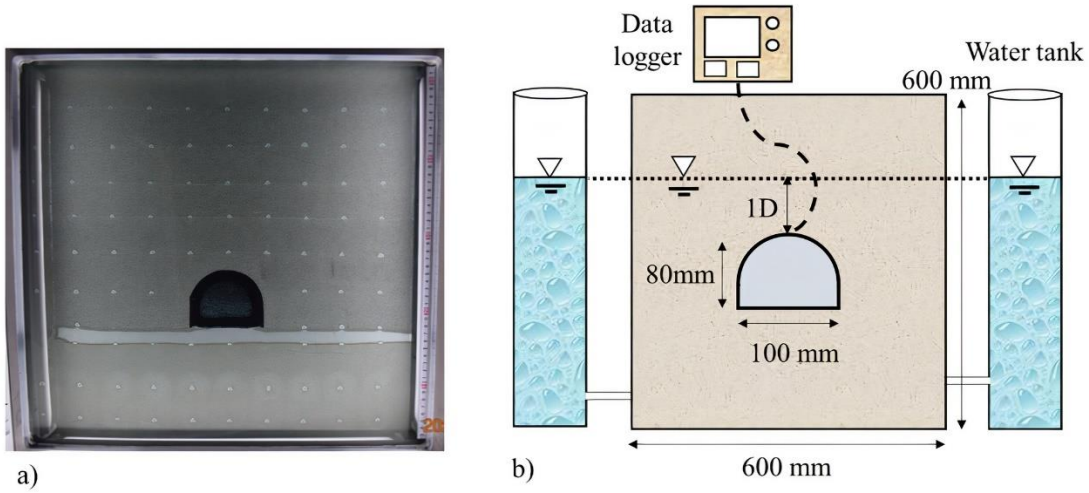

Figure 4-1 Model test equipment and its schematic diagram

The gauges were ultra-small and sensitive pressure measuring equipment optimal for the model tests. The gauges were specifically designed for the model test by Tokyo measuring instruments laboratory (TML) and designated as PDB-200KPB. The gauges had the ability to measure pressure

under water as well. The ideal temperature for measurement was 22ºC while optimum humidity was 25%. These gauges were installed on both sides of the tunnel and were guided out of the model tank through an opening from the tunnel and the supportive back ring installed on the tank to keep tunnel in its position. The tunnel invert was placed at a height of 17 mm from the base of the tank.

Table 4- 2 Contents of the model tests

Element	Contents and conditions for experiment
Soil Chamber	The tank was designed for evaluating the expansion impacts on the tunnel with expansive soil and surrounding ground material. (600 mm * 600 mm * 200 mm).
Tunnel Model	Horseshoe shaped tunnel, (100 mm * 80 mm * 200 mm).
Model Scale	The model is downscaled to 1:100.
Expansive soil	As the expansion is caused by specific expansive soils, lab prepared expansive soil samples were used.
Surrounding Ground	The surrounding ground was prepared by Silica Sand No. 8, No. 6, and concrete block

The gauges were connected to a data logger for continuous recording of the pressure on them. The water inlets at the base were connected with the water tanks for carrying out the process of saturation. The water level could be controlled in water tanks as per the different conditions of the test.

The location of gauges on tunnel model is represented in Figure 4-2. The nomenclature for the gauges was adopted as C for crown, S for shoulder, SL for spring-line, W for wall and I for invert section. The subscripts ‘l’ represents the left side while ‘r’ represents the right and ‘c’ for centre. The overburden pressure was simply the pressure exerted by the surrounding ground material on the gauges. The expansion process is demonstrated in this study by placing the expansive soils sample around the tunnel model as depicted in Figure 4-2. The glass front of the model was installed to assist the photography during the performance of the test as the surrounding ground movements in context of expansion of expansive soils were evaluated through particle image velocimetry (PIV). The objective of the model tests is to reproduce the expansion mechanism and behavior and to verify its detrimental effects on tunnels. Table 4-2 summarizes the contents of the model tests.

The tunnel material was rigid and non-deformable. If the tunnel lining is considered deformable, the tendency of the swelling pressure application on tunnel will significantly impact the pressure application as compared to what evaluated in this study. Considering the field conditions, the tunnel structures are in between the rigid and the free state. As in the model test conducted for this study,

the tunnel was firmly fixed in its position, the swelling impacts evaluated in this research are closer towards fixed tunnels. As the prime purpose of this research was to evaluate the time-dependent swelling pressure application on tunnels, therefore, for simplification of the model tests, the boundary conditions of a fixed tunnel structure were adopted. Although not perfectly in plain-strain conditions, this was one of the testing circumstances. The further evaluation can be carried out with partially fixed or free tunnel structure and a comparison can be drawn for future study.

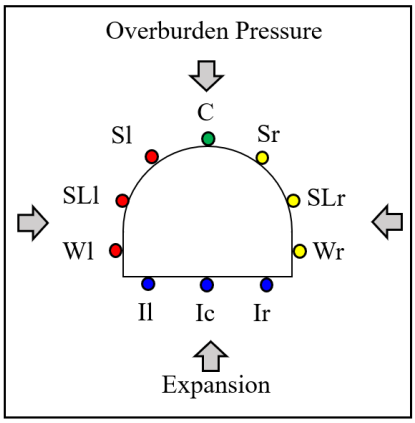

Figure 4-2 Location and description of gauges installed in tunnel model

4.4 EXPERIMENTAL PROCEDURE FOR THE MODEL TESTS

The experimental procedure involved placing the porous wire gauze along with filter paper at the bottom of the model tank. The glass front of the model was marked with grading lines for placing of surrounding ground material and expansive soil location as the case may be. The preparation of the base ground of the tunnel was next step. Silica sand No. 8, No. 6, and concrete blocks were used in this study as the ground under the tunnel. The sand was placed in layers of 50 mm thick each to ensure constant density throughout the base ground. Each layer was pointed by white clay dots for specifying the grid for PIV analysis. The expansive soil layer was placed on its location as per the experimental conditions explained in the section to follow. In all the model test cases, the expansive soil layer was not placed throughout the length of the model to help quicken the saturation procedure. The expansive soil length of 50mm on both sides of the model was discontinued thus making it be saturated from both top and bottom in the process. The tunnel was placed on its fixed location and locked by the back ring which had an opening for the wires of the gauges installed in the tunnel to be connected to the data logger. The remaining surrounding ground around the tunnel was prepared. This study was carried out by keeping the overburden height equal to three times the diameter of the tunnel which makes it a shallow to deep tunnel (Andreotti and Lai, 2019).

As the tunnel was placed in its location, the gauges were connected to the data logger for continuous data recording of the pressure on the gauges. The frequency of data recording was set to 10 seconds interval. The increment of pressure by placing each layer was represented by the gauges until the overburden material was completed as per the methodology of the model test. As soon as the setup was completed and initial pressures on the gauges due to overburden was recorded, the water was

inserted from the inlets to start the saturation process. Water movement was modeled from bottom to top replicating the upward groundwater movement in geological repositories.

The density of the expansive soil sample was maintained by placing it in smaller sections in the model and compacting until the required volume was achieved. These sections were separated by acrylic plate structure designed to divide the layer's area into equivalent sections as represented in the methodology flow chart of the model test in Figure 4-3. Swelling pressure of an expansive soil with identified preliminary physical conditions, is the pressure at which saturation of the soil does not originate a failure or swelling distortions in the sample. It is simply the stress state to keep constant volume of soil sample without distortion during soaking mechanism (Serratrice and Soyez, 1996). The water intrusion in the assembly triggered the swelling mechanisms and depending upon the location of the expansive soil layer, the corresponding gauges responded with additional pressure in addition to the overburden pressure.

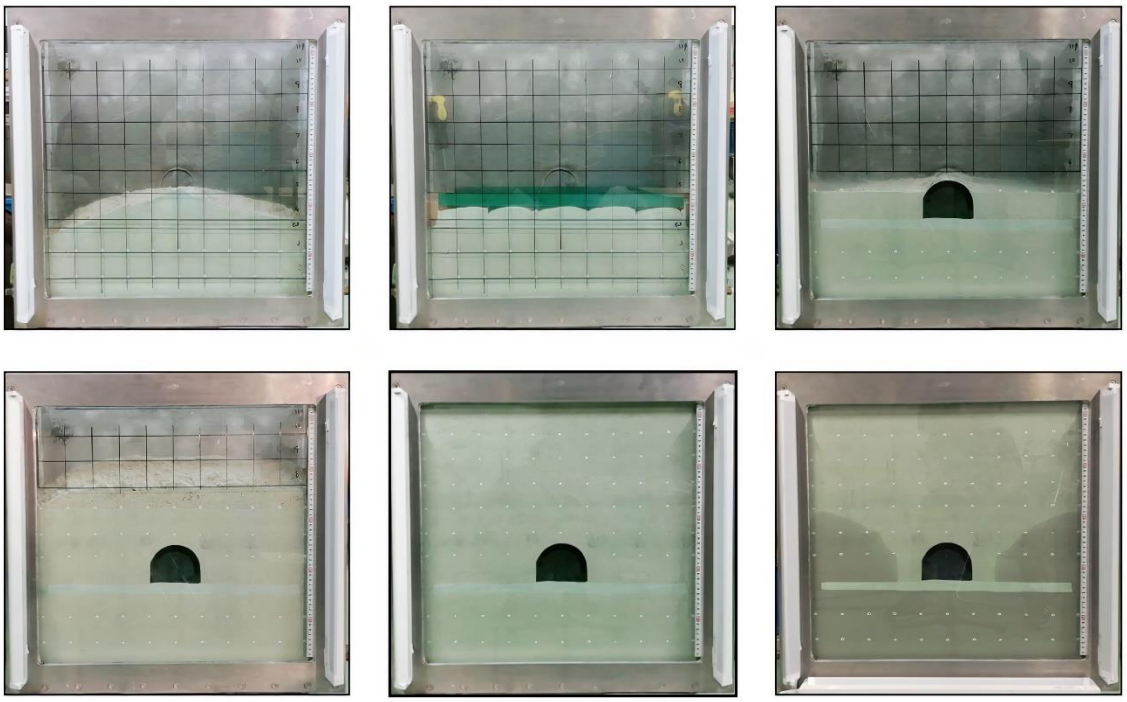

Figure 4-3 Step by step procedure for model tests

The glass front of the assembly was captured through a camera for specified time-period. The images were analyzed for the movements of the surrounding ground soil in response to the expansion of expansive layer. The pressure variation on the gauges was recorded and the model test was continued until the gauges gained a constant state of final pressure or showed negligible change (<0.1%) in swelling pressures with further elapse in time. The step-by-step procedure of model tests is further illustrated in Figure 4-3. The figure represents the model test S8-B in detail and other tests were conducted in similar way for other conditions. The different conditions of the model tests adopted for this study are explained in detail in section 4.5 of this chapter.

4.5 EXPERIMENTAL SCENARIOS FOR THE MODEL TESTS

This model test-based study has been divided into various scenarios to evaluate the time-dependent impacts of expansive strata on tunnels. These scenarios are explained in this section in detail.

4.5.1 Presence of expansive soils

The model tests-based study was carried out based on different conditions. Initially the test was carried out by using silica sand No. 8 as the surrounding material around the tunnel with no expansive soil in the model. The soil was placed in layers and compacted at 80% of the relative density of the sand followed by saturation. The outcomes were compared with another test in which a 20 mm thick expansive soil layer was placed at the invert section of the tunnel with rest of the process identical. The comparison was made between the pressure recorded on gauges corresponding to the presence of the expansive soil. These tests are correspondingly represented as 'S8' and 'S8-B' in Table 4-3 which summarizes the experimental conditions of the model tests. As explained in Chapter 3, the stiffness of Silica sand No. 8 was measured to be 1.86 Mpa, the stiffness of No.8 did not reflect a significant percentage of expansive pressure on gauges in tunnel model as compared to the free swell pressure of the expansive soil sample in free swell tests. Therefore, the surrounding ground was replaced by a stiffer Silica sand No. 6 having stiffness of 2.06 MPa and model tests were repeated as for sand No. 8 case. These tests were named as S6 and S6-B in the experimental conditions. The comparison of all these tests was made to evaluate how the presence of expansive soil in the geological layer around the tunnel invert would impact the tunnel security in context of time. Since the surrounding ground was replaced by silica sand No. 6 in the later half, a part of this condition also signifies how the surrounding ground stiffness is involved in presenting the expansive soil's ability to impact the tunnel structure. Figure 4-4 represents the front view of these tests.

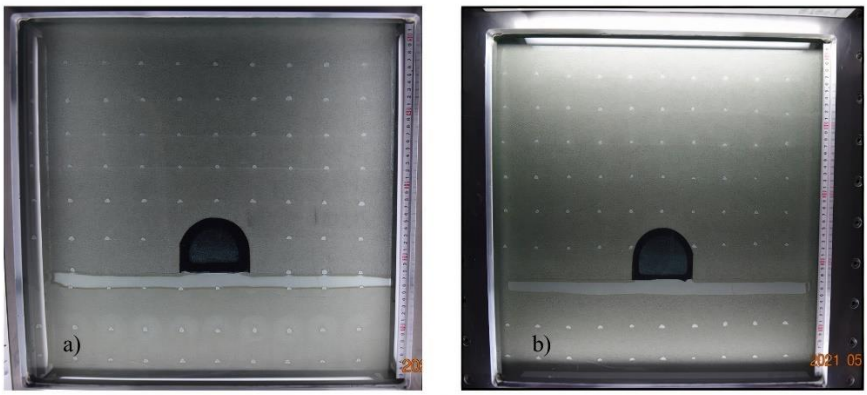

Figure 4-4 Model tests for expansive soil presence a) S8-B and b) S6-B

4.5.2 Location of expansive soils around tunnels

In further testing, a scenario was developed to signify how the location of expansive soil layer around the tunnel would impact the corresponding sections of the tunnel structure. In this condition, the expansive soil layer was placed around the crown section, shoulders and walls of the tunnel

thereby helping to comprehend the impacts of location of expansive soils on the tunnel sections. The surrounding ground for these tests was kept as silica sand no. 6 at 80% of its relative density. The S6-B case explained in earlier section was included in discussion as the location of expansive soil in that case was the invert section of the tunnel. These four tests helped in adjudicating the effects of location of expansive soil in the geological strata and the time-dependent deteriorations of the tunnel structure in response to this additional pressure. These model tests are abbreviated as S6-T for top case, S6-S for shoulder case, and S6-W for the expansive soil placed around walls of the tunnel on both sides. The term S6 with each of these tests represents that the surrounding ground was prepared with silica sand No. 6 at 80% of its relative density. Figure 4-5 represents the model tests performed for location of expansive soil at Crown, shoulder and wall section of the tunnel.

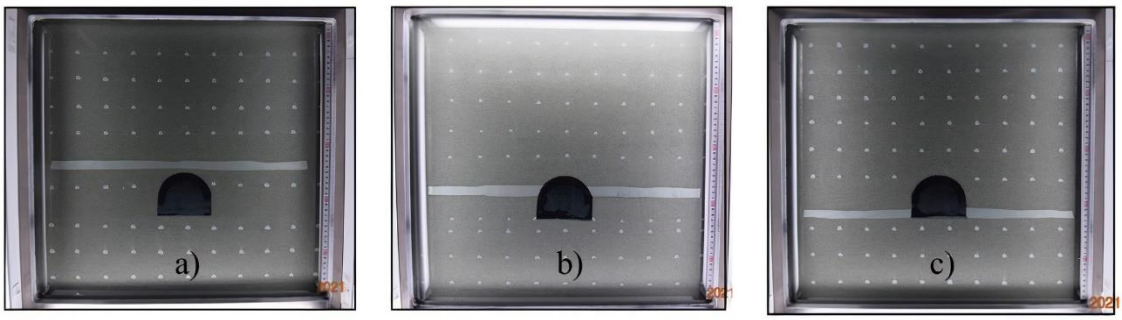

Figure 4-5 Model tests for expansive soil location a) S6-T, b) S6-S, and c) S6-W

4.5.3 Varying the ground under the tunnel

The impacts of expansive soils on tunnels in context of time was also studied by variation of the stiffness of the surrounding ground beneath the tunnel model. The impacts of surrounding ground stiffness were studied by comparing the time-dependent expansive pressure variation on the tunnel heave section using silica sand No. 8 and No. 6 beneath the tunnel at 90% of their relative densities while the rest of the ground being silica sand no. 6 at 80% of its relative density. As for all the model tests, a 20 mm thick expansive soil layer was placed under the tunnel in all these cases. These model tests are nominated as S8(90)-B and S6(90)-B respectively. In another test, the ground under the tunnel was replaced by stiff concrete blocks and expansive soil layer over them with the rest of the ground being silica sand No. 6 at 80% of its relative density. The perforated concrete blocks were overlaid by holed aluminium sheets to allow water to interact with expansive soil layer thereby making an identical condition with the rest of the two cases. This test is represented as Bk-B in this study. In all the model tests explained above, the expansive soil layer was discontinued by 50 mm on both sides of the model to ensure that water can pass by the layer and interact with the soil above the expansive layer to ensure that the layer is being saturated from both top and bottom side. This was done to shorten the saturation period and keep the boundary conditions identical. Figure 4-6 represents the model tests for different ground under the tunnel for studying the impacts of surrounding ground stiffness on expansion representation on the tunnels.

Table 4- 3 Experimental scenarios for the model tests

Location / S. Ground	Relative Density	No ES	Bottom	Top	Wall	Shoulder
Sand No. 8	80%	S8	S8-B	--	--	--
Sand No. 6	80%	S6	S6-B	S6-T	S6-W	S6-S
Sand No.8 UT, else No.6	90% UT, 80% above	--	S8(90)-B	--	--	--
Sand No.6 UT, else No.6	90% UT, 80% above	--	S6(90)-B	--	--	--
Blocks UT, else No.6	80% above	--	Bk-B	--	--	--
Sand No.6 UT, else No.6	90% UT, 80% above	S6-1D (Expansive soil at 1D below tunnel invert				

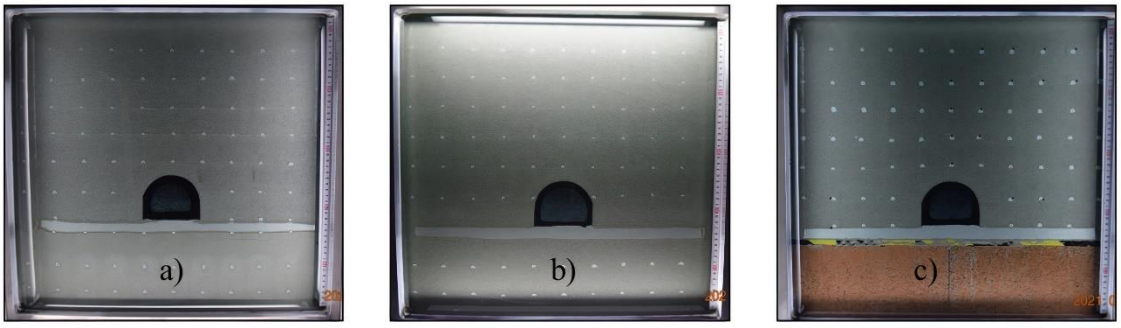

Figure 4-6 Model tests for ground stiffness a) S8(90)-B, b) S6(90)-B, and c) Bk-B

The model tests conditions explained in this section are summarized in Table 4-3. The nomenclature adopted for each test is listed. The 'UT' stands for the ground characteristics under the tunnel and above for the soil above the tunnel. Similarly, 'ES' is for expansive soil.

4.6 CALIBRATION AND VALIDATION OF PRESSURE GAUGES

The model test explanation included the installation of the gauges in the tunnel model. The gauges were designed to capture the pressure increment during the performance of the test owing to expansion of expansive soils. The gauges were made by Tokyo measurement instruments lab. As the gauges were installed in the tunnel model, it was deemed necessary to calibrate the gauges against known loads to validate their accuracy during the model test performance. For this purpose, the tunnel with installed gauges was placed in the model tank in vertical position such that all the gauges were at same level of 100 mm from the bottom of the model. The horizontal lines for 100 mm height were drawn on the glass to specify the water level for reference pressure. The model tank was filled with water until the centre of the gauges. As the water stabilized, the data logger was started to collect the pressure data for the gauges in level with water level.

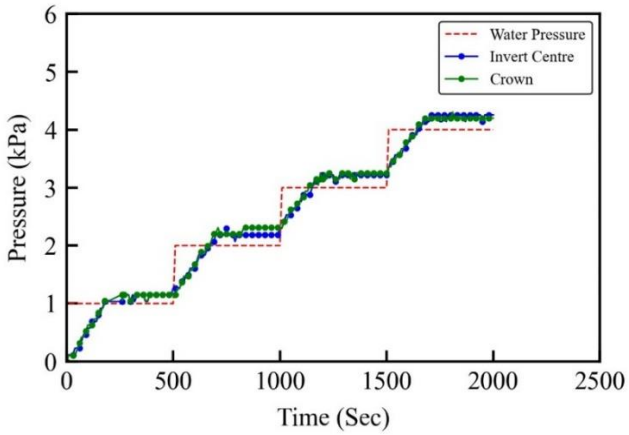

Figure 4-7 Pressure comparison for invert centre and crown gauges before calibration

The pressure increment of 100 mm of water was set as the limit and the gauges were initially loaded with 100mm height of water for which the corresponding pressure was 0.98 kPa. The pressure was allowed to settle down and measured for 500 seconds until a further addition of 100 mm height of water in the model tank which took the pressure level to 1.96 kPa. I the similar way, the pressure for 400mm column of water was added on the gauges and their corresponding response to this added pressure was recorded. Figure 4-7 represents the pressure on the crown and invert centre gauges with the coefficients as supplied by the company.

The pressure represented by the gauges was a bit over-estimated. The pressure of 4 cm column of water is 3.92 kPa whereas the pressure gauges represented was 4.25 and 4.2 kPa respectively. Consequently, the pressure coefficients of these gauges were adjusted / reduced to get the right pressure as per the actual pressure on the gauges.

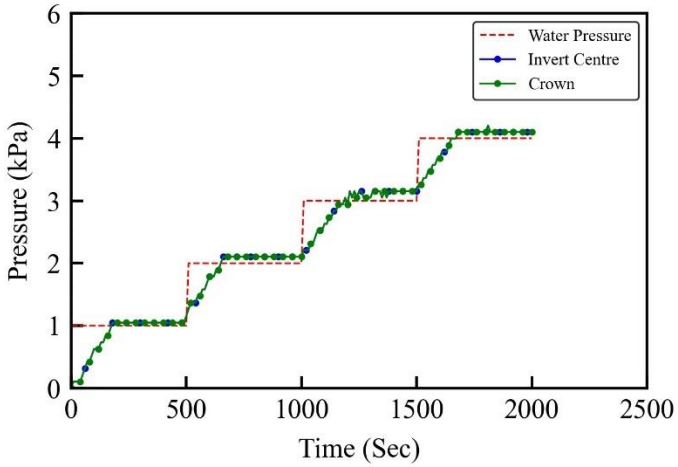

Figure 4-8 Pressure comparison for invert centre and crown gauges after calibration

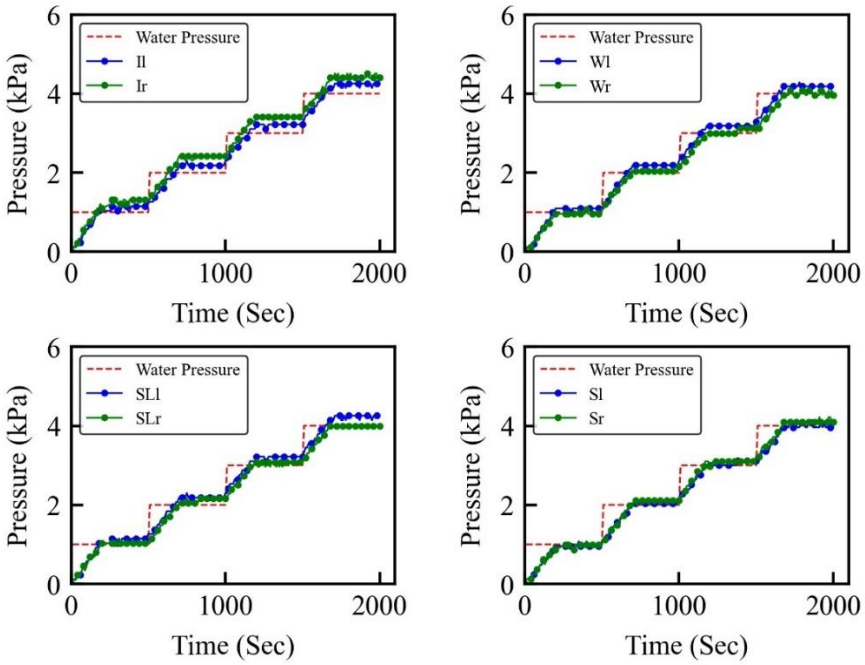

Figure 4-9 Pressure comparison for mirror-image gauges before calibration

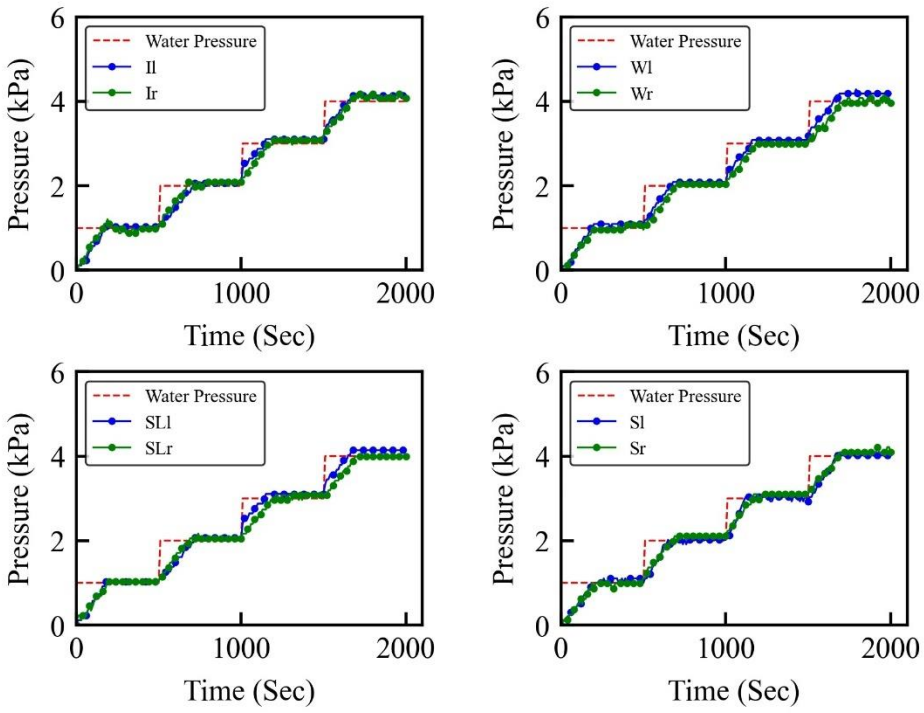

Figure 4-10 Pressure comparison for mirror-image gauges after calibration

Figure 4-8 represents the pressure on the same gauges after calibrating the gauges and justifying the validation for further using the gauges for model test for actual and correct representation of the pressure. On the similar lines, Figure 4-9 and Figure 4-10 represent the sub-plots for water pressure before and after calibrating the gauges and performing the water column pressure test. It is to be noted gauges on the invert edges, shoulders, spring-lines and wall sections are combined in these plots.

4.7 PARTICLE IMAGE VELOCIMETRY (PIV) ANALYSIS

The particle image velocimetry (PIV) analysis technique was utilized in this study to evaluate the displacement of the nodes of the surrounding ground in response to the expansion of expansive soils. PIV is a visual tool to estimate the velocity of the particles and was initially utilized in the field of fluid mechanics for flowing particles (McKenna and McGillis, 2002). The analysis can be utilized in the field of geotechnical engineering to assess the movement of the soil particles as the particles act as the tracers themselves. The photos taken during a soil mechanism can be used to evaluate various deformations as was done in this research (White et al., 2003). The model tests were further analysed using the images captured at the beginning, during and at the completion of the tests. Particle image velocimetry (PIV) analysis was performed using the PIV module of FLOWNIZER 2D, a state-of-the-art image processing engine transforming the flow/movement into vectors. The software divides the image into a mesh of equally spaced grids and creates a displacement vector for each grid. The displacement function was applied on consecutive images and co-relation function is developed between them to estimate the amount of displacement (Cao et al., 2014). The corelation coefficient (R) can calculate the intensity of examination between two photos. The nodal displacements were converted into volumetric and deviatoric strains of elements formed as a matrix of four displacement nodes integrated through Gauss integration method.

4.7.1 Parametric settings for PIV analysis

The parametric settings of the PIV software FLOWNIZER included the setting of the target image for calibration. A know displacement of two points as measured during the model test performance by placing the clay particles at grids was initial input to the software. The particle image was selected as the first image for analysing the displacement with the consequent following images at different intervals of time to analyse the time-dependent displacement in accordance with time dependent swelling response simultaneously. As soon as the model assembly was provided water, the hourly images from the front were started. In this way, the first image was taken when the soil state was dry (or nearly dry as 3-5% water was added to the soil before placing in model to assist in damping). As the water interaction with whole assembly took only 5-10 minutes initially, the brightness of the second image until the completion of the test remained more or less at the same level. Consequently, the image analysis was performed by comparing the second image of the camera with consequent following images in which the displacement was monitored. However, the difference of the displacement for the first- and second-hour image was evaluated to assess the displacement for dry and partially saturated initial state of the soil in the model test. It was found that for S8-B case, that displacement of 0.0097 mm occurred as compared to final displacement of nearly 2 mm. This displacement is less than 5% of the total displacement. To ensure the accuracy of image analysis, the second image was used to evaluate the time-dependent displacement of the whole

model test and the dry state image was not incorporated. In this way the brightness of the images was kept more or less constant for whole duration of model tests.

The tunnel front was masked as it was fixed in its location and no displacement was expected. Although the analysis includes velocimetry, for simplicity, unit time was considered between images converting the velocity into simple displacement. The interrogation grid was set equal to the glass front of the model tank. A grid interval of 10mm by 10mm was set to evaluate the nodal displacement. The output after the analysis was set to represent the displacement both through contours and vectors. The vectors depicting both the direction and the magnitude of the displacement for each node were utilized.

4.7.2 Validation of PIV analysis

The validation of th PIV analysis was carried out before the actual displacement analysis. One photo of the model test was cropped from top by one pixel. The same photo was cropped from the bottom by one pixel. The total difference between the two cropped images was two pixels. The photos taken during all the model tests had DPI (dots per inch) of 300. The cropping of 1 pixel from top and bottom would mean a displacement of 0.085 mm of the image for one pixel cropping. A cumulative displacement of 0.17 mm was expected to be calculated by the PIV analysis for this case as the relationship between the DPI and distance is given by following formula:

$$\text{Distance in mm} = (\text{Pixels of the image} * 25.4) / \text{DPI}$$

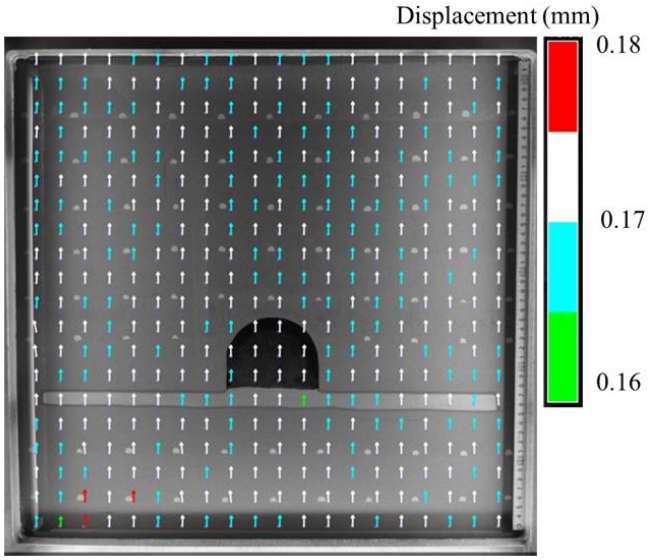

Figure 4-11 Validation of PIV analysis for known displacements

The validation of the PIV analysis was carried out by using these two images in FLOWNIZER software and a pre-determined displacement of 0.17 mm was expected to be a part of the outcomes. Figure 4-11 represents the calculated displacement for this scenario. The output represents that most of the image moved by a distance within a range of 0.17 mm justifying the accuracy of the PIV analysis for this model-based study. The validation was carried out for higher number of pixels as

well and similar results were observed that were in correspondence with the displacement initiated with the original image after cropping.

4.8 SUMMARY

This chapter summarizes the similitude analysis performed for carrying out the model test for evaluating the impacts of expansive soils on long-term stability of mountainous tunnels constructed in vicinity of expansive strata. The lab-prepared model equipment was explained in detail followed by the experimental procedure adopted. There were different scenarios developed for understanding the tunnel response to expansive soils involving their presence, location and surrounding ground stiffness etc. These scenarios were outlined. The process of calibrating and validating the pressure gauges installed on the model of tunnel was discussed. The surrounding ground displacements were calculated through PIV analysis in this study. A section of this chapter explained the PIV technique along with relevant software used in this study and the process of validating it for accurate estimation of displacements for the model tests.

CHAPTER 5 RESPONSE OF TUNNEL LINING TO EXPANSIVE SOILS

5.1 INTRODUCTION

As per the experimental conditions and the outline of the model tests explained in chapter 4, this chapter concentrates on the evaluation of the time-dependent variation of swelling pressure on tunnels due to presence of expansive soils in the rock-mass around the tunnels. The model tests were conducted by preparation of surrounding ground around the tunnel using the silica sand No. 8 and No. 6. Initially, the response of the tunnel lining was adjudicated by placing the non-expansive soils below and above the tunnel to capture the magnitude of the overburden pressure in the model tests. In the later model tests, same conditions were applied but with provision of 20 mm thick expansive soil layer placed at the invert section of the tunnel. The swelling of the layer upon saturation imposed additional pressure on the tunnel invert section which was recorded for each time step to evaluate the time-dependent impacts of expansive soil availability in the geological repositories around the tunnels. The surrounding ground movements and the corresponding strains were evaluated for both of these cases. In addition, a comparison was made between the two cases based on the difference of the material used as the surrounding ground. The time-dependent deformation due to presence of expansive soils is explained in detail in this chapter.

5.2 MODEL TESTS FOR SILICA SAND NO. 8 AS SURROUNDING GROUND

5.2.1 Silica sand No. 8 test (S8)

Figure 5-1 represents the experimental conditions for the model test in which the tunnel is surrounded by silica sand No. 8 as the surrounding ground. The surrounding ground was initially prepared by placing 50 mm layers of the sand at 80% of its relative density and with 5% of water content to help in the dumping of the material in the available volume as per the relative density and the mass of the sand. The relative density of Silica sand no. 8 was calculated by the laboratory test performed for maximum and minimum density test. The maximum density was calculated as 1.54 g/cm^3. Consequently, the 80 % relative density was 1.232 g/cm^3. The tunnel was placed in its position. The pressure measurement gauges were connected to the data logger for continuous recording of the pressure variation during the model test. The rest of the surrounding was correspondingly prepared in accordance with the relative density of 80% in layers to ensure the correctness of the overburden pressure measurements. Upon the completion of the application of the overburden pressure on the tunnel, the model was saturated from the inlets provided at the base of the assembly to evaluate the saturated overburden pressure applied on different sections of the tunnel with the surrounding ground as Silica sand No. 8. This test is designated as **S8** in the nomenclature adopted for different model tests carried out for this research program as highlighted in the model test scenarios in Chapter 4.

5.2.2 Expansive soil at invert section (S8-B)

The evaluation of time-dependent impacts of expansive soils on tunnels was carried out by performing another model test. The experimental conditions in this case were kept same as S8 test but a 20 mm thick layer of expansive soil was placed at the invert section of the tunnel. The ground beneath the tunnel was prepared as per the previous test including the expansive soil layer placed in

different sections with fixed volume and dry density of the bentonite-Toyoura sand mixture. These sections collectively constituted the expansive soil layer under the tunnel invert. The mass of the expansive soil sample was calculated by keeping the dry density of the mixture of Toyoura sand and bentonite as 1.60 Mg/m^3 (Cui et al., 2015).

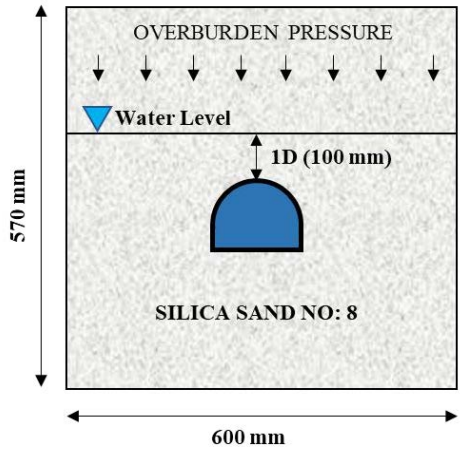

Figure 5-1 Schematic diagram for S8 model test

The remaining surrounding ground preparations were kept same as S8 test. The tunnel gauges were connected to data logger as soon as the tunnel was placed in its position to ensure the recording of the overburden pressure with addition of each overlaying layer of sand No. 8. The surrounding ground was prepared until the height of the overlaying soil was maintained at a height equal to three times the diameter of the tunnel (3D) which was 300 mm in this case. Having completed the assembly, the whole soil mass was saturated by water provisions at the inlets at the base of the model. The water level was maintained at a height equal to the diameter of the tunnel (1D) in the water tanks placed aside.

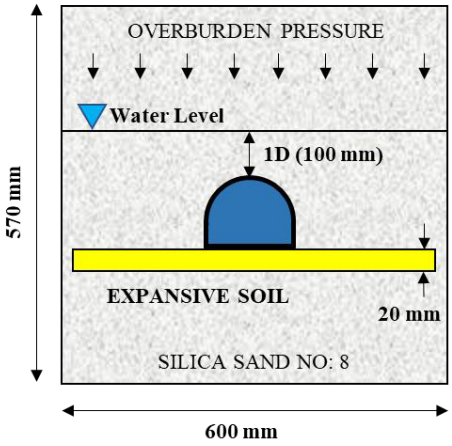

Figure 5-2 Schematic diagram for **S8-B** model test

The water started interacting with the expansive soil layer and the process of expansion began. This test was referred to as S8-B in the nomenclature adopted in this study where 'B' signifies the

location of the expansive soil layer at the bottom of the tunnel invert. The schematic diagram of this test is represented in Figure 5-2.

5.3 RESPONSE OF TUNNEL LINING IN SILICA SAND NO. 8

5.3.1 Tunnel response to S8

Figure 5-3 represents the response of the tunnel lining to the pressure exerted by overburden soil for S8 test. The pressure kinetics showed that the as the overburden layers were placed the consequent rise in pressure was observed by the corresponding gauges. Upon the completion of the surrounding ground preparation, the water insertion slightly added to the pressure by amount that was required to saturate the soil and is represented as 'Ss' in the graphic signifying the start of saturation. The pressure variation for the pressure measurement gauges installed at the invert section are intentionally represented in different colours as these gauges would experience additional pressure in the S8-B case where expansive soil was placed at the invert section.

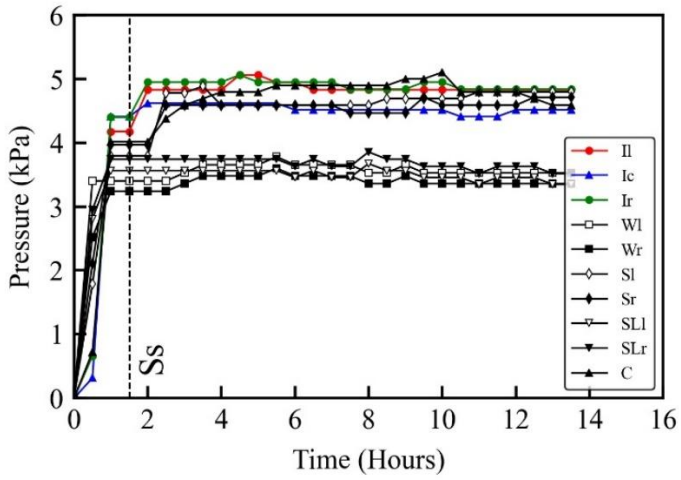

Figure 5-3 Pressure kinetics at different sections of the tunnel for **S8** model test

The invert section of the tunnel experienced 4.83 kPa of saturated overburden pressure on the left and right gauges. There was a slight reduction of pressure at centre invert gauge which represented 4.5 kPa of overburden pressure. As the tunnel was locked in its position, this reduction in pressure was observed for the centre gauge. The gauges on the wall experienced 3.52 kPa pressure as these gauges were perpendicular to the overburden pressure of soil. The gauges on spring-line and shoulder sections of the tunnel on both sides represented 3.5 and 4.8 kPa respectively. Similarly, crown represented an overburden pressure of 4.58 kPa. The test was continued for certain period until the rate of change in pressure was negligible for a long enough time. Figure 5-4 represents the pressure magnitude on each gauge on tunnel based on their location for S8 model test.

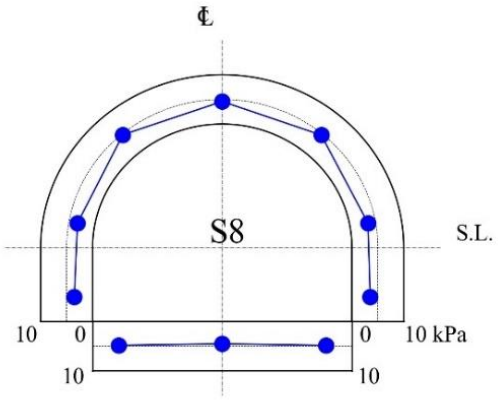

Figure 5-4 Representation of pressure at different sections of the tunnel for **S8**

5.3.2 Tunnel response to S8-B

Figure 5-5 represents the kinetics of the pressure on tunnel for S8-B model test. The pressure increment was in line with S8 test initially and the magnitude of the overburden pressure was comparable. As the overlying layers of the surrounding ground were completed and saturation started, the expansive soil layer responded to water interaction and started to expand. The swelling of the layer imposed additional pressure to the invert section of the tunnel. The invert left and right gauges (Il & Ir) immediately responded to additional pressure within first 10 hours of the test and showed a rising trend with further time passing. The pressure on these sections fell down during the next 20 hours span. The reason could be the settling of the expansive soil minerals as the voids went on filling by water with the passing time. Also, the water interaction caused change in the degree of saturation of the soil. The expansive layer started to saturate from the bottom as the layer with immediate contact with tunnel invert was yet to experience the saturation because of being tightly packed under the tunnel. The sections of the expansive soil other than under the tunnel were getting saturated from both side top and bottom. Only the layer right beneath the tunnel was being saturated from the bottom side. This caused the pressure increment to relax for some time but did not remain declined for long. As the saturation of the expansive layer kept on increasing with passing time, the pressure started to rise again.

The pressure kept on rising on the invert section gauges. As the saturation kept rising, the vicinity of expansive pressure expanded and took the impacts to the wall section of the tunnel being relatively close to the expansive soil layer. The wall gauges on both sides of the tunnel started responding to the additional pressure to the swelling at a delayed span as compared to the invert section. The stuttering in the pressure representation was expected to occur as the layer beneath the tunnel kept on saturating with respect to time.

As the expansive layer pushed the tunnel structure upwards along with the surrounding ground, the gauges on spring-line and shoulder section represented with slight reduction in pressure. This happened because the upward push relieved the overburden pressure on these sections insignificantly. As the layer approached full saturation, the rate of rise of expansive pressure subsided and finally it remained constant for long enough time representing that the expansive layer has reached its limiting swell potential.

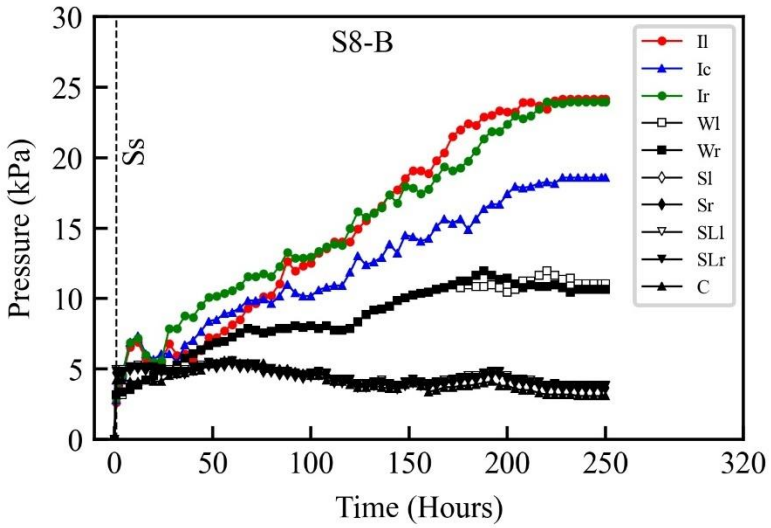

Figure 5-5 Pressure kinetics at different sections of the tunnel for **S8-B** model test

The invert edge gauges represented final pressure of 24.15 kPa while the center gauge showed 18.58 kPa at the end of the test representing a typical heaving of invert section. The wall sections represented 10.65 kPa. The rate of swelling pressure recorded on gauges was swiftest in the beginning and subsided slowly as the test went on to completion. Figure 5-6 represents the final pressure distribution on different sections of the tunnel at completion.

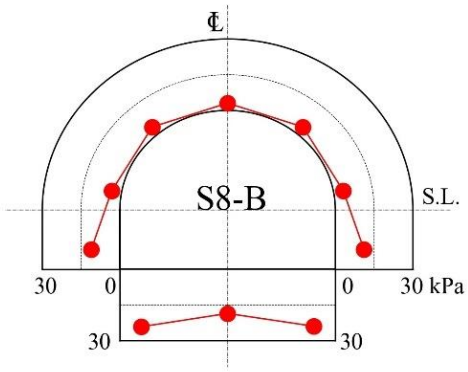

Figure 5-6 Representation of pressure at different sections of the tunnel for **S8-B**

The pressure recorded on invert gauges is around 15% of the free swell pressure of the same expansive soil in free swell test. The reason for depicting such lower percentage of expansion pressure as compared to the free-swell pressure was the absorption of the pressure by the soft surrounding ground in case of model test and the difference of boundary conditions and corresponding confining pressure. Nonetheless, the expansive pressure exerted on the invert section is nearly 5 times of the pressure as compared to the S8 case with no expansive soil around.

5.3.3 Time-dependent expansive pressure variation for S8-B

To further elaborate the time-dependent pressure variation on the tunnel, different time steps were selected from Figure 5-5 and the expansive pressure variation on the tunnel was comprehended to evaluate the time-dependent impacts of expansive soils on tunnels. Consequently, Figure 5-7 represents this variation for various time-periods for S8-B. The above transformation of time-dependent pressure variation signifies the stability of tunnel with increase in degree of saturation of expansive soil. The consequent impacts of expansive soil with time showed the critical phase where pressure significantly rose. As for this case, the pressure between 100 hours and 175 hours rose to almost double of the pressure at 100 hours. To further elaborate the time-dependent stability of tunnels in expansive strata, a dissection of the swelling curve for invert section can be divided into four zones and are enlisted below:

1- Acceleration zone
As the expansive soil came in contact with water, a sharp rise in pressure was observed. Consequently, the invert gauges represented a pressure higher than the initial overburden. The pressure kept rising and peaked until a specific value at an early stage of the swelling. It is presumed that the pressure experienced within this range would bring about the elastic response of tunnel to expansion.

2- Creep zone
Although it is for a short period of time and not very significant for this particular case, the creep zone is the region where swelling pressure tended to seize and slight reduction in pressure was observed and then remained constant for some time. The region discriminates the elastic and visco-elastic response of the tunnel to addition pressure due to expansion of surrounding soil. The zone specifies the initial setting of the soil particles. It is hard to realize time similitude for field tunnels yet, this zone signifies that although the structure may look perfectly stable, it might have undergone the elastic deformations and is now going through a probable stable zone of creep. The pressure rose initially and represented a decline within 20 hours of testing for S8-B identified as the creep zone.

3- Renaissance zone
The swelling pressure started to rise again in the renaissance zone after undergoing a pause in the creep zone. The invert gauges responded to this rise and depicted increasing pressure. The pressure increment in this phase was not as sharp as for the acceleration case, yet it kept on rising. The curve included linear and non-linear portions of rising until it reached the slow rise trend representing the limiting visco-plastic response of the surrounding ground. The range for S8-B was within 20-200 hours. The tunnel structure might start to depict structural damages like heaving and spalling of lining depending upon the location of pressure due to the expansive soil layer. The surrounding rock would start taking up the additional pressure around the tunnel and undergo deteriorations due to volume change. The consequent strength parameters of surrounding ground would reduce, and typical failures might occur.

4- Steady zone
The maximum swelling pressure of the expansive soil would be realized as the sample underwent near complete saturation. The pressure on gauges directly in contact with the expansive soil showed a steady pressure for long enough time depicting that swelling pressure had reached its limiting

value. The stability of structure depends upon the strength of the tunnel lining and surrounding ground's ability to take up the additional pressure. Majority of damage would have occurred in the renaissance zone and the stability would be investigated however if no significant damage is observed until the steady zone has reached, the structure is deemed to have taken up the additional stresses due to expansion and is referred to as benign against swelling pressure. This time-dependent analysis can be utilized to evaluate the life of the tunnels constructed in swelling strata and can help in quantifying the magnitude of swelling pressures that can be experienced by the tunnel during different phases of expansion with respect to time.

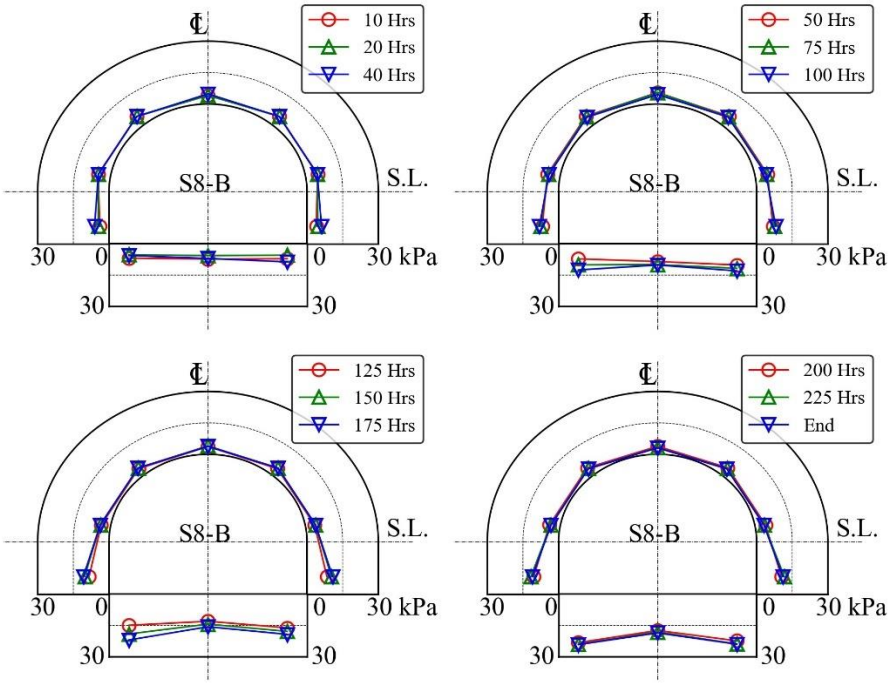

Figure 5-7 Time-dependent expansive pressure variation for **S8-B**

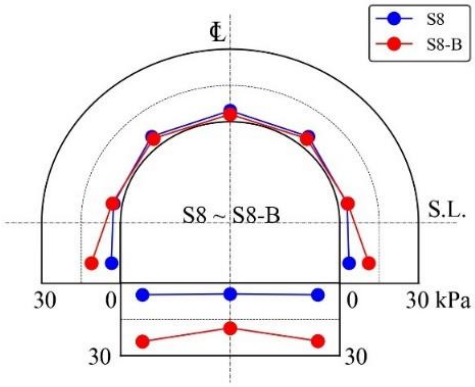

Figure 5-8 Comparison of pressure on tunnel sections for **S8** and **S8-B**

The wall sections of the tunnel on both sides also represented the same trend of swelling pressure representation as explained in four zones for invert sections however, it was slightly delayed as these sections were not in direct contact with the expansive soil. A slight imbalance in the final pressure at the invert edge gauges represent the heterogeneous degree of saturation on either side of the tunnel yet, at the completion of the test a symmetrical representation was observed on gauges that are placed on identical locations on each side of the tunnel. Having comprehend the time-dependent impacts, Figure 5-8 compares the pressure on various gauges of the tunnel for S8 and S8-B thereby signifying the impacts of presence of expansive soil undergoing saturation in soil strata around the tunnel.

5.3.4 Surrounding ground movement for S8-B

As explained in the model test setup, the model photos were captured continuously during the testing procedure. The glass front of the model was divided into a mesh to adjudicate the movement of the surrounding ground upon expansion. Figure 5-9 represents the time-dependent displacement of the node nearest to the gauge which was in direct contact with the expansive soil layer. As the expansive soil was at the invert section, the pressure observed by the invert left and right gauges is plotted against the time along with displacement of the nearest node to these gauges on the secondary axis. The term IL(P) and IR(P) consequently represent the pressure variation on left and right invert gauges respectively while IL(D) and IR(D) are the corresponding displacement curves for left and right side in the graph.

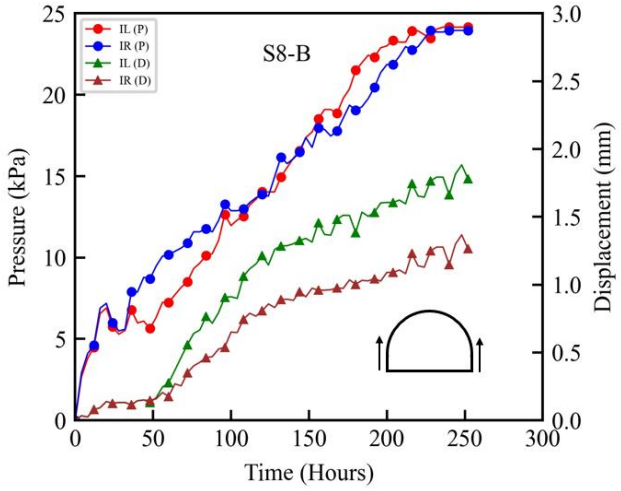

Figure 5-9 Time-dependent nodal displacement and expansive pressure near invert for **S8-B**

The displacement in the initial pressure rise zone of the expansive soil was very small as compared to the cumulative final displacement observed. During this range the expansive soil was undergoing saturation and the volumetric strain was developing to overcome the overburden pressure. This zone could also represent the stabilization of strain rate and corresponds to the constant creep state where the surrounding ground experienced no deformation for an extended period of time. As soon as the expansive push reached the limiting magnitude of overburden pressure and the swelling pressure

kept rising, a sudden surge in the displacement was observe on both sides of the invert of the tunnel. The rate of rise was quickest in this region. A slight difference in magnitude of displacement was observed in this case on both sides of the invert. The reason could be the amount of expansive pressure being applied heterogeneously on the surrounding ground on both sides based on degree of saturation of expansive soil.

As the time went on, the rate of rise of displacement got slower and its magnitude supressed significantly until the final stage reached where swelling pressure became constant. The image analysis through PIV performed for this case represented the time-dependent directional displacement of the nodes. Based on the swelling kinetics graph, different time spans were evaluated for the visual representation of the surrounding ground movements with time. Figure 5-10 represents the said displacement through contours and vectors of displacement for these specific time periods.

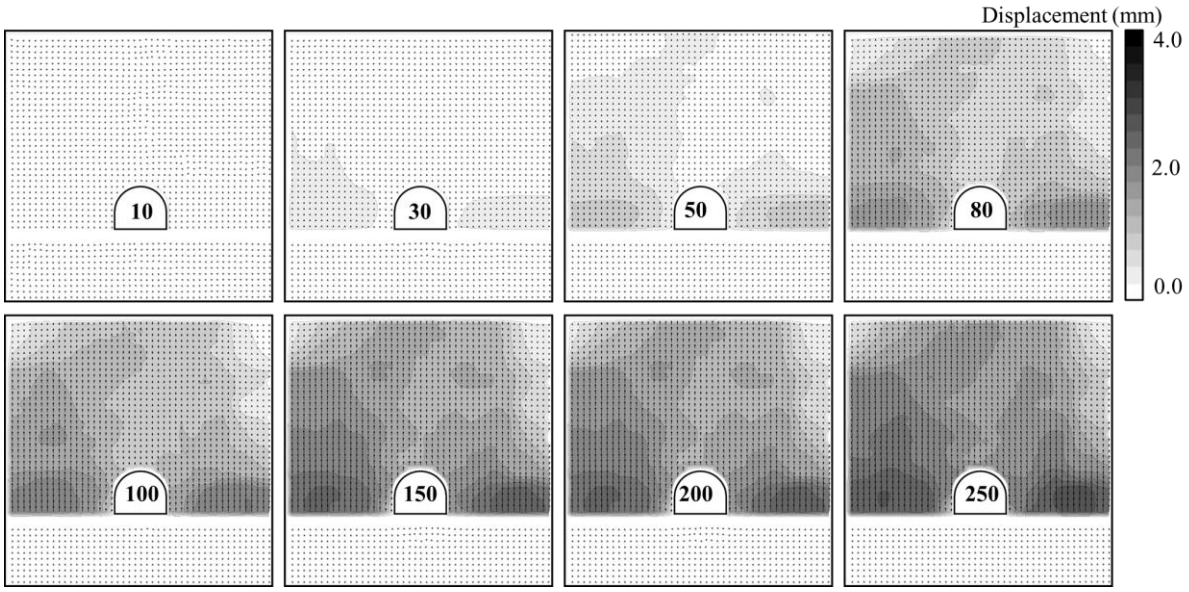

Figure 5-10 Time-dependent nodal displacement around tunnel invert for **S8-B**

The deformation of the surrounding ground initiates slowly due to swelling pressure and rises with further water interaction and rise in degree of saturation of expansive soil strata around the tunnel. Majority of displacement occurred during the creep zone where swelling pressure slightly subsided and reached a steady state with expansive soil being saturated. The results suggest that even the structure itself might be experiencing huge additional pressure of expansion yet, the surrounding ground may seem to exist in stable conditions.

A cumulative displacement of 1.76mm and 1.26mm was observed near the invert section on left and right side respectively. The displacement right above the tunnel is ceased as the tunnel model is locked in its position and the pressure exertion above the crown is restrained vertically. Major displacement is observed right above the expansive soil layer and as the distance from the layer increases, the displacement slowed down. The analysis reflects that the magnitude of the deterioration near the tunnel buried underground would be a lot more as compared to experience at the exposed surface.

5.4 MODEL TESTS FOR SILICA SAND NO. 6 AS SURROUNDING GROUND

5.4.1 Silica sand No. 6 test (S6)

Figure 5-11 represents the experimental conditions for the model test in which the tunnel is surrounded by silica sand No. 6 as the surrounding ground. The surrounding ground was initially prepared by placing 50 mm layers of the sand at 80% of its relative density and with 5% of water content to help in the dumping of the material in the available volume as per the relative density and the mass of the sand used. The relative density of Silica sand no. 6 was calculated by the laboratory test performed for maximum and minimum density test. The maximum dry density was calculated as 1.578 g/cm^3. Consequently, the relative density of 80% was 1.265 g/cm^3. The tunnel was placed on its relevant position. The rest of the procedure was the same as explained for S8 test. This test is designated as **S6** in the nomenclature adopted for different model tests carried out for this research program as highlighted in the model test scenarios in Chapter 4.

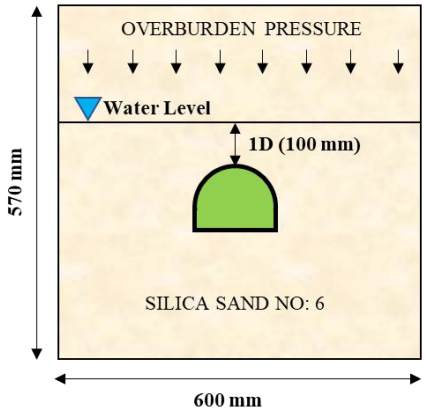

Figure 5-11 Schematic diagram for S6 model test

5.4.2 Expansive soil at invert section test (S6-B)

The experimental conditions in this case were kept same as S6 test but a 20 mm thick layer of expansive soil was placed at the invert section of the tunnel.

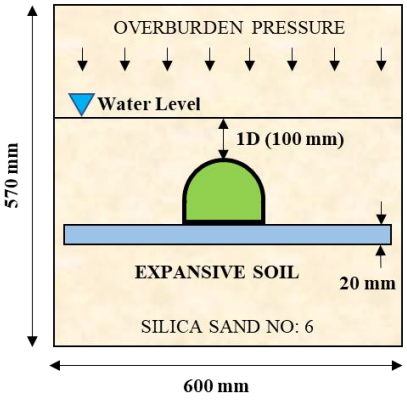

Figure 5-12 Schematic diagram for **S6-B** model test

The ground beneath the tunnel was prepared as per the previous test including the expansive soil layer placed in different sections with fixed volume and dry density of the bentonite-Toyoura sand mixture. Just like S8-B, the expansive soil was not placed throughout the length of the model. The expansive layer was discontinued at 50mm on each side. This discontinuity was kept ensuring that water would percolate through the silica sand openings provided on each side of expansive soil and the process of saturation would be carried out at a quick pace. The rest of the procedure followed was the same as adopted for S8-B test. The overburden height was kept to 3D and water level for saturation maintained at 1D. The water insertion caused the expansive soil layer to expand. This test was referred to as **S6-B** in the nomenclature adopted in this study where 'B' again signifies the location of the expansive soil layer at the tunnel invert. The schematic diagram of this test is represented in Figure 5-12.

5.5 RESPONSE OF TUNNEL LINING IN SILICA SAND NO. 6

5.5.1 Tunnel response to S6

Figure 5-13 represents the response of the tunnel lining to the pressure exerted by overburden soil for S6 test. The pressure kinetics showed that the as the overburden layers were placed the consequent rise in pressure was observed by the corresponding gauges. Upon the completion of the surrounding ground preparation, the water insertion slightly added to the pressure by amount that was required to saturate the soil. As for S6 case, the pressure variation for the pressure measurement gauges installed at the invert section are again represented in different colours intentionally as these gauges would experience additional pressure in the S6-B case where expansive soil was placed at the invert section.

The invert section of the tunnel experienced 4.84 kPa of saturated overburden pressure on the left and right gauges. There was a reduction of pressure at centre invert gauge which represented 4.09 kPa of overburden pressure as compared to 4.5 kPa for S8. The gauges on the wall experienced 3.72 kPa pressure as these gauges were normal to the overburden soil. Considerable changes were observed in overburden pressure for shoulder sections on both side of the tunnel and the crown section as compared to S8. The gauges on shoulder sections of the tunnel on both sides represented 4.96 kPa and 5.25 kPa respectively. The rise in pressure is credited to the dense material of sand No. 6 as compared to No. 8. Also, the void ratio for No. 6 was higher hence having the ability to retain more water as compared to No. 8 in the previous case.

Similarly, crown represented an overburden pressure of 5.26 kPa in comparison to 4.58 kPa. The pressure represented by the spring-line gauges on left and right gauges was 4.33 and 4.21 kPa respectively. The test was continued for certain period of time until the rate of change in pressure was negligible for a long enough time. Figure 5-15 represents the pressure magnitude on each gauge on tunnel based on its location for S6.

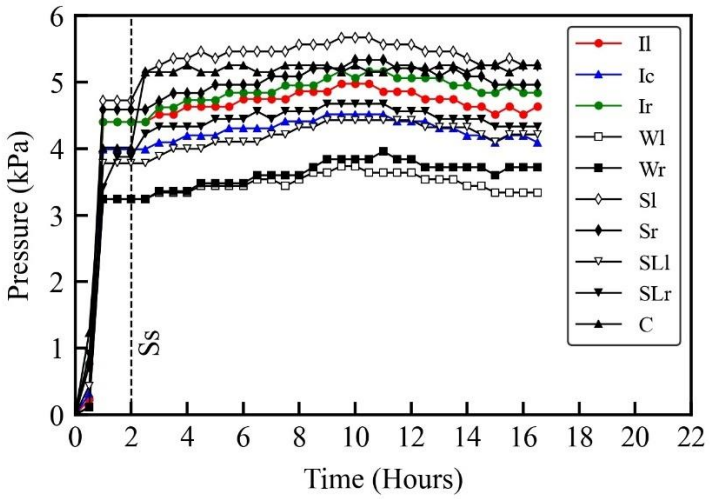

Figure 5-13 Pressure kinetics at different sections of the tunnel for **S6** model test

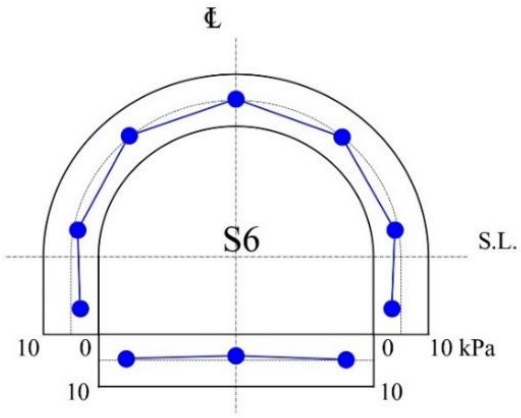

Figure 5-14 Representation of pressure at different sections of the tunnel for **S6**

5.5.2 Tunnel response to S6-B

Figure 5-15 represents the kinetics of the pressure on tunnel for S6-B model test. The pressure increment was in line with S6 test initially and the magnitude of the overburden pressure was comparable. As the overlying layers of the surrounding ground were completed and saturation was started, the expansive soil layer responded to water interaction and started to expand. The swelling of the layer imposed additional pressure to the invert section of the tunnel. The invert left and right gauges (Il & Ir) immediately responded to additional pressure within first 5 hours of the test and showed a rising trend which was a lot swifter as compared to S8-B case.

The swelling pressure did not drop and kept on rising quickly with further time passing. By the 20th hour, the pressure stabilized and remained constant for a significant time until 75th hour. The reason could be the strain hardening zone where the soil kept on taking the expansion load without depicting changes in the pressure. Also, the expansive soil minerals settled as the voids went on filling by water with the passing time. The water interaction caused change in the degree of

saturation of the soil. The expansive layer started to saturate from the bottom as the layer with immediate contact with tunnel invert was yet to experience the saturation because of being tightly packed under the tunnel. The sections of the expansive soil other than under the tunnel were getting saturated from both side top and bottom. Only the layer right beneath the tunnel was being saturated from the bottom side. This caused the pressure increment to relax for some time but did not remain constant for long. As the saturation of the expansive layer kept on increasing with passing time, the pressure started to rise again until it remained constant again for a long enough period. The pressure kept on rising on the invert section gauges. As the saturation kept rising, the vicinity of expansive pressure expanded and took the impacts to the wall section of the tunnel being relatively close to the expansive soil layer. The wall gauges on both sides of the tunnel started responding to the additional pressure to the swelling at a delayed span as compared to the invert section but this pressure was not as significant as in S8-B case. The surrounding ground did not absorb the swelling as much being harder than S8. The pressure variation was smooth as the impacts were directly taken up by the gauges installed in the tunnel model. The layer beneath the tunnel kept on saturating with respect to time and pressure kept rising.

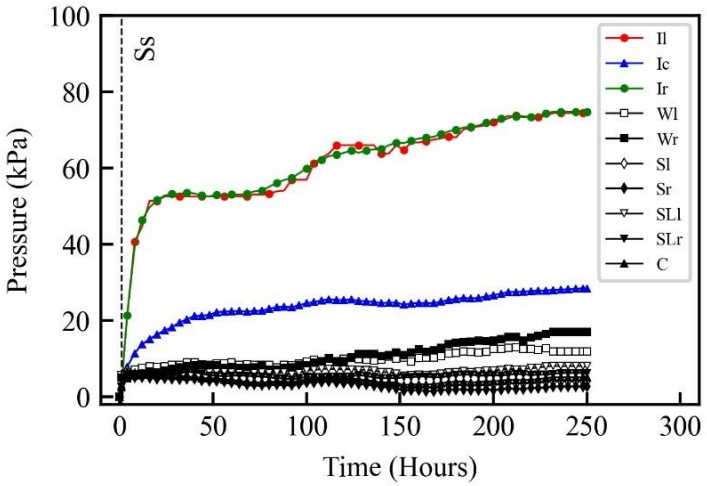

Figure 5-15 Pressure kinetics at different sections of the tunnel for **S6-B** model test

As the expansive layer pushed the tunnel structure upwards along with the surrounding ground, the gauges on spring-line and shoulder section represented with slight reduction in pressure. This happened because the upward push relieved the overburden pressure on these sections insignificantly. As the layer approached full saturation, the rate of rise of expansive pressure subsided and finally it remained constant for long enough time representing that the expansive layer has reached its limiting swell potential.

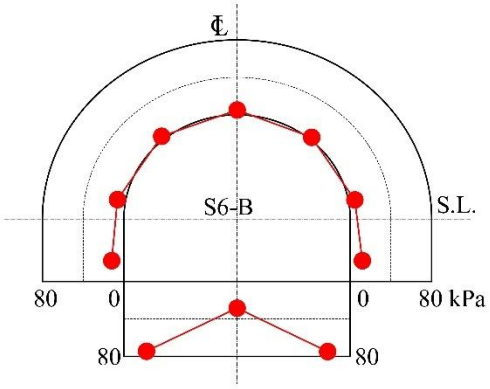

Figure 5-16 Representation of pressure at different sections of the tunnel for **S6-B**

The invert edge gauges in this case represented final pressure of 74.73 and 74.8 kPa respectively. The center gauge showed 28.48 kPa at the end of the test representing typical heaving of invert section. The wall sections represented 17.4 and 12 kPa on left and right side respectively. The rate of swelling pressure recorded on gauges was swiftest in the beginning and subsided slowly as the test went on to completion. Figure 5-16 represents the final pressure distribution on different sections of the tunnel at completion.

Around 46.25% of the free swell pressure was recorded with slight increase (0.2 MPa) in stiffness of the surrounding ground. Also, the rate of swelling got much higher for this case in the initial hours and almost 83% of the total swelling pressure observed was already recorded on bottom gauges within initial 50 hours of the test. The remaining swelling pressure kept on rising with passing time. This rise is significantly more than the S8-B case. However, this pressure is still lower than the free swell pressure of expansive soil the reason being the absorption of the expansive pressure by the sand No. 6 surrounding ground in case of model test and the difference of boundary conditions and corresponding confining pressure. Nonetheless, the expansive pressure exerted on the invert section of the tunnel is nearly 15 times of the pressure as compared to the S6 case with no expansive soil around implying significant pressure increment on tunnel structure constructed in strata comprising of expansive rocks / soils.

5.5.3 Time-dependent expansive pressure variation for S6-B

As explained for earlier model test, to further elaborate the time-dependent pressure variation on the tunnel for S6-B, different time steps were selected from Figure 5-15 and the expansive pressure variation on the tunnel was comprehended to evaluate the time-dependent impacts of expansive soils on tunnels. Consequently, Figure 5-17 represents this variation for various time-periods. The above transformation of time-dependent pressure variation signifies the stability of tunnel with increase in degree of saturation of expansive soil. The consequent impacts of expansive soil with time showed the critical phase where pressure significantly rose. As for this case, the pressure for initial 50 hours had reached around 83% of the total pressure and kept on rising rather steadily thereafter. Similar to S8-B case, the time-dependent stability of tunnels in expansive strata for this case is elaborated by carrying out a dissection of the swelling curve for invert section and is divided into four similar zones enlisted below:

1- Acceleration zone

The acceleration zone for this case reflected a lot quicker pressure on the invert section as the expansive soil came in contact with water. Consequently, the invert gauges represented a pressure higher than the initial overburden. The pressure kept rising quickly in a smaller time frame and peaked until a specific value at an early stage of the swelling. The increment of pressure was a lot more and signified the difference in the surrounding ground stiffness as dense silica sand No. 6 was used. The pressure experienced within this range covered the elastic response of tunnel to expansion.

2- Creep zone

S6-B represented a longer duration for creep zone in which the pressure remained constant while expansive soil underwent saturation. No particular decline in constant swelling pressure attained in the acceleration zone was observed in this case. The pressure remained around 55 kPa including the overburden pressure on the invert section from 20^{th} hour to 70^{th} hour. This region signifies the visco-elastic response of the tunnel to addition pressure due to expansion of surrounding soil in a comparatively stiffer non-swelling surrounding ground. The zone identifies the preliminary deterioration and temporal setting of the soil elements. As it is hard to realize time similitude for field tunnels yet, this zone implies that underground passageways have experienced a significant rise in external pressure although they might look perfectly stable and elastic deformations have occurred and temporary stable zone of creep is going on.

3- Renaissance zone

The swelling pressure on the invert section of tunnel started to rise again in this zone after undergoing a pause in the creep zone. The pressure increase in this period was not as intense as for the earlier case, however it kept on escalating. The slope of the curve in this zone was very mild in contrary to the steep slope in acceleration zone. The rate of rise of pressure kept declining until reaching the limiting visco-elastic response of the surrounding ground. Majority of swelling pressure was observed earlier but the rise in this region was around 15 kPa. This range was within 70-220 hours for S6-B and expansive soil attained higher degree of saturation. The tunnel structure might start to depict structural damages like heaving and spalling of lining depending upon the location of pressure provided by the expansive layer which was at the invert section. The surrounding rock would start taking up the additional pressure around the tunnel and undergo deteriorations due to volume change. The consequent strength parameters of surrounding ground would reduce, and typical failures might occur.

4- Steady zone

The maximum swelling pressure of the expansive soil was attained in zone. The expansive soil around the invert edges had attained maximum degree of saturation and has impacted the tunnel structure to its maximum potential. The firmness of tunnel depends upon the strength of its lining and the ability of the surrounding ground to cater the additional swelling pressure. Majority of damage would have occurred in the renaissance zone and the stability would be examined however if no significant damage like heaving or spalling is observed until this zone has reached, the structure is deemed to have taken up the additional swelling stresses and is designed to cater expansion and is referred to as safe against swelling pressure. This time-dependent analysis can be utilized to evaluate the life of the tunnels constructed in swelling strata with denser surrounding ground as compared to

S8-B case and can help in quantifying the magnitude of swelling pressures that can be experienced by the tunnel during different phases of expansion with respect to time.

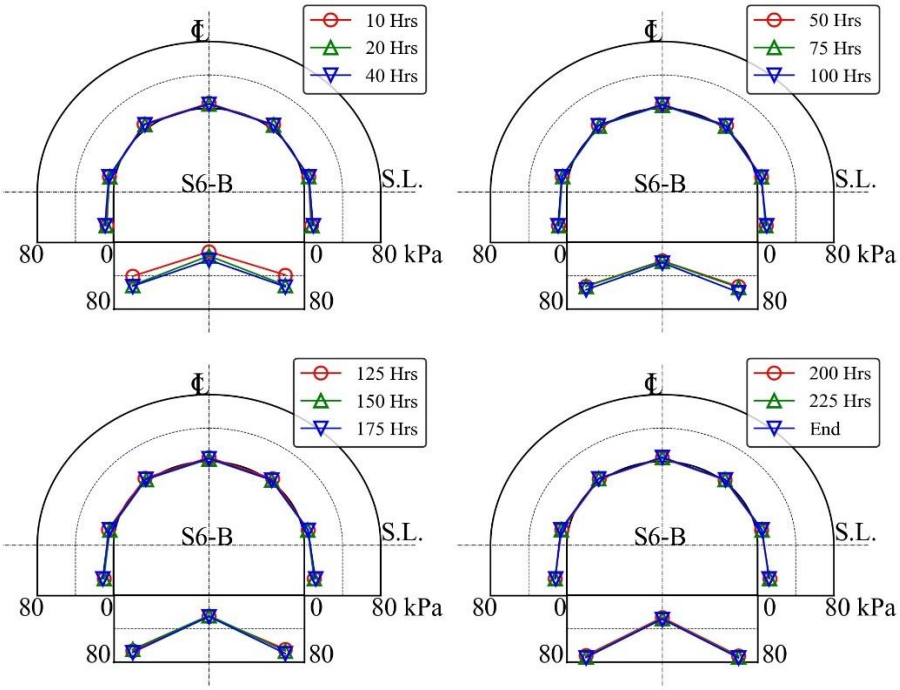

Figure 5-17 Time-dependent expansive pressure variation for **S6-B**

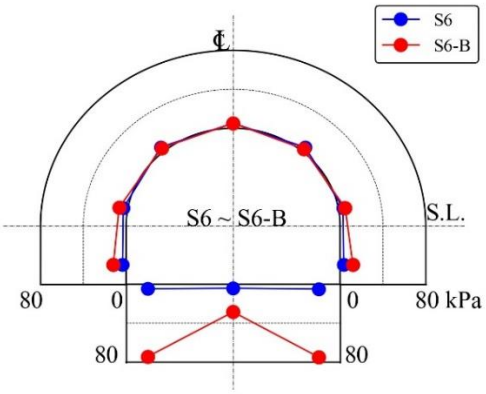

Figure 5-18 Comparison of pressure on tunnel sections for **S6** and **S6-B**

A symmetrical representation of pressure variation was observed on gauges that are placed on identical locations on each side of the tunnel. Having comprehended the time-dependent impacts, Figure 5-18 compares the pressure on various gauges of the tunnel for S6 and S6-B thereby signifying the impacts of presence of expansive soil undergoing saturation in soil strata around the tunnel. The expansive soil location at the invert section significantly enhanced the swelling pressure

on tunnel in addition to the overburden pressure. As the time went on, the pressure bulb is extended to wall section of the tunnel too. This comparison signified the criticality of expansive soil in the geological repositories around the tunnel structures and the number of damages that could occur due to water interaction of the expansive geology and consequent long-term stability of mountainous tunnels.

5.5.4 Surrounding ground movement for S6-B

The PIV analysis carried out for S6-B is represented in Figure 5-19 below. The time-dependent displacement of the node nearest to the invert gauge which was in direct contact with the expansive soil layer is evaluated. The term IL(P) and IR(P) consequently represent the expansive pressure variation on left and right invert gauges respectively while IL(D) and IR(D) are the corresponding displacement curves in the graph.

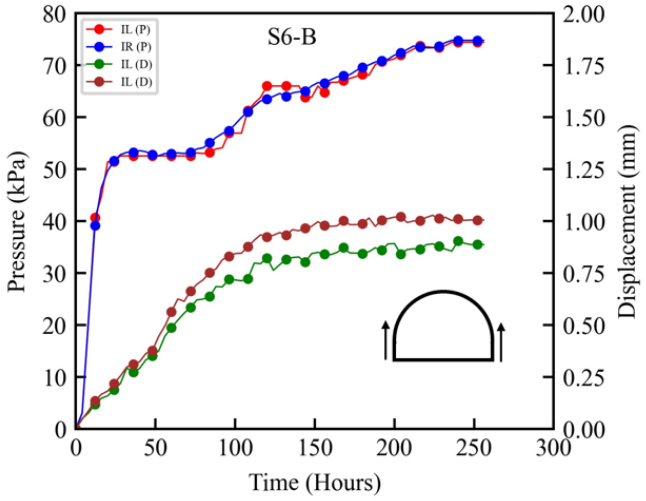

Figure 5-19 Time-dependent nodal displacement and expansive pressure near invert for **S6-B**

Owing to the increased surrounding ground stiffness as compared to earlier case, the displacement in the initial pressure rise zone of the expansive soil was swift as compared to the cumulative final displacement observed. During this range the expansive soil was undergoing saturation and the volumetric strain was developing to overcome the overburden pressure, but it was observed quickly as the surrounding ground is not taking much of the expansive pressure being stiffer now. This zone represented the continuous rate of strain and continued in the constant creep state where the surrounding ground kept displacing and showed deformation for an extended period of time. As the creep zone finished, the displacement tended to stabilize

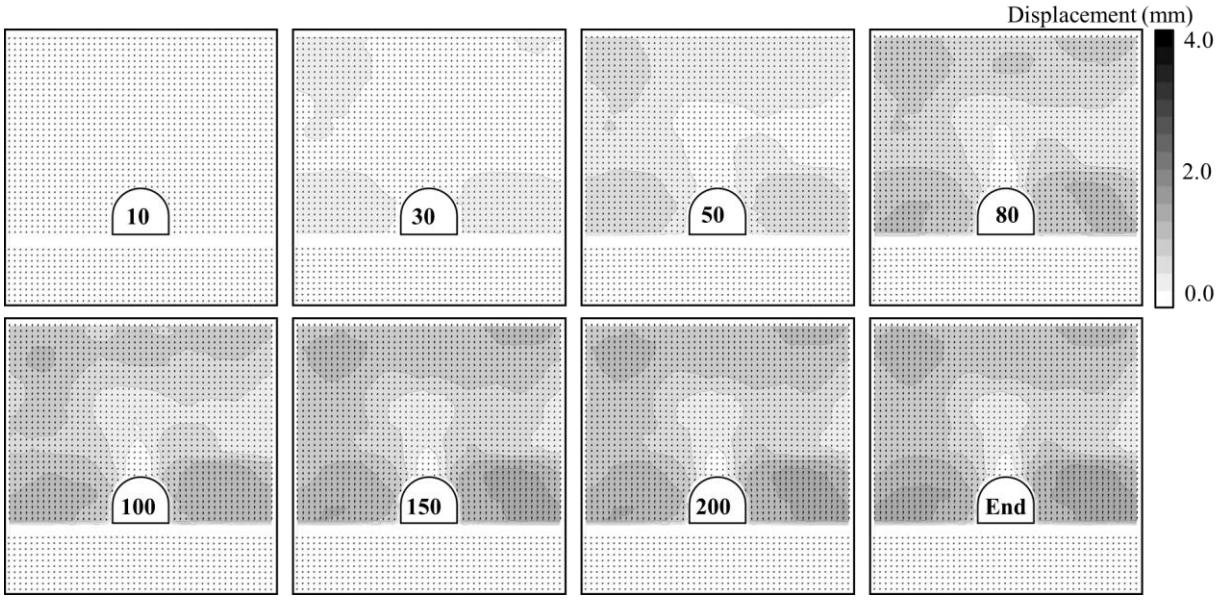

Figure 5-20 Time-dependent nodal displacements around tunnel invert for **S6-B**

A slight difference in magnitude of displacement was observed in this case on both sides of the invert. The reason could be the amount of expansive pressure being applied heterogeneously on the surrounding ground on both sides based on degree of saturation of expansive soil. As the time went on, the rate of rise of displacement got slower and its magnitude supressed significantly until the final stage reached where swelling pressure and corresponding nodal displacement became constant. The image analysis performed for this case represented the time-dependent directional displacement of the nodes. Based on the swelling kinetics graph, different time spans were evaluated for the visual representation of the surrounding ground movements with time. Figure 5-20 represents the said displacement through contours and vectors of displacement for these specific time periods similar to S8-B case.

The deformation of the surrounding ground initiated quickly in this case due to surge in swelling pressure and water interaction of expansive soil with stiffer surrounding ground around the tunnel. Majority of displacement occurred during the creep zone where swelling pressure slightly subsided and reached a steady state with expansive soil being saturated. The results suggest that as the surrounding ground gets stiffer, the swelling pressure and ground displacement occur simultaneously. But with stiffer ground the magnitude of displacement was almost half of what was observed in S8-B case. An accumulative displacement of 0.88 mm and 1.01 mm was observed near the invert section on left and right side respectively. The displacement right above the tunnel is significantly ceased as the tunnel model is locked in its position and the pressure exertion above the crown is restrained vertically. Major displacement is observed right above the expansive soil layer and as the distance from the layer increases, the displacement got reduced. The analysis reflects that the magnitude of the deterioration near the tunnel buried underground would be a lot more as compared to what would be experienced at the ground level.

5.5.5 Comparison for S8-B and S6-B

The model test performed for different surrounding ground stiffness also signifies the role of the surrounding rock stiffness on the expansive pressure exerted on tunnel by swelling soils. A softer ground may absorb the expansive pressure and vice-versa.

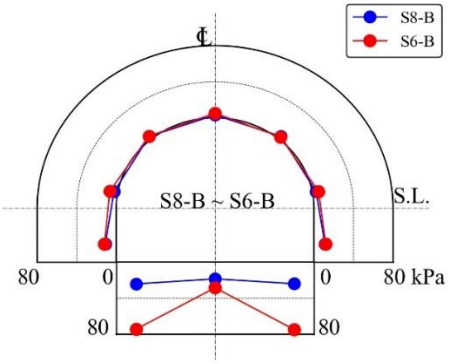

Figure 5-21 Comparison of pressure on tunnel sections for **S8-B** and **S6-B**

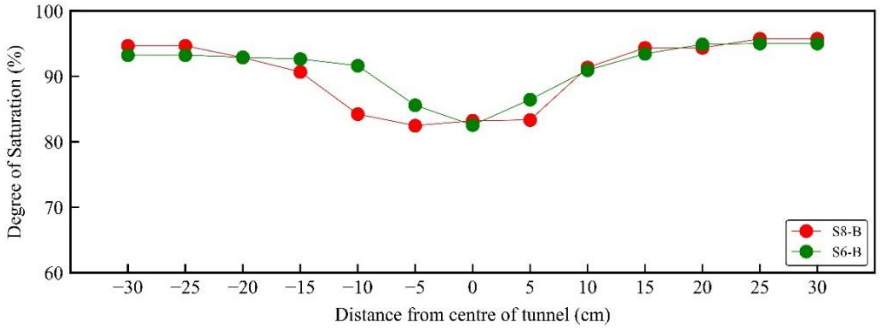

Figure 5-22 Saturation level of expansive soil at the completion of **S8-B** and **S6-B** model test

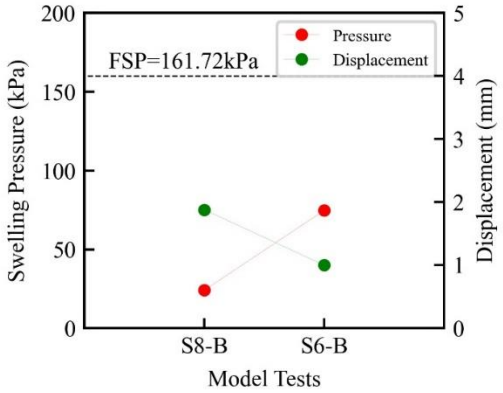

Figure 5-23 Comparison of final swelling pressure and displacement for **S8-B** and **S6-B** model test

Figure 5-21 compares the final pressure observed by different gauges on different location for S6-B and S8-B. Figure 5-22 represents the final degree of saturation of the expansive layer at the

completion of tests. The reduced saturation level under the tunnel is one of the reasons for expansive pressure being less than the pressure observed in free swell tests along with changes in confinements and boundary conditions. Figure 5-23 draws the final comparison of expansive pressure and nodal displacement at the completion of the tests.

5.6 SUMMARY

In this chapter, the impacts of expansive soil on tunnels in the geological repositories where expanding rocks could be encountered were studied through model tests. The expansive soil sample was placed at the invert section of the tunnel and made saturated by water insertion. The expansive pressure of an expansive soil sample is proportional to the amount of expansive mineral present in it. Expansive soils have substantial impacts on structures around them owing to their swelling ability and volume change during water content variation as found in this chapter. The pressure increment of 5 times was observed with S8 as surrounding ground while it was 15 times for S6. Such additional pressures can pose serious threats on tunnel securities causing invert heaving or lining dysfunctionalities. Many cases of tunnel failures are reported in literature owing to the insufficient support provided by the surrounding rock media comprising of expansive rocks. The design of tunnels often skips the high possibility of excessive pressures exerted by the expansive soils upon saturation on them. Underestimation of these swelling pressures during design is one of the key reasons of tunnel failures during their service period. As soon as geological survey of the site presents the possibility of presence of expansive soil minerals, it is essential to device a method that clearly specifies the detection of their occurrence and consequent rock support mechanisms to cater the probability of high pressures on tunnel upon expansion. So, an effort has been made to quantify the time-dependent magnitude of the pressure that can be expected for existing tunnels in expansive geological rock layers. This process can also help in devising the mitigation measures at very early stage of tunnel deterioration to overcome such tremendous amount of pressure that can very swiftly rise and may cause a complete failure of the tunnel with passing time.

CHAPTER 6 IMPACTS OF LOCATION OF EXPANSIVE SOILS ON TUNNELS

6.1 INTRODUCTION

As per the experimental conditions and the outline of the model tests explained in chapter 4, this chapter concentrates on the evaluation of the time-dependent variation of swelling pressure on tunnels due to variation of location of expansive soils in the rock-mass around the tunnels. The model tests were conducted by preparation of surrounding ground around the tunnel using the silica sand No. 6. The response of the tunnel was adjudicated by placing the expansive soils at different locations of the tunnel. A 20 mm thick expansive soil layer was placed at crown, shoulder and wall section of the tunnel on both sides. The swelling of the layer upon saturation imposed additional pressure on the tunnel sections which was recorded for each time step to evaluate the time-dependent impacts of expansive soil availability in the geological repositories around the tunnels at different locations. The time-dependent surrounding ground movements were evaluated for each case using image analysis. In addition, a comparison was made between different cases based on the difference of the location of expansive soil in the surrounding ground. The time-dependent deformation due to presence of expansive soils is explained in detail in this chapter.

6.2 EXPANSIVE SOIL ON TOP OF THE TUNNEL

6.2.1 Experimental conditions for S6-T

Figure 6-1 represents the experimental conditions for the model test S6-T in which the tunnel is surrounded by silica sand No. 6 as the surrounding ground.

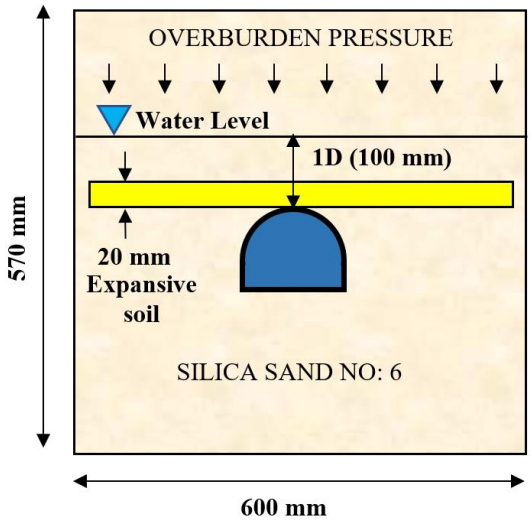

Figure 6-1 Schematic diagram for S6-T model test

The surrounding ground was initially prepared by placing 50 mm layers of the sand at 80% of its relative density and with 5% of water content to help in the dumping of the material in the available volume as per the relative density and the mass of the sand used. The tunnel was placed in its

location and the pressure measurement gauges were connected to the data logger for continuous recording of the pressure variation during the model test. A 20 mm layer of expansive soil was placed above the crown and the rest of the surrounding was correspondingly prepared in accordance with the relative density value of 80% in layers to ensure the correctness of the overburden pressure measurements. Upon the completion of the application of the overburden pressure on the tunnel, the model was saturated from the inlets provided at the base of the assembly to evaluate the saturated overburden pressure applied on different sections of the tunnel with the surrounding ground as Silica sand No. 6 and the expansive soil layer placed on top of the tunnel. This test is designated as S6-T in the nomenclature adopted for different model tests carried out for this research program.

6.2.2 Tunnel response to S6-T

Figure 6-2 represents the kinetics of the pressure on tunnel for S6-T model test. The pressure increment was in line with S6 test initially and the magnitude of the overburden pressure was comparable. As the overlying layers of the surrounding ground were completed and saturation was started, the expansive soil layer responded to water interaction and started to expand. The swelling of the layer imposed additional pressure to the crown section of the tunnel. The crown gauge (C) immediately responded to additional pressure and showed a swift rise. The pressure on other sections like shoulder, spring-line and wall also responded to the vertical pressure of swelling. The degree of saturation of expansive soil kept on rising with time.

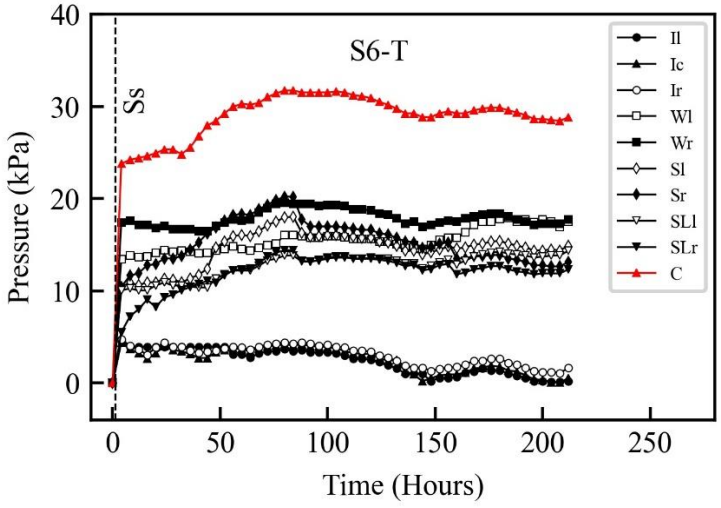

Figure 6-2 Pressure kinetics at different sections of the tunnel for S6-T model test

The pressure rose to about 25 kPa and relaxed a bit until 40 hours. The expansive pressure was taken to the shoulder, spring-line and wall sections of the tunnel being tightly packed between the tunnel and the model boundary. The wall gauges on both sides of the tunnel responding to the additional pressure to the swelling at a same time as compared to the crown section. As the expansive layer pushed the tunnel structure downwards along with the surrounding ground, the gauges on spring-line and shoulder section represented with slight increase in pressure. This happened because the downward swelling push added to the overburden pressure on these sections significantly. Contrary to this, the invert gauges represented reduction in pressure as the time went on as the downward push

relieved a part of pressure on them. As the layer approached full saturation, the rate of rise of expansive pressure subsided and finally remained constant for long enough time representing that the expansive layer has reached its limiting swell potential.

The crown gauge projected a gross pressure of 29 kPa. The wall sections represented 17.65 kPa on both sides. The rate of swelling pressure recorded on gauges was swiftest in the beginning and subsided slowly as the test went on to completion. Figure 6-3 represents the final pressure distribution on different sections of the tunnel at completion.

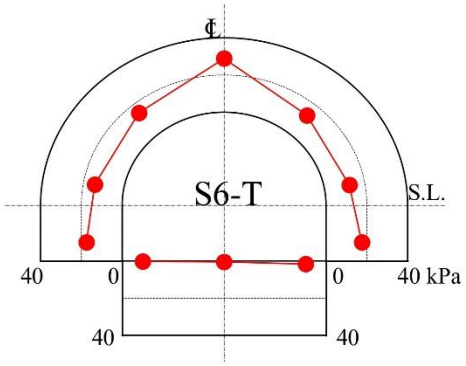

Figure 6-3 Final pressure at different sections of the tunnel for **S6-T**

The pressure recorded on crown gauge was around 18% of the free swell pressure of the same expansive soil in free swell test. The reason for depicting such lower percentage of expansion pressure as compared to the free-swell pressure is the location of expansive soil. The soil being on top of the crown expanded upwards and most of the pressure is applied to the ground over the tunnel. The difference of boundary conditions and corresponding confining pressure as compared to free swell test is another reason. Nonetheless, the expansive pressure exerted on the crown section is nearly 6 times of the pressure as compared to the S6 case with no expansive soil around.

6.2.3 Time-dependent expansive pressure variation for S6-T

To further elaborate the time-dependent pressure variation on the tunnel, different time steps were selected from Figure 6-2 and the expansive pressure variation on the tunnel was comprehended to evaluate the time-dependent impacts of expansive soils on tunnels. Consequently, Figure 6-4 represents this variation for various time-periods for S6-T. The above transformation of time-dependent pressure variation signifies the stability of tunnel with increase in degree of saturation of expansive soil. The consequent impacts of expansive soil with time showed the critical phase where pressure rose significantly. As for this case, the pressure within the first 5 hours rose very swiftly. To further elaborate the time-dependent stability of tunnels in expansive strata, a dissection of the swelling curve for crown can be divided into four zones as for the previous cases and are enlisted below:

1- Acceleration zone

As the expansive soil came in contact with water, a sharp rise in pressure was observed. Consequently, the gauge in direct contact with expansive soil, the crown gauge represented a

pressure higher than the initial overburden. The pressure rose very swiftly and peaked until a specific value at an early stage of the swelling. It is presumed that the pressure experienced within this range would bring about the elastic response of tunnel to expansion.

2- Creep zone

S6-T represented a longer duration for creep zone in which the pressure remained constant while expansive soil underwent saturation. No particular decline in constant swelling pressure attained in the acceleration zone was observed in this case. The pressure remained around 25 kPa including the overburden pressure on the invert section from 5^{th} hour to 35^{th} hour. This region signifies the creep zone of the tunnel to addition pressure due to expansion of surrounding soil in a comparatively stiffer non-swelling surrounding ground. The zone identified the preliminary deterioration and temporal setting of the soil elements. As it is hard to realize time similitude for field tunnels yet, this zone implies that underground passageways have experienced a significant rise in external pressure although they might look perfectly stable. This zone represents that elastic deformations have occurred and temporary stable zone of creep is going on.

3- Renaissance zone

The swelling pressure started to rise again in the renaissance zone after undergoing a pause in the creep zone. The crown, shoulder and the wall gauges responded to this rise and depicted increasing pressure. The pressure increment in this phase was not as sharp as for the acceleration case, yet it kept on rising and fell down to a final pressure position with a slight stuttering up and down. The curve included non-linear portions of rising and fall until it reached the slow rise trend representing the limiting visco-elastic response of the surrounding ground. The range for S6-T was within 40-175 hours. The tunnel structure might start to depict structural damages like deterioration of lining and contractions around wall depending upon the location of pressure provided by the expansive layer. The surrounding rock would start taking up the additional pressure around the tunnel and undergo deteriorations due to volume change of expansive soil. The consequent strength parameters of surrounding ground would reduce, and typical failures might occur.

4- Steady zone

The maximum swelling pressure of the expansive soil would be realized as the sample underwent near complete saturation. The pressure on gauges directly in contact with the expansive soil showed a steady pressure for long enough time depicting that swelling pressure had reached its limiting value. The stability of structure depends upon the strength of the tunnel lining and surrounding ground's ability to take up the additional pressure. Majority of damage would have occurred in the renaissance zone and the stability would be investigated however if no significant damage is observed until the steady zone has reached, the structure is deemed to have taken up the additional stresses due to expansion and is referred to as benign against swelling pressure. This time-dependent analysis can be utilized to evaluate the life of the tunnels constructed in swelling strata and can help in quantifying the magnitude of swelling pressures that can be experienced by the tunnel during different phases of expansion with respect to time.

The wall sections of the tunnel on both sides also represented the same trend of swelling pressure representation as explained in four zones for crown as it was confined between the vertical section of tunnel and model tank boundaries. However, this behaviour was very slightly delayed for the shoulder and spring-line sections as these sections were not in direct contact yet closer to the

expansive soil. A slight reduction in the final pressure at the invert edge gauges represents the reduction of overburden pressure due expansive layer making an arch above crown. At the completion of the test a symmetrical representation was observed on gauges that are placed on identical locations on each side of the tunnel. Having comprehend the time-dependent impacts, Figure 6-5 compares the pressure on various gauges of the tunnel for S6 and S6-T thereby signifying the impacts of presence of expansive soil undergoing saturation in soil strata around the tunnel.

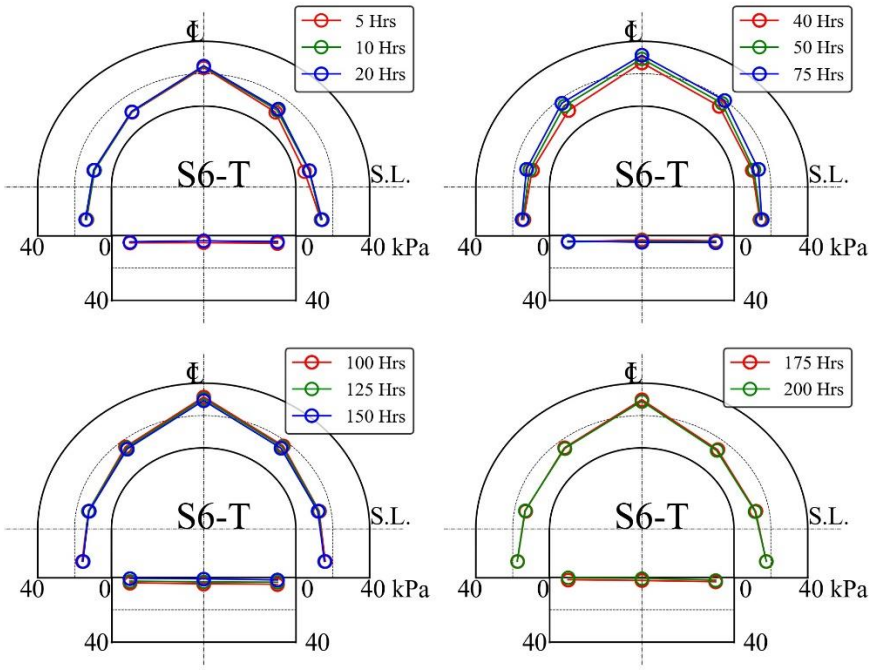

Figure 6-4 Time-dependent expansive pressure variation for **S6-T**

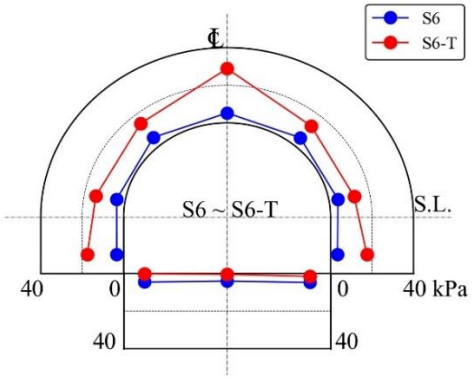

Figure 6-5 Comparison of pressure on tunnel sections for **S6** and **S6-T**

6.2.4 Surrounding ground movement for S6-T

As explained in the model test setup, the model photos were captured continuously during the testing procedure. The glass front of the model was divided into a mesh to adjudicate the movement of the surrounding ground upon expansion. Figure 6-6 represents the time-dependent displacement of the node nearest to the crown gauge which was in direct contact with the expansive soil layer.

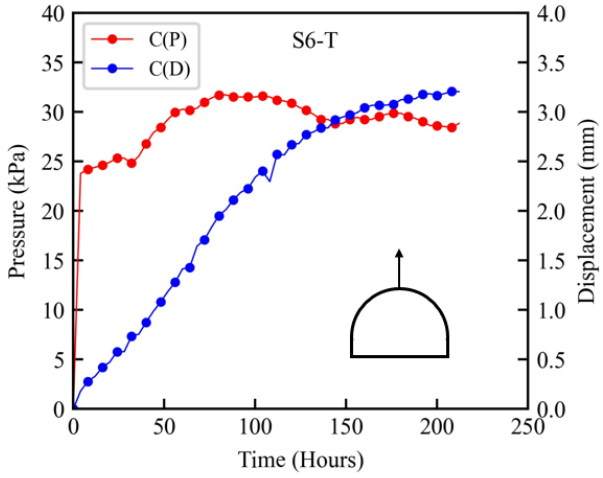

Figure 6-6 Time-dependent displacement and expansive pressure near crown for **S6-T**

As the expansive soil was at the crown section, the pressure observed by the crown gauge is plotted against the time along with displacement of the nearest node to it on the secondary axis. The term C(P) and C(D) represent the pressure variation and consequent surrounding ground displacement on crown gauge respectively in the graph.

The displacement in the initial pressure rise zone of the expansive soil was very small as compared to the cumulative final displacement observed in comparison to sharp rise in pressure. During this range the expansive soil was undergoing saturation and the volumetric strain was developing to overcome the overburden pressure. This zone could also represent the development of strain rate and corresponded to the constant creep state where the surrounding ground experienced no deformation for an extended period of time. As soon as the expansive push reached the limiting magnitude of overburden pressure and the swelling pressure kept rising, the displacement kept on rising above the tunnel crown. As the time went on, the rate of rise of displacement got slower and its magnitude supressed significantly until the final stage reached where swelling pressure became constant. The image analysis represented the time-dependent directional displacement of the nodes. Based on the swelling kinetics graph, different time spans were evaluated for the visual representation of the surrounding ground movements. Figure 6-7 represents the displacement through contours and vectors of displacement for these time periods.

The deformation of the surrounding ground initiates slowly due to swelling pressure and rises with further water interaction and rise in degree of saturation of expansive soil strata above the tunnel.

Majority of displacement occurred during the creep zone where swelling pressure slightly subsided and reached a steady state with expansive soil being saturated.

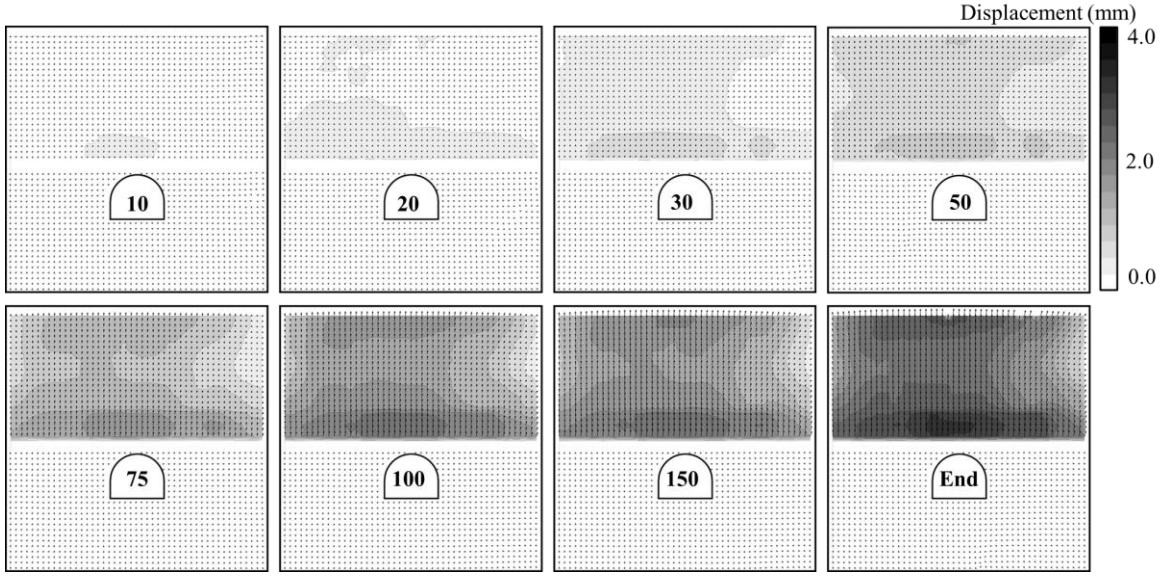

Figure 6-7 Time-dependent nodal displacement around tunnel crown for **S6-T**

The results suggest that even the structure itself might be experiencing huge additional pressure of expansion yet, the surrounding ground may seem to exist in stable conditions. A cumulative displacement of 3.2 mm was observed near the crown of the tunnel. Major displacement is observed right above the expansive soil layer and as the distance from the layer increases, the displacement reduced. The analysis reflects that the magnitude of the deterioration near the tunnel buried underground would be a lot more as compared to experience at the exposed surface.

6.3 EXPANSIVE SOIL NEAR SHOULDERS OF THE TUNNEL

6.3.1 Experimental conditions for S6-S

The experimental conditions in this case were kept same as S6-T test but a 20 mm thick layer of expansive soil was placed at the shoulder section of the tunnel on both sides. The ground beneath the tunnel was prepared as per the previous test including the expansive soil layer placed with fixed volume and dry density of the bentonite-Toyoura sand mixture. The expansive soil layer in this case was divided into two parts as the tunnel portion was missed. The soil was kept in direct contact with the shoulder gauges. The external 50 mm length was discontinued to allow the water to escape the layer and help saturation from both sides. The rest of the procedure followed was the same as adopted for S6-T test. The overburden height was kept to 3D and water level for saturation maintained at 1D. The water insertion caused the expansive soil layer to expand. This test was referred to as S6-S in the nomenclature adopted in this study where ‘S’ signifies the location of the expansive soil layer at the shoulders of the tunnel. The schematic diagram of this test is represented in Figure 6-8.

6.3.2 Tunnel response to S6-S

Figure 6-9 represents the kinetics of the pressure on tunnel for S6-S model test. The pressure increment was in line with S6 test initially and the magnitude of the overburden pressure was comparable. As the overlying layers of the surrounding ground were completed and saturation was started, the expansive soil layer responded to water interaction and started to expand.

The swelling of the layer imposed additional pressure to the shoulder gauges of the tunnel. The shoulder left and right gauges (Sl & Sr) immediately responded to additional pressure within first 10 hours of the test and showed a rising trend which was a lot sharper initially. The swelling pressure did not drop and kept rising quickly with further time passing. By the 25th hour, the pressure peaked and then started to fall.

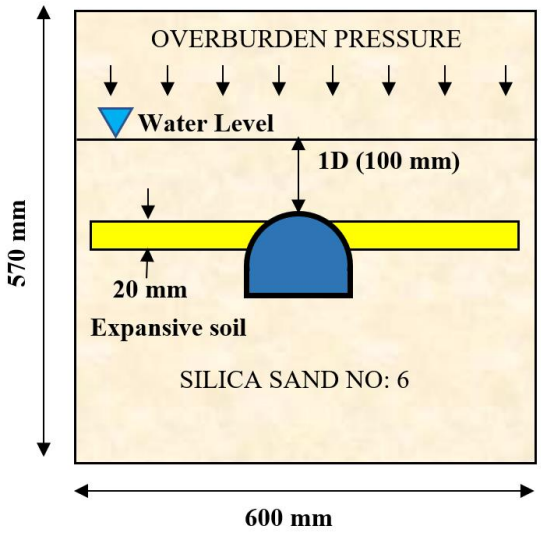

Figure 6-8 Schematic diagram for **S6-S** model test

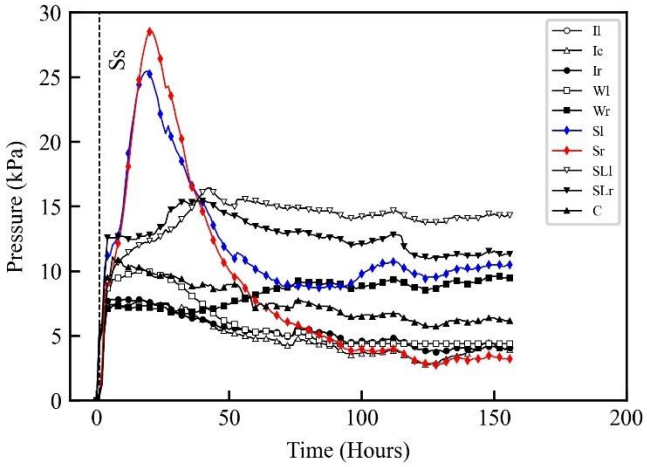

Figure 6-9 Pressure kinetics at different sections of the tunnel for **S6-S** model test

Usually in other cases, the pressure would remain constant after a certain peak but for this case the pressure fell, and the reason could be the location of expansive soil. The soil was placed near the centroid of the tunnel and almost all the gauges responded to changes in pressure. As the pressure on the wall gauges rose after the 50th hour, the pressure on the shoulder gauges fell further down because the impacts were transferred to the lower part of the tunnel to spring-line and wall sections. Meanwhile, the expansive soil minerals settled as the voids went on filling by water with the passing time. The water interaction caused change in the degree of saturation of the soil. The pressure on the crown and spring-line gauges rose initially and followed the acceleration, creep, rerise and steady zone trend as earlier cases however, it remained more or less constant for majority of the test duration thereafter. The invert gauges also responded to slight rise in pressure initially but steadily reduced afterwards. The expansive layer at the shoulder section of the tunnel kept on saturating with respect to time and the pressure increment suggest that the tunnel is being squeezed from both sides due to confining expansive pressure. As the saturation of the expansive layer kept on increasing with passing time, the pressure on shoulder gauges kept falling and remained constant again for a long enough period to conclude the test.

The invert edge gauges in this case represented final pressure of 4.06 and 4.07 kPa respectively. The invert center gauge showed 3.95 kPa at the end of the test representing no serious impact on invert section of the tunnel. The wall sections represented 4.38 and 9.48 kPa on left and right side respectively. The rate of swelling pressure recorded on gauges was swiftest in the beginning and subsided slowly as the test went on to completion. The shoulder gauges ended up with 10.49 and 3.22 kPa of final pressure. The impacts were taken by the spring-line gauges majorly and the final pressure for them was 11.3 and 10.5 kPa on left and right side respectively. Figure 6-10 represents the final pressure distribution on different sections of the tunnel at completion for S6-S case.

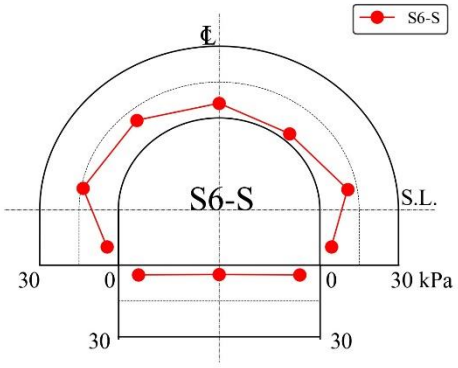

Figure 6-10 Representation of pressure at different sections of the tunnel for **S6-S**

Around 22.62% of the free swell pressure was recorded on shoulder gauges during the test and fell down to 6.48%. Also, the rate of swelling got much higher for this case in the initial hours and almost all of the total swelling pressure observed was already recorded on the gauges within initial 30 hours of the test. Nonetheless, the expansive pressure exerted on the shoulder section of the tunnel is nearly 7 times of the pressure as compared to the S6 case with no expansive soil around implying significant pressure increment on tunnel structure constructed in strata comprising of expansive rocks / soils.

6.3.3 Time-dependent expansive pressure variation for S6-S

For the time-dependent pressure variation on the tunnel for S6-S, different time steps were selected from Figure 6-9 and the expansive pressure variation on the tunnel was comprehended. Consequently, Figure 6-11 represents this variation for various time-periods. The above transformation of time-dependent pressure variation signifies the stability of tunnel with increase in degree of saturation of expansive soil. The consequent impacts of expansive soil with time showed the critical phase where pressure significantly rose. As for this case, the pressure for initial 25 hours had already reached its maximum potential and then fell down drastically. The time-dependent stability of tunnels in expansive strata for this case was elaborated by carrying out a dissection of the swelling curve for shoulder section to evaluate how the pressure varied in this test and is divided into three zones enlisted below:

1- Acceleration zone

The acceleration zone for this case reflected a lot quicker pressure on the shoulder section as the expansive soil came in contact with water. Consequently, the shoulder gauges represented a pressure higher than the initial overburden. The pressure kept rising quickly in a smaller time frame and peaked until a specific value at an early stage of the swelling. The increment of pressure was a lot more and signified the difference in the surrounding ground stiffness as dense silica sand No. 6 was used. The pressure experienced within this range covered the elastic response of tunnel to expansion.

2- Creep zone

S6-S represented a different response for creep zone in which the pressure did not remain constant while expansive soil underwent saturation. A particular decline in swelling pressure attained in the acceleration zone was observed in this case. The pressure dropped from 28 kPa to 7 kPa including the overburden pressure on the shoulder section from 25^{th} hour to 60^{th} hour. The creep zone was significantly represented by the spring-line gauges. This region signifies the changes in the pressure distribution on the other sections of the tunnel due to expansion of expansive soil in a comparatively stiffer non-swelling surrounding ground. The zone identifies the preliminary deterioration and temporal setting of the soil elements. As it is hard to realize time similitude for field tunnels yet, this zone implies that underground passageways have experienced a significant rise in external pressure and the tunnel is undergoing squeezing from the shoulder and spring-line sections for different time periods. The structure might look perfectly stable but elastic deformations have occurred and an equilibrium state had been achieved.

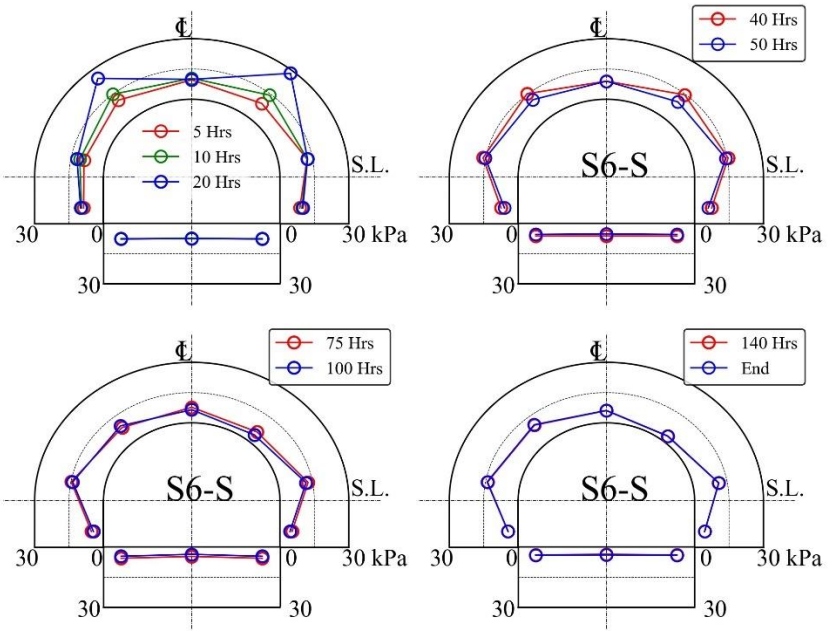

Figure 6-11 Time-dependent expansive pressure variation for **S6-S**

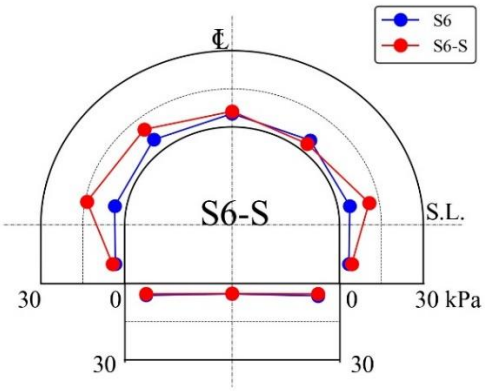

Figure 6-12 Comparison of pressure on tunnel sections for **S6** and **S6-S**

3- Steady zone

The maximum swelling pressure of the expansive soil was attained in zone. The expansive soil had attained maximum degree of saturation and has impacted the tunnel structure to its maximum potential. The firmness of tunnel depends upon the strength of its lining and the ability of the surrounding ground to cater the additional swelling pressure. Majority of damage would have occurred in the creep zone and the stability would be examined however if no significant damage like heaving or spalling is observed until this zone has reached, the structure is deemed to have taken up the additional swelling stresses and is designed well to cater expansion and is referred to as safe against swelling pressure. There was no renaissance zone for shoulder section as the pressure fell significantly thereafter however, the renaissance zone was represented by the shoulder and wall section gauges. This time-dependent analysis can be utilized to evaluate the life of the tunnels

constructed in swelling strata around shoulder sections and can help in quantifying the magnitude of swelling pressures that can be experienced by the tunnel during different phases of expansion with respect to time.

Slight unsymmetrical representation of pressure variation was observed on gauges that are placed on identical locations on each side of the tunnel as the layer was discontinued at the tunnel. The reason could be the swelling pressure being higher on one side of the tunnel trying to overturn the structure. Having comprehended the time-dependent impacts, Figure 6-12 compares the final pressure on various gauges of the tunnel for S6 and S6-S thereby signifying the impacts of location of expansive soil undergoing saturation in soil strata around the shoulder section of the tunnel.

6.3.4 Surrounding ground movement for S6-S

The PIV analysis carried out for S6-S is represented in Figure 6-13. The time-dependent displacement of the node nearest to the shoulder gauge which was in direct contact with the expansive soil layer is evaluated. The term SL(P) and SR(P) consequently represent the expansive pressure variation on left and right shoulder gauges respectively while SL(D) and SR(D) are the corresponding displacement curves in the graph.

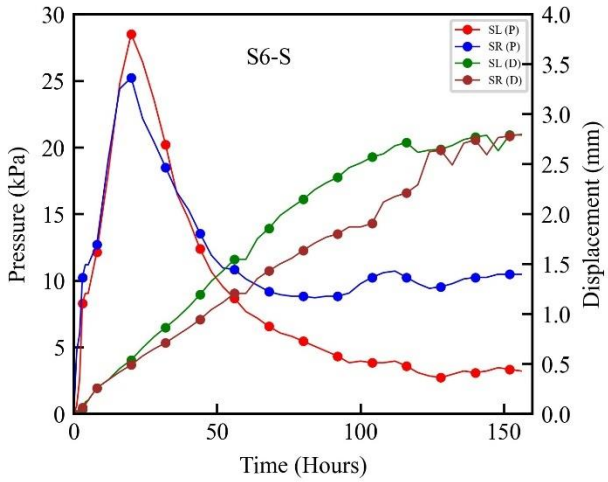

Figure 6-13 Time-dependent nodal displacement and expansive pressure near shoulder for **S6-S**

The displacement in the initial pressure rise zone of the expansive soil was small as compared to the cumulative final displacement observed. During this range the expansive soil was undergoing saturation and the volumetric strain was developing to overcome the overburden pressure, but it was observed quickly as the surrounding ground is not taking much of the expansive pressure being stiffer S6 sand. This zone represented the continuous rate of strain and continued in the falling creep state where the surrounding ground kept displacing and showed deformation for an extended period of time. As the creep zone finished, the displacement tended to stabilize A slight difference in magnitude of displacement was observed in this case on both sides of the shoulder. The reason could be the amount of expansive pressure being applied heterogeneously on the surrounding ground on both sides based on degree of saturation of expansive soil. As the time went on, the rate of rise of

displacement got slower and its magnitude supressed significantly until the final stage was reached where swelling pressure and corresponding nodal displacement became constant.

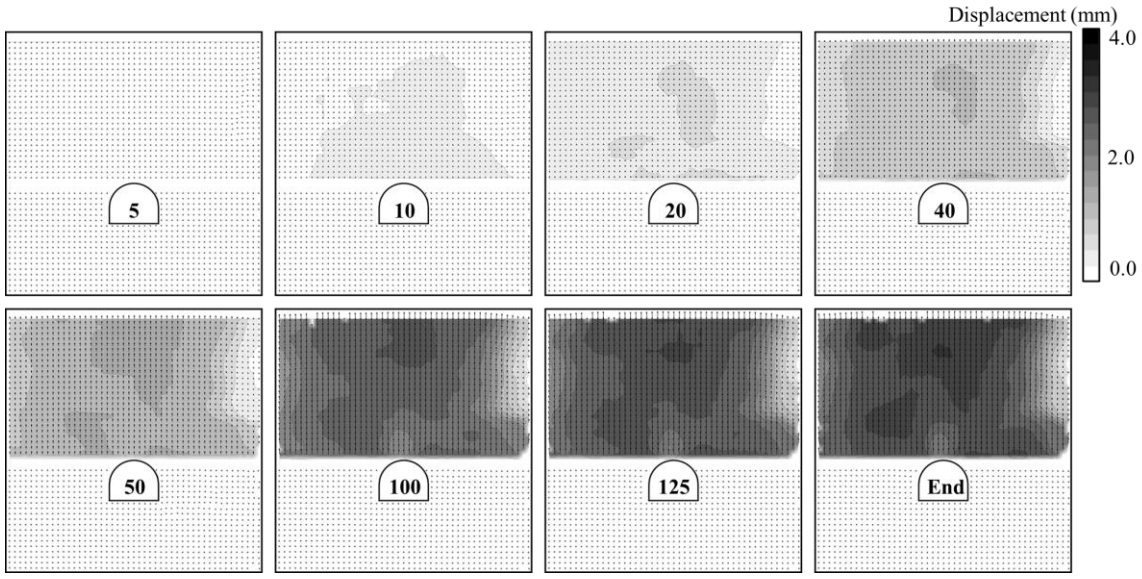

Figure 6-14 Time-dependent nodal displacement around tunnel shoulder for **S6-S**

The image analysis through PIV performed for this case represented the time-dependent directional displacement of the nodes. Based on the swelling kinetics graph, different time spans were evaluated for the visual representation of the surrounding ground movements with time. Figure 6-14 represents the said displacement through contours and vectors of displacement for these specific time periods for S6-S case.

The deformation of the surrounding ground initiated quickly in this case due to surge in swelling pressure and water interaction of expansive soil. Majority of displacement occurred during the falling creep zone where swelling pressure subsided on shoulder section and reached a steady state. The results suggest that as the surrounding ground gets stiffer, the swelling pressure and ground displacement occur simultaneously. An accumulative displacement of 2.80 mm and 2.79 mm was observed near the shoulder section on left and right side respectively. The displacement right above the tunnel is slightly reduced and ceased as the tunnel model is locked in its position and the expansive soil is discontinued here.

Major displacement is observed right above the expansive soil layer and as the distance from the layer increases, the displacement got reduced. This case presented with higher magnitude of displacement as the overburden pressure is reduced owing to its location. The analysis reflects that the magnitude of the deterioration near the tunnel buried underground would be a lot more as compared to what would be experienced at the ground level just like other cases.

6.4 EXPANSIVE SOIL NEAR WALLS OF THE TUNNEL

6.4.1 Experimental conditions for S6-W

The experimental conditions in this case were kept same as S6-S test. The ground beneath the tunnel was prepared as per the previous test including the expansive soil layer placed with fixed volume and dry density of the bentonite-Toyoura sand mixture. The expansive soil layer in this case was divided into two parts as the tunnel portion was missed. The soil was kept in direct contact with the wall gauges. The external 50 mm length was discontinued to allow the water to escape the layer and help saturation from both sides. The rest of the procedure followed was the same as adopted for S6-T and S6-S test. The overburden height was kept to 3D and water level for saturation maintained at 1D. The water insertion caused the expansive soil layer to expand. This test was referred to as S6-W in the nomenclature adopted in this study where 'W' signifies the location of the expansive soil layer at the walls of the tunnel invert. The schematic diagram of this test is represented in Figure 6-15 below:

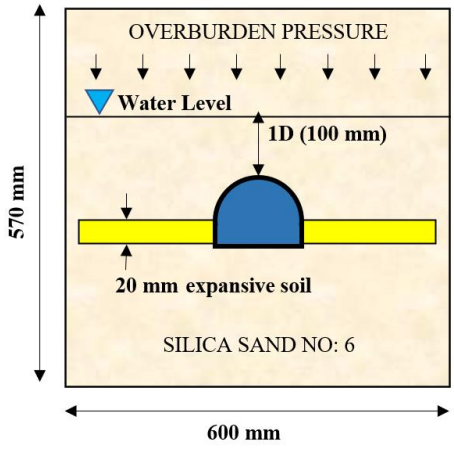

Figure 6-15 Schematic diagram for **S6-W** model test

6.4.2 Tunnel response to S6-W

Figure 6-16 represents the kinetics of the pressure on tunnel for S6-W model test. The pressure increment was in line with S6 test initially and the magnitude of the overburden pressure was comparable. As the overlying layers of the surrounding ground were completed and saturation was started, the expansive soil layer responded to water interaction and started to expand. The swelling of the layer imposed additional pressure to the wall gauges of the tunnel. The wall left and right gauges (Wl and Wr) immediately responded to additional pressure within first 10 hours of the test and showed a rising trend which was a lot sharper initially. The swelling pressure did not drop and kept on rising quickly with further time passing. By the 50^{th} hour, the pressure peaked and then slightly fell down. Also, the expansive soil minerals settled as the voids went on filling by water with the passing time. The water interaction rose the degree of saturation of the soil with time.

The expansive layer started to saturate from both bottom and top side. The pressure on all the other gauges rose initially however it remained constant for majority of the test duration. The pressure variation was smooth as the impacts were directly taken up by the gauges installed in the tunnel

model. The expansive layer at the wall section of the tunnel kept on saturating with respect to time and the pressure increment suggest that the tunnel is being squeezed from the side confining pressure. As the saturation of the expansive layer kept on increasing with passing time, the pressure on wall gauges did not fall anymore and remained constant again for a long enough period to conclude the test.

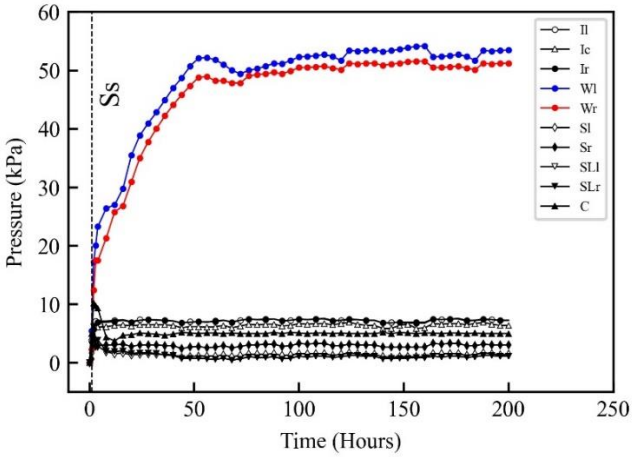

Figure 6-16 Pressure kinetics at different sections of the tunnel for **S6-W** model test

The invert edge gauges in this case represented final pressure of 7.2 kPa respectively. The invert centre gauge showed 6.4 kPa at the end of the test. The crown section represented 5 kPa. The rate of swelling pressure recorded on gauges was swiftest in the beginning and subsided slowly as the test went on to completion. The wall gauges ended up with 51.22 and 53.5 kPa of final pressure. Figure 6-17 represents the final pressure distribution on different sections of the tunnel at completion for S6-W case.

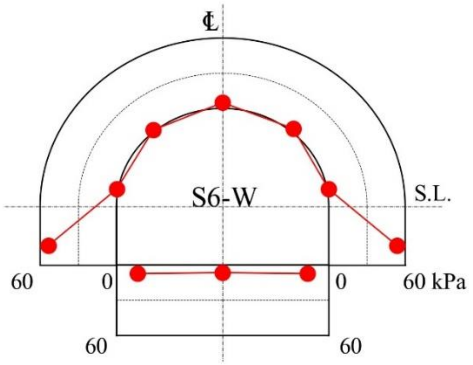

Figure 6-17 Representation of pressure at different sections of the tunnel for **S6-W**

Around 33% of the free swell pressure was recorded on wall gauges. Also, the rate of swelling got much higher for this case in the initial hours and almost all of the total swelling pressure observed was already recorded on the gauges within initial 50 hours of the test. Nonetheless, the expansive

pressure exerted on the wall section of the tunnel is nearly 10 times of the pressure as compared to the S6 case with no expansive soil around implying significant pressure increment on tunnel structure constructed in strata comprising of expansive rocks / soils.

6.4.3 Time-dependent expansive pressure variation for S6-W

For the time-dependent pressure variation on the tunnel for S6-W, different time steps were selected and the expansive pressure variation on the tunnel was comprehended to evaluate the time-dependent impacts of expansive soils on tunnels. Consequently, Figure 6-18 represents this variation for various time-periods. The time-dependent pressure variation signifies the stability of tunnel with increase in degree of saturation of expansive soil. The consequent impacts of expansive soil with time showed the critical phase where pressure significantly rose. As for this case, the pressure for initial 50 hours had already reached its maximum potential and then fell down slightly. The time-dependent stability of tunnels in expansive strata for this case is elaborated by carrying out a dissection of the swelling curve for shoulder section to evaluate how the pressure varied in this test and is divided into three zones enlisted below:

1- Acceleration zone

The acceleration zone for this case reflected a lot quicker pressure on the wall section as the expansive soil came in contact with water. Consequently, the wall gauges represented a pressure higher than the initial overburden. The pressure kept rising quickly in a smaller time frame and peaked until a specific value at an early stage of the swelling. The pressure experienced within this range covered the elastic response of tunnel to expansion.

2- Creep zone

S6-W represented a different response for creep zone in which the pressure did not remain constant while expansive soil underwent saturation. A decline in swelling pressure attained in the acceleration zone was observed in this case. The pressure dropped from 49 kPa to 48 kPa including the overburden pressure on the shoulder section from 50^{th} hour to 75^{th} hour and then back to 51 kPa showing a small rerise zone. This region signifies the changes in the pressure distribution on the other sections of the tunnel due to expansion of expansive soil near walls of the tunnel. The zone identified the preliminary deterioration and temporal setting of the soil elements. As it is hard to realize time similitude for field tunnels yet, this zone implies that underground passageways have experienced a significant rise in external pressure and the tunnel is undergoing squeezing from the wall section. Although the structure might look perfectly stable but elastic deformations have occurred and an equilibrium state has been achieved.

3- Steady zone

The maximum swelling pressure of the expansive soil was attained in zone. The expansive soil had attained maximum degree of saturation and has impacted the tunnel structure to its maximum potential. The firmness of tunnel depends upon the strength of its lining and the ability of the surrounding ground to cater the additional swelling pressure. Majority of damage would have occurred in the creep zone and the stability would be examined however if no significant damage like heaving or spalling is observed until this zone has reached, the structure is deemed to have taken up the additional swelling stresses and is designed well to cater expansion and is referred to as safe against swelling pressure. This time-dependent analysis can be utilized to evaluate the life of the tunnels constructed in swelling strata around wall sections and can help in quantifying the magnitude

of swelling pressures that can be experienced by the tunnel during different phases of expansion with respect to time.

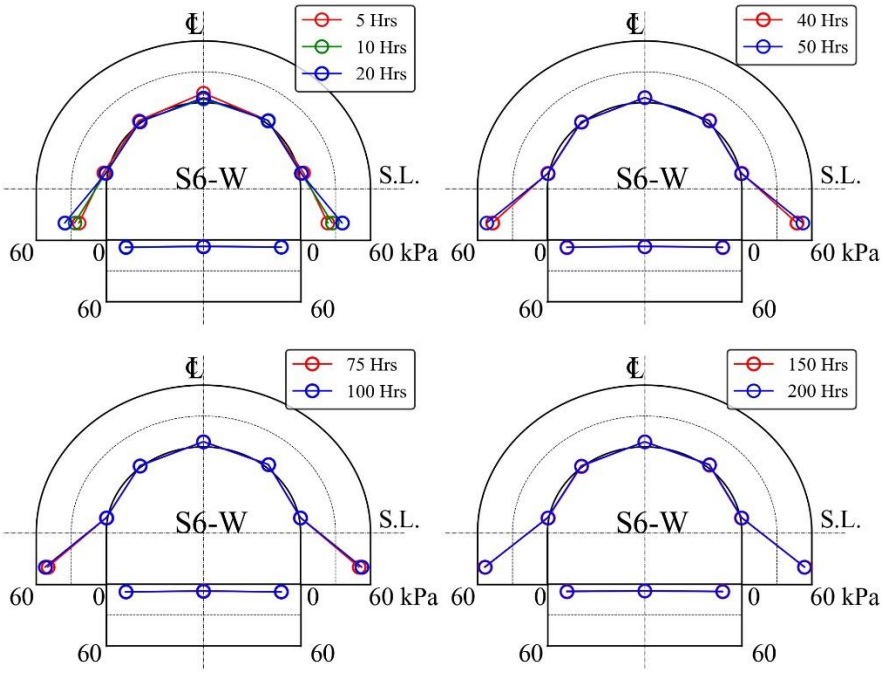

Figure 6-18 Time-dependent expansive pressure variation for **S6-W**

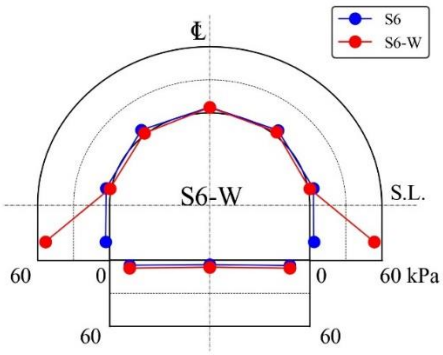

Figure 6-19 Comparison of pressure on tunnel sections for **S6** and **S6-W**

A symmetrical representation of pressure variation was observed on gauges that are placed on identical locations on each side of the tunnel. Having comprehended the time-dependent impacts, Figure 6-19 compares the final pressure on various gauges of the tunnel for S6 and S6-W thereby signifying the impacts of location of expansive soil undergoing saturation in soil strata around the wall section of the tunnel.

6.4.4 Surrounding ground movement for S6-W

The PIV analysis carried out for S6-W is represented in Figure 6-20. The time-dependent displacement of the node nearest to the wall gauge which was in direct contact with the expansive soil layer is evaluated. The term WL(P) and WR(P) consequently represent the expansive pressure variation on left and right shoulder gauges respectively while WL(D) and WR(D) are the corresponding displacement curves in the graph.

The displacement in the initial pressure rise zone of the expansive soil was slow as compared to the cumulative final displacement. During this range the expansive soil was undergoing saturation and the volumetric strain was developing to overcome the overburden pressure. The displacement rose quickly as the surrounding ground is not taking much of the expansive pressure being stiffer S6 sand than S8. This zone represented the continuous rate of strain and continued in the constant creep state where the surrounding ground showed deformation for an extended period of time. As the creep zone finished, the displacement tended to stabilize. A slight difference in magnitude of displacement was observed in this case on both sides of the wall. The reason could be the amount of expansive pressure being applied heterogeneously on the surrounding ground on both sides of the tunnel based on degree of saturation of expansive soil.

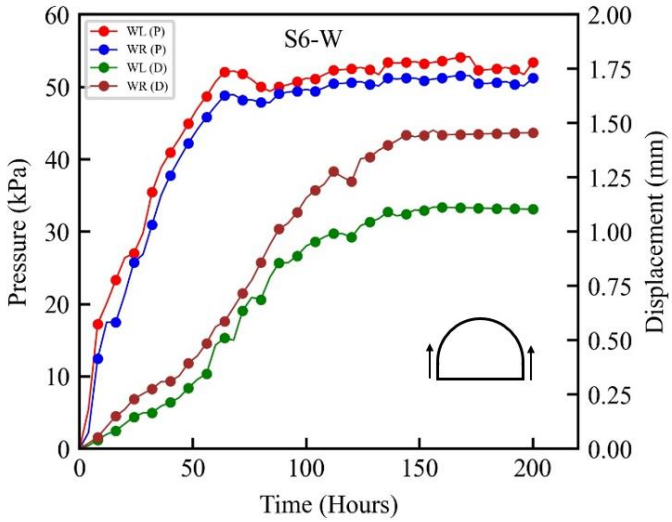

Figure 6-20 Time-dependent nodal displacement and expansive pressure near walls for **S6-W**

As the time went on, the rate of rise of displacement ceased and its magnitude supressed significantly until the final stage reached where swelling pressure and corresponding nodal displacement became constant. The image analysis performed for this case represented the time-dependent directional displacement of the nodes. Based on the swelling kinetics graph, different time spans were evaluated for the visual representation of the surrounding ground movements with time. Figure 6-21 represents the said displacement through contours and vectors of displacement for these specific time periods for S6-W case.

The deformation of the surrounding ground initiated quickly in this case due to surge in swelling pressure and water interaction of expansive soil with stiffer surrounding ground around the tunnel. Majority of displacement occurred during the creep zone where swelling pressure slightly subsided

and fell and reached a steady state with expansive soil being saturated. The results suggest that as the surrounding ground gets stiffer, the swelling pressure and ground displacement occur simultaneously. An accumulative displacement of 1.1 mm and 1.45 mm was observed near the wall section on left and right side respectively. The displacement right above the tunnel is significantly ceased as the tunnel model is locked in its position and the expansive soil is discontinued here. The pressure exertion above the crown is negligible. Major displacement is observed right above the expansive soil layer and as the distance from the layer increases, the displacement got reduced. This case presented with higher magnitude of displacement as the overburden pressure is reduced owing to its location. The analysis reflects that the magnitude of the deterioration near the tunnel buried underground would be a lot more as compared to what would be experienced at the ground level just like other cases.

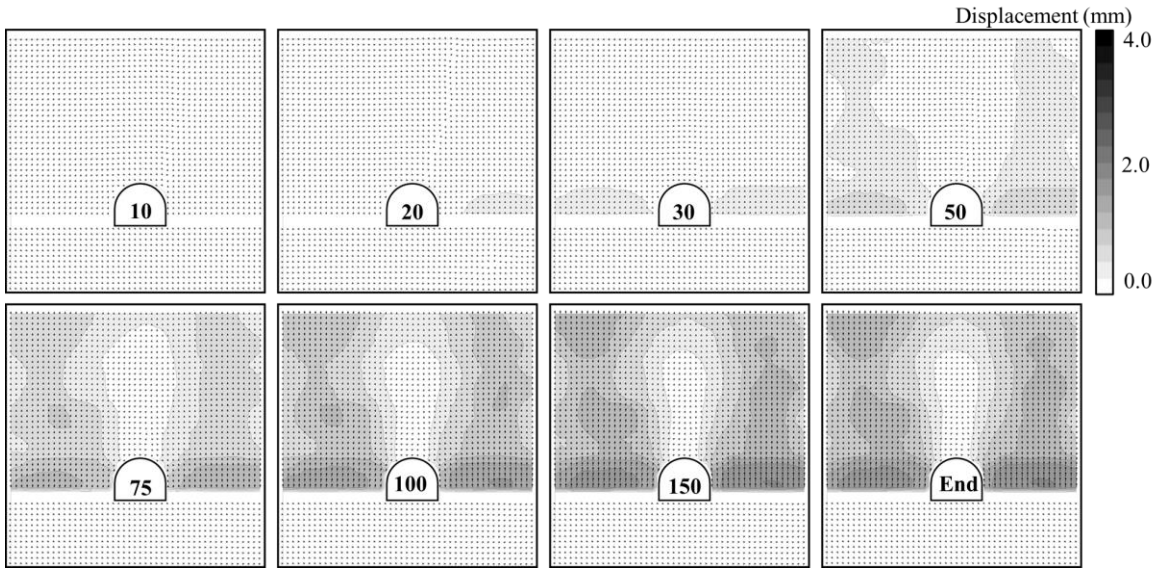

Figure 6-21 Time-dependent nodal displacement around tunnel shoulder for **S6-W**

6.4.5 Impacts of location of expansive soils on tunnels

The model tests explained in this chapter signify the key role played by the location and corresponding expansive pressure exerted on tunnels due to swelling forces. As represented in the results, the location of expansive soil influenced the corresponding section of the tunnel. Figure 6-22 compares the pressure observed by different gauges on different location for the model tests conducted by varying the location of the expansive soil. The final pressures for model tests namely S6-B, S6-W, S6-S and S6-T are represented. Figure 6-23 represents the final degree of saturation of the expansive layer at the completion of tests. The reduced water level at completion is one of the reasons for expansive pressure being less than the pressure observed in free swell tests along with changes in confinements and boundary conditions. Figure 6-24 draws the final comparison of expansive pressure and nodal displacement at the completion of the tests for varying locations.

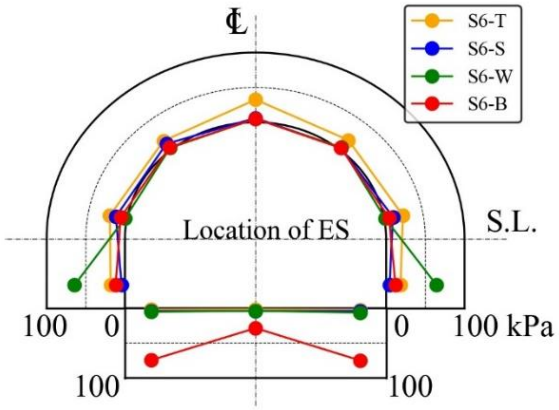

Figure 6-22 Comparison of pressure on tunnel sections for varied location of expansive soil

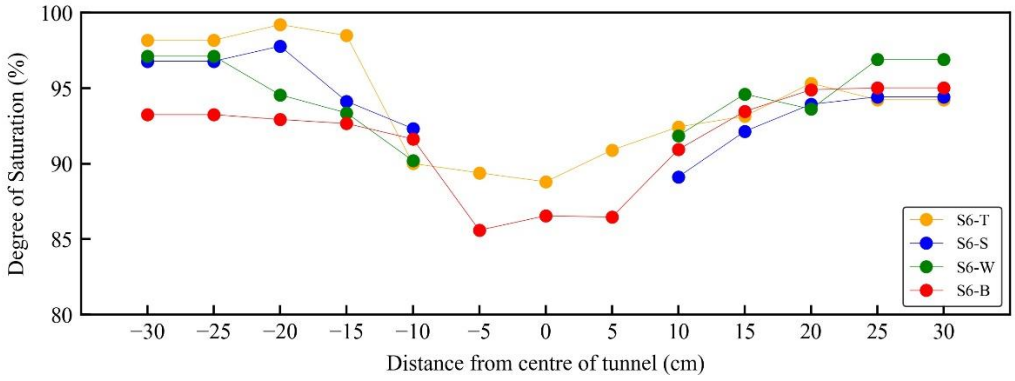

Figure 6-23 Saturation level of expansive soil at the completion of model test

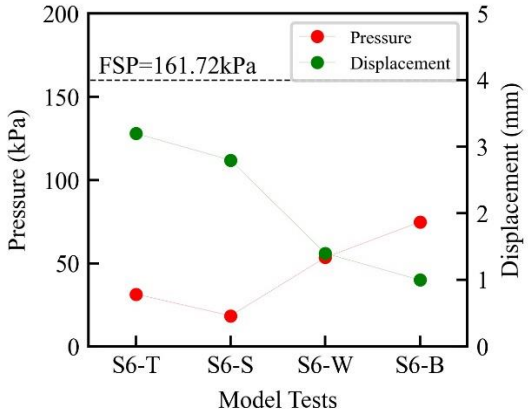

Figure 6-24 Comparison of final swelling pressure and displacement for model tests based on location of expansive soil

6.5 SUMMARY

This chapter summarized the long-term impacts of expansive soils on stability of tunnels based on the location of expansive soil. The impacts were evaluated by considering the locality of expansive soil around crown, shoulder and wall sections of the tunnel. The swelling impacts were evaluated by pressure increments with respect to time and the corresponding displacements in the vicinity of expansive soil around tunnel were calculated by PIV analysis. It was found that the location of expansive soil significantly impacts the time-dependent response of the tunnel to expansive soils. As the soil is near the crown section, the crown portion of the tunnel is severely impacted due to intensifying pressures. The ground above the crown moved upward by this pressure. The magnitude of this pressure was about 6 times the overburden pressure and 18% of the free swell pressure measured in the oedometer test. The shoulder section of the tunnel was near the centroid of the tunnel hence almost all the pressure points of the tunnel responded to the expansive pressure exerted by expansive soil placed at the shoulder of the tunnel. The surrounding ground moved vertically and time-dependent variation in the gauges in the vicinity of expansive layer varied differently for different gauges. The shoulder section experienced an additional pressure of 7 times the over burden pressure that fell down to normal overburden as the impacts were taken by spring-line gauges thereafter. This pressure is significant enough to squeeze the tunnel and cause damage to lining. Similarly expansive soil at wall sections of the tunnel tended to squeeze the tunnel with an enhanced pressure of about 10 times the overburden pressure. The time-dependent strains in the surrounding ground evaluated in this study suggest that swelling pressure application is quicker as compared to the heaving of the ground and the tunnel structure may look perfectly safe and no ground movement may be seen yet, the tunnel might be going through intense addition in pressure due to presence of expansive soil in the vicinity. The time-dependent pressure also suggested that the water contact with expansive soil will speedily increase the pressure before going into creep zone and majority of damage is expected as soon as the expansive soil interacts with water.

CHAPTER 7 IMPACTS OF SURROUNDING GROUND STIFFNESS AND EXPANSIVE SOILS ON TUNNELS

7.1 INTRODUCTION

This chapter concentrates on the evaluation of the time-dependent variation of swelling pressure on tunnels due to presence of expansive soils in the rock-mass around the tunnels and difference in the stiffness and strength of the surrounding ground present beneath the tunnel. The model tests were conducted by preparation of ground under the tunnel using the silica sand No. 8 and No. 6 but their relative density was increased to 90% rather than 80% as for S8-B and S6-B cases. These cases are designated as S8(90)-B and S6(90)-B. The expensive soil in both the cases was placed at the invert section of the tunnel while the rest of the ground above the tunnel was prepared by silica sand No. 6 at 80% of its relative density. In another test, the ground beneath the tunnel was prepared by using concrete blocks while rest of the procedure being same as for above mentioned tests. This test is referred to as Bk-B. The response of the tunnel lining was adjudicated by placing the 20 mm expansive soil under the tunnel for all these cases. The swelling of the layer upon saturation imposed additional pressure on the tunnel invert section but for these cases the surrounding ground under the tunnel was different hence, the impacts were evaluated based on two conditions namely the expansive soil at invert and variation of surrounding ground stiffness under the expansive layer. These conditions evaluated the time-dependent impacts of expansive soil availability in the geological repositories around the tunnels with difference in surrounding ground stiffness. The testing conditions like water intrusion and ground movements evaluation through PIV analysis etc. were kept same as for all the previous cases. The ground above the tunnel was always kept as silica sand No. 6 at 80% of its relative density. The density of the ground above the tunnel could not be increased as to avoid the impacts of greater dumping effort to affect the gauges on the tunnel. In addition, a comparison was made among these cases based on the difference of the material used as the surrounding ground under the tunnel was different. The time-dependent deformation due to expansive soils at heave and different surrounding ground stiffness is explained in detail in this chapter. Table 7-1 represents these conditions.

7.2 EXPANSIVE SOIL AND STIFFER S8 AS BASE GROUND

7.2.1 Experimental conditions for S8(90)-B

As explained earlier, the experimental conditions in this case include placing silica sand No. 8 at 90% of its relative density overlaid by a 20 mm thick layer of expansive soil placed at direct contact with the invert section of the tunnel. The ground beneath the tunnel was prepared as per the previous tests including the expansive soil layer placed in different sections with fixed volume and dry density of the bentonite-Toyoura sand mixture. Again, the expansive soil was not placed throughout the length of the model rather it was discontinued at 50mm on each side. This discontinuity was kept ensuring that water would percolate through the silica sand openings provided on each side of expansive soil and the process of saturation would be carried out at a quick pace. The overburden height was kept to 3D and water level for saturation maintained at 1D. This test was referred to as S8(90)-B in the nomenclature adopted in this study where 90 signifies the relative density of sand under the tunnel and ‘B’ signifies the location of the expansive soil layer at the bottom of the tunnel invert. The schematic diagram of this test is represented in Figure 7-1 below:

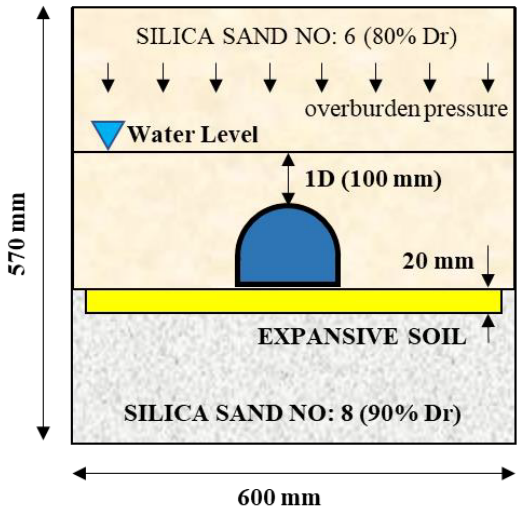

Figure 7-1 Schematic diagram for **S8(90)-B** model test

Table 7- 1 Experimental conditions for surrounding ground stiffness model tests

Location / S. Ground	Relative Density	Name
Sand No.8 UT, else No.6	90% UT, rest 80%	S8(90)-B
Sand No.6 UT, else No.6	90% UT, rest 80%	S6(90)-B
Blocks UT, else No.6	80% above tunnel	Bk-B

7.2.2 Tunnel response to S8(90)-B

Figure 7-2 represents the kinetics of the pressure on tunnel for S8(90)-B model test. The pressure increment was in line with S6 test initially and the magnitude of the overburden pressure was comparable. As the overlying layers of the surrounding ground were completed and saturation was started, the expansive soil layer responded to water interaction and started to expand. The swelling of the layer imposed additional pressure to the invert section of the tunnel. The invert left and right gauges (Il & Ir) did not immediately respond to additional pressure for first 20 hours of the test as it took a bit longer for water to go up through finer silica sand No. 8 for this case. As the water crept up, the invert gauges showed a rising trend in pressure which was a lot swifter as compared to S8-B case. The swelling pressure kept on rising quickly with further time passing and became constant for a long enough time until the completion of the test. No significant strain hardening zone was observed in this case in which the soil kept on taking the expansion load without depicting changes in the pressure. The expansive soil minerals settled as the voids went on filling by water with the passing time. The water interaction caused change in the degree of saturation of the soil. The expansive layer started to saturate from the bottom as the layer with immediate contact with tunnel invert was yet to experience the saturation because of being tightly packed under the tunnel. This was the reason that invert centre gauge responded a lot later as compared to the invert edge gauges. The sections of the expansive soil other than under the tunnel were getting saturated from both side

top and bottom. Only the layer right beneath the tunnel was being saturated from the bottom side. The wall gauges for this test experienced a lot more pressure and even greater than the invert centre gauge. As the saturation of the expansive layer kept on increasing with passing time, the pressure kept on rising until it remained constant again for a long enough period. The pressure on the gauges above wall sections felt relieving of the pressure and a decline was observed in pressure for these gauges which even fell below the over burden pressure as the swelling force was stronger owing to dense ground under the tunnel. The rise of pressure on wall gauges was not as quick as for the invert gauges being not in direct contact with the expansive soil. The duration of the test was 250 hours. A mismatch in the swelling curves was observed initially for invert edge gauges owing to variation in water contact of expansive soil.

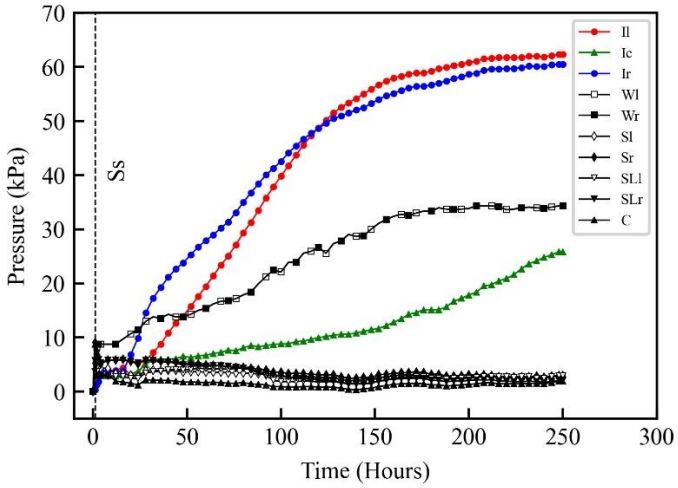

Figure 7-2 Pressure kinetics at different sections of the tunnel for **S8(90)-B** model test

The surrounding ground especially under the invert did not absorb the swelling as much being harder than S8-B. The pressure variation was smooth as the impacts were directly taken up by the gauges installed in the tunnel. As the layer approached full saturation, the rate of rise of expansive pressure subsided and finally it remained constant for long enough time representing that the expansive layer has reached its limiting swell potential. The invert edge gauges in this case represented final pressure of 62.33 and 60.5 kPa respectively. The centre gauge showed 25.83 kPa at the end of the test and was still rising. The wall sections represented 34.32 kPa pressure on left and right sides. Figure 7-3 represents the final pressure distribution on different sections of the tunnel at completion.

Around 38.53% of the free swell pressure was recorded with slight increase (0.18 MPa) in stiffness of the surrounding ground under the tunnel (refer to Chapter 3 Table 3-5). This rise is significantly more as compared to the S8-B case. However, this pressure is still lower than the free swell pressure of expansive soil the reason being the absorption of the expansive pressure by the sand No. 6 surrounding ground above the tunnel, the difference of boundary conditions and corresponding confining pressure.

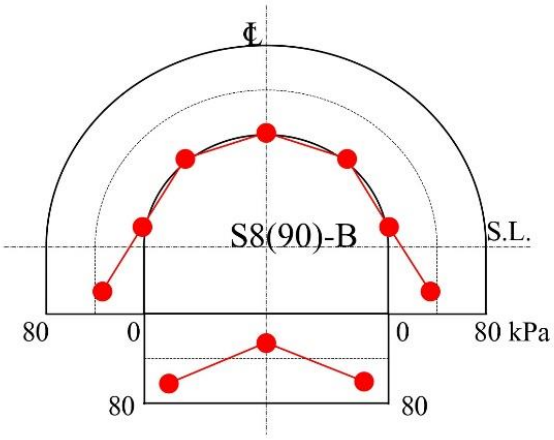

Figure 7-3 Representation of pressure at different sections of the tunnel for **S8(90)-B**

Nonetheless, the expansive pressure exerted on the invert section of the tunnel is nearly 12 times of the pressure as compared to the S8 case with no expansive soil around implying significant pressure increment on tunnel structure constructed in strata comprising of expansive soils laid above the stiffer base.

7.2.3 Time-dependent expansive pressure variation for S8(90)-B

Different time steps were selected from Figure 7-2 and the expansive pressure variation on the tunnel was comprehended to evaluate the time-dependent impacts of expansive soils on tunnels. Consequently, Figure 7-4 represents this variation for various time-periods. The above transformation of time-dependent pressure variation signifies the stability of tunnel with increase in degree of saturation of expansive soil. The consequent impacts of expansive soil with time showed the critical phase where pressure significantly rose. As for this case, the pressure for initial 30 hours remained comparable with the overburden pressure. The expansion pressure did not shoot up as for other cases. The test is comparable with S8-B as the ground beneath the tunnel was Sand No. 8 but at a higher relative density. The pressure on invert gauges started to rise around 30th hour and kept on rising rather steadily thereafter. Similar to S8-B case, the time-dependent stability of tunnels in expansive strata for this case is elaborated by carrying out a dissection of the swelling curve for invert section and is divided into four similar zones enlisted below:

1- Acceleration zone

The acceleration zone for this case was delayed as expansive soil underwent saturation. The acceleration zone for this case started from 30th hour. Consequently, the invert gauges represented a pressure higher than the initial overburden and the delayed response could be attributed to a denser S8 and it took some time for water to penetrate through dense finer particles to reach the expansive layer. The pressure kept rising quickly in a smaller time frame and peaked until a specific value at an early stage of the swelling. The increment of pressure was a lot more and signified the difference in the surrounding ground stiffness as dense silica sand No. 8 was used. The pressure experienced within this range covered the elastic response of tunnel to expansion.

2- Creep and renaissance zone

The creep zone was not very dominant in this case and got mixed with the acceleration zone. As explained earlier, the stiffness of S8 is lower than S6 even at higher density, a part of swelling pressure was still absorbed by the soft surrounding ground, but the overall pressure was higher than S8-B case implying the importance of surrounding ground stiffness around expansive soil. No particular declining trend in swelling pressure attained in the acceleration zone was observed in this case. The pressure reached around 50 kPa including the overburden pressure on the invert section until 120^{th} hour. This region signifies the elastic response of the tunnel to additional pressure due to expansion of surrounding expansive soil in a comparatively stiffer non-swelling surrounding ground beneath. The zone identifies the preliminary deterioration and temporal setting of the soil elements. As it is hard to realize time similitude for field tunnels yet, this zone implies that underground passageways have experienced a significant rise in external pressure although they might look perfectly stable and elastic deformations have occurred and temporary stable zone of creep is going on.

The swelling pressure on the invert section of tunnel kept rising in renaissance part of this zone however, the rate of rise of pressure in this zone was subsided after undergoing a quick rise in the acceleration zone. The pressure increase in this period was not as intense as for the earlier case, however it kept on escalating. The slope of the curve in this zone was very mild in contrary to the steep slope in acceleration zone. The rate of rise of pressure kept declining until reaching the limiting visco-plastic response of the surrounding ground. Majority of swelling pressure was observed earlier but the rise in this region was around 12 kPa. The time range for this state was within 120-220 hours. The tunnel structure might start to depict structural damages like heaving and spalling of lining depending upon the location of pressure provided by the expansive layer which was at the invert section. The surrounding rock would start taking up the additional pressure around the tunnel and undergo deteriorations due to volume change. The consequent strength parameters of surrounding ground would reduce, and typical failures might occur.

3- Steady zone

The maximum swelling pressure of the expansive soil was attained in this zone. The expansive soil around the invert edges had attained maximum degree of saturation and has impacted the tunnel structure to its maximum potential. The firmness of tunnel depends upon the strength of its lining and the ability of the surrounding ground to cater the additional swelling pressure. Majority of damage would have occurred in the creep and renaissance zone and the stability would be examined. If no significant damage like heaving or spalling is observed until this zone has reached, the structure is deemed to have taken up the additional swelling stresses and is designed well to cater expansion and is referred to as safe against swelling pressure. This time-dependent analysis can be utilized to evaluate the life of the tunnels constructed in swelling strata with denser surrounding ground under the tunnel as compared to S8-B case and can help in quantifying the magnitude of swelling pressures that can be experienced by the tunnel during different phases of expansion with respect to time.

A symmetrical representation of pressure variation was observed on gauges that are placed on identical locations on each side of the tunnel. Initial unsymmetrical representation is subjected to water interaction at different time spans with different gauges.

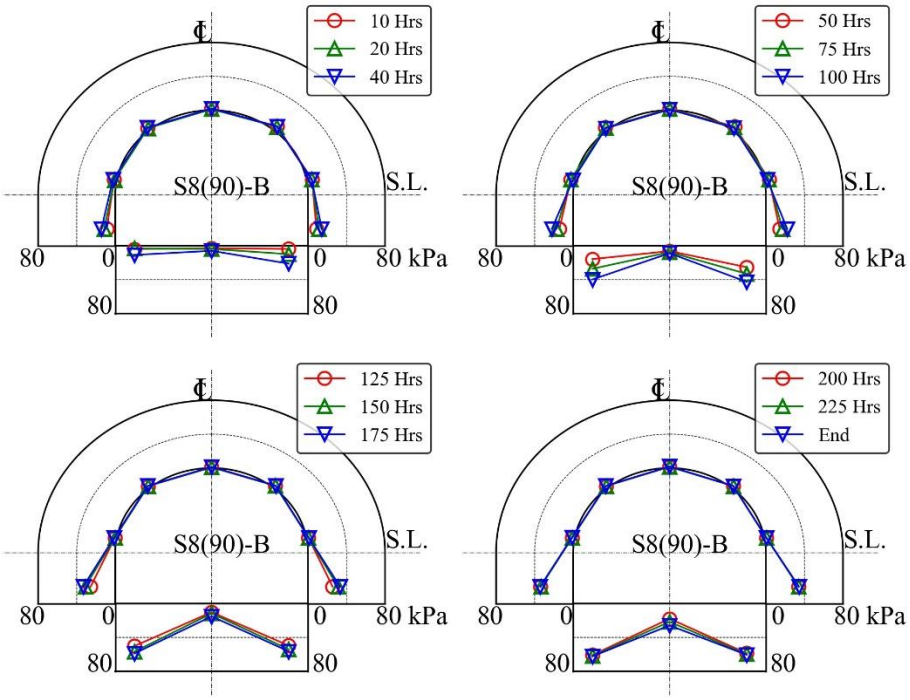

Figure 7-4 Time-dependent expansive pressure variation for **S8(90)-B**

7.2.4 Surrounding ground movements for S8(90)-B

The PIV analysis carried out for S8(90)-B is represented in Figure 7-5 below. The time-dependent displacement of the node nearest to the invert gauge which was in direct contact with the expansive soil layer was evaluated. The term IL(P) and IR(P) consequently represent the expansive pressure variation on left and right invert gauges respectively while IL(D) and IR(D) are the corresponding displacement curves in the graph.

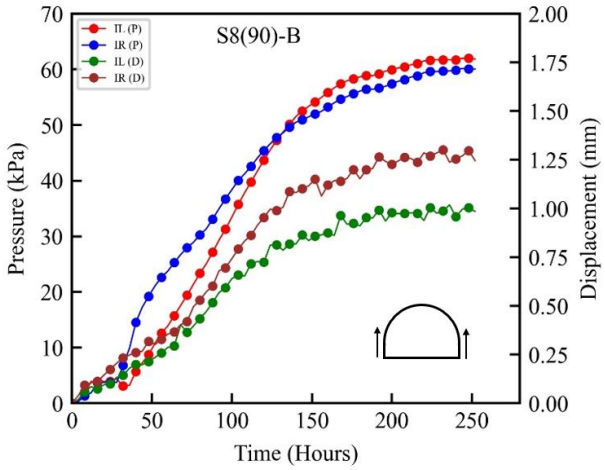

Figure 7-5 Time-dependent nodal displacement and expansive pressure near invert for **S8(90)-B**

Owing to the increased surrounding ground stiffness under the tunnel as compared to earlier case (S8-B), the displacement in the initial pressure rise zone of the expansive soil was swift as compared to the cumulative final displacement observed. During this range the expansive soil was undergoing saturation and the volumetric strain was developing to overcome the overburden pressure, but it was observed quickly as the surrounding ground is not taking much of the expansive pressure being stiffer now. This zone represented the continuous rate of strain and continued in the constant creep state where the surrounding ground kept displacing and showed deformation for an extended period of time. As the creep and renaissance zone finished, the displacement tended to stabilize A slight difference in magnitude of displacement was observed in this case on both sides of the invert. The reason could be the amount of expansive pressure being applied heterogeneously on the surrounding ground on both sides based on degree of saturation of expansive soil. As the time went on, the rate of rise of displacement got slower and its magnitude supressed significantly until the final stage reached where swelling pressure and corresponding nodal displacement became constant. The image analysis through PIV performed for this case represented the time-dependent directional displacement of the nodes. Based on the swelling kinetics graph, different time spans were evaluated for the visual representation of the surrounding ground movements with time. Figure 7-6 represents the said displacement through contours and vectors of displacement for these specific time periods. The deformation of the surrounding ground initiated slowly in this case and as the pressure surged and water interacted with expansive soil along with stiffer surrounding ground around the tunnel, the displacements enhanced. Majority of displacement occurred during the strain hardening zone where swelling pressure slightly subsided and reached a steady state with expansive soil being saturated. The results suggest that as the surrounding ground gets stiffer, the swelling pressure and ground displacement occur simultaneously. But the magnitude of displacement was nearly half of what was observed in S8-B case.

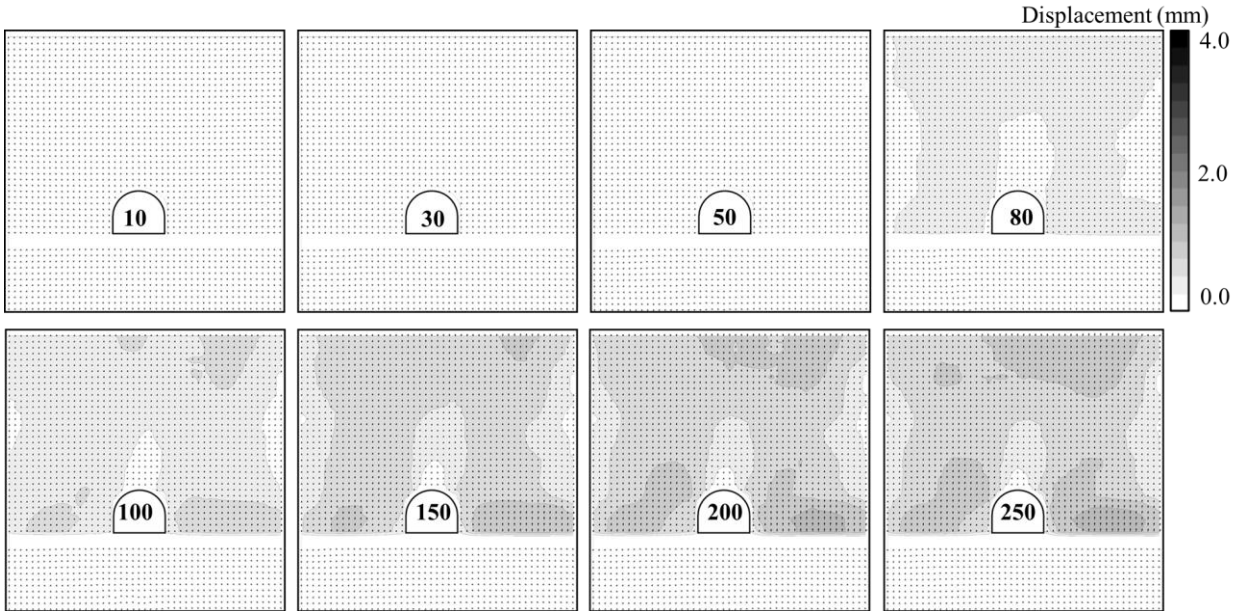

Figure 7-6 Time-dependent nodal displacement around tunnel invert for **S8(90)-B**

An accumulative displacement of 1.00 mm and 1.23 mm was observed near the invert section on left and right side respectively. The displacement right above the tunnel is significantly ceased as the tunnel model is locked in its position and the pressure exertion above the crown is restrained vertically. Major displacement is observed right above the expansive soil layer and as the distance from the layer increases, the displacement got reduced. The analysis reflects that the magnitude of the deterioration near the tunnel buried underground would be a lot more as compared to what would be experienced at the ground level.

7.3 EXPANSIVE SOIL AND STIFFER S6 AS BASE GROUND

7.3.1 Experimental conditions for S6(90)-B

As explained earlier, the experimental conditions in this case include placing silica sand No. 6 at 90% of its relative density overlaid by a 20 mm thick layer of expansive soil placed at direct contact with the invert section of the tunnel. The ground beneath the tunnel was prepared as per the previous tests including the expansive soil layer placed in different sections with fixed volume and dry density of the bentonite-Toyoura sand mixture. Again, the expansive soil was not placed throughout the length of the model rather it was discontinued at 50mm on each side. The overburden height was kept to 3D and water level for saturation maintained at 1D. This test was referred to as S6(90)-B in the nomenclature adopted in this study where 90 signifies the relative density of sand under the tunnel and 'B' signifies the location of the expansive soil layer at the bottom of the tunnel invert. The schematic diagram of this test is represented in Figure 7-7.

7.3.2 Tunnel response to S6(90)-B

Figure 7-8 represents the kinetics of the pressure on tunnel for S6(90)-B model test. The pressure increment was in line with S6 test initially and the magnitude of the overburden pressure was comparable. As the overlying layers of the surrounding ground were completed and saturation was started, the expansive soil layer responded to water interaction and started to expand. The swelling of the layer imposed additional pressure to the invert section of the tunnel. The invert left and right gauges (Il & Ir) immediately respond to additional pressure for first 25 hours of the test as the test conditions were very close to S6-B test. The reason for slight change in the slope of the curve making it delayed for gauges to respond was a bit longer time for water to go up through relatively dense silica sand No.6 for this case. As the water crept up, the invert gauges showed a rising trend in pressure which was a lot swifter as compared to S6-B case.

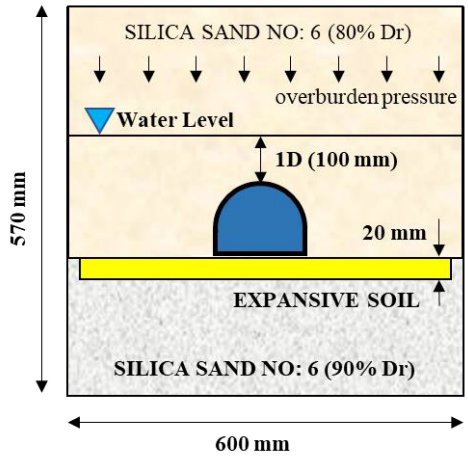

Figure 7-7 Schematic diagram for **S6(90)-B** model test

By the 30th hour, the pressure stabilized and remained constant for a significant time until 60th hour. The reason could be the strain hardening zone where the soil kept on taking the expansion load without depicting changes in the pressure. Also, the expansive soil minerals settled as the voids went on filling by water with the passing time. The water interaction caused change in the degree of saturation of the soil. The expansive layer started to saturate from the bottom as the layer with immediate contact with tunnel invert was yet to experience the saturation because of being tightly packed under the tunnel. The sections of the expansive soil other than under the tunnel were getting saturated from both top and bottom. Only the layer right beneath the tunnel was being saturated from the bottom side. This caused the pressure increment to relax for some time but did not remain constant for long. As the saturation of the expansive layer kept on increasing with passing time, the pressure started to rise again until it remained constant again for a long enough period. The pressure kept on rising on the invert section gauges. As the saturation kept rising, the vicinity of expansive pressure expanded and took the impacts to the wall section of the tunnel being relatively close to the expansive soil layer. The wall gauges on both sides of the tunnel started responding to the additional pressure to the swelling at a delayed span as compared to the invert section but this pressure was not as significant as in S6-B case because the ground beneath the tunnel was stiffer in this case and more expansive pressure was taken up by the tunnel itself. The surrounding ground did not absorb the swelling as much being harder than before. The pressure variation was smooth as the impacts were directly taken up by the gauges installed in the tunnel model. The layer beneath the tunnel kept on saturating with respect to time and pressure kept rising. As the expansive layer pushed the tunnel structure upwards along with the surrounding ground, the gauges on spring-line and shoulder section represented with slight reduction in pressure. This happened because the upward push relieved the overburden pressure on these sections insignificantly. As the layer approached full saturation, the rate of rise of expansive pressure subsided and finally it remained constant for long enough time representing that the expansive layer has reached its limiting swell potential.

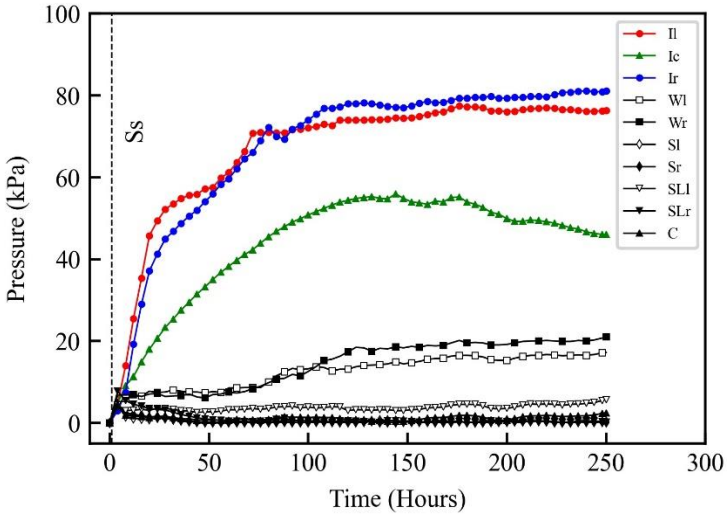

Figure 7-8 Pressure kinetics at different sections of the tunnel for **S6(90)-B** model test

The invert edge gauges in this case represented final pressure of 76.4 and 81.13 kPa respectively. The invert center gauge showed 46.07 kPa at the end of the test. The wall sections represented 21 and 17.23 kPa on left and right side respectively. The rate of swelling pressure recorded on gauges was swiftest in the beginning and subsided slowly as the test went on to completion. Figure 7-9 represents the final pressure distribution on different sections of the tunnel at completion.

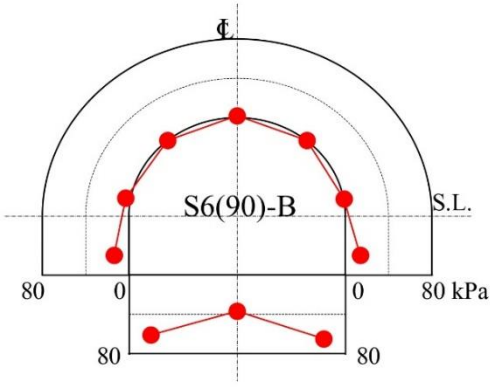

Figure 7-9 Representation of pressure at different sections of the tunnel for **S6(90)-B**

Around 50.31% of the free swell pressure was recorded with slight increase (0.19 MPa) in stiffness of the surrounding ground under the tunnel where silica sand No.6 was placed at 90% of its relative density. Also, the rate of swelling got much higher for this case in the initial hours and almost 80% of the total swelling pressure observed was already recorded on bottom gauges within initial 70 hours of the test. The remaining swelling pressure kept on rising with passing time. This rise is slightly more than the S6-B case. However, this pressure is still lower than the free swell pressure of expansive soil the reason being the absorption of the expansive pressure by the sand No. 6 surrounding ground in case of model test and the difference of boundary conditions and

corresponding confining pressure. Nonetheless, the expansive pressure exerted on the invert section of the tunnel is nearly 16 times of the pressure as compared to the S6 case with no expansive soil around implying significant pressure increment on tunnel structure constructed in strata comprising of expansive rocks / soils.

7.3.3 Time-dependent expansive pressure variation for S6(90)-B

As explained for earlier model test, to further elaborate the time-dependent pressure variation on the tunnel for S6(90)-B, different time steps were selected from Figure 7-8 and the expansive pressure variation on the tunnel was comprehended to evaluate the time-dependent impacts of expansive soils on tunnels. Consequently, Figure 7-10 represents this variation for various time-periods. The above transformation of time-dependent pressure variation signifies the stability of tunnel with increase in degree of saturation of expansive soil. The consequent impacts of expansive soil with time showed the critical phase where pressure significantly rose. As stated earlier, the pressure for initial 80 hours had reached around 80% of the total pressure and kept on rising rather steadily thereafter. So, it was deemed necessary to dissect the pressure changes within this range to examine the time-dependent stability of tunnels in expansive strata. As for this case, it is elaborated by carrying out an examination of the swelling curve for invert section and is divided into four similar zones as for all the model tests and are enlisted below:

1- Acceleration zone

The acceleration zone for this case reflected a lot quicker pressure on the invert section as the expansive soil came in contact with water. Consequently, the invert gauges represented a pressure higher than the initial overburden. The pressure kept rising quickly in a smaller time frame and peaked until a specific value at an early stage of the swelling. The increment of pressure was a lot more and signified the difference in the surrounding ground stiffness as dense silica sand No. 6 at 90% of its relative density was used. The pressure experienced within this range covered the elastic response of tunnel to expansion.

2- Creep zone

S6(90)-B represented a shorter duration for creep zone in which the pressure remained constant while expansive soil underwent saturation. There was no decline in constant swelling pressure attained in the acceleration zone, but the slower rise was observed in this case. The pressure remained around 55 kPa including the overburden pressure on the invert section from 25^{th} hour to 50^{th} hour. This region signifies the visco-elastic response of the tunnel to addition pressure due to expansion of surrounding soil in a comparatively stiffer non-swelling surrounding ground. The zone identifies the preliminary deterioration and temporal setting of the soil elements. As it is hard to realize time similitude for field tunnels yet, this zone implies that underground passageways have experienced a significant rise in external pressure although they might look perfectly stable and elastic deformations have occurred and temporary stable zone of creep is going on.

3- Renaissance zone

The swelling pressure on the invert section of tunnel started to rise again in this zone after undergoing a pause in the creep zone. The pressure increase in this period was not as intense as for the acceleration case, however it kept on growing. The slope of the curve in this zone was very mild in contrary to the steep slope in acceleration zone. The rate of rise of pressure kept declining until

reaching the limiting visco-elastic response of the surrounding ground. Majority of swelling pressure was observed earlier but the rise in this region was around 20 kPa. This range was within 70-100 hours for S6(90)-B and as expansive soil attained higher degree of saturation thereafter, a minute rise in expansive pressure was observed. The tunnel structure might start to depict structural damages like heaving and spalling of lining depending upon the location of pressure provided by the expansive layer which was at the invert section. The surrounding rock would start taking up the additional pressure around the tunnel and undergo deteriorations due to volume change. The consequent strength parameters of surrounding ground would reduce, and typical failures might occur.

4- Steady zone

The maximum swelling pressure of the expansive soil was attained in zone. The expansive soil around the invert edges had attained maximum degree of saturation and has impacted the tunnel structure to its maximum potential. The firmness of tunnel depends upon the strength of its lining and the ability of the surrounding ground to cater the additional swelling pressure. Majority of damage would have occurred in the renaissance zone and the stability would be examined however if no significant damage like heaving or spalling is observed during this zone has reached, the structure is deemed to have taken up the additional swelling stresses and is designed well to cater expansion and is referred to as safe against swelling pressure. This time-dependent analysis can be utilized to evaluate the life of the tunnels constructed in swelling strata with denser surrounding ground as compared to S6-B case and can help in quantifying the magnitude of swelling pressures that can be experienced by the tunnel during different phases of expansion with respect to time.

A symmetrical representation of pressure variation was observed on gauges that are placed on identical locations on each side of the tunnel. The expansive soil location at the invert section with strengthening the soil beneath the tunnel significantly enhanced the swelling pressure on tunnel in addition to the overburden pressure. This case was nearly the same as S6-B however the expansive pressure observed by the invert section was more than the earlier case. This test also strengthens the repeatability of model tests performed in this study. As the time went on, the pressure bulb is extended to wall section of the tunnel too. This comparison signified the criticality of expansive soil in the geological repositories around the tunnel structures and the number of damages that could occur due to water interaction of the expansive geology and consequent long-term stability of mountainous tunnels.

7.3.4 Surrounding ground movements for S6(90)-B

The PIV analysis carried out for S6(90)-B is represented in Figure 7-11. The time-dependent displacement of the node nearest to the invert gauge which was in direct contact with the expansive soil layer is evaluated. The term IL(P) and IR(P) consequently represent the expansive pressure variation on left and right invert gauges respectively while IL(D) and IR(D) are the corresponding displacement curves in the graph. Owing to the increased surrounding ground stiffness under the tunnel as compared to earlier case (S6-B), the displacement in the initial pressure rise zone of the expansive soil was sluggish as compared to the cumulative final displacement observed. During this range the expansive soil was undergoing saturation and the volumetric strain was developing to overcome the overburden pressure, but it was observed quickly as the surrounding ground is not taking much of the expansive pressure being stiffer now.

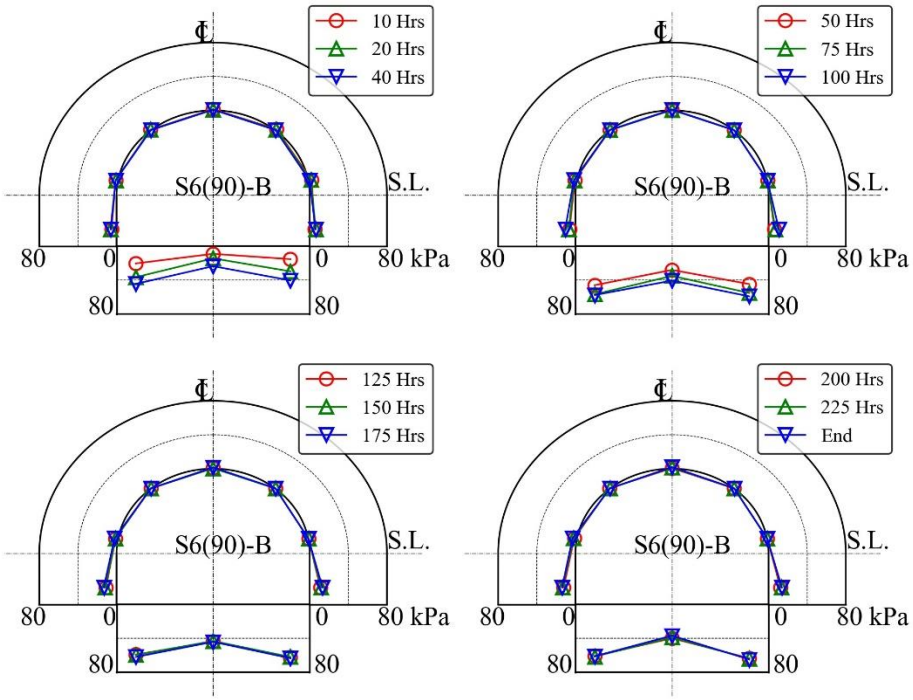

Figure 7-10 Time-dependent expansive pressure variation for **S6(90)-B**

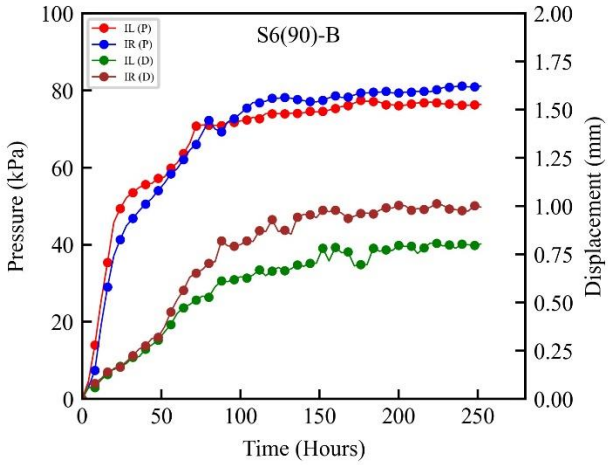

Figure 7-11 Time-dependent nodal displacement and expansive pressure near invert for **S6(90)-B**

This zone represented the continuous rate of strain and continued in the constant creep state where the surrounding ground displaced quickly and showed deformation for an extended period of time. As the creep zone finished, the displacement kept on rising in renaissance zone. A slight difference in magnitude of displacement was observed in this case on both sides of the invert. The reason could be the amount of expansive pressure being applied heterogeneously on the surrounding ground on both sides based on degree of saturation of expansive soil. As the time went on, the rate of rise of

displacement got slower and its magnitude supressed significantly until the final stage reached where swelling pressure and corresponding nodal displacement became constant. The image analysis through PIV performed for this case represented the time-dependent directional displacement of the nodes. Based on the swelling kinetics graph, different time spans were evaluated for the visual representation of the surrounding ground movements with time.

Figure 7-12 represents the said displacement through contours and vectors of displacement for these specific time periods. The deformation of the surrounding ground initiated slowly in this case and as the pressure surged and water interacted with expansive soil along with stiffer surrounding ground under the tunnel, the displacements enhanced. Majority of displacement occurred during the strain hardening zone where swelling pressure slightly subsided and reached a steady state with expansive soil being saturated. The results suggest that as the surrounding ground particularly under the tunnel gets stiffer, the swelling pressure and ground displacement occur simultaneously. But with stiffer ground under the tunnel, the magnitude of upward displacement was nearly the same as compared to displacement observed in S6-B case. It means that if the rock mass under the tunnel is stiff, more upward displacement will occur strengthening the repeatability of PIV analysis too.

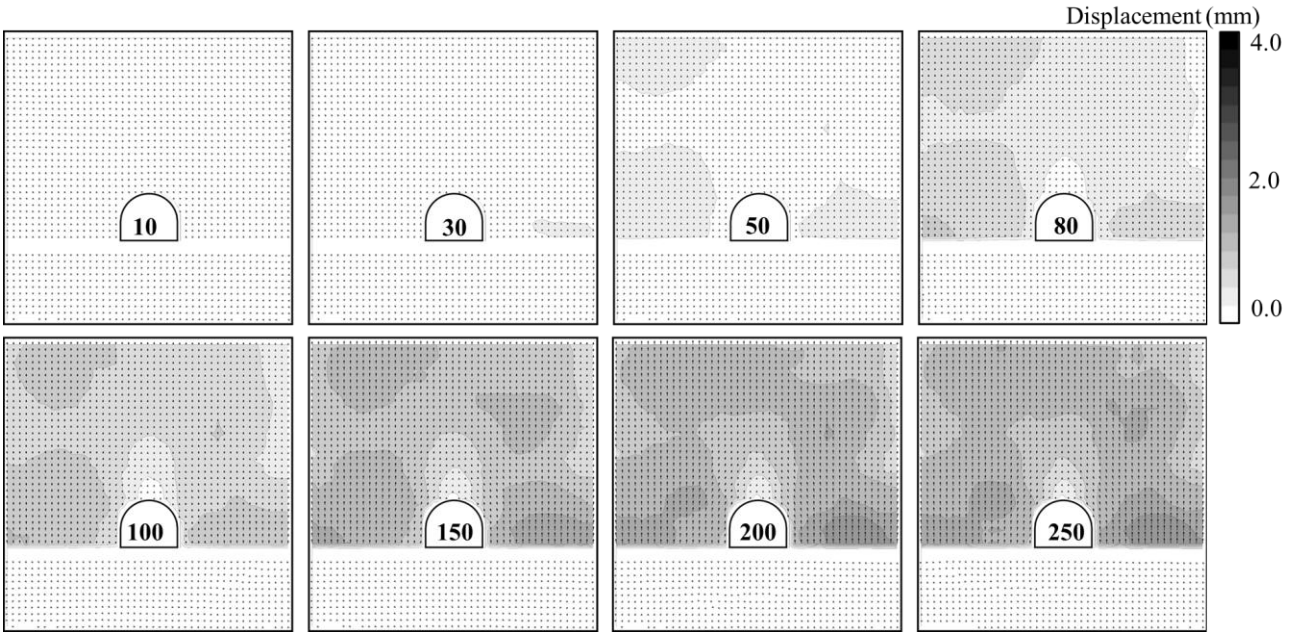

Figure 7-12 Time-dependent nodal displacement around tunnel invert for **S6(90)-B**

An accumulative displacement of 1.00 mm and 0.79 mm was observed near the invert section on left and right side respectively. The displacement right above the tunnel is significantly ceased as the tunnel model is locked in its position and the pressure exertion above the crown is restrained vertically. Major displacement is observed right above the expansive soil layer and as the distance from the layer increases, the displacement got reduced. The analysis reflects that the magnitude of the deterioration near the tunnel buried underground would be a lot more as compared to what would be experienced at the ground level.

7.4 EXPANSIVE SOIL AND CONCRETE AS BASE GROUND

7.4.1 Experimental conditions for BK-B

As explained earlier, the experimental conditions in this case include placing concrete blocks at bottom of the tunnel overlaid by a 20 mm thick layer of expansive soil placed at direct contact with the invert section of the tunnel. To keep the experimental conditions identical with previous tests with this one, aluminium plates were placed on top of blocks with perforations.

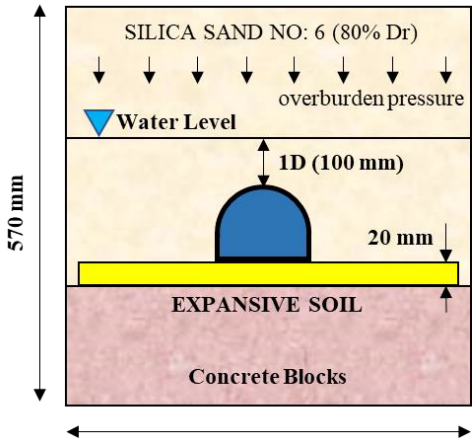

Figure 7-13 Schematic diagram for BK-B model test

Again, the expansive soil was not placed throughout the length of the model rather it was discontinued at 50mm on each side. This discontinuity was kept ensuring that water would percolate through the silica sand openings provided on each side of expansive soil and the process of saturation would be carried out at a quick pace. The overburden height was kept to 3D and water level for saturation maintained at 1D. This test was referred to as BK-B in the nomenclature adopted in this study where 'Bk' signifies the concrete blocks under the tunnel and 'B' signifies the location of the expansive soil layer at the bottom of the tunnel invert. The schematic diagram of this test is represented in Figure 7-13.

7.4.2 Tunnel response to BK-B

Figure 7-14 represents the kinetics of the pressure on tunnel for BK-B model test. The pressure increment was in line with S6 test initially and the magnitude of the overburden pressure was comparable. As the overlying layers of the surrounding ground above the tunnel were completed and saturation was started, the expansive soil layer responded to water interaction and started to expand. The swelling of the layer imposed additional pressure to the invert section of the tunnel. The invert left, right and invert centre gauges (Il, Ir, Ic) immediately respond to additional pressure for first 10 hours of the test as the test conditions were very close to S6(90)-B test. Interestingly, the invert centre gauge in this case responded rather quickly as compared to edge gauges. The reason was the stiff blocks under the tunnel which were transforming the entire expansive pressure to the entire invert section of the tunnel. The slope of the rising line was steepest for this case as compared to the two previous cases. The rising trend was uniform for all the invert gauges and there was no delay in

experiencing the pressure rise. As the water crept up rapidly through porous blocks and aluminium plates, the invert gauges showed a swift rising trend in pressure.

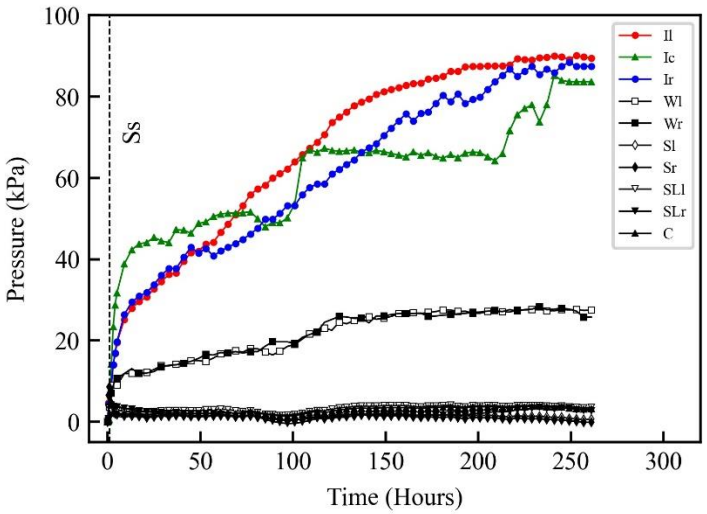

Figure 7-14 Pressure kinetics at different sections of the tunnel for BK-B model test

By the 20th hour, the pressure rose but not at the same rate as earlier and remained increasing for a significant time until 50th hour for edge gauges and 30th hour for invert centre gauge. There was no particular zone where a constant swelling pressure or declining swelling pressure was seen apart for invert centre gauge. The strain hardening zone where the soil kept on taking the expansion load without depicting changes in the pressure was not significant yet, existent. Also, the expansive soil minerals settled as the voids went on filling by water with the passing time. The water interaction caused change in the degree of saturation of the soil. The expansive layer started to saturate from the bottom as the layer with immediate contact with tunnel invert was yet to experience the saturation because of being tightly packed under the tunnel. But in this case, since the bottom ground was concrete blocks, all the pressure was transformed to tunnel invert. The sections of the expansive soil other than under the tunnel were getting saturated from both side top and bottom. Only the layer right beneath the tunnel was being saturated from the bottom side. This caused the rate of rise of pressure increment to relax for some time specifically for invert centre gauge but did not remain constant for long. As the saturation of the expansive layer kept on increasing with passing time, the pressure kept on rising until it remained stable for a long enough period. The pressure kept on rising on the invert section gauges. As the saturation started, the vicinity of expansive pressure expanded and took the impacts to the wall section of the tunnel quickly being relatively close to the expansive soil layer. The wall gauges on both sides of the tunnel also responded to rise in initial pressure however the rise was not as prominent as the invert gauges. Also, the wall gauges responded to the additional pressure to the swelling in the beginning of the test at same time span as compared to the invert section. The surrounding ground under the tunnel did not absorb the swelling pressure as much as before being harder. The pressure variation at invert centre was haphazard owing to the impacts being directly taken up by the tunnel centre as the saturation progressed. The layer beneath the tunnel kept on saturating with respect to time and pressure kept rising. As the expansive layer pushed the tunnel structure upwards along with the surrounding ground, the gauges on spring-line and shoulder section represented with reduction in pressure. This happened because the upward push

relieved the overburden pressure on these sections. As the layer approached full saturation, the rate of rise of expansive pressure subsided and finally it remained constant for long enough time representing that the expansive layer has reached its limiting swell potential.

The invert edge gauges in this case represented final pressure of 89.42 and 87.45 kPa respectively, the highest of the three cases. The center gauge showed 83.68 kPa at the end of the test representing uplifting of the invert section altogether. The wall sections represented 25.8 and 27.51 kPa on left and right side respectively. The rate of swelling pressure recorded on gauges was swiftest in the beginning and subsided slowly as the test went on to completion. Figure 7-15 represents the final pressure distribution on different sections of the tunnel at completion.

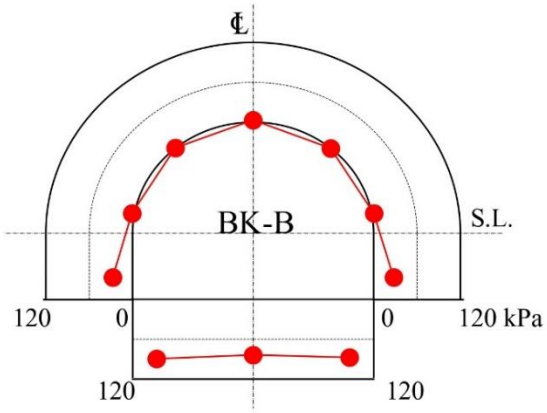

Figure 7-15 Representation of pressure at different sections of the tunnel for **BK-B**

Around 56.64% of the free swell pressure was recorded with increase in stiffness of the surrounding ground under the tunnel where concrete blocks were used. Also, the rate of swelling got much higher for this case in the initial hours and almost half of the total swelling pressure observed was already recorded on bottom gauges within initial 50 hours of the test. The remaining swelling pressure kept on rising with passing time. This rise is 10 kPa more than the S6(90)-B case. However, this pressure is still lower than the free swell pressure of expansive soil the reason being the absorption of the expansive pressure by the sand No. 6 surrounding ground above the tunnel in case of model test, the difference of boundary conditions and corresponding confining pressure. Nonetheless, the expansive pressure exerted on the invert section of the tunnel is nearly 18 times of the pressure as compared to the S6 case with no expansive soil around implying significant pressure increment on tunnel structure constructed in strata comprising of expansive rocks / soils.

7.4.3 Time-dependent expansive pressure variation for BK-B

The time-dependent pressure variation on the tunnel for BK-B was further elaborated by taking different time steps from Figure 7-14 and the expansive pressure variation on the tunnel was comprehended to evaluate the time-dependent impacts of expansive soils on tunnels. Consequently, Figure 7-18 represents this variation for various time-periods. This transformation of time-dependent pressure variation signifies the stability of tunnel with increase in degree of saturation of expansive soil. The consequent impacts of expansive soil with time showed the critical phase where pressure significantly rose. This was a unique case where pressure for initial 80 hours was half of the total

pressure measured. Thereafter the pressure kept on rising rather steadily. So, it was deemed necessary to dissect the pressure changes within this range to examine the time-dependent stability of tunnels in expansive strata. As for this case, it is elaborated by carrying out an examination of the swelling curve for invert section and is divided into four similar zones as for all the earlier explained model tests and are enlisted below:

1- Acceleration zone

The acceleration zone for this case reflected a lot quicker pressure on the invert section as the expansive soil came in contact with water. Consequently, the invert gauges represented a pressure higher than the initial overburden. The differentiating fact was the slope of the rising curve which was almost vertical in the beginning. The pressure kept rising quickly in a smaller time frame and peaked until a specific value at an early stage of the swelling. The increment of pressure was a lot more and signified the difference in the surrounding ground stiffness as concrete blocks were a lot dense as compared to silica sand No. 6 or 8 at 90% of its relative density. The pressure experienced within this range covered the elastic response of tunnel to expansion. Also, the additional swelling pressure was directly taken by the expansive layer and almost none was taken by the blocks.

2- Creep zone

BK-B represented a shorter duration for creep zone in which the pressure remained constant while expansive soil underwent saturation, and this trend was mainly observed for invert centre gauge. There was no decline in constant swelling pressure attained in the acceleration zone, but the pressure on edge gauges at invert section responded to slowly to additional swelling pressure in this zone. The pressure remained around 50 kPa including the overburden pressure on the invert centre section from 10^{th} hour to 100^{th} hour. Whereas for the invert edge gauges it slowly rose from 30 to 45 kPa in the same time span. This region signifies the visco-elastic response of the tunnel to addition pressure due to expansion of surrounding soil in a comparatively stiffer non-swelling surrounding ground of concrete blocks under the tunnel. The zone identifies the preliminary expansion and temporal setting of the expansive soil elements. As it is hard to realize time similitude for field tunnels yet, this zone implies that underground passageways have experienced a significant rise in external pressure even with a strong rock under the tunnel invert although the structure might look perfectly stable under elastic deformations and temporary stable zone of creep is going on.

3- Renaissance zone

The swelling pressure on the invert section of tunnel started to rise again with steeper slope as compared to creep zone in this zone after undergoing a pause. The pressure increase in this period was not as intense as for the acceleration case, however it kept on growing. The rate of rise of pressure kept declining until reaching the limiting visco-elastic response of the surrounding ground. Majority of swelling pressure was observed earlier but the rise in this region was significant too which differentiates this case from the earlier ones. This range was within 70-225 hours for BK-B and as expansive soil attained higher degree of saturation thereafter, a minute rise in expansive pressure was observed. The tunnel structure might start to depict structural damages like heaving and spalling of lining depending upon the location of pressure provided by the expansive layer which was at the invert section. The surrounding rock would start taking up the additional pressure around the tunnel and undergo deteriorations due to volume change. The consequent strength parameters of surrounding ground would reduce, and typical failures might occur in this range.

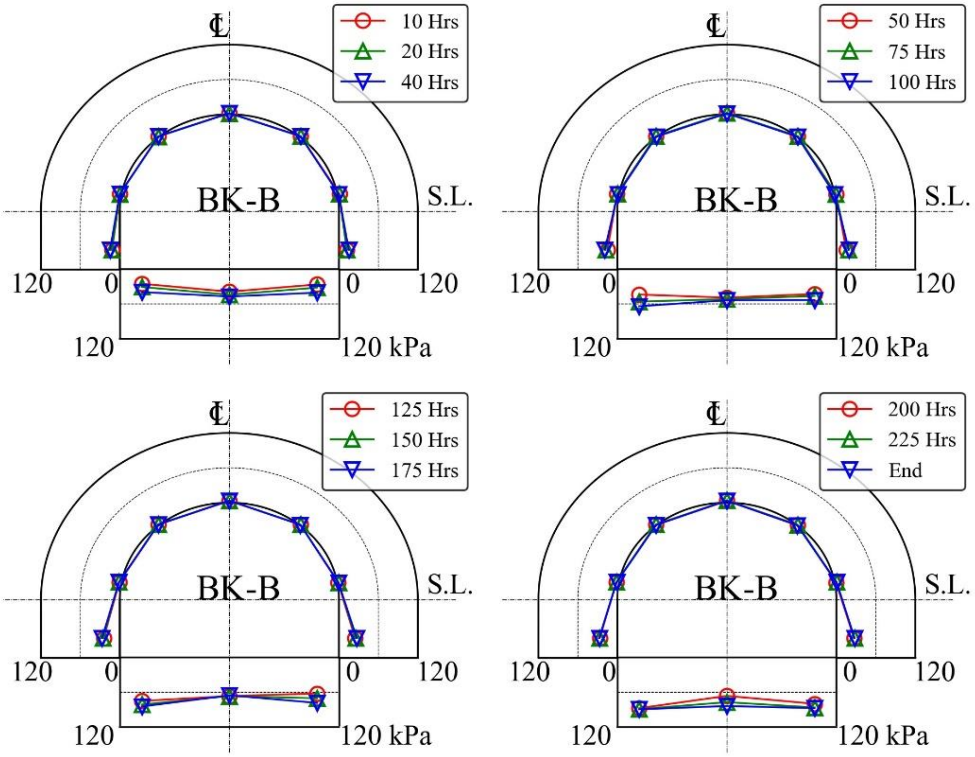

Figure 7-16 Time-dependent expansive pressure variation for **BK-B**

4- Steady zone

The maximum swelling pressure of the expansive soil was attained in zone. The expansive soil around the invert edges had attained maximum degree of saturation and has impacted the tunnel structure to its maximum potential. The firmness of tunnel depends upon the strength of its lining and the ability of the surrounding ground to cater the additional swelling pressure. Majority of damage would have occurred in the renaissance zone and the stability would be examined however if no significant damage like heaving or spalling is observed until this zone has reached, the structure is deemed to have taken up the additional swelling stresses and is designed well to cater expansion and is referred to as safe against swelling pressure.

This time-dependent analysis can be utilized to evaluate the life of the tunnels constructed in swelling strata with denser surrounding ground under the tunnel invert as compared to sand No.8 and 6 cases and can help in quantifying the magnitude of swelling pressures that can be experienced by the tunnel during different phases of expansion with respect to time. The final pressure on tunnel invert in this case was maximum for this model test series thereby justifying that with stronger surrounding ground, higher swelling pressure is transformed on the tunnel in geological formations where expansive soils interact with moisture variation.

A symmetrical representation of pressure variation was observed on gauges that are placed on identical locations on each side of the tunnel. The expansive soil location at the invert section with strengthening the base beneath the tunnel significantly enhanced the swelling pressure on tunnel in

addition to the overburden pressure. This case was different while discussing the invert centre gauge and the expansive pressure observed by the invert section was more than the earlier case. This test also strengthens the repeatability of model tests performed in this study. Also, the pressure bulb is extended to wall section of the tunnel rather quickly too. This comparison signified the criticality of expansive soil in the geological repositories around the tunnel structures and the number of damages that could occur due to water interaction of the expansive geology and consequent long-term stability of mountainous tunnels.

7.4.4 Surrounding ground movements for BK-B

The PIV analysis carried out for BK-B is represented in Figure 7-17. The time-dependent displacement of the node nearest to the invert gauge which was in direct contact with the expansive soil layer was evaluated. The term IL(P) and IR(P) consequently represent the expansive pressure variation on left and right invert gauges respectively while IL(D) and IR(D) are the corresponding displacement curves in the graph. Owing to the increased surrounding ground stiffness under the tunnel as compared to earlier cases, the displacement in the initial pressure rise zone of the expansive soil was quick as compared to the displacement observed in cases where sand was placed at higher density under the tunnel. During this range the expansive soil was undergoing saturation and the volumetric strain was developing to overcome the overburden pressure, but it was observed quickly as the surrounding ground specially under the tunnel was not taking much of the expansive pressure being stiffer now.

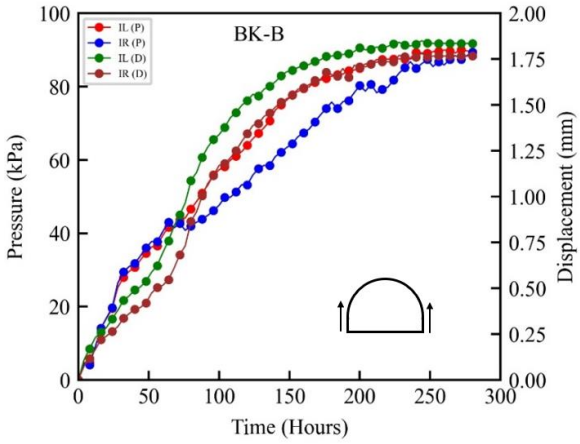

Figure 7-17 Time-dependent nodal displacement and expansive pressure near invert for BK-B

This zone represented the continuous rate of strain and continued in the constant creep state where the surrounding ground kept on displacing quickly and showed deformation for an extended period of time. As the creep zone finished, the displacement kept on rising in renaissance zone too. A slight difference in trend of displacement curve was observed in this case on both sides of the invert. The reason could be the amount of expansive pressure being applied heterogeneously on the surrounding ground on both sides based on degree of saturation of expansive soil. As the time went on, the rate of rise of displacement got slower and its magnitude supressed significantly until the final stage

reached where swelling pressure and corresponding nodal displacement became constant. The image analysis through PIV performed for this case represented the time-dependent directional displacement of the nodes. Based on the swelling kinetics graph, different time spans were evaluated for the visual representation of the surrounding ground movements with time. Figure 7-18 represents the said displacement through contours and vectors of displacement for these specific time periods.

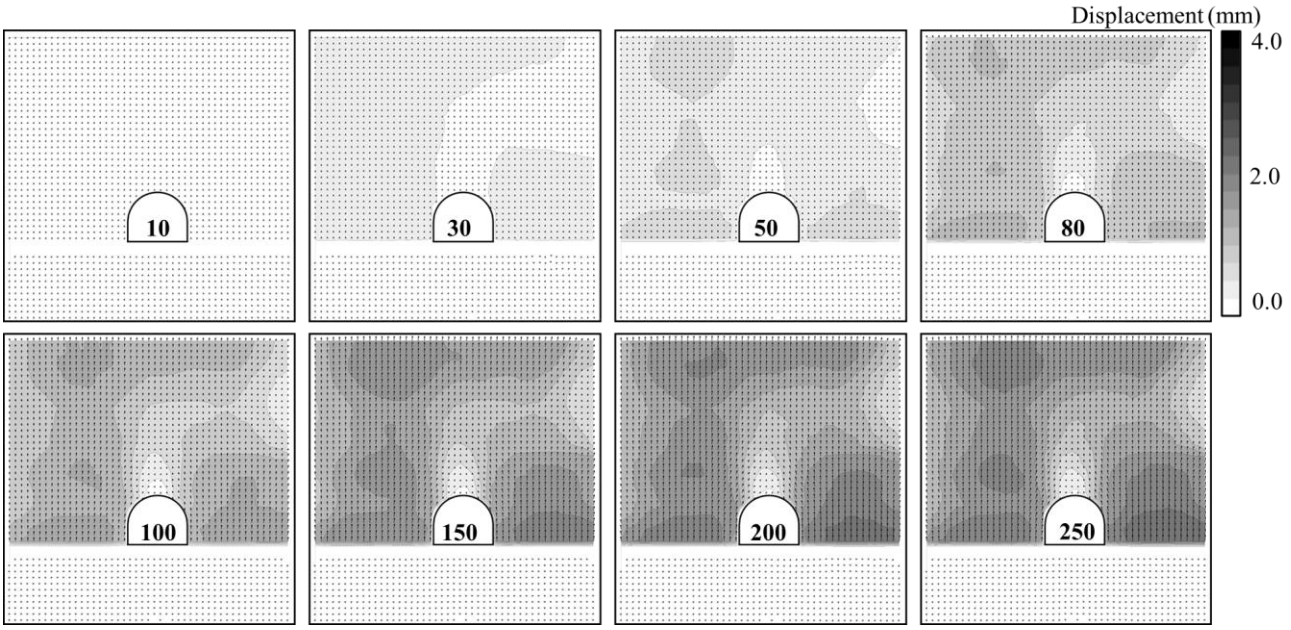

Figure 7-18 Time-dependent nodal displacement around tunnel invert for BK-B

The deformation of the surrounding ground initiated rather swiftly in this case and as the pressure surged and water interacted with expansive soil along with stiffer surrounding ground below the tunnel, the displacements enhanced. Majority of displacement occurred during the strain hardening zone where swelling pressure slightly subsided and reached a steady rising state with expansive soil being saturated. The results suggest that as the surrounding ground particularly under the tunnel gets stiffer, the swelling pressure and ground displacement occur simultaneously. Also, with stiffer ground under the tunnel, the magnitude of upward displacement was more as compared to what was observed in S6(90)-B case. It means that if the rock mass under the tunnel is stiff, more upward displacement will occur.

An accumulative displacement of 1.74 mm and 1.75 mm was observed near the invert section on left and right side respectively. The displacement right above the tunnel is significantly ceased as the tunnel model is locked in its position and the pressure exertion above the crown is restrained vertically. Major displacement is observed right above the expansive soil layer and as the distance from the layer increases, the displacement got reduced. The analysis reflects that the magnitude of the deterioration near the tunnel buried underground would be a lot more as compared to what would be experienced at the ground level.

7.4.5 Impacts of surrounding ground stiffness and expansive soils on tunnels

Figure 7-19 represents the water content of the expansive soil layer after the test was finished. The water content of the layer was minimum at the centre because of the layer being tightly packed under the fixed tunnel. This is one of the reasons that the swelling pressure recorded was lower than the pressure found through free swell tests.

Figure 7-20 summarizes the outcomes of this chapter by comparing the final pressure on different gauges on tunnel in response to variation of surrounding ground stiffness. The comparison clarified that with increase in stiffness of base ground, higher pressure is transformed to the tunnel structure.

Figure 7-21 draws the comparison on how the pressure and corresponding displacement varied with variation of surrounding ground stiffness under the tunnel structure in model test-based study. The linear relationship suggested that the displacements of ground strata increase with the increase in the stiffness of surrounding ground with the swelling pressure on the tunnel simultaneously.

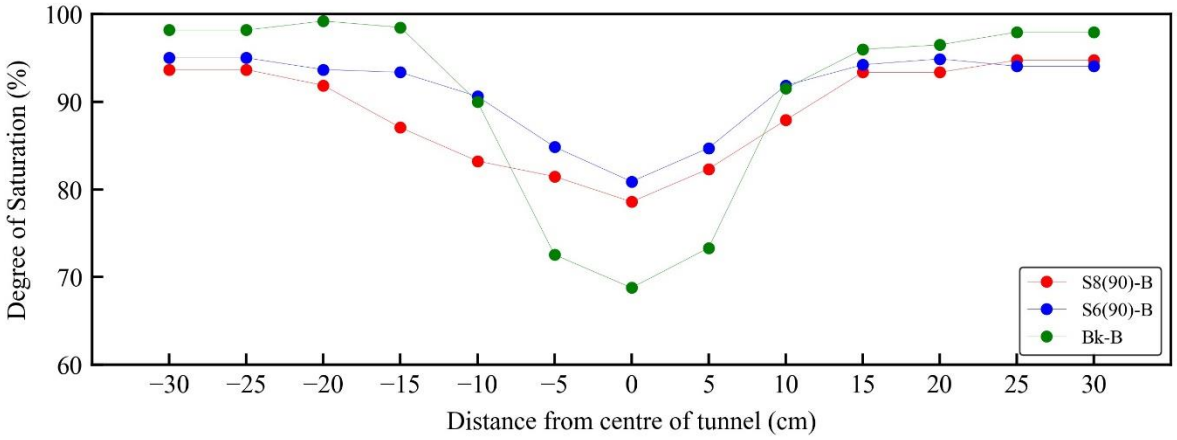

Figure 7-19 Final saturation level of expansive soil layer for model tests

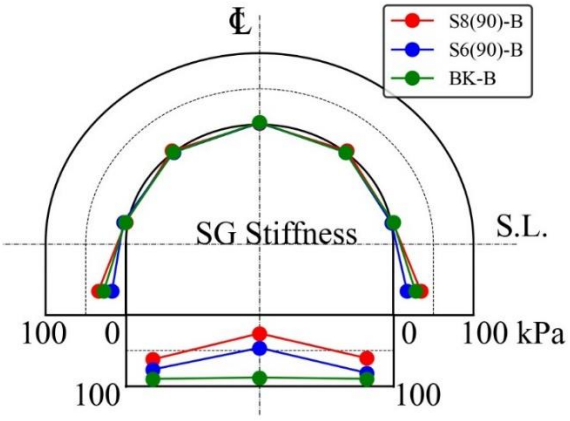

Figure 7-20 Impacts of surrounding ground stiffness and expansive soils on tunnels

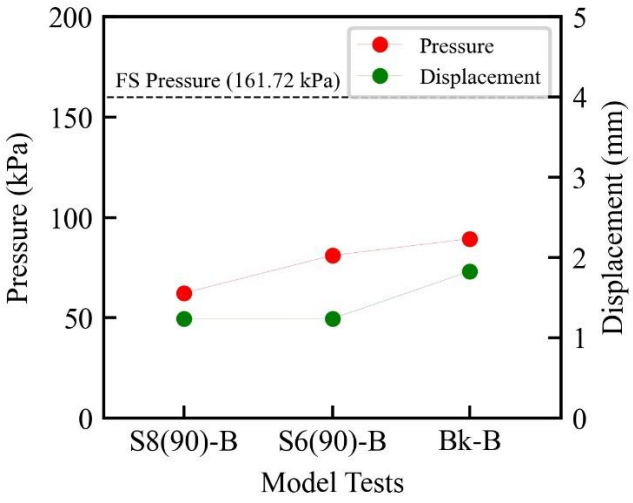

Figure 7-21 comparison of swelling pressure on tunnel and ground displacements in its vicinity

7.5 SUMMARY

This chapter summarized the long-term impacts of expansive soils on stability of tunnels based on the location of expansive soil at invert section and variation in the stiffness of the surrounding ground under the tunnel invert. The impacts were evaluated by considering the locality of expansive soil at invert of the tunnel in all the cases but the ground under the tunnel was made by silica sand No.8 and 6 at 90% of their relative densities. In another case the base ground was made by using concrete blocks. The swelling impacts were evaluated by pressure increments with respect to time and the corresponding displacements in the vicinity of expansive soil and tunnel were calculated by PIV analysis. It was found that the stiffness of base ground along with location of expansive soil significantly impacts the time-dependent response of the tunnel to expansive soils. As the ground under the tunnel is softer, the expansive pressure exerted on tunnel is curtailed because a part of the pressure is absorbed by the soft ground. However, the surrounding ground displacement got higher as the ground got stiffer. The stiffness of base ground also depicted how the invert section of the tunnel responded to excess pressure of swelling. The magnitude of this pressure was about 18 times the overburden pressure and 55.6% of the free swell pressure measured in the oedometer test for base ground being concrete blocks. The surrounding ground moved vertically and time-dependent variation in the gauges in the vicinity of expansive layer varied differently for different gauges. The tunnel sections in softer ground were relieved as much of the expansive force acted on softer ground above the tunnel and tried to displace it vertically upwards. The time-dependent strains in the surrounding ground evaluated in this study suggest that swelling pressure application is quicker as compared to the heaving of the ground and the tunnel structure may look perfectly safe and no ground movement may be seen yet, the tunnel might be going through intense addition in pressure due to presence of expansive soil in the vicinity and stiffness of ground under the tunnel. The time-dependent pressure also suggested that the water contact with expansive soil will speedily increase the pressure before going into creep zone and majority of damage is expected as soon as the expansive soil is in contact with water.

CHAPTER 8 TIME-DEPENDENT IMPACTS OF EXPANSIVE SOIL AT A DISTANCE FROM TUNNEL INVERT

8.1 INTRODUCTION

This chapter investigates the time-dependent impacts of expansive soils on tunnel when the location of the soil layer is beneath the tunnel invert. The replication of possible location of expansive soil for this study was made by placing the expansive soil at a distance of one time the diameter of the tunnel (1D) from the invert section. The model test assembly was used as for the earlier tests. In this case, the surrounding ground was prepared by Silica sand No. 6 at 90% of its relative density under the tunnel while the ground above the tunnel was sand No. 6 at 80% of its relative density. The density above the tunnel was reduced to ensure that the dumping efforts may not hamper the gauges to record haphazard pressure other than the overburden pressure. The response of the tunnel lining was adjudicated by placing the 20 mm expansive soil under the tunnel at a distance of 100 mm in this case. The swelling of the layer upon saturation imposed additional pressure on the tunnel invert section but for this case, the expansive soil was deeper under the tunnel, hence, the impacts were evaluated based on the field conditions in which the probability of expansive layer presence was at a distance of 1D from the tunnel invert. These conditions evaluated the time-dependent impacts of expansive soil availability in the geological repositories beyond the excavation for tunnel construction. The testing conditions like water intrusion and ground movements evaluation through PIV analysis etc. were kept same as for all the previous cases. This test is referred to as S6-1D for this study.

8.2 MODEL TEST FOR S6-1D

8.2.1 Experimental conditions for S6-1D

As explained earlier, the experimental conditions in this case included placing silica sand No. 6 under the tunnel overlaid by a 20 mm thick layer of expansive soil placed at distance of 100 mm (1D) from the tunnel invert. The expansive soil was not in direct contact with the invert section of the tunnel. To keep the experimental conditions identical with previous tests, the expansive soil layer was discontinued at edges by 50 mm and water was supplied from the side inlets for saturating the soil assembly. The overburden height was kept to 3D and water level for saturation maintained at 1D. This test was referred to as S6-1D in the nomenclature adopted in this study where ‘S6’ signifies the surrounding ground being silica sand No. 6, and ‘1D’ signifying the location of expansive soil being at a distance of one time the diameter from the tunnel invert. The schematic diagram of this test is represented in Figure 8-1.

8.2.2 Tunnel response to S6-1D

Figure 8-2 represents the kinetics of the pressure on tunnel for S6-1D model test. The pressure increment was in line with S6 test initially and the magnitude of the overburden pressure was comparable. As the overlying layers of the surrounding ground over the tunnel were completed and saturation was started, the expansive soil layer responded to water interaction and started to expand. The swelling of the layer imposed additional pressure to the invert section of the tunnel. The invert left, right and invert centre gauges (Il, Ir, Ic) immediately respond to additional pressure as the test

conditions were close to tests with expansive soil being placed in direct contact with the invert of the tunnel. Interestingly, the response of all the invert gauges in this case was relatively identical throughout the test. The reason was the location of the expansive soil deep under the tunnel which were transforming the entire expansive pressure to the entire invert section of the tunnel. The slope of the rising line was uniform for this case as compared to the cases discussed in chapter 7. The rising trend was uniform for all the invert gauges and there was no delay in experiencing the pressure rise. As the water crept up rapidly through silica sand, the invert gauges showed a swift rising trend in pressure.

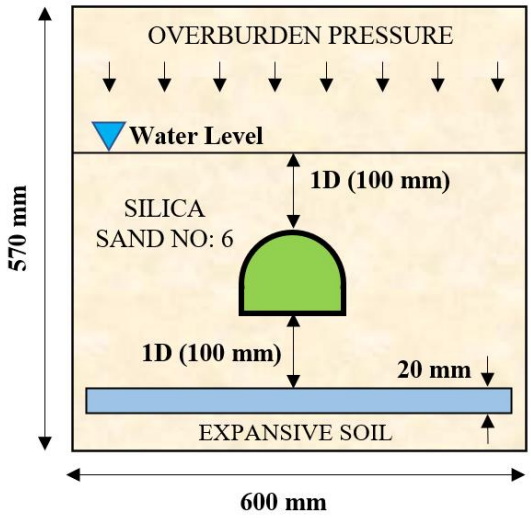

Figure 8-1 Schematic diagram for **S6-1D** model test

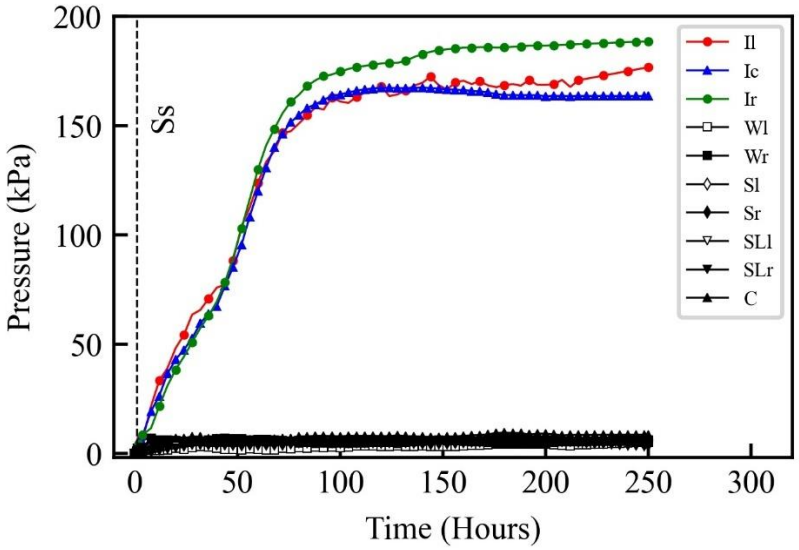

Figure 8-2 Pressure kinetics at different sections of the tunnel for **S6-1D** model test

The swelling kinetics curve for this case represented a continuous rise in swelling pressure until the 100th hour. The rate of swelling rose swiftly until 50th hour but rather than going into the creep zone where pressure would remain constant, the pressure rose rather swiftly in the renaissance. There was no particular zone where a constant swelling pressure or declining swelling pressure was seen. The strain hardening zone where the soil kept on taking the expansion load without depicting changes in the pressure was not significant yet, existent. Also, the expansive soil minerals settled as the voids went on filling by water with the passing time. The water interaction caused change in the degree of saturation of the soil. The expansive layer started to saturate from the bottom as well as top as the expansive layer was surrounded by silica sand and was not in immediate contact with tunnel invert.

As the saturation of the expansive layer kept on increasing with passing time, the pressure kept on rising until it remained stable for a long enough period. The pressure kept on rising on the invert section gauges. As the saturation kept rising, the vicinity of expansive pressure expanded but the gauges on wall, shoulder and spring-line sections did not reflect any particular changes in pressure being relatively far from the expansive soil layer for this case.

The surrounding ground of expansive soil being stiffer S6, almost all the expansive pressure was taken up by the tunnel invert itself. The pressure variation at invert section was smooth owing to the impacts being directly taken up by the tunnel centre as the saturation progressed. As the expansive layer pushed the tunnel structure upwards along with the surrounding ground, the gauges on spring-line and shoulder section represented with slight reduction in pressure. This happened because the upward push relieved the overburden pressure on these sections insignificantly. As the layer approached full saturation, the rate of rise of expansive pressure subsided and finally it remained constant for long enough time representing that the expansive layer has reached its limiting swell potential.

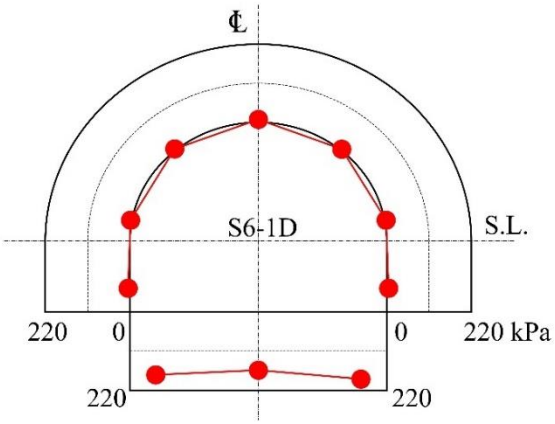

Figure 8-3 Representation of pressure at different sections of the tunnel for **S6-1D**

This test represented very high pressure on gauges. The invert edge gauges in this case represented final pressure of 176.7. 163.5, and 188.6 kPa for invert left, center and right gauge respectively, representing uplifting of the invert section altogether. The other sections represented the same pressure as the overburden pressure on left and right side of the tunnel. The rate of swelling pressure recorded on gauges was swiftest in the beginning and subsided slowly as the test went on to

completion. Figure 8-3 represents the final pressure distribution on different sections of the tunnel at completion.

Interestingly, the pressure recorded on invert gauges for this case exceeded the free swell pressure recorded in oedometer test. Also, the rate of swelling got much higher for this case in the initial hours and almost 80% of the total swelling pressure observed was already recorded on bottom gauges within initial 60 hours of the test. The remaining swelling pressure kept on rising with passing time. This rise is more than the tests explained in Chapter 7. The expansive pressure exerted on the invert section of the tunnel is nearly 38 times of the pressure as compared to the S6 case with no expansive soil around implying significant pressure increment on tunnel structure constructed in strata comprising of expansive rocks / soils even below the tunnel structure.

8.2.3 Time-dependent expansive pressure variation for S6-1D

The time-dependent pressure variation on the tunnel for S6-1D was further elaborated by taking different time steps from Figure 8-2 and the expansive pressure variation on the tunnel was comprehended to evaluate the time-dependent impacts of expansive soils on tunnels. Consequently, Figure 8-4 represents this variation for various time-periods. This transformation of time-dependent pressure variation signifies the stability of tunnel with increase in degree of saturation of expansive soil. The consequent impacts of expansive soil with time showed the critical phase where pressure significantly rose. This was a unique case where pressure for initial 100 hours had already nearly reached the final swelling pressure of the expansive soil. So, it was deemed necessary to dissect the pressure changes within this range to examine the time-dependent stability of tunnels in expansive strata. As for this case, it is elaborated by carrying out an examination of the swelling curve for invert section and is divided into four similar zones as for all the earlier explained model tests and are enlisted below:

1- Acceleration zone

The acceleration zone for this case reflected a lot quicker pressure on the invert section as the expansive soil came in contact with water. Consequently, the invert gauges represented a pressure higher than the initial overburden. The differentiating fact was the slope of the rising curve which rose at a comparable rate with previous cases in the beginning. The pressure kept rising quickly in a smaller time frame and peaked until a specific value at an early stage of the swelling. The increment of pressure signified the difference in the surrounding ground stiffness and location of expansive soil being far below the invert. The pressure experienced within this range covered the elastic response of tunnel to expansion. Also, the additional swelling pressure was directly taken by the expansive layer and almost none was taken by the surrounding ground around the expansive soil layer being denser at 90% of the relative density of silica sand No. 6.

2- Creep and Renaissance zone

S6-1D represented almost negligible duration for creep zone in which the pressure remained constant while expansive soil underwent saturation, and this trend was mainly observed for invert centre gauge. There was no decline in rising swelling pressure attained in the acceleration zone, but the pressure on edge gauges at invert section responded rather swiftly to additional swelling pressure in this zone. This region signifies the visco-elastic response of the tunnel to addition pressure due to expansion of surrounding soil in a comparatively stiffer non-swelling surrounding ground and the

expansive soil far below the invert section. The zone identifies the preliminary expansion and temporal setting of the expansive soil elements. As it is hard to realize time similitude for field tunnels yet, this zone implies that underground passageways have experienced a significant rise in external pressure even with a strong rock under the tunnel invert.

The swelling pressure on the invert section of tunnel started to rise with steeper slope as compared to acceleration and creep zone in renaissance zone after undergoing a change in curve. The pressure increase in this period was very intense as for the acceleration case because the expansive soil layer saturation was not rendered by the location of tunnel being tightly locked under the tunnel as for previous cases. The rate of rise of pressure kept declining thereafter until reaching the limiting visco-elastic response of the surrounding ground. Majority of swelling pressure was observed earlier but the rise in this region was significant too which differentiates this case from the earlier ones. This range was within 50-75 hours for S6-1D, and as expansive soil attained higher degree of saturation thereafter, a rise in expansive pressure was observed. The tunnel structure might start to depict structural damages like heaving and spalling of lining depending upon the location of pressure provided by the expansive layer which was at the distance of 1D from the invert section. The surrounding rock would start taking up the additional pressure around the tunnel and undergo deteriorations due to volume change. The consequent strength parameters of surrounding ground would reduce, and typical failures might occur in this range.

3- Steady zone

The maximum swelling pressure of the expansive soil was attained in zone. The expansive soil at 1D from the invert edges had attained maximum degree of saturation and has impacted the tunnel structure to its maximum potential. The firmness of tunnel depends upon the strength of its lining and the ability of the surrounding ground to cater the additional swelling pressure. Majority of damage would have occurred in the renaissance zone and the stability would be examined however if no significant damage like heaving or spalling is observed until this zone has reached, the structure is deemed to have taken up the additional swelling stresses and is designed well to cater expansion and is referred to as safe against swelling pressure.

This time-dependent analysis can be utilized to evaluate the life of the tunnels constructed in strata where expansive soil is located at a distance of 1D from the tunnel invert and can help in quantifying the magnitude of swelling pressures that can be experienced by the tunnel during different phases of expansion with respect to time. The final pressure on tunnel invert in this case was maximum and even exceeded the free swell pressure in oedometer test for this model test study thereby justifying that with stronger surrounding ground and expansive soil located at 1D from heave of the tunnel, higher swelling pressure is transformed on the tunnel in geological formations where expansive soils can interact with moisture variation.

A symmetrical representation of pressure variation was observed on gauges that are placed on identical locations on each side of the tunnel. The expansive soil location at the invert section with strengthening the base beneath the tunnel significantly enhanced the swelling pressure on tunnel in addition to the overburden pressure. This case was different while discussing the invert centre gauge and the expansive pressure observed by the invert section was more than the earlier cases. This test also strengthens the repeatability of model tests performed in this study. This comparison signified the criticality of expansive soil in the geological repositories even far below the tunnel structures and

the number of damages that could occur due to water interaction of the expansive geology and consequent long-term stability of mountainous tunnels.

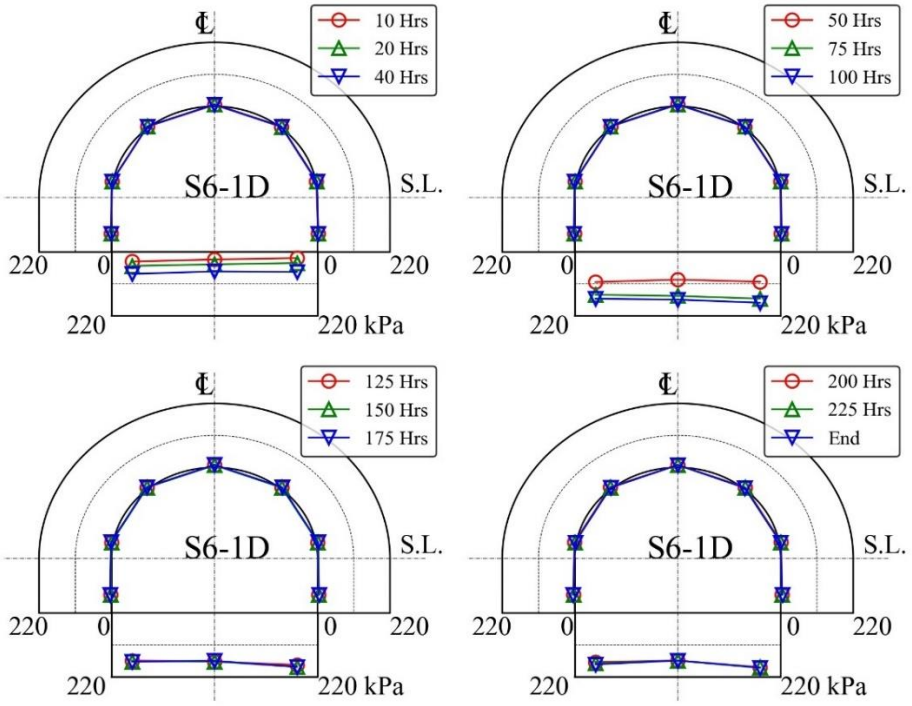

Figure 8-4 Time-dependent expansive pressure variation for **S6-1D**

8.2.4 Surrounding ground movements for S6-1D

The PIV analysis carried out for S6-1D is represented in Figure 8-5. The time-dependent displacement of the node nearest to the invert gauge which was in direct contact with the tunnel is evaluated. The term IL(P) and IR(P) consequently represent the expansive pressure variation on left and right invert gauges respectively while IL(D) and IR(D) are the corresponding displacement curves in the graph. Owing to the increased surrounding ground stiffness and expansive soil being far from the invert under the tunnel, the displacement in the initial pressure rise zone of the expansive soil was slow as compared to the displacement observed in cases where sand was placed at higher density under the tunnel. During this range the expansive soil was undergoing saturation and the volumetric strain was developing to overcome the overburden pressure of the sand above the expansive layer, but it was observed quickly as the surrounding ground specially under the tunnel was not taking much of the expansive pressure.

This zone represented the continuous rate of strain and continued in the constant creep state where the surrounding ground kept on displacing quickly and showed deformation for an extended period of time. The displacement kept on rising in renaissance zone too. A slight difference in trend of displacement curve was observed in this case on both sides of the invert. The reason could be the amount of expansive pressure being applied heterogeneously on the surrounding ground on both sides based on degree of saturation of expansive soil. As the time went on, the rate of rise of displacement got slower and its magnitude supressed significantly until the final stage reached where

swelling pressure and corresponding nodal displacement became constant. The image analysis through PIV performed for this case represented the time-dependent directional displacement of the nodes. Based on the swelling kinetics graph, different time spans were evaluated for the visual representation of the surrounding ground movements with time.

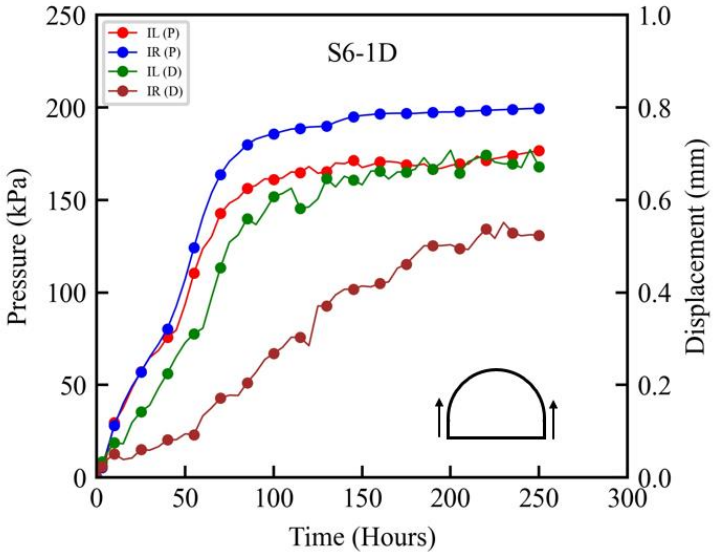

Figure 8-5 Time-dependent nodal displacement and expansive pressure near invert for S6-1D

Figure 8-6 represents the said displacement through contours and vectors of displacement for these specific time periods. The deformation of the surrounding ground initiated rather slowly in this case and as the pressure surged and water interacted with expansive soil along with stiffer surrounding ground around the tunnel, the displacements enhanced. Majority of displacement occurred during the renaissance zone and reached a steady rising state with expansive soil being saturated. The results suggest that as the expansive soil is placed at a distance below the tunnel invert, the swelling pressure experienced was higher because now the saturation of expansive layer was aided from both top and bottom while the ground displacement was reduced as compared to what was observed in S6(90)-B case.

An accumulative displacement of 0.67 mm and 0.52 mm was observed near the invert section on left and right side respectively. The displacement right above the tunnel is significantly ceased as the tunnel model is locked in its position and the pressure exertion above the crown is restrained vertically. Major displacement is observed right above the expansive soil layer and as the distance from the layer increases, the displacement got reduced. The analysis reflects that the magnitude of the deterioration near the tunnel buried underground would be a lot more as compared to what would be experienced at the ground level.

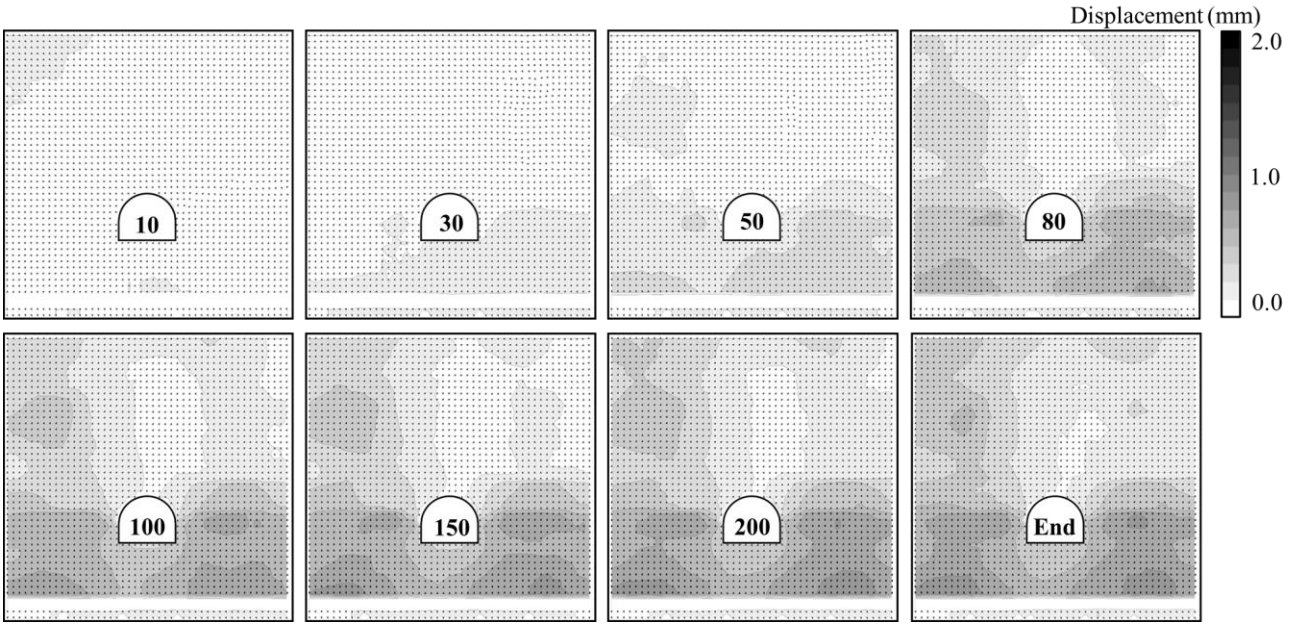

Figure 8-6 Time-dependent nodal displacement around tunnel invert for S6-1D

8.2.5 Trapdoor behaviour of the fixed tunnel

Terzaghi's formula (1943) for active earth pressure on the trap door is often applied for the design of tunnel support systems. The main objective of this theory is to evaluate the magnitude of the total active earth pressure on the geotechnical structures. The information of the distribution of the passive earth pressure outside of the lowering trap door is more important as the surrounding ground of the tunnel is subjected to the distribution of the passive earth pressure. This distribution of the passive earth pressure is vital considering the stability of the surrounding ground. In this experiment the fixed tunnel in its position acted as a trapdoor. The initial value of pressure recorded on the gauges installed on the tunnel invert was same as the overburden pressure. In classic trap door experiments, the frame of the trap door is movable and is lowered or raised to estimate the active or passive earth pressure whereas in this case, the expansive soil placed at a distance of 1D from the base of the tunnel acted as a source of upward pressure on the tunnel invert and the tunnel was fixed in its position. This makes the condition for passive state of raising the tunnel due to swelling pressure of expansive soil. The pressure on tunnel invert was recorded by three gauges installed at invert left, right and centre position just like all the other model tests. Therefore, the critical earth pressure for this experiment would be the maximum value of pressure for the passive state case. Figure 8-7 represents the relationship between the passive earth pressure and the upward displacement recorded on the invert gauge for an overburden height of 30 cm (Silica sand No. 6). The graph represents that the initial passive earth pressure suddenly changes within 1-2 mm of the displacement recorded on the position of the gauge and remained steady thereafter during the whole experiment.

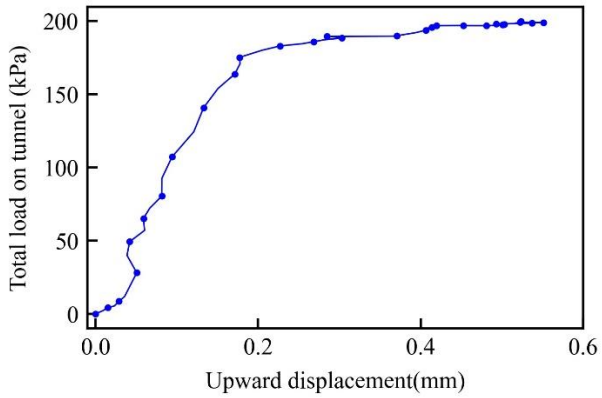

Figure 8-7 Upward displacement vs pressure for S6-1D at invert section of tunnel

8.2.6 Earth pressure on trap door formation due to tunnel

As the pressure experienced at the invert of the tunnel exceeded the free swell pressure, an analytical solution was proposed and is explained in Figure 8-8 where an element of layer is considered under tunnel with thickness dz. The solution is as follows:

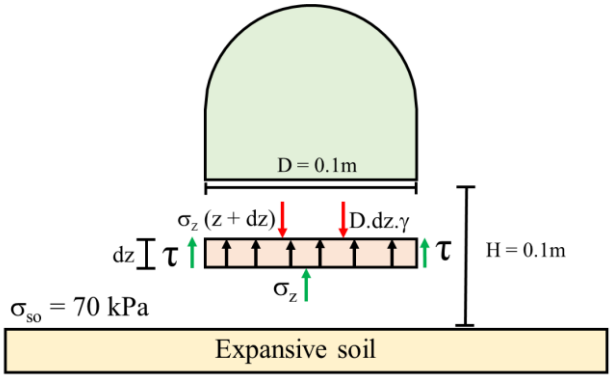

Figure 8-8 Equilibrium of forces acting at tunnel invert for S6-1D

Downward forces = σ_z (z + dz). D + D.γ.dz

Upward forces =σ_z (z). D + 2. τ. dz

At equilibrium

σ_z (z + dz). D + D.γ.dz = σ_z (z). D + 2. τ. dz …….... (1)

Using Taylor's expansion:

σ_z (z + dz) = σ_z (z) + ($\partial\sigma_z$ (z) / ∂z). dz……. (2)

Putting 2 in 1

{σ_z (z) + ($\partial\sigma_z$ (z) / ∂z). dz} * D + D.γ.dz = σ_z (z). D + 2. τ. dz …… (3)

The terms σ_z (z). D and dz will cancel out, simplifying

$\{\partial\sigma_z (z) / \partial z\} + D.\gamma.dz = (2\ \tau) / D - \gamma$ …… (4)

As σ_{so} >> overburden so $D.\gamma.dz \sim 0$

$\partial\sigma_z (z) / \partial z = \{(2\ \tau) / D\} - \gamma$ ……...…… (5)

According to the Mohr-Coulomb's Failure criteria

$\tau = k_o.\ \sigma_z(z).\ \text{Tan}\ \phi$ ……. (6)

Putting equation 6 in 5

$\partial\sigma_z (z) / \partial z = \{(2\ k_o.\ \sigma_z(z).\ \text{Tan}\ \phi) / D\} - \gamma$……. (7)

Let $\{(2\ k_o.\ \text{Tan}\ \phi) / D\}$ be a constant value 'a'

Therefore:

$\partial\sigma_z (z) / \partial z = a.\ \sigma_z(z) - \gamma$ ……. (8)

This is a first order differential equation. The boundary conditions for solution of this equation are: At z =0, $\sigma_z (0) = \sigma_{so}$, where σ_{so} is swell pressure on top of expansive layer. Rearranging 8:

$\partial\sigma_z (z) / a.\ \sigma_z(z) - \gamma = \partial z$ ……. (9)

Let $\mu(z) = -e^{-az}$ so multiplying $\mu(z)$ on both sides of (9)

$\{-e^{-az} * \partial\sigma_z (z) / \partial z\} - a\ (-e^{-az})\ \sigma_z = -e^{-az}\ \gamma$ …… (10)

$(e^{-az}\ \sigma_z) / dz = e^{-az}\ \gamma$ ……. (11)

$e^{-az}\ \sigma_z = \int -e^{-az}\ \gamma\ dz$ ……. (12)

Applying simple integration function

$$e^{-az}\ \sigma_z = e^{-az}\ (-\gamma/a) + C \quad \text{…. Solution (13)}$$

Using boundary conditions z =0, $\sigma_z (0) = \sigma_{so}$:

$\sigma_{so} = C - (\gamma/a)$ …… (14)

Or $C = \sigma_{so} + (\gamma/a)$ …… (15)

For our model test data:

D	0.1m,	H	0.1m,	σ_{so}	70 kPa
ρ	1.6 g/cm^3,	g	9.81 m/s^2,	Ko	0.5
φ	42.34^0,	tan φ	0.911,	a	9.11
γ	15.69 kN/m^2,	C = 71.72			

σ_z = 176.67 kPa (Theoretical)

σ_z = 176.33 kPa (Experimental average pressure at tunnel invert)

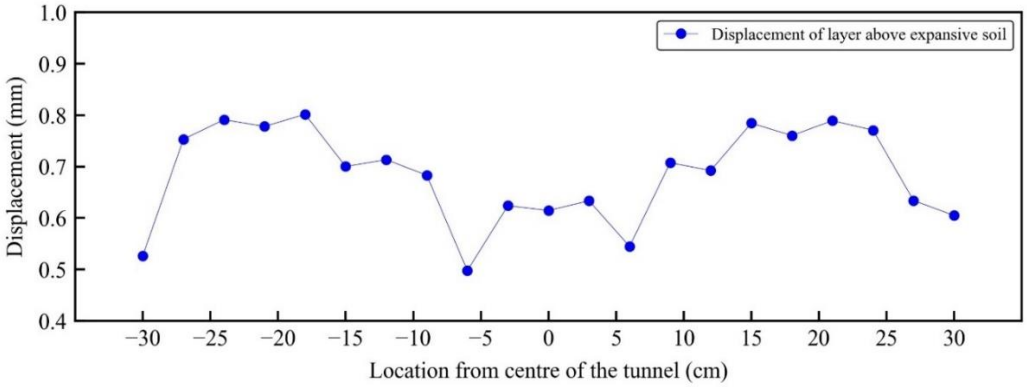

Figure 8-9 Final displacement of the ground above expansive soil layer for **S6-1D**

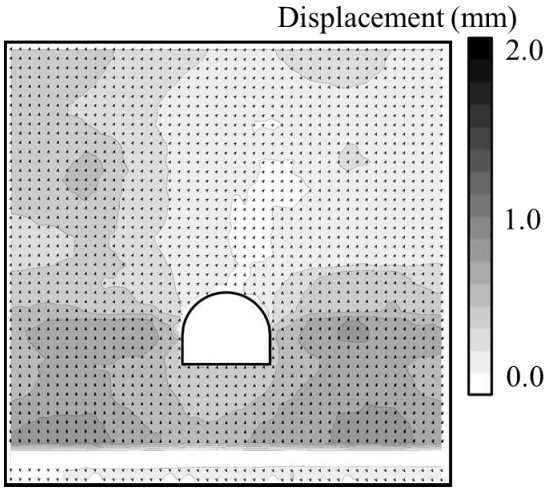

Figure 8-10 Final nodal displacement around tunnel for S6-1D

As a vivisection of the displacement of the surrounding ground right above the expansive layer was carried out specifically for this case, an interesting feature of trapdoor behaviour was observed as represented in Figure 8-9. The stresses induced by the expansion of expansive soil re-distributed and made an arching action on the surrounding non-swelling ground. The trapdoor can be active, or passive as explained widely in the literature. In case of an active trapdoor, the stresses above it are reduced causing an increase in the stresses in the adjacent layers of soil and vice-versa is observed for the passive case. The main component defining the role of trapdoor are the relation between the soil cover height to the width of trapdoor (which was acted by the fixed tunnel invert in this case), the engineering properties of soil and its geometric situation. The outcomes of this model test are classic example of aspects of the trapdoor phenomenon for underground structures and is limited in literature. The failure mechanisms and formation of trapdoor under the buried tunnel structure due to presence of expansive soil layer at a distance of 1D under the tunnel heave was novel.

The contour map clearly represented the formation of trapdoor and the role played by the fixed location of the tunnel. The walls of the tunnel acted as the key components of providing friction to the expansive pressure imposed by the swelling soil depicted in Figure 8-10. This could be the reason that the pressure recorded on invert gauges in this case was a lot more as compared to other cases in fact it exceeded the free swell pressure observed during the performance of the free swell test on the same soil sample in oedometer.

8.3 SUMMARY

This chapter summarized the long-term impacts of expansive soils on stability of tunnels based on the location of expansive soil at a distance of 1D from the invert section of the tunnel invert. The impacts were evaluated by considering the locality of expansive soil at a depth of one time the diameter of the tunnel below the invert of the tunnel. The surrounding ground under the tunnel was made by silica sand No. 6 at 90% of its relative density. The swelling impacts were evaluated by pressure increments with respect to time and the corresponding displacements in the vicinity of expansive soil and tunnel were calculated by PIV analysis. It was found that the stiffness of base ground along with location of expansive soil significantly impacts the time-dependent response of the tunnel to expansive soils. The stiffness of the ground above the expansive soil layer depicted how the invert section of the tunnel responded to excess pressure of swelling even if the expansive layer is placed below the tunnel invert. The surrounding ground moved vertically and time-dependent pressure variation on the gauges in the vicinity of expansive layer varied differently for different gauges. The time-dependent strains in the surrounding ground evaluated in this study suggest that swelling pressure application is quicker as compared to the heaving of the ground and the tunnel structure may look perfectly safe and no ground movement may be seen yet, the tunnel might be going through intense addition in pressure due to presence of expansive soil in the vicinity and stiffness of ground under the tunnel. The fixity of the tunnel may impose additional load on the tunnel replicating a situation where trapdoor formation can exist. An interesting outcome of this model test was pressure application on tunnel invert which was even more than the free swell pressure of expansive soil exerted in oedometer test. The time-dependent pressure also suggested that the water contact with expansive soil will speedily increase the pressure after entering into the post-creep zone and majority of damage is expected as the expansive soil underwent saturation.

CHAPTER 9 CONCLUSIONS AND RECOMMENDATIONS

9.1 SUMMARY OF THE KEY OUTCOMES

Expansive soils are considered an engineering problem in development projects owing to their ability to drastically expand upon contact with water. It is one of the major causes of heaving of the tunnel structures even long after construction thereby posing serious threats to their long-term stabilities. In this research the time-dependent impacts of expansive soils on tunnel stability and consequent surrounding ground movements were studied through various model experiments based on their presence, location, and conditions of the surrounding ground. The key outcomes are summarized below:

1. The expansive pressure of an expansive soil sample is proportional to the amount of expansive mineral present in it. Expansive soils have substantial impacts on structures around them owing to their swelling ability and volume change during water content variation as found in this study through free swell test on laboratory prepared Toyoura sand and bentonite mixtures. Specifically, the B2575 sample indicated 161.72 kPa of swelling pressure.

2. The presence of expansive soil in soil strata can pose additional pressures on tunnel section. The pressure increment of 6.6 times was observed with S8 as surrounding ground while it was 15 times for S6. Such additional pressures can pose serious threats on tunnel securities causing invert heaving or lining dysfunctionalities.

3. The location of the expansive soil strata significantly impacts the consequent tunnel section. As compared to non-expansive overburden pressure, this research projected 7.8 times of additional swelling pressure on crown section with expansive soil over it, 10 times for wall section, and 9 time for the shoulder section justifying the criticality of expansive soil location in the strata around tunnels. Such pressure exertion and corresponding tunnel response to this pressure and can encourage the vulnerability of tunnel failure.

4. The surrounding ground stiffness other than expansive soil around the tunnel can play an imperative role regarding expansive pressures on tunnels. Soft surrounding ground can absorb a part of the expansive pressure. As the surrounding ground stiffness rises, more and more expansive pressure is exerted on tunnels. As for this study, the S8 soil test exerted 62.33 kPa pressure on invert section which rose to 81 kPa for S6 and 89 kPa for concrete block's case as compared to 5 kPa of overburden pressure thereby validating the assertion.

5. The surrounding ground movement in response to expansion of expansive soils is one of the prime causes of heave at invert section of the tunnels and it aids in the deteriorations in the geological strata around. The strain in the strata depends on the location of the expansive soil and stiffness of the rock mass itself around the tunnels. The softer ground although absorb expansive pressure yet it displaces more. As the rock bed under the tunnel gets stiffer, more pressure is exerted on the upper strata thereby displacing it more.

6. The time-dependent impacts of expansive soils can be sub-divided into several zones. The key zones for stability considerations encountered in this study were the acceleration zone, creep zone, renaissance zone and steady zone. Each zone identified a particular response of the tunnel thereby directly impacting the long-term stability of tunnels constructed in geological repositories with expansive soils.

7. As the expansive soil was placed at a distance of 1D from the invert, the swelling pressure significantly increased owing to formation of passive trapdoor because of tunnel being fixed in its position. The friction on the walls of the tunnel added to swelling pressure making the tunnel stability conditions further critical.

9.2 FUTURE RECOMMENDATIONS FOR RESEARCH

The research was performed by taking maximum considerations contemplating natural phenomenon occurring in the geology comprising of expansive soils interacting with underground structures. The outcomes of reduced-scale model tests do not entirely represent the field conditions. The thickness of the expansive soil layer was pre-identified to enable saturation within certain length of time hence it is recommended to consider different thickness and setting of expansive soil layer for future research intentions. The water movement was entirely based on saturation happening due to water supplied at the base which moved upwards replicating groundwater level increasing however, the water interaction can also happen from top and coming down towards the expansive layers in geology which can be applied in further research. Different combinations of expansive soils can also be considered. The current study incorporated horse-shoe tunnel whereas other kinds of shapes like circular or box tunnels can be employed as well. Also, heterogeneous surrounding ground conditions along with varying stiffness can be considered. The water used in this research was normal drinkable water however underground structures may encounter chemically polluted or saline water hence more impacts can be studied through changing the quality of water interacting with expansive soils near tunnel structures. The overburden height was kept to three times the diameter of the tunnel, for future research, the overburden pressure can be increased replicating the cases of deep tunnels.

Nonetheless, in this research the time-dependent impacts of expansive soils on tunnels along with consequent surrounding ground movements were successfully evaluated and it can be used as a reference to evaluate the long-term stability of mountainous tunnels in such strata to quantify the additional pressures and ground displacements for field tunnels constructed in expansive rocks vicinity.

REFERENCES

Abdellah, W.R., Ali, M.A., Yang, H.S., 2018. Studying the effect of some parameters on the stability of shallow tunnels. J. Sustain. Min. 17, 20–33. https://doi.org/10.1016/j.jsm.2018.02.001

Adem, H.H., Vanapalli, S.K., 2013. Constitutive modeling approach for estimating 1-D heave with respect to time for expansive soils. Int. J. Geotech. Eng. 7, 199–204. https://doi.org/10.1179/1938636213Z.00000000024

Al-Rawas, A.A., Hago, A.W., Al-Sarmi, H., 2005. Effect of lime, cement and Sarooj (artificial pozzolan) on the swelling potential of an expansive soil from Oman. Build. Environ. 40, 681–687. https://doi.org/10.1016/j.buildenv.2004.08.028

Alonso, E. E., Gens, A. & Josa, A., 1990. A constitutive model for partially saturated soils. Geotechnique 40, No. 3, 405–430. 405–430. https://doi.org/10.1680/geot.1990.40.3.405

Alonso, E.E., Berdugo, I.R., Ramon, A., 2013. Extreme expansive phenomena in anhydritic-gypsiferous claystone: The case of lilla tunnel. Geotechnique 63, 584–612. https://doi.org/10.1680/geot.12.P.143

Alonso, E.E., Vaunat, J., Gens, A., 1999. Modelling the mechanical behaviour of expansive clays. Eng. Geol. 54, 173–183. https://doi.org/10.1016/S0013-7952(99)00079-4

Anagnostou, G., 1993. A model for swelling rock in tunnelling. Rock Mech. Rock Eng. 26, 307–331. https://doi.org/10.1007/BF01027115

Andreotti, G., Lai, C.G., 2019. Use of fragility curves to assess the seismic vulnerability in the risk analysis of mountain tunnels. Tunn. Undergr. Sp. Technol. 91, 103008. https://doi.org/10.1016/j.tust.2019.103008

Ashayeri, I., Yasrebi, S., 2009. Free-swell and swelling pressure of unsaturated compacted clays; experiments and neural networks modeling. Geotech. Geol. Eng. 27, 137–153. https://doi.org/10.1007/s10706-008-9219-y

ASTM, 2013. D4546 − 08 Standard Test Methods for One-Dimensional Swell or Collapse of Cohesive Soils 1. ASTM Int. 1–9. https://doi.org/10.1520/D4546-14.

Bahlouli, T. El, Bahi, L., 2013. Analysis of the swelling behavior of the tirs of gharb (Morocco) compared with factors related to the change of soil-moisture. Int. J. Eng. Technol. 5, 3649–3659.

Barla, M., 2008. Numerical simulation of the swelling behaviour around tunnels based on special triaxial tests. Tunn. Undergr. Sp. Technol. 23, 508–521. https://doi.org/10.1016/j.tust.2007.09.002

Basma, A.A., Al-Homoud, A.S., Husein, A., 1995. Laboratory assessment of swelling pressure of expansive soils. Appl. Clay Sci. 9, 355–368. https://doi.org/10.1016/0169-1317(94)00032-L

Bei-xiao Shi, Sheng-shui Chen, H.H. andCheng-fengZheng, 2014. Expansive Soil Crack Depth under Cumulative Damage Beixiao Shi 1,2 , Shengshui Chen 3 , and Chengfeng Zheng 4. Hindawi Publ. Corp. ?e Sci. World Journa 2014, 1–14.

Beloborodov, R., Pervukhina, M., Han, T., Josh, M., 2017. Experimental Characterization of Dielectric Properties in Fluid Saturated Artificial Shales. Geofluids 2017, 1–9.

https://doi.org/10.1155/2017/1019461

Bonini, M., Debernardi, D., Barla, M., Barla, G., 2009. The mechanical behaviour of clay shales and implications on the design of tunnels. Rock Mech. Rock Eng. 42, 361–388. https://doi.org/10.1007/s00603-007-0147-6

Butscher, C., Huggenberger, P., Zechner, E., Einstein, H.H., 2011. Relation between hydrogeological setting and swelling potential of clay-sulfate rocks in tunneling. Eng. Geol. 122, 204–214. https://doi.org/10.1016/j.enggeo.2011.05.009

Cao, X., Liu, J., Jiang, N., Chen, Q., 2014. Particle image velocimetry measurement of indoor airflow field: A review of the technologies and applications. Energy Build. 69, 367–380. https://doi.org/10.1016/j.enbuild.2013.11.012

Castro, R., Trueman, R., Halim, A., 2007. A study of isolated draw zones in block caving mines by means of a large 3D physical model. Int. J. Rock Mech. Min. Sci. 44, 860–870. https://doi.org/10.1016/j.ijrmms.2007.01.001

Cui, Y., Kodaka, T., Furuyama, S., 2015. Deformation and strength characteristics of high-density bentonite-sand mixture under unsaturated conditions. 15th Asian Reg. Conf. Soil Mech. Geotech. Eng. ARC 2015 New Innov. Sustain. 1829–1832. https://doi.org/10.3208/jgssp.JPN-085

Cui, Y.J., Nguyen, X.P., Tang, A.M., Li, X.L., 2013. An insight into the unloading/reloading loops on the compression curve of natural stiff clays. Appl. Clay Sci. 83–84, 343–348. https://doi.org/10.1016/j.clay.2013.08.003

D.G. Fredlund, A.X., 1994. Equations for the soil-water characteristic ' curve '. Can. Geotech. J.

Daraei, A., Herki, B.M.A., Sherwani, A.F.H., Zare, S., 2018. Slope Stability in Swelling Soils Using Cement Grout: A Case Study. Int. J. Geosynth. Gr. Eng. 4, 0. https://doi.org/10.1007/s40891-018-0127-9

Dennis, K.C., 1994. Expansive soils. Constr. Specif. 47, 1–7. https://doi.org/10.1007/978-3-642-41714-6_52078

Du Mingqing, Dong Fei, Li Ao, Cao Xi, Zeng Kehan, Z.Q., 2019. Mechanism and failure mode of floor heave in tunnel invert of high speed railway under expansive surrounding rock. China Railw. Sci. Vol. 40. N.

El Bahlouli, T., Bahi, L., 2014. Assessment of the swelling pressure of the green clay of tangier (Morocco) compared with the soil-moisture conditions. MATEC Web Conf. 11, 1–5. https://doi.org/10.1051/matecconf/20141103011

Estabragh, A.R., Moghadas, M., Javadi, A.A., 2013. Effect of different types of wetting fluids on the behaviour of expansive soil during wetting and drying. Soils Found. 53, 617–627. https://doi.org/10.1016/j.sandf.2013.08.001

Faezehossadat, K., Jeff, B., 2016. Expansive Soil: Causes and Treatments. i-manager's J. Civ. Eng. 6, 1. https://doi.org/10.26634/jce.6.3.8083

Fattah, M.Y., Al-Lami, A.H.S., 2016. Behavior and characteristics of compacted expansive

unsaturated bentonite-sand mixture. J. Rock Mech. Geotech. Eng. 8, 629–639. https://doi.org/10.1016/j.jrmge.2016.02.005

Fredlund, D.G., Morgenstern, N.R., Widger, R.A., 1978. Shear Strength of Unsaturated Soils. Can. Geotech. J. 15, 313–321. https://doi.org/10.1139/t78-029

Gens, A., Alonso, E.E., 1992. A framework for the behaviour of unsaturated expansive clays. Can. Geotech. J. 29, 1013–1032. https://doi.org/10.1139/t92-120

Gens, A., Sánchez, M., Sheng, D., 2006. On constitutive modelling of unsaturated soils. Acta Geotech. 1, 137–147. https://doi.org/10.1007/s11440-006-0013-9

Htut, Z.M., Mohammed Azhar, M.M., Chao, K.C., 2019. Evaluation of the relationship between swelling pressures determined by consolidation-swell test and constant volume test. 7th Asia-Pacific Conf. Unsaturated Soils, AP-UNSAT 2019 250–255. https://doi.org/10.3208/jgssp.v07.039

Huang, F., Zhu, H., Xu, Q., Cai, Y., Zhuang, X., 2013. The effect of weak interlayer on the failure pattern of rock mass around tunnel - Scaled model tests and numerical analysis. Tunn. Undergr. Sp. Technol. 35, 207–218. https://doi.org/10.1016/j.tust.2012.06.014

ISRM, 1999. Suggested methods for laboratory testing of swelling rocks. Int. J. Rock Mech. Min. Sci. 36, 307–322.

Jan, M.A., Walker, R.D., 1963. Effect of Lime, Moisture and Compaction on a Clay Soil. Highw. Res. Rec. 1–12.

Komine H. and Ogata N., 1999. Experimental study on swelling characteristics of sand-bentonite mixture for nuclear waste disposal. Soils Found. 39, 83–97. https://doi.org/https://doi.org/10.3208/sandf.39.2_83

Komine, H., Ogata, N., 2004. Predicting Swelling Characteristics of Bentonites. J. Geotech. Geoenvironmental Eng. 130, 818–829. https://doi.org/10.1061/(asce)1090-0241(2004)130:8(818)

Kong, L.W., Guo, A.G., 2011. Bearing strength and swelling behavior of jingmen expansive soil. Road Mater. Pavement Des. 12, 441–450. https://doi.org/10.1080/14680629.2011.9695253

Kyokawa, H., Ohno, S., Kobayashi, I., 2020. A method for extending a general constitutive model to consider the electro-chemo-mechanical phenomena of mineral crystals in expansive soils. Int. J. Numer. Anal. Methods Geomech. 44, 749–771. https://doi.org/10.1002/nag.3026

Latar, S., Hardiyatmo, H.C., Adi, A.D., 2015. Relationship with the Degree of Saturation of the Swelling Strain 5, 51–56.

Li, L., Shang, C., Chu, K., Zhou, Z., Song, S., Liu, Z., Chen, Y., 2021. Large-scale geo-mechanical model tests for stability assessment of super-large cross-section tunnel. Tunn. Undergr. Sp. Technol. 109, 103756. https://doi.org/10.1016/j.tust.2020.103756

Liu, N., Li, N., Xu, C., Li, G., Song, Z., Yang, M., 2020. Mechanism of Secondary Lining Cracking and its Simulation for the Dugongling Tunnel. Rock Mech. Rock Eng. 53, 4539–4558. https://doi.org/10.1007/s00603-020-02183-3

McKenna, S.P., McGillis, W.R., 2002. Performance of digital image velocimetry processing techniques. Exp. Fluids 32, 106–115. https://doi.org/10.1007/s003480200011

Miao, L., Liu, S., Lai, Y., 2002. Research of soil-water characteristics and shear strength features of Nanyang expansive soil. Eng. Geol. 65, 261–267. https://doi.org/10.1016/S0013-7952(01)00136-3

Nature of expansive soils, 1938. https://doi.org/10.1016/B978-0-444-41393-2.50006-5

Nelson, J.D., 2015. Time dependence of swelling in oedometer tests on expansive soil. 15th Asian Reg. Conf. Soil Mech. Geotech. Eng. ARC 2015 New Innov. Sustain. 490–493. https://doi.org/10.3208/jgssp.OTH-35

Nujid, M.M., Taha, M.R., 2016. Numerical Modelling of Embankment on Soft Clay. IOP Conf. Ser. Mater. Sci. Eng. 136. https://doi.org/10.1088/1757-899X/136/1/012021

Ofoegbu, G.I., Dasgupta, B., Manepally, C., Stothoff, S.A., Fedors, R., 2017. Modeling the mechanical behavior of unsaturated expansive soils based on Bishop principle of effective stress. Environ. Earth Sci. 76, 1–18. https://doi.org/10.1007/s12665-017-6884-2

Osman, K.T., 2018. Management of soil problems. Manag. Soil Probl. 1–474. https://doi.org/10.1007/978-3-319-75527-4

Panji, M., Koohsari, H., Adampira, M., Alielahi, H., Asgari Marnani, J., 2016. Stability analysis of shallow tunnels subjected to eccentric loads by a boundary element method. J. Rock Mech. Geotech. Eng. 8, 480–488. https://doi.org/10.1016/j.jrmge.2016.01.006

Pedroso, D.M., Farias, M.M., 2011. Extended Barcelona Basic Model for unsaturated soils under cyclic loadings. Comput. Geotech. 38, 731–740. https://doi.org/10.1016/j.compgeo.2011.02.004

Pham, H.Q., Fredlund, D.G., 2008. Equations for the entire soil-water characteristic curve of a volume change soil. Can. Geotech. J. 45, 443–453. https://doi.org/10.1139/T07-117

Pimentel, E., 2015. Existing Methods for Swelling Tests - A Critical Review. Energy Procedia 76, 96–105. https://doi.org/10.1016/j.egypro.2015.07.857

Pruška, J., Šedivý, M., 2015. Prediction of Soil Swelling Parameters. Procedia Earth Planet. Sci. 15, 219–224. https://doi.org/10.1016/j.proeps.2015.08.052

Qi, S., Vanapalli, S.K., 2016. Influence of swelling behavior on the stability of an infinite unsaturated expansive soil slope. Comput. Geotech. 76, 154–169. https://doi.org/10.1016/j.compgeo.2016.02.018

Robert, W., 2006. Foundatin Engineering Handbook. 1st ed., ISBN 0-07-144769-5, Library of Congress, Ed. ASCE press, USA: Mcgraw-Hill Professional, 2006.

Seki, S., Kaise, S., Morisaki, Y., Azetaka, S., Jiang, Y., 2008. Model experiments for examining heaving phenomenon in tunnels. Tunn. Undergr. Sp. Technol. 23, 128–138. https://doi.org/10.1016/j.tust.2007.02.007

Selen, L., Panthi, K.K., Vergara, M.R., Mørk, M.B., 2021. Investigation on the Effect of Cyclic Moisture Change on Rock Swelling in Hydropower Water Tunnels. Rock Mech. Rock Eng. 54, 463–476. https://doi.org/10.1007/s00603-020-02266-1

Selmer-Olsen, R., Palmstrom, A., Stromme, B., 1989. Tunnel collapses in swelling clay zones. Tunnels Tunn. Int. 21, 49–51. https://doi.org/10.1016/0148-9062(90)94784-q

Serratrice, J.F., Soyez, B., 1996. Les essais de gonflement. Bull. des Lab. des Ponts Chaussees 0, 65–85.

Shi, B., Jiang, H., Liu, Z., Fang, H.Y., 2002. Engineering geological characteristics of expansive soils in China. Eng. Geol. 67, 63–71. https://doi.org/10.1016/S0013-7952(02)00145-X

Simms, P.H., Yanful, E.K., 2002. Predicting soil-water characteristic curves of compacted plastic soils from measured pore-size distributions. Geotechnique 52, 269–278. https://doi.org/10.1680/geot.2002.52.4.269

Soltani, A., Deng, A., Taheri, A., Mirzababaei, M., 2019. A sulphonated oil for stabilisation of expansive soils. Int. J. Pavement Eng. 20, 1285–1298. https://doi.org/10.1080/10298436.2017.1408270

Soltani, A., Taheri, A., Khatibi, M., Estabragh, A.R., 2017. Swelling Potential of a Stabilized Expansive Soil: A Comparative Experimental Study. Geotech. Geol. Eng. 35, 1717–1744. https://doi.org/10.1007/s10706-017-0204-1

Sridharan, A., Prakash, K., 2000. Classification procedures for expansive soils. Proc. Inst. Civ. Eng. Geotech. Eng. 143, 235–240. https://doi.org/10.1680/geng.2000.143.4.235

Stille, H., Palmström, A., 2008. Ground behaviour and rock mass composition in underground excavations. Tunn. Undergr. Sp. Technol. 23, 46–64. https://doi.org/10.1016/j.tust.2006.11.005

Stoltz, G., Cuisinier, O., Masrouri, F., 2012. Multi-scale analysis of the swelling and shrinkage of a lime-treated expansive clayey soil. Appl. Clay Sci. 61, 44–51. https://doi.org/10.1016/j.clay.2012.04.001

Tahasildar, J., Erzin, Y., Rao, B.H., 2018. Development of relationships between swelling and suction properties of expansive soils. Int. J. Geotech. Eng. 12, 53–65. https://doi.org/10.1080/19386362.2016.1250040

Takagi, T., 1994. Bentonite in Japan – Geology and Industries –. Open file Rep. Geol. Surv. JApan 1–13.

Tang, S.B., Tang, C.A., 2012. Numerical studies on tunnel floor heave in swelling ground under humid conditions. Int. J. Rock Mech. Min. Sci. 55, 139–150. https://doi.org/10.1016/j.ijrmms.2012.07.007

Tang, Y.H., Bao, C.G., Wang, M.Y., Ding, J.H., 2008. Experimental study on the strength characteristics of expansive soil reinforced with synthetic fibers. Geosynth. Civ. Environ. Eng. - Geosynth. Asia 2008 Proc. 4th Asian Reg. Conf. Geosynth. 369–373. https://doi.org/10.1007/978-3-540-69313-0_71

Tiwari, N., Satyam, N., 2021a. Coupling effect of pond ash and polypropylene fiber on strength and durability of expansive soil subgrades: An integrated experimental and machine learning approach. J. Rock Mech. Geotech. Eng. https://doi.org/10.1016/j.jrmge.2021.03.010

Tiwari, N., Satyam, N., 2021b. Coupling effect of pond ash and polypropylene fiber on strength and

durability of expansive soil subgrades: An integrated experimental and machine learning approach. J. Rock Mech. Geotech. Eng. 13, 1101–1112. https://doi.org/10.1016/j.jrmge.2021.03.010

Tiwari, N., Satyam, N., Kumar Shukla, S., 2020. An experimental study on micro-structural and geotechnical characteristics of expansive clay mixed with EPS granules. Soils Found. 60, 705–713. https://doi.org/10.1016/j.sandf.2020.03.012

Tong, F., Jian-Hua, Y., 2011. Nonlinear creep and swelling behavior of bentonite mixed with different sand contents under oedometric condition. Mar. Georesources Geotechnol. 29, 346–363. https://doi.org/10.1080/1064119X.2011.560824

Tran, T.D., Cui, Y.J., Tang, A.M., Audiguier, M., Cojean, R., 2014. Effects of lime treatment on the microstructure and hydraulic conductivity of Héricourt clay. J. Rock Mech. Geotech. Eng. 6, 399–404. https://doi.org/10.1016/j.jrmge.2014.07.001

Vanapalli, S.K., Pufahl, D.E., Fredlund, D.G., 1998. The Effect of Stress State on the Soil-Water Characteristic Behavior of a Compacted Sandy Clay Till. Proc. 51st Can. Geotech. Conf. 87–94.

Wang, F.N., Guo, Z.B., Qiao, X.B., Fan, J.Y., Li, W., Mi, M., Tao, Z.G., He, M.C., 2021. Large deformation mechanism of thin-layered carbonaceous slate and energy coupling support technology of NPR anchor cable in Minxian Tunnel: A case study. Tunn. Undergr. Sp. Technol. 117. https://doi.org/10.1016/j.tust.2021.104151

Wang, G., Wei, X., 2015. Modeling swelling–shrinkage behavior of compacted expansive soils during wetting–drying cycles. Can. Geotech. J. 52, 783–794. https://doi.org/10.1139/cgj-2014-0059

Wang, Y.X., Shan, S.B., Zhang, C., Guo, P.P., 2019. Seismic response of tunnel lining structure in a thick expansive soil stratum. Tunn. Undergr. Sp. Technol. 88, 250–259. https://doi.org/10.1016/j.tust.2019.03.016

Wang, Y., Zheng, S., Li, Y., Wang, Yueming, Huang, Y., 2021. The failure characteristics around shallow buried tunnels under rainfall conditions. Geomatics, Nat. Hazards Risk 12, 363–380. https://doi.org/10.1080/19475705.2021.1875058

Wanjun, Y.E., Chenyang, C.U.I., Zhuowu, X.I.E., Yuntao, W.U., Xihao, D., 2019. Influence of Water Content Difference on Construction Mechanical Behavior of Expansive R ed Clay Tunnel.

White, D.J., Take, W.A., Bolton, M.D., 2003. Soil deformation measurement using particle image velocimetry (PIV) and photogrammetry. Geotechnique 53, 619–631. https://doi.org/10.1680/geot.2003.53.7.619

Wittke-Gattermann and Wittke, 2004. Computation of strains and pressures for tunnels in swelling rocks. Tunn. Undergr. Sp. Technol. 19, 422–423. https://doi.org/10.1016/j.tust.2004.02.040

Xu, Y., Sun, D.E.A.N., 2001. Determination of Expansive Soil 9, 51–60.

Yan, X., Yu, H., Yuan, Y., Yuan, J., 2015. Multi-point shaking table test of the free field under non-uniform earthquake excitation. Soils Found. 55, 985–1000.

https://doi.org/10.1016/j.sandf.2015.09.031

Yin, J.H., Tong, F., 2011. Constitutive modeling of time-dependent stress- strain behaviour of saturated soils exhibiting both creep and swelling. Can. Geotech. J. 48, 1870–1885. https://doi.org/10.1139/T11-076

Yu, J., Liu, G., Cai, Y., Zhou, J., Liu, S., Tu, B., 2020. Time-Dependent Deformation Mechanism for Swelling Soft-Rock Tunnels in Coal Mines and Its Mathematical Deduction. Int. J. Geomech. 20, 04019186. https://doi.org/10.1061/(asce)gm.1943-5622.0001594

Yuzo OKUI, Kazuo NISHIMURA, N.I., 2020. 軟岩の膨潤と強度低下を考慮した 弾塑性時間依存モデルと変状トンネルへの適用 76, 1–20.

Zaini, M.S.I., Hasan, M., Yie, L.S., Masri, K.A., Putra Jaya, R., Hyodo, M., Winter, M.J., 2021. Effect of optimum utilization of silica fume and eggshell ash to the engineering properties of expansive soil. J. Mater. Res. Technol. 14, 1401–1418. https://doi.org/10.1016/j.jmrt.2021.07.023

Zamin, B., Nasir, H., Mehmood, K., Iqbal, Q., Farooq, A., Tufail, M., 2021. An Experimental Study on the Geotechnical, Mineralogical, and Swelling Behavior of KPK Expansive Soils. Adv. Civ. Eng. 2021. https://doi.org/10.1155/2021/8493091

Zeng, Z., Cui, Y.J., Conil, N., Talandier, J., 2020. Investigating the contribution of claystone to the swelling pressure of its mixture with bentonite. E3S Web Conf. 195, 0–3. https://doi.org/10.1051/e3sconf/202019503043

Zhang, C.L., Wieczorek, K., Xie, M.L., 2010. Swelling experiments on mudstones. J. Rock Mech. Geotech. Eng. 2, 44–51. https://doi.org/10.3724/SP.J.1235.2010.00044

Zhang, W., Wu, K., Wu, H., Wang, Y., Yu, Y., 2016. Assessing the influence of humidity on the stability of expansive soil rock surrounding tunnels. Int. J. Simul. Syst. Sci. Technol. 17, 1–5. https://doi.org/10.5013/IJSSST.a.17.44.29